

An eccentric perspective on brain networks

Marcel Alexander de Reus

The studies described in this thesis were performed at the Brain Center Rudolf Magnus,
Department of Psychiatry, University Medical Center Utrecht

Cover design: Nadja de Bruin
Printed by: Proefschriftmaken.nl || Uitgeverij BOXPress
Published by: Uitgeverij BOXPress, 's-Hertogenbosch
ISBN: 978-94-6295-357-4

© 2015 Marcel de Reus

All rights reserved. No part of this publication may be reproduced or distributed in any form or by any means, or stored in a database or retrieval system, without prior permission of the author.

An eccentric perspective on brain networks

Een andere kijk op hersennetwerken
(met een samenvatting in het Nederlands)

Proefschrift

ter verkrijging van de graad van doctor aan de Universiteit Utrecht op gezag van de rector magnificus, prof. dr. G.J. van der Zwaan, ingevolge het besluit van het college voor promoties in het openbaar te verdedigen op dinsdag 29 september 2015 des middags te 2.30 uur

door

Marcel Alexander de Reus

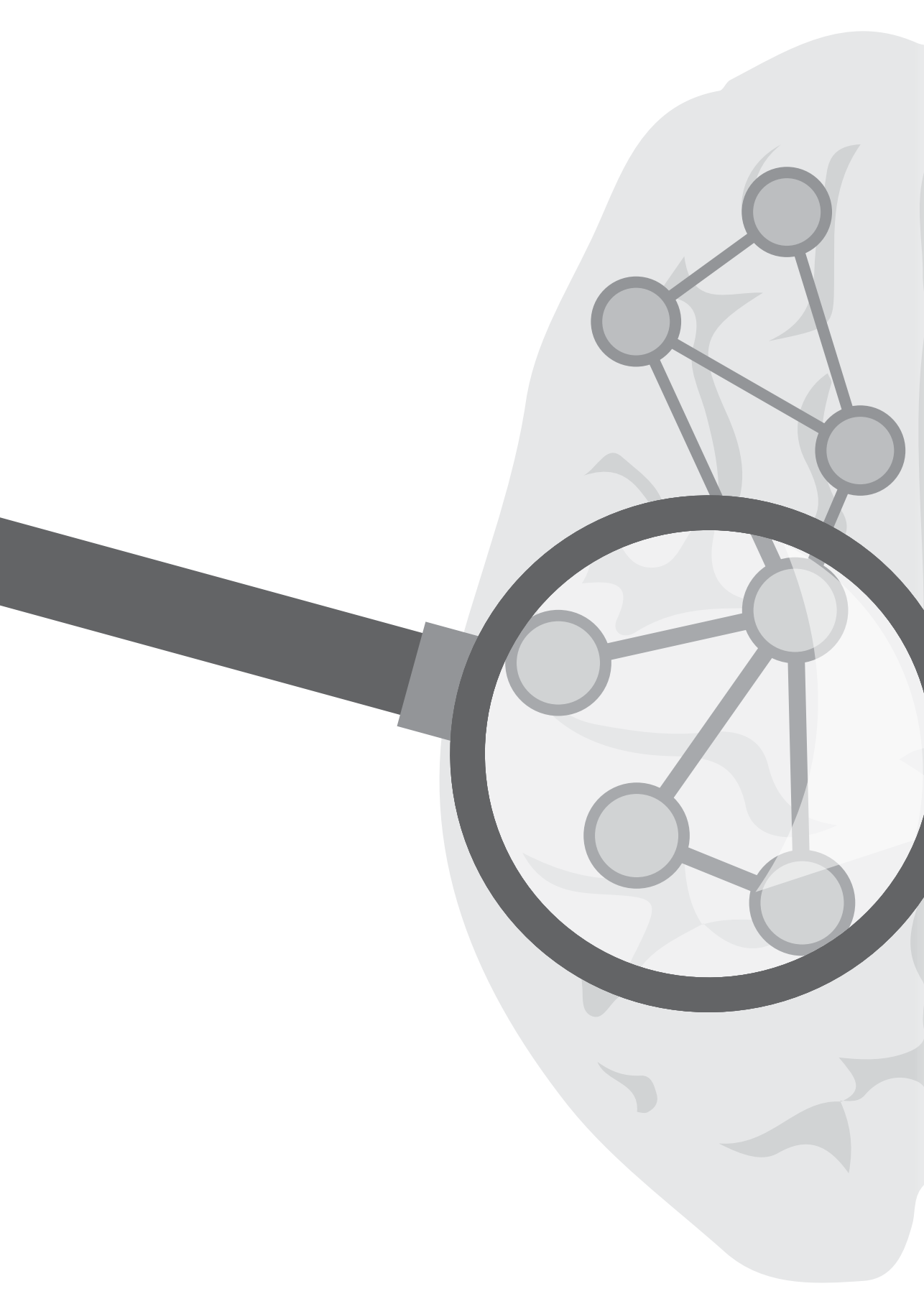
geboren op 1 februari 1987 te Rotterdam

Promotor: Prof. dr. R.S. Kahn

Copromotor: Dr. M.P. van den Heuvel

Table of contents

Chapter 1	Introduction	7
Chapter 2	Mapping the wires of our brain: Automated connectome reconstruction using diffusion tractography	27
Chapter 3	The parcellation-based connectome: Limitations and extensions	53
Chapter 4	Estimating false positives and negatives in brain networks	77
Chapter 5	Rich club organization and intermodule communication in the cat connectome	111
Chapter 6	Simulated rich club lesioning in brain networks: a scaffold for communication and integration?	143
Chapter 7	Mapping and examining the rodent connectome Part I: Chasing the dreams of early connectionists Part II: Topological organization of connectivity strength in the rat connectome	163 168
Chapter 8	Link communities in the human brain	197
Chapter 9	Spectral fingerprints of neural networks Part I: The Laplacian spectrum of neural networks Part II: The role of symmetry in neural networks and their Laplacian spectra	226 249
Chapter 10	Summary and discussion	273
	Nederlandse samenvatting	311
	List of publications	322
	Acknowledgments	324
	Curriculum vitae	326



Chapter 1

Introduction

Our brain is a formidably complex network. The adult human brain comprises an estimated number of about 80-100 billion neurons, interconnected to each other through circa 100-500 trillion neuronal connections. To put these staggering numbers into perspective: if you would go to the beach to fill one-liter soda bottles with sand, you would need about 100,000 bottles to collect enough grains of sand to match the number of neurons in the brain and a thousandfold more to match the number of neuronal connections. Although perhaps one of science's ultimate goals, mapping all neurons and neuronal connections, together forming the so-called *connectome*, is currently far from feasible, as would it be to extract sensible information from such an overwhelmingly detailed map. This does not mean, however, that the organization of the neural infrastructure which enables us to move, sense, memorize, and think has to remain elusive. On a larger and more comprehensible scale, neurons are organized into anatomically and functionally distinguishable brain regions and their neuronal connections form large-scale white matter fibers. This *macroscale* connectome of brain regions and white matter fibers can be mapped – even *in vivo* – and studied, allowing us to investigate the intriguing network architecture supporting the almost perpetual flow of information in our brain.

Even though the, especially during the last decade, quickly increasing number of studies on macroscale brain networks has started to lift a little corner of the veil, our understanding of the principles behind large-scale brain wiring is still a work in progress. Why is the brain wired like it is? What features characterize brain networks? And how is information from different brain regions combined? The aim of this thesis is to add some new pieces to this scientific puzzle by exploring new, eccentric, perspectives on macroscale brain networks. The idea of exploring these eccentric perspectives is two-fold. On the one hand, we here wish to further uncover wiring principles of the healthy brain and examine their validity across mammalian species (including human, cat, mouse, rat, and macaque). On the other hand, we expect the approaches and views presented here to be useful instruments for exposing differences between the healthy and diseased brain and hope this thesis will catalyze their adoption in clinically oriented con-

nectome studies.

Charting brain wires

An essential first step in providing any perspective on brain networks is to form a map of their elements. Ever since Marcello Malpighi showed that the white matter of the brain comprises “fibers” (1664; see Schmahmann and Pandya (2006) for a historical overview), scientists have tried, as suggested by Niels Stensen in 1665, to follow “the nerve threads through the substance of the brain to find out where they go and where they end” (cited in Schmahmann and Pandya (2006, p. 11)). Unfortunately, this turned out to be easier said than done. Although meticulous dissection of postmortem brain tissue allowed anatomists to get a global impression of the course of white matter fiber bundles, it was “quite impossible to trace the fibres to their ultimate ending” (Beevor (1891) as cited in Schmahmann and Pandya (2006, p. 25)). In fact, reliable estimation of white matter connections remained out of reach for more than three hundred years, until the introduction of physiological neuronal tract-tracing methods in the late 1970s marked the first of two major breakthroughs in the mapping of macroscale brain wiring.

Neuronal tract-tracing

The principle of neuronal tract-tracing methods is somewhat comparable to that of classic high school experiments in which coloring agents are used to visualize the flow of otherwise transparent fluids. First, a special substance with visualizable components is injected in a specific site of interest in the brain of a living animal. After the visualizable components have been allowed to spread, the animal is sacrificed and the experimenter determines where the visualizable components ended up. The crux of the approach is that the injected components are not just simple coloring agents, as in the high school experiments, but special compounds that are designed to enter neurons and use the intrinsic transport mechanisms within a neuron to move along the axon. As a result, the presence of visualizable components in brain regions other than the injection

site provides direct evidence for the existence of a neuronal connection between that region and the injection site.

The finer details of neuronal tract-tracing depend on the specific compound used. Since the introduction in the 1970s, many different neural tracers have been developed, which differ from one another on several aspects (Marotte, 1998). For instance, visualization of the tracer substance may depend on radioactivity, fluorescence, or a histochemical reaction, and the tracer may or may not be self-replicating (i.e., viral). Moreover, depending on the tracer substance, transport along the axon can be directed from the cell body to the axonal terminal (anterograde tracing), or from the terminal to the cell body (retrograde tracing), or involve a mixture of anterograde and retrograde movement. Every combination of these features has its own advantages and disadvantages and it may depend on the specific research question which compound is most suitable. The gross result, however, is always the same: an estimation of the macroscale white matter projections of the injection site, typically including an indication of the strength of the projections, as well as information about their direction (with anterograde tracers identifying outgoing projections and retrograde tracers identifying incoming projections of the injection site).

The relatively direct way in which neuronal tract-tracing allows assessment of neural connectivity makes that it is generally considered to be the gold standard and still in use today. Unfortunately, there are two major drawbacks which limit the usability of neuronal tract-tracing in some common scenarios in modern neuroscience. The first, most obvious, drawback is that, due to its invasive nature, neuronal tract-tracing techniques are limited to studies on animal brains and cannot be used to investigate the human brain. The second limitation is that one can only study the connectivity of a single (or, in case of fluorescent tracers, a few) injection site(s) within the same brain. After all, the source of detected visualizable components must be unambiguous to be able to infer the existence of neuronal projections. Examination of larger networks of white matter connections, such as macroscale connectomes, is therefore only possi-

ble by combining data from multiple animals, either by collating findings across tract-tracing literature or by landmark efforts involving hundreds of brains. As will also be shown in **chapters 5-7** and **chapter 9**, such “compiled” animal connectomes are well-suited to examine brain network architecture. However, they do not permit assessment of intersubject variability – a necessary precondition to elucidate potential links between the connectome and topics such as cognitive performance, brain development, and brain disorders.

Diffusion-weighted magnetic resonance imaging

On July 3, 1977, decades of research on a physical phenomenon known as *nuclear magnetic resonance* culminated in the first magnetic resonance imaging (MRI) body scan of a (living) human being (Damadian et al., 1976). While the practical usability of MRI was still limited at that time (the first scan took nearly five hours to complete and only produced a single image of the subject’s thorax), a number of subsequent improvements would quickly turn MRI into a widely used and indispensable technique in both research and clinic, crowned with the Nobel Prize in Physiology or Medicine in 2003. Advantages of MRI include its ability to provide high contrasts between different types of soft tissue and the absence of ionizing radiation, making it possible to examine almost any subject and to perform relatively long or repeated measurements.

In the brain, MRI provides excellent contrast between gray and white matter and therefore allows *in vivo* examination of several aspects of brain anatomy (volume of specific structures, thickness and gyration of the cortical mantle, etc.). However, on a conventional MRI scan, there is not much contrast *within* the white matter and there is no trace of any large-scale fibers. Instead, like in actual postmortem sections of the brain, the white matter appears as a more or less homogeneous substance. That MRI can also be used to delineate white matter fibers is indirectly related to Albert Einstein, who, in addition to his famous theories on relativity and the photoelectric effect, described why and how particles suspended in water, including water molecules themselves, randomly move or *diffuse* (Einstein, 1905). Eight decades later, Denis Le Bihan, a resident

in radiology at the time, realized that this diffusion of water could provide insight in the microstructural architecture of tissues. He anticipated that the random movement of water molecules would be altered by the presence and layout of cells and designed a new type of MRI scan able to measure diffusion of water molecules (Le Bihan et al., 1986). For fibrous tissue such as the brain's white matter, it was then shown that the net displacement of water molecules is largest in the direction parallel to the fibers (Moseley et al., 1990) – the suspected mechanism being that water molecules "bump" into the fibers when moving perpendicular to them. This observation is still central in present day MRI-based connectome reconstruction and allows quick and *in vivo* estimation of the course of white matter pathways in a single individual on the basis of MRI diffusion measurements. Given the current importance of MRI-based connectome reconstruction, the topic of charting white matter fibers using MRI is further and more elaborately discussed in **chapter 2**.

Graph theory

Obtaining connectome maps in itself does not provide new information on how our brain may process information or coordinate complex tasks. When reduced to its essence, connectome mapping basically provides us with a list of brain regions, which can be thought of as "dots", and a large collection of seemingly haphazardly placed "lines" (i.e., connections) between those dots. Unraveling this complex network of dots and lines by extracting useful information from it is one of the key challenges when examining connectomes. Help in tackling this challenge comes from a perhaps unexpected corner – a branch of mathematics known as *graph theory*, which finds its origin in an old riddle about Königsberg.

The seven bridges of Königsberg

In 1736, the famous Swiss mathematician Leonhard Euler published a solution to a riddle about Königsberg (Euler, 1741), an old Prussian city now known as Kaliningrad and birthplace of many renowned mathematicians (including Christian Goldbach, Otto Hesse, Carl Neumann, Rudolf Lipschitz, Alfred Clebsch, David

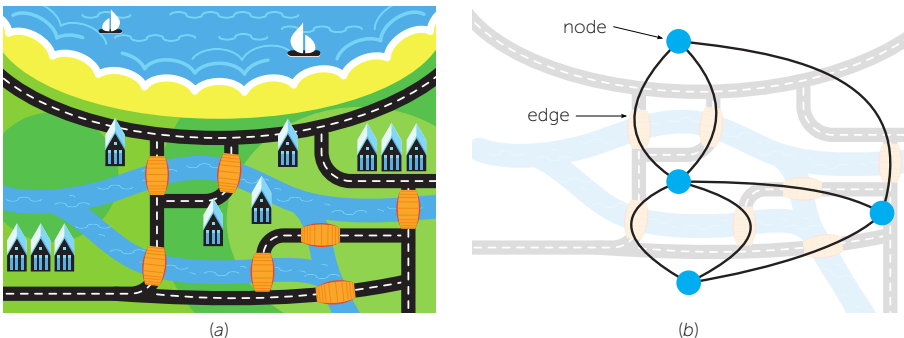


Figure 1.1. (a) Schematic illustration of the seven bridges of Königsberg in the early eighteenth century. At the time, a widely known, yet unsolved, riddle about these bridges drew the attention of the famous Swiss mathematician Leonhard Euler: is there a way to make a closed walk through the city, crossing each of the seven bridges exactly once? Euler realized that only the abstract pattern of connections between the land masses had to be taken into account and demonstrated more generally that a walk of the desired type can only exist if all land masses have an even number of connections, which was not the case in Königsberg. (b) Euler's abstract approach to the riddle laid the foundations for the formal study of *graphs*; mathematical objects consisting of a collection of *nodes* and a collection of interconnecting *edges*. Contrary to the graph associated to the Königsberg bridge problem, brain networks are usually represented by graphs with at most one edge between a pair of nodes.

Hilbert and Hermann Minkowski). At the time, there were seven bridges in the city center of Königsberg, connecting the northern and southern part of the city and two central islands, geographically separated from each other by the river Pregel (Figure 1.1a). Inhabitants of the city wondered whether it would be possible to make a closed walk through the city, crossing each of the seven bridges exactly once. In his solution, Euler recognized that only the abstract pattern of connections between the four land masses had to be taken into account, the precise shape and size of the land masses and the length of the bridges being irrelevant. He then demonstrated that for any configuration of land masses and bridges, a walk of the desired type can only exist if all land masses have an even number of connections, which was not the case in Königsberg. The inhabitants of the city could therefore stop wondering and the riddle was solved.

Nodes and edges

With his solution to the Königsberg bridge problem, achieved by reducing the problem to its essential structure, Euler laid the foundations for the mathematical field of graph theory, concerning objects called *graphs* that consist of a collection of *nodes* or *vertices* (e.g., land masses) and a collection of interconnecting *edges* or *links* (e.g., bridges) (Figure 1.1b). Almost three centuries later, graph theory has not only become a flourishing field of research within mathematics, dealing with very diverse questions about abstract graphs, but has also proven to be useful as an instrument for the analysis of many “real-world” networks appearing in nature and society. Such real-world networks – including the connectome, but also, for instance, social networks such as Facebook and Twitter, protein-protein interaction networks, computer networks, food webs, and transportation networks – can almost always be conceptualized as collections of nodes (dots) and edges (lines). As a result, they can be analyzed using general graph theoretical tools oblivious to the specific meaning of the nodes and edges. For example, in a graph representation of Facebook, people can be represented by nodes and Facebook friendships between people by edges, while in a food web, nodes can represent species and edges may reflect predator-prey relationships. As already indicated by the description of connectome maps in terms of dots and lines, for the connectome graphs central in this thesis, nodes will reflect brain regions and edges will reflect white matter fibers. The formation of these connectome graphs is more extensively discussed in **chapters 2–4**, with **chapter 3** focusing on the choice of nodes and **chapter 4** on the presence of edges.

Examining network organization

Because the universal nature of graph theory makes it easy to share new concepts and inventions between scientific disciplines, there is an impressive, and still increasing, number of graph theoretical instruments available to examine and describe the features and organization of (large) complex networks such as the connectome (Rubinov and Sporns, 2010). The commonly used network metrics and concepts presented below give an impression of what kind of fea-

tures such instruments can capture.

Path length and efficiency

Given a pair of nodes i and j , one might wonder how many “steps” are needed to “walk” from node i to j along the edges of the network. The minimum number of edges that needs to be traversed to accomplish this transition from node i to j is known as the *path length* between i and j (Figure 1.2a). A popular application of path length is measuring the “degree of separation” between people in social networks, using units such as handshakes, friendships, e-mail contacts, or scientific collaborations. An exponent of the latter is the *Erdős number*, which measures the collaborative distance of scientists to the prolific 20th century mathematician Paul Erdős. Averaging the path length across all node pairs results in the *characteristic path length* of the network as a whole. This characteristic path length is typically used to provide an indication of the communication efficiency in the network, with shorter characteristic path lengths taken to be more efficient.

Clustering coefficient

Introduced in a seminal paper of Watts and Strogatz (1998), the (local) *clustering coefficient* of a given node i measures how strongly the neighbors of i (that is, the nodes connected to i) are interconnected (Figure 1.2b). More specifically, the clustering coefficient is the ratio between the number of existing connections between node i ’s neighbors and the total number of neighbor-to-neighbor connections possible, with a value of 0 indicating that none of the neighbors are connected to each other and a value of 1 indicating that all neighbors are interconnected. An intuitive interpretation of the clustering coefficient arises in friendship networks, where it measures how often someone’s friends are also friends of one another. Similar to path length, the clustering coefficient is often averaged (in this case over all nodes) to get a global score for the entire network.

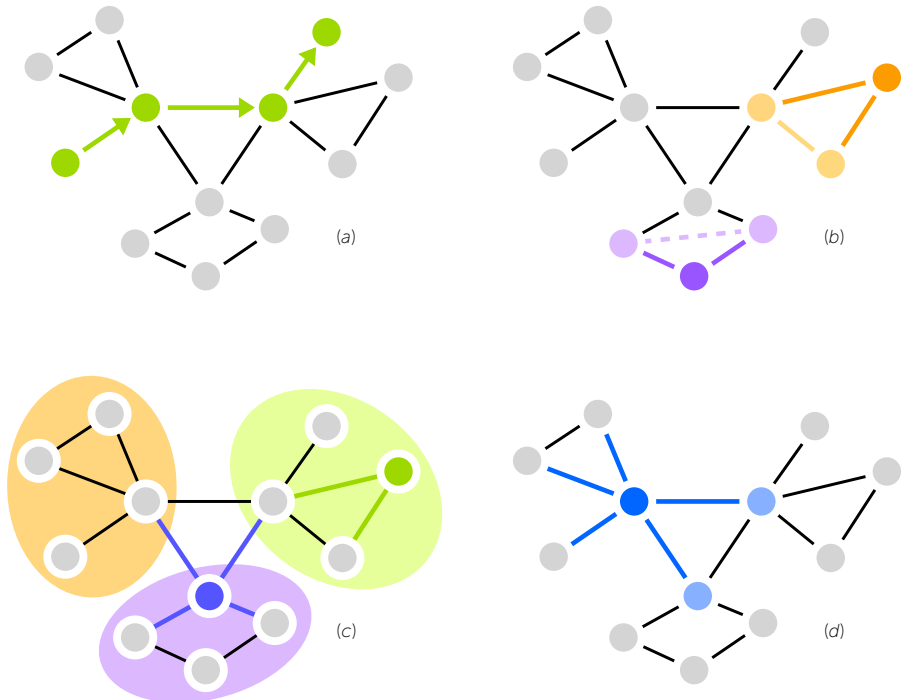


Figure 1.2. Illustration of some commonly used graph theoretical concepts and metrics. (a) The *path length* between two nodes is the minimum number of edges that needs to be traversed to get from one node to the other. The inverse of the average path length over all node pairs is often interpreted as a measure of communication efficiency. (b) The *clustering coefficient* of a node measures to what extent the neighbors of a node are also neighbors of one another. The orange node has a high clustering coefficient because its neighbors (the light orange nodes) are connected, whereas the purple node has a low clustering coefficient. (c) Given a subdivision of the network into *modules* of densely interconnected nodes (indicated by the ellipses), the *participation coefficient* of a node measures how well its neighbors are distributed over the different modules. Since the neighbors of the green node all belong to the same module, this node has a very low participation coefficient. In contrast, the neighbors of the highlighted node in the purple module are almost equally distributed over the three modules, thus resulting in a high participation coefficient. (d) The number of edges of a node is known as its *degree*. Nodes with a high degree and a central position in the network are referred to as *hubs*. In the example network, the dark blue node has a degree of five. Both the dark blue node and the light blue nodes have a relatively high degree and a topologically central position (being part of the trajectory of many of the shortest paths and being, on average, relatively close to all other nodes) and would therefore classify as hubs.

Communities, modularity and participation

Someone's friends also being friends of one another is more likely if all are part of the same *community*, which, in case of friendship networks, could for in-

stance be a sports team, school class, group of colleagues, or knitting club. In the large complex networks encountered in nature and society, such communities (or *modules*) of densely interconnected nodes are typically not *a priori* apparent, but are instead identified with specialized computer-driven algorithms to provide insight in the structure of the network (Porter et al., 2009). Using a quality function to rate possible subdivisions of the network, these algorithms try to find the best partitioning of a network into communities. A commonly used quality function is the so-called *modularity* metric, which provides a normalized estimate of the proportion of intramodule (i.e., within-community) edges (Newman, 2006). The optimal modularity score returned by the community detection algorithm is also referred to as *the modularity* of the network and indicates to what extent the network can be subdivided into separate modules. Identified communities can shed light on the organization of the network and can be incorporated in subsequent analyses. For instance, the *participation coefficient* of a node captures how its neighbors are distributed over the communities (Figure 1.2c), producing the highest value if the node's neighbors are (approximately) equally divided (i.e., if the node is in contact with many different communities) and the lowest value if the node's neighbors are concentrated within a single community (Guimerà and Amaral, 2005).

Hubs and centrality measures

In many real-world networks, the number of connections per node, known as the node's *degree*, is far from evenly distributed. Instead, there tends to be a small collection of nodes with a disproportionately large number of connections (Figure 1.2d). These high-degree *hub* nodes often play a more prominent role in the organization of the network and are therefore studied with special interest. Examples of hubs include Utrecht Central Station in the Dutch railway network and London Heathrow Airport for international flight traffic. These examples already indicate that the existence of hubs in a network may have both upsides (e.g., providing shortcuts and easy switching between communities) and downsides. Indeed, mist above Heathrow or a power disruption at Utrecht Central Station can have a cascading impact on the entire system. Although hubs are

classically distinguished on the basis of degree alone, one may also incorporate other nodal metrics that support the intuitive concept of hubs. Such additional metrics may, for instance, assess the centrality of a node in the network, with *closeness centrality* (the average distance of a node to all other nodes in the network) and *betweenness centrality* (the average fraction of shortest paths in which a node is involved) being two common examples.

Unraveling the connectome

Over the past years, the adoption of graph theoretical instruments to unravel the architecture of brain networks has taken an enormous flight, resulting in the discovery of several important properties of the human and animal connectome (Bullmore and Sporns, 2009). First, brain networks have been shown to exhibit a *small-world* organization (Gong et al., 2009; He et al., 2007; van den Heuvel et al., 2008; Sporns and Zwi, 2004; Stam, 2004); a term used for networks that have both high levels of local clustering and a short characteristic path length (Watts and Strogatz, 1998). This combination of features in brain networks may represent a balance between the occurrence of specialized processing of neural information within local clusters and global integration of information via short communication routes (Bassett and Bullmore, 2006; Sporns, 2013). Another organizational characteristic potentially related to local information processing is the existence of communities in connectome graphs (Alexander-Bloch et al., 2012; Chen et al., 2008; He et al., 2009; Hilgetag et al., 2000). Rather than being composed of a single layer of clear-cut modules, the community structure of the brain appears to be an intricate affair, with multiple levels of (hierarchically nested) communities and the existence of nodes without a clear allegiance to a single community (Betzel et al., 2013; Meunier et al., 2010; Wu et al., 2011). A commonly investigated factor which may partially drive such connectome characteristics is the concept of *wiring optimization* and its relation to the spatial embedding of the connectome in the skull (Achard and Bullmore, 2007; Bassett et al., 2010; van den Heuvel et al., 2012; Kaiser and Hilgetag, 2006; Raj and Chen, 2011). Based on the notion that the construction and use of long and thick wires is likely to demand more resources than that of short and thin ones,

Bullmore and Sporns (2012) hypothesized that "brain organization is shaped by an economic trade-off between minimizing costs and allowing the emergence of adaptively valuable topological patterns".

A prominent example of putative high-cost elements which are nevertheless present in the brain is presented by highly connected hub regions. The existence of such brain hubs – being the neural analogs of Heathrow Airport and Utrecht Central Station – has been consistently demonstrated in many types of connectome maps across several species (Hagmann et al., 2008; van den Heuvel and Sporns, 2011; Li et al., 2013; Nijhuis et al., 2013; Power et al., 2013; Sporns et al., 2007; Zamora-López et al., 2010). Corroborating an important role for hubs in healthy brain function, neural hubs have high metabolic demands (Liang et al., 2013; Tomasi et al., 2013; Vaishnavi et al., 2010) and are frequently reported to be implicated in brain-related disorders (Achard et al., 2012; Bassett et al., 2008; Buckner et al., 2009; Crossley et al., 2014; van den Heuvel et al., 2010; Stam et al., 2009). Interestingly, neural hubs are not only individually "rich" in connectivity, but are also densely interconnected to each other, thus forming a central core or *rich club* (Hagmann et al., 2008; van den Heuvel and Sporns, 2011). The role of this collective of hub nodes and interconnecting hub-to-hub connections in brain network organization will be a recurring theme in **chapters 5-8**.

New perspectives?

One might have noticed that the commonly used network metrics and concepts described above mainly characterize the organization of the connectome in terms of (average) properties of nodes or groups of nodes. It can therefore be argued that the graph theoretical instruments currently used for the analysis of brain networks provide a rather *node-centric* perspective on the connectome. This focus on nodes, and thus brain regions, as "main characters" also makes a lot of sense. Brain regions are, for instance, typically quite well-described; they have names which can be used to refer to them and there often is data available related to their potential function (e.g., which tasks they might be involved in), microscale and macroscale anatomy, and gene expression. Moreover, the

presence of brain regions is believed to be fairly robust across subjects and their number (ranging from tens to hundreds depending on the adopted methodology for delineation, see **chapter 3**) is foreseeable. In other words, brain regions are convenient and familiar elements to work with and newly derived knowledge about their role in the connectome (being a hub or not, level of clustering or participation, community assignment, etc.) can be relatively seamlessly integrated with previous insights.

Although the “conventional” node-centric perspective on brain networks is thus perfectly sensible, it remains odd that in a framework with two types of elements (i.e., nodes and edges), there is such a strong imbalance towards investigating one of them. In this thesis, we therefore go off the beaten track and turn our focus to the network properties of the edges of the connectome; an approach that can be labeled as both edge-centric and eccentric. In contrast to the brain regions which constitute the nodes of the connectome, the connectome’s edges – reflecting large-scale white matter fibers – are plentiful in number and generally do not have specific names. One way to get a grip on this myriad of connectome edges is to divide the collection of all edges into logical subgroups or *edge categories*. For instance, given the classification of nodes into hubs and non-hubs, the edges of the connectome can be divided into hub-to-hub *rich club* connections, non-hub-to-hub *feeder* connections, and non-hub-to-non-hub *local* connections (van den Heuvel et al., 2012). Here, we further develop this concept by exploring different ways to define edge categories, as well as new methods that may provide insight in the role that specific (types of) edges have in brain networks.

A strong motivation to pursue this edge-centric perspective is that (graph theoretical) connectome variation between subjects is preeminently encoded by the connections. While the nodes of the connectome are considered to be uniform across subjects and treated as “dimensionless dots” in graph analyses, the edges may vary in position (i.e., be absent or present, **chapter 4**) and typically also carry information about the *strength* of the represented white matter projections

(**chapter 2**). One of the most direct ways to assess connectome changes during healthy brain development and aging, as well as changes related to brain disorders, is therefore to monitor the connectivity strength of connectome edges. Suitably chosen edge categories and computational methods that assess the network role of edges may subsequently help to inspect what kind of connections are involved in changes in connectivity strength and may thus indirectly contribute to a better understanding of disease- or age-related changes in brain wiring.

Another, less edge-centric, but certainly not less eccentric, perspective that is more briefly explored in this thesis is given by the so-called *Laplacian spectrum* of neural networks. Rather than considering network properties of individual nodes or edges, or averaging such individual properties into global network estimates, the Laplacian spectrum essentially blends all aspects of a network into a single curve or “fingerprint”. Although perhaps somewhat less intuitive and more mathematical in nature, this fingerprint provides a truly systems-level point of view and may therefore elucidate different aspects of macroscale connectome organization than standard node-centric and our own edge-centric approaches.

Outline by chapter

Before exploring new perspectives on the connectome, **chapter 2** reviews the reconstruction of macroscale connectomes on the basis of diffusion-weighted MRI. Tracing back the steps taken to develop a new software package for automated connectome reconstruction, this chapter provides an in-depth overview of the process used to turn images produced by an MRI scanner into connectome maps. Part of the process of connectome mapping is delineating the macroscale brain regions that constitute the nodes of the network. **Chapter 3** discusses several delineation approaches and addresses how the choices involved in delineation may affect connectome maps and their network properties. Still more on the side of connectome mapping than connectome analysis, **chapter 4** shifts focus to the edges of the connectome by estimating the influence

of a simple parameter on the amount of false positive and false negative white matter connections (inherently present due to the reconstruction process) in group-averaged connectome maps. Since connections form the main objects of investigation when taking an edge-centric angle on connectome analysis, knowledge and reduction of such errors is especially important.

Although typically presented in conjunction with findings derived using conventional graph theoretical approaches, **chapters 5-8** all contribute to the edge-centric perspective pursued in this thesis. In **chapter 5**, several edge categories are used to examine the role of hubs in the cat connectome, dividing the connections of the connectome in unidirectional and bidirectional edges, intermodule and intramodule edges, and in rich club, feeder, and local connections. **Chapter 6** introduces a simulated lesioning framework to estimate network properties of individual edges and uses this framework to further develop insight in the role of rich club, feeder, and local connections, both in the human and cat connectome. **Chapter 7** explores whether the rodent brain exhibits similar network properties and continues along the edge-centric path by defining edge categories based on the strength of connections. These edge categories are analyzed using both conventional metrics and our simulated lesioning framework to answer the question whether connections of different strengths also have different roles in the network. Aiming to identify new edge categories independent of morphology (directedness, strength) or node labels, **chapter 8** generalizes the concept of communities to edges and investigates the presence and location of communities of white matter fibers in the human connectome.

The potential of the less edge-centric, but nevertheless eccentric, "spectral fingerprints" is probed in **chapter 9**, revolving around the investigation and interpretation of Laplacian spectra of animal and human connectomes. **Chapter 10** briefly recapitulates the insights on connectome organization provided by the perspectives adopted here and discusses their relative context and future potential.

References

- Achard, S., Bullmore, E., 2007. Efficiency and Cost of Economical Brain Functional Networks. *PLoS Computational Biology* 3, e17.
- Achard, S., Delon-Martin, C., Vértes, P.E., Renard, F., Schenck, M., Schneider, F., Heinrich, C., Kremer, S., Bullmore, E.T., 2012. Hubs of brain functional networks are radically reorganized in comatose patients. *Proceedings of the National Academy of Sciences* 109, 20608-20613.
- Alexander-Bloch, A., Lambiotte, R., Roberts, B., Giedd, J., Gogtay, N., Bullmore, E., 2012. The discovery of population differences in network community structure: New methods and applications to brain functional networks in schizophrenia. *NeuroImage* 59, 3889-3900.
- Bassett, D.S., Bullmore, E., 2006. Small-World Brain Networks. *The Neuroscientist* 12, 512-523.
- Bassett, D.S., Bullmore, E., Verchinski, B.A., Mattay, V.S., Weinberger, D.R., Meyer-Lindenberg, A., 2008. Hierarchical Organization of Human Cortical Networks in Health and Schizophrenia. *The Journal of Neuroscience* 28, 9239-9248.
- Bassett, D.S., Greenfield, D.L., Meyer-Lindenberg, A., Weinberger, D.R., Moore, S.W., Bullmore, E.T., 2010. Efficient Physical Embedding of Topologically Complex Information Processing Networks in Brains and Computer Circuits. *PLoS Computational Biology* 6, e1000748.
- Beevor, C.E., 1891. On the Course of the Fibres of the Cingulum and the Posterior Parts of the Corpus Callosum and Fornix in the Marmoset Monkey. *Philosophical Transactions of the Royal Society of London B: Biological Sciences* 182, 135-199.
- Betzel, R.F., Griffa, A., Avena-Koenigsberger, A., Goñi, J., Thiran, J.P., Hagmann, P., Sporns, O., 2013. Multi-scale community organization of the human structural connectome and its relationship with resting-state functional connectivity. *Network Science* 1, 353-373.
- Buckner, R.L., Sepulcre, J., Talukdar, T., Krienen, F.M., Liu, H., Hedden, T., Andrews Hanna, J.R., Sperling, R.A., Johnson, K.A., 2009. Cortical Hubs Revealed by Intrinsic Functional Connectivity: Mapping, Assessment of Stability, and Relation to Alzheimer's Disease. *The Journal of Neuroscience* 29, 1860-1873.
- Bullmore, E., Sporns, O., 2009. Complex brain networks: graph theoretical analysis of structural and functional systems. *Nature Reviews Neuroscience* 10, 186-198.
- Bullmore, E., Sporns, O., 2012. The economy of brain network organization. *Nature Reviews Neuroscience* 13, 336-349.
- Chen, Z.J., He, Y., Rosa-Neto, P., Germann, J., Evans, A.C., 2008. Revealing Modular Architecture of Human Brain Structural Networks by Using Cortical Thickness from MRI. *Cerebral Cortex* 18, 2374-2381.
- Crossley, N.A., Mechelli, A., Scott, J., Carletti, F., Fox, P.T., McGuire, P., Bullmore, E.T., 2014. The hubs of the human connectome are generally implicated in the anatomy of brain disorders. *Brain*, epub ahead of print.
- Damadian, R., Goldsmith, M., Minkoff, L., 1976. NMR in cancer: XVI. FONAR image of the live human body. *Physiological Chemistry and Physics* 9, 97-100.
- Einstein, A., 1905. Über die von der molekularkinetischen Theorie der Wärme geforderte Bewegung von in ruhenden Flüssigkeiten suspendierten Teilchen. *Annales de Physique* 322, 549-560.
- Euler, L., 1741. Solutio problematis ad geometriam situs pertinentis. *Commentarii academiae scientiarum Petropolitanae* 8, 128-140.
- Gong, G., He, Y., Concha, L., Lebel, C., Gross, D.W., Evans, A.C., Beaulieu, C., 2009. Mapping Anatomical Connectivity Patterns of Human Cerebral Cortex Using In Vivo Diffusion Tensor Imaging Tractography. *Cerebral Cortex* 19, 524-536.
- Guimerà, R., Amaral, L.A.N., 2005. Functional cartography of complex metabolic networks. *Nature* 433, 895-900.
- Hagmann, P., Cammoun, L., Gigandet, X., Meuli, R., Honey, C.J., Wedeen, V.J., Sporns, O., 2008. Mapping the Structural Core of Human Cerebral Cortex. *PLoS Biology* 6, e159.
- He, Y., Chen, Z.J., Evans, A.C., 2007. Small-World Anatomical Networks in the Human Brain Revealed by Cortical Thickness from MRI. *Cerebral Cortex* 17, 2407-2419.
- He, Y. et al., 2009. Uncovering Intrinsic Modular Organization of Spontaneous Brain Activity in Humans. *PLoS ONE* 4, e5226.

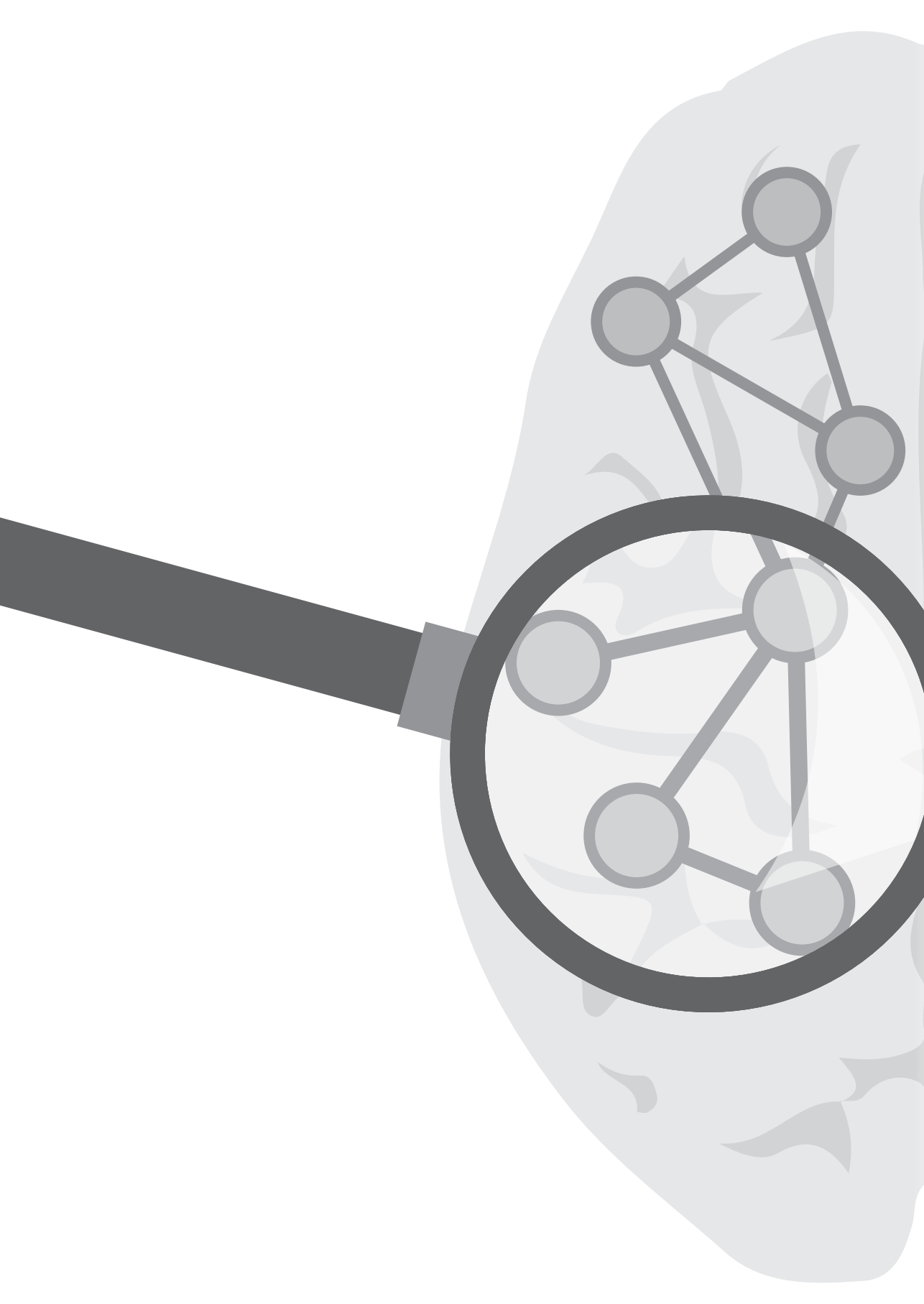
- van den Heuvel, M.P., Kahn, R.S., Goñi, J., Sporns, O., 2012. High-cost, high-capacity backbone for global brain communication. *Proceedings of the National Academy of Sciences* 109, 11372-11377.
- van den Heuvel, M.P., Mandl, R.C.W., Stam, C.J., Kahn, R.S., Hulshoff Pol, H.E., 2010. Aberrant Frontal and Temporal Complex Network Structure in Schizophrenia: A Graph Theoretical Analysis. *The Journal of Neuroscience* 30, 15915-15926.
- van den Heuvel, M.P., Sporns, O., 2011. Rich-Club Organization of the Human Connectome. *The Journal of Neuroscience* 31, 15775-15786.
- van den Heuvel, M.P., Stam, C.J., Boersma, M., Hulshoff Pol, H.E., 2008. Small-world and scale-free organization of voxel-based resting-state functional connectivity in the human brain. *NeuroImage* 43, 528-539.
- Hilgetag, C.C., Burns, G.A., O'Neill, M.A., Scannell, J.W., Young, M.P., 2000. Anatomical connectivity defines the organization of clusters of cortical areas in the macaque monkey and the cat. *Philosophical Transactions of the Royal Society of London B: Biological Sciences* 355, 91-110.
- Kaiser, M., Hilgetag, C.C., 2006. Nonoptimal Component Placement, but Short Processing Paths, due to Long-Distance Projections in Neural Systems. *PLoS Computational Biology* 2, e95.
- Le Bihan, D., Breton, E., Lallemand, D., Grenier, P., Cabanis, E., Laval-Jeantet, M., 1986. MR imaging of intravoxel incoherent motions: application to diffusion and perfusion in neurologic disorders. *Radiology* 161, 401-407.
- Li, L., Hu, X., Preuss, T.M., Glasser, M.F., Damen, F.W., Qiu, Y., Rilling, J., 2013. Mapping putative hubs in human, chimpanzee and rhesus macaque connectomes via diffusion tractography. *NeuroImage* 80, 462-474.
- Liang, X., Zou, Q., He, Y., Yang, Y., 2013. Coupling of functional connectivity and regional cerebral blood flow reveals a physiological basis for network hubs of the human brain. *Proceedings of the National Academy of Sciences* 110, 1929-1934.
- Marotte, L.R., 1998. Anatomical Tracing of Neuronal Connections. In: Martin, R. (Ed.), *Neuroscience Methods: A Guide for Advanced Students*. Harwood Academic Publishers, Amsterdam.
- Meunier, D., Lambiotte, R., Bullmore, E.T., 2010. Modular and hierarchically modular organization of brain networks. *Frontiers in Neuroscience* 4, 200.
- Moseley, M.E., Cohen, Y., Kucharczyk, J., Mintorovitch, J., Asgari, H.S., Wendland, M.F., Tsuruda, J., Norman, D., 1990. Diffusion-weighted MR imaging of anisotropic water diffusion in cat central nervous system. *Radiology* 176, 439-445.
- Newman, M.E.J., 2006. Modularity and community structure in networks. *Proceedings of the National Academy of Sciences* 103, 8577-8582.
- Nijhuis, E.H.J., van Cappellen van Walsum, A.M., Norris, D.G., 2013. Topographic Hub Maps of the Human Structural Neocortical Network. *PLoS ONE* 8, e65511.
- Porter, M.A., Onnela, J.P., Mucha, P.J., 2009. Communities in networks. *Notices of the American Mathematical Society* 56, 1082-1097.
- Power, J., Schlaggar, B., Lessov-Schlaggar, C., Petersen, S., 2013. Evidence for Hubs in Human Functional Brain Networks. *Neuron* 79, 798-813.
- Raj, A., Chen, Y., 2011. The Wiring Economy Principle: Connectivity Determines Anatomy in the Human Brain. *PLoS ONE* 6, e14832.
- Rubinov, M., Sporns, O., 2010. Complex network measures of brain connectivity: Uses and interpretations. *NeuroImage* 52, 1059-1069.
- Schmahmann, J.D., Pandya, D.N., 2006. *Fiber Pathways of the Brain*. Oxford University Press, New York.
- Sporns, O., 2013. Network attributes for segregation and integration in the human brain. *Current Opinion in Neurobiology* 23, 162-171.
- Sporns, O., Honey, C.J., Kotter, R., 2007. Identification and Classification of Hubs in Brain Networks. *PLoS ONE* 2, e1049.
- Sporns, O., Zwi, J., 2004. The small world of the cerebral cortex. *Neuroinformatics* 2, 145-162.
- Stam, C.J., 2004. Functional connectivity patterns of human magnetoencephalographic recordings: a 'small-world' network? *Neuroscience Letters* 355, 25-28.
- Stam, C.J. et al., 2009. Graph theoretical analysis of magnetoencephalographic functional connectivity in Alzheimer's disease. *Brain* 132, 213-224.
- Tomasi, D., Wang, G.J., Volkow, N.D., 2013. Energetic cost of brain functional connectivity. *Proceedings of the National Academy of Sciences* 110, 13642-13647.

Vaishnavi, S.N., Vlassenko, A.G., Rundle, M.M., Snyder, A.Z., Mintun, M.A., Raichle, M.E., 2010. Regional aerobic glycolysis in the human brain. *Proceedings of the National Academy of Sciences* 107, 17757-17762.

Watts, D.J., Strogatz, S.H., 1998. Collective dynamics of 'small-world' networks. *Nature* 393, 440-442.

Wu, K. et al., 2011. The Overlapping Community Structure of Structural Brain Network in Young Healthy Individuals. *PLoS ONE* 6, e19608.

Zamora-López, G., Zhou, C., Kurths, J., 2010. Cortical hubs form a module for multisensory integration on top of the hierarchy of cortical networks. *Frontiers in Neuroinformatics* 4, 1.



Chapter 2

Mapping the wires of our brain:
Automated connectome reconstruction
using diffusion tractography

Abstract

The neural connections in our brain constitute the wiring of a complex network, known as the human connectome. Advances in magnetic resonance imaging techniques have made it possible to study the macroscale architecture of this fascinating network *in vivo* and within a single individual, catalyzing the adoption of connectomics for a wide variety of topics. Over the past years, connectome studies have provided insight into healthy brain organization, brain development and aging, and in brain alterations associated with neurological and neuropsychiatric disorders. This blossoming of connectomics goes hand in hand with an increasing demand for reconstruction of connectome maps, which is often considered to be a somewhat challenging task. To prevent connectome reconstruction from becoming a limiting factor and minimize the time needed for the preparation of new connectome maps, we developed special connectome reconstruction software, optimized to fabricate large amounts of high-quality connectome maps in a quick, consistent, and automated manner. In this chapter, we give an overview of the principles and techniques involved in this automated connectome reconstruction.

Introduction

In 1827, the botanist Robert Brown observed through his “simple microscope ... made ... by Mr. Dollond” that pollen grains immersed in water spontaneously moved around in a seemingly random fashion (Brown, 1829). Fascinated by the discovery of these “active molecules”, Brown extended his investigation to particles obtained from other materials (including gum resins, fossil wood, glass, rocks, and metals) and “inferred that these molecules were not limited to organic bodies, nor even to their products” (Brown, 1828). In hindsight, the abundance of materials comprising “active” particles makes perfect sense. In one of his seminal 1905 (*annus mirabilis*) papers, Albert Einstein namely demonstrated that the Brownian motion of particles suspended in water is not attributable to the suspended particles themselves, like Brown implicitly assumed, but instead results from the kinetic energy of the water molecules, which “bump” into the

suspended particles (Einstein, 1905). In other words, all (small) particles will display the seemingly random motion observed by Brown when suspended in water, even water molecules themselves. This self-diffusion of water molecules is the cornerstone of diffusion-weighted magnetic resonance imaging – a modern imaging technique allowing *in vivo* estimation of the brain's white matter fibers.

As will be more elaborately discussed in **chapter 3**, conventional (T1-weighted) magnetic resonance imaging (MRI) provides a clear contrast between the brain's gray and white matter and can be used to reconstruct the form and position of anatomically distinguishable *brain regions*; contiguous portions of gray matter whose boundaries are typically based on macroscale landmarks or transitions in microscale architecture as incorporated in a reference atlas. Rather than constituting independently operating components, these brain regions are tightly intertwined parts of a complex neural network, known as the macroscale connectome (Sporns et al., 2005). The large-scale bundles of nerve fibers which are situated in the white matter and form the connections of this neural network are, however, not deducible from conventional MRI scans, on which the white matter appears as a roughly homogeneous substance. This is where Brownian motion comes, quite literally, into the picture. As recognized by Denis Le Bihan, the finer architecture of apparently homogeneous tissues can namely be observed indirectly through the self-diffusion of water molecules, whose random movement is altered by the layout of the cells (Le Bihan, 2014; Le Bihan et al., 1986). In case of fibrous tissue such as the brain's white matter, movement perpendicular to the fibers tends to be impeded and diffusion is largest in the direction of the fibers (Figure 2.1a) (Moseley et al., 1990). Le Bihan and colleagues therefore proposed a new type of MRI scan able to measure local diffusion of water in all voxels (i.e., three-dimensional pixels) of an MRI volume; an approach that would become known as diffusion-weighted imaging (DWI).

Although the precise implementation of DWI is rather technical and has been subject to many improvements over the years, its key principle is quite intuitive (see Hagmann et al. (2006) for a review). First, hydrogen atoms are “labeled”

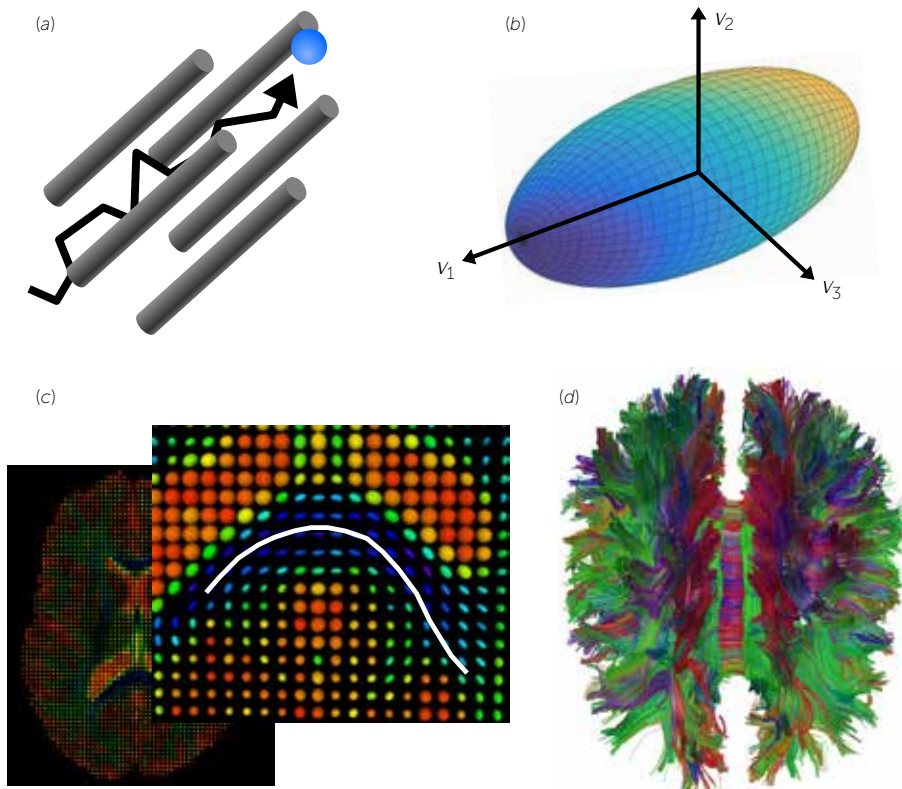


Figure 2.1. Estimating the course of white matter pathways using diffusion tractography. (a) In fibrous tissue such as the brain's white matter, a randomly moving water molecule (here depicted as a blue sphere) is hindered when moving perpendicular to the fibers, causing the net displacement of water molecules to be largest in the direction parallel to the fibers. (b) Assuming the self-diffusion of water to be Gaussian, local diffusion profiles can be characterized by a diffusion tensor, which can be visualized as an ellipsoid. The distance from the ellipsoid's center to a point on the surface is proportional to the root mean square displacement of water molecules in the direction of that point. (c) After a diffusion tensor has been fitted in every voxel (i.e., three-dimensional pixel) of the diffusion-weighted images, white matter fibers can be reconstructed by following the main diffusion axis (v_1 in panel b) from voxel to voxel. (d) Starting from evenly distributed seed points in the white matter, hundreds of thousands of so-called streamlines are formed using this tractography principle, providing an estimation of the brain's large-scale anatomical pathways.

The schematic illustration in panel a is based on a figure from Mori (2007).

according to their position along a chosen gradient axis by briefly creating a magnetic field whose strength deliberately varies along the gradient axis (called a gradient pulse), causing location-dependent phase shifts in the so-called spin of the hydrogen atoms. Then, after a short interval in which the hydrogen atoms

are allowed to diffuse, the same gradient pulse is applied a second time, but now in combination with a radio-frequency pulse which effectively reverses its phase shift effect (Stejskal and Tanner, 1965). The net phase shift after the two gradient pulses is therefore directly related to the movement of a hydrogen atom parallel to the gradient axis: if the atom did not move along the gradient axis, the two shifts are of equal magnitude but in opposite direction and cancel each other out, while any movement along the gradient axis results in a discrepancy proportional to that movement. Remaining phase shifts in turn influence (to be precise, decrease) the MR signal (Hahn, 1950), so that the measured signal intensity for each voxel can be related to the mean net displacement of local hydrogen atoms along the gradient axis (Hagmann et al., 2006).

In this chapter, we discuss how DWI allows us to estimate local fiber orientations and quality metrics and how this local information can be “knitted” together to reconstruct the wiring of the macroscale connectome. Since DWI-based connectome reconstruction is situated on the interface of several active fields of research, there tends to be a rich spectrum of approaches available for each individual processing step. Here, we follow the paradigm implemented in our recently developed connectome reconstruction software, optimized to fabricate large amounts of high-quality connectome maps in a quick, consistent, and automated manner.

Estimating the diffusion profile: diffusion tensor imaging

For the reconstruction of local diffusion profiles of water in the brain, it is not sufficient to obtain just a single diffusion-weighted MR scan. After all, as discussed in the introduction, a diffusion-weighted MR scan only provides information about the (rate of) diffusion in the direction parallel to the applied diffusion gradient. Full reconstruction of the so-called probability density function (PDF) for each voxel, constituting a complete probability map of where a water molecule departing from that voxel might end up, would therefore require the acquisition of very many, theoretically even infinite, diffusion-weighted scans (each using

a different gradient). Although it is in practice possible to reduce the number of scans necessary to about a couple of hundred (for instance, using diffusion spectrum imaging (Wedeen et al., 2005)), the time needed to reconstruct PDF's "from scratch" remains substantial. As an alternative to starting from scratch, further reductions in the number of required measurements could be achieved by adding *a priori* information about what the PDF might look like. Indeed, in line with Einstein's calculations predicting simple Brownian motion to be Gaussian (Einstein, 1905), Peter Basser and Denis Le Bihan showed that if one adopts a Gaussian model for self-diffusion of water in the brain, the diffusion profile can be reconstructed using only six diffusion-weighted and one diffusion-unweighted scan (Basser et al., 1994a); a set obtainable in just a few minutes. Because the Gaussian assumption implies that diffusion can be fully characterized by a so-called tensor (represented by a symmetric 3×3 matrix), this approach is known as *diffusion tensor imaging*.

Fitting the diffusion tensor

The key objective when processing diffusion tensor imaging (DTI) data is to obtain an estimate for the diffusion tensor in every voxel of the acquired brain images. As DTI has been around for over two decades now, the procedures for fitting the diffusion tensor have had ample time to mature, culminating in a reliable algorithm with a high level of robustness against measurement errors. Below, we first discuss two basic approaches, followed by the robust tensor fitting algorithm for which they form the ingredients.

Linear fit

Under the assumption of Gaussian diffusion, the relationship between the signal intensity S_k appearing in a diffusion-weighted image and the signal intensity S_0 appearing in a diffusion-unweighted image is given by (a form of) the Stejskal-Tanner equation (Stejskal and Tanner, 1965):

$$\frac{S_k}{S_0} = \exp(-bg_k^t Dg_k). \quad (2.1)$$

In this equation, D denotes the diffusion tensor, g_k is a unit vector pointing in the direction of the applied diffusion gradient, and b is the so-called b -value, a combined factor comprising some physical constants and imaging parameters which together determine the "amount of diffusion-weighting". Since the 3×3 matrix which represents the diffusion tensor is symmetric, there are just six unique coefficients which have to be determined. Collecting these coefficients in a vector $d = (D_{xx}, D_{yy}, D_{zz}, D_{xy}, D_{xz}, D_{yz})^t$ and forming another vector $H_k = b(g_{kx}, g_{ky}, g_{kz}, 2g_{kx}g_{ky}, 2g_{kx}g_{kz}, 2g_{ky}g_{kz})$ using the components of g_k , the argument of the exponential in formula (2.1) can be rewritten as

$$-bg_k^t D g_k = -H_k d. \quad (2.2)$$

So, if multiple diffusion-weighted measurements S_1, S_2, \dots, S_n are combined in a vector S and their associated H_k vectors are merged to a matrix H (having H_k as its k th row), taking the logarithm over equation (2.1) shows

$$\log\left(\frac{S}{S_0}\right) = -Hd, \quad (2.3)$$

where the logarithm is understood to act on each vector component separately (Kingsley, 2006). Formula (2.3) reduces the problem of finding the diffusion tensor D to a system of linear equations, which can be solved using standard methods if there are at least six diffusion-weighted measurements obtained with sufficiently different gradients (such that the rows of H are linearly independent). With exactly six measurements, H is invertible and there is a unique solution d that satisfies equation (2.3). In case of more than six measurements, there generally does not exist a vector d that exactly satisfies equation (2.3). Instead, applying the pseudoinverse of H provides the tensor components which best explain the measurements in the usual least-squares sense.

Although six diffusion-weighted measurements are in principle sufficient to determine D , the inevitable occurrence of measurement errors makes it generally preferable to perform more measurements. After all, with just six measurements, the diffusion tensor D is uniquely and directly determined by the measurements,

including their errors, while the addition of extra data points in combination with a least-squares approach potentially provides some robustness against the influence of errors. In the standard (unweighted) least-squares procedure described above, based on the application of the pseudoinverse of H to $\log(S/S_0)$, the same weight is assigned to each data point $\log(S_k/S_0)$. However, it has been pointed out that if the original measurements S_k are assumed to be equally reliable, the reliability (and hence weight) of $\log(S_k/S_0)$ should be taken to be proportional to S_k (Basser et al., 1994b; Kingsley, 2006). This so-called weighted least-squares fit is established by introducing a diagonal matrix $W^{1/2}$ with the signal intensities S_k on the diagonal to both sides of equation (2.3), giving

$$W^{\frac{1}{2}} \log\left(\frac{S}{S_0}\right) = -W^{\frac{1}{2}} H d, \quad (2.4)$$

and instead computing the least-squares solution to this system of linear equations (i.e., by applying the pseudoinverse of $W^{1/2} H$ to $W^{1/2} \log(S/S_0)$).

Non-linear fit

Even with adjusted weights, approximating the diffusion tensor on the basis of a linear fit is not ideal (Kingsley, 2006). This is because the linear fitting procedures approximate $\log(S/S_0)$ instead of S/S_0 and thus evaluate the goodness of fit in terms of the squared distances $(\log(S_k/S_0) - \hat{g}_k)^2$ between the predicted values \hat{g}_k and the logarithm of the observed values S_k/S_0 . The problem here is that if two proposed predictions are equally good in terms of their distance to $\log(S_k/S_0)$, there associated predictions for S_k/S_0 are generally not equally good. Indeed, as nicely illustrated by Kingsley (2006), if $S_k/S_0 = 1/10$, then $\log(1/5)$ and $\log(1/20)$ are equally good predictions for $\log(S_k/S_0)$, while S_k/S_0 and $1/5$ are twice as far apart as S_k/S_0 and $1/20$.

Better results may therefore be obtained by using an iterative, non-linear approach to find tensor components, as collected in the vector d , that (approximately) minimize

$$\chi^2 = \sum_{k=1}^n w_k \left(\frac{S_k}{S_0} - \exp(-H_k d) \right)^2, \quad (2.5)$$

where the term w_k allows the use of custom weighting factors. An algorithm commonly employed to perform this non-linear fit is the Levenberg-Marquardt (LM) method, which is a standard method to solve non-linear least-squares problems. In the general context in which a function $\hat{y}(x; p)$ should be fitted to measurements $y_1(x_1), y_2(x_2), \dots, y_n(x_n)$ to determine the parameters p of \hat{y} , the LM method iteratively updates – depending on some conditions – the parameters p to $p + \delta_p$, with δ_p given by Marquardt's update rule (Marquardt, 1963):

$$J^t W J + \lambda \text{diag}(J^t W J) \delta_p = J^t (y - \hat{y}). \quad (2.6)$$

In this equation, W is a diagonal matrix with weighting factors w_k on the diagonal, \hat{y} is interpreted as a vector-valued function $\hat{y}(p) = (\hat{y}(x_1; p), \hat{y}(x_2; p), \dots, \hat{y}(x_n; p))^t$ and $J = \partial \hat{y} / \partial p$ is the Jacobian matrix, measuring “the local sensitivity of the function \hat{y} to variation in the parameters p ” (Gavin, 2011). Furthermore, λ is an algorithmic, self-updating parameter reflecting the core idea behind the LM approach, namely to use the gradient descent method to update the parameters when still far from a suitable solution (corresponding to large values for λ) and to use the Gauss-Newton method when the parameters approach a minimum (corresponding to small values for λ). An excellent overview of the LM method, including MATLAB code, is provided by Gavin (2011) in a privately published paper.

Since standard implementations of the LM method do not assume any knowledge about the model function \hat{y} , the Jacobian J is usually numerically approximated. However, when applying LM to fit the diffusion tensor, it is possible to compute the required derivatives analytically. In this case, the vector-valued function $\hat{y}(p)$ is equal to $\exp(-Hd)$, with the components of d serving as fitting parameters p (note that the exponent is understood to act component-wise). Using standard calculus, it then follows that

$$J = -\text{diag}(\exp(-Hd))H, \quad (2.7)$$

which can be very efficiently computed from the matrix H , supplied as input for the algorithm, and the already evaluated $\hat{y} = \exp(-Hd)$. Considering that the Jacobian has to be computed many times during a single non-linear fit, that many non-linear fits are performed for each voxel (see next section), and that there are many voxels, using this analytic expression for the Jacobian instead of numerical approximation may result in substantial reductions in computational time.

Robust tensor estimation

The acquisition of more than six diffusion-weighted measurements in combination with a (linear or non-linear) least-squares fit already provides some robustness against the influence of measurement errors. However, some measurements may include much larger errors than others – for instance due to sudden subject motion during the measurement – and the presence of such outliers will have a large influence on the fit, which is basically dragged towards the outliers and therefore becomes less accurate with respect to the measurements with “regular” error levels. In order to make tensor estimation more robust to deviating measurements, Chang et al. (2005) proposed the *Robust Estimation of Tensors by Outlier Rejection* (RESTORE) method. The idea behind this method is to identify outliers on the basis of non-linear least-squares fits with iteratively adjusted weights and to remove these outliers before performing a final tensor fit. Complementing the original RESTORE approach with elements based on a later update (Chang et al., 2012), we arrived at an implementation of the algorithm which – except for some practical modifications – closely follows “the RESTORE algorithm with added constraints” as described by Chang et al. (2012).

The implemented procedure starts with a weighted linear least-squares fit, the output of which is used as the starting point for a non-linear least-squares fit with constant weights. It is then checked using a robust median absolute deviation (MAD) estimate of the variability

$$\sigma = \sqrt{\frac{n}{n-6} \text{median}_i(|r_i - \text{median}_j r_j|)} \quad (2.8)$$

whether any of the residuals r_1, r_2, \dots, r_n give reason to believe that there might be outlying measurements (being poorly explained by the initial fit, implemented as $|r_i| \geq 3\sigma$). If so, the non-linear fit is iteratively repeated with the previous estimate as starting point and custom weighting factors set to $w_i = 1/(r_i^2 + C^2)$, with

$$C = 1.4826 \text{median}_i(|r_i - \text{median}_j r_j|). \quad (2.9)$$

Because the weighting factors are inversely related to the residuals of the previous fit, the influence of outlying measurements is effectively reduced during the iterations and the fitting procedure gets more and more focused on properly explaining the regular measurements. As soon as the tensor estimates become stable (percentage change of all components < 0.1%) or the number of iterations has reached a maximum (set to 400), the iterative fitting is ended and the same procedure as before is used to determine whether there are any outliers with respect to the obtained fit (i.e., satisfying $|r_i| \geq 3\sigma$, with σ computed as in equation (2.8)). If the set of measurements is still sufficiently representative after removing the identified outliers (see next paragraph), a final non-linear tensor fit with constant weights is performed on the basis of just the non-outlying measurements, resulting in an estimate for the diffusion tensor which is robust to the presence of outliers.

Checking whether the non-outlying measurements are sufficiently representative is necessary to avoid poor combinations of diffusion gradients, not providing enough information to get reliable tensor estimates (Chang et al., 2012) – a case in which it is preferable to use all measurements (including outliers) for the estimation. The suitability of the set of diffusion gradients corresponding to non-outlying measurements is evaluated using two criteria which must both be met. The first criterion is that the so-called condition number of the matrix H introduced in equation (2.3) is smaller than a certain threshold t_c after eliminating all rows corresponding to outlying measurements. Roughly speaking, this con-

dition number measures the sensitivity of the linear least-squares estimate of the diffusion tensor to measurement errors, with large condition numbers indicating that small changes in the measurements may lead to large changes in the estimate. For the second criterion, the variation in the average projection scores p_1, p_2, \dots, p_n of the original normalized gradient vectors on the set of remaining gradients after outlier removal is asserted:

$$p_i = \frac{1}{|R|} \sum_{j \in R} |g_i \cdot g_j|, \quad (2.10)$$

with R representing the set of indices of non-outlying measurements. If the variation across projection scores is small, all original gradients are roughly equally “surrounded” by remaining gradients, implying that a directionally balanced set of gradients remains after outlier removal. This is implemented by requiring that the coefficient of variation $\text{std}(p)/\text{mean}(p)$ must be smaller than a certain threshold t_d .

The achievable values for the condition number and projection variation largely depend on the set of original gradient vectors used to acquire the data, something which should be kept in mind when choosing the thresholds t_c and t_d . Reference distributions for these values can be obtained by considering bootstrap samples in which a fixed random percentage of the gradient vectors has been removed. We found that, in practice, good results are typically achieved by choosing the thresholds such that about 75% of the random samples with 5% of the gradients removed and about 25% of the random samples with 50% of the gradients removed pass the criteria (allowing some, but not too much, measurements to be labeled as outliers), which is a rule of thumb that can easily be automated for autonomous threshold selection.

Interpreting the diffusion tensor

Once a diffusion tensor D has been estimated for all (relevant) voxels, the applicable information for white matter fiber reconstruction can be extracted. This information is derived from the eigenvalue decomposition of the 3×3 matrix

representing the tensor, resulting in three eigenvectors v_1 , v_2 , v_3 and their associated eigenvalues λ_1 , λ_2 , λ_3 . These eigenvectors and eigenvalues respectively represent the principal axes of diffusion and the diffusivity along these axes. Although the laws of nature dictate the diffusivities (and hence eigenvalues) to be non-negative, there is no such constraint in the above-described fitting procedures, meaning that measurement noise may cause negative eigenvalues to occur (note, however, that the matrix D is symmetric by construction, so the eigenvalues λ_1 , λ_2 , λ_3 are automatically real). To reduce the effects of these putative errors on the tensor-derived quantities discussed below, any negative eigenvalues are replaced by zeros (Koay et al., 2006). Having only non-negative eigenvalues, the diffusion tensor can be visualized as an ellipsoid, with the principal axes of the ellipsoid spanning the same lines as the individual eigenvectors and the length of the principal axes proportional to the square root of the eigenvalues (Figure 2.1b). The distance from the center of this ellipsoid to a point on the surface is then proportional to the root mean square displacement of water molecules in the direction of that point, so that the ellipsoid gives a visual impression of the diffusion profile.

The most important piece of information that can be derived from the diffusion tensor is the axis along which local water molecules show the largest displacement. As first noticed by Moseley et al. (1990), this main diffusion axis tends to align with the white matter fibers in the examined voxel, constituting the key ingredient for their reconstruction. Using the eigenvalue decomposition of the tensor D , the main diffusion axis is simply given by the eigenvector corresponding to the largest eigenvalue (representing the diffusivity along the eigenvector axis). It should be noted that the length and sign (i.e., considering v or $-v$) of the eigenvector are irrelevant, both from a mathematical and physical perspective. Indeed, diffusion-weighted measurements only provide information about the extent of diffusion along a certain axis, not about the direction of diffusion along that axis. Moreover, there is currently no indication that the direction in which water molecules diffuse along the main axis would provide any additional information about, for instance, the direction in which neural signals travel along the

white matter fibers. In the ellipsoid representation of the diffusion tensor, the main diffusion axis is easily identified as the axis along which the ellipsoid is most strongly elongated.

Complementing the main diffusion axis, there are several commonly used metrics that quantify the size and shape of the diffusion ellipsoid, the latter of which can basically vary from a sphere to a thin cigar-shaped ellipsoid. The "pointedness" of the diffusion ellipsoid is measured by the *fractional anisotropy* (FA)

$$\text{FA} = \sqrt{\frac{1}{2} \frac{\sqrt{(\lambda_1 - \lambda_2)^2 + (\lambda_2 - \lambda_3)^2 + (\lambda_3 - \lambda_1)^2}}{\sqrt{\lambda_1^2 + \lambda_2^2 + \lambda_3^2}}} = \sqrt{\frac{3}{2} \frac{\text{std}(\lambda)}{\text{rms}(\lambda)}}, \quad (2.11)$$

quantifying the extent to which the diffusion is anisotropic (i.e., different for different directions) (Basser and Pierpaoli, 2011). An FA value of 0 indicates that the diffusion in the examined voxel is completely isotropic, corresponding to a spherical ellipsoid, while an FA value of 1 indicates that the diffusion is completely restricted to the main diffusion axis. Other tensor-derived metrics include: *axial diffusivity* (AD), measuring the diffusivity along the main diffusion axis as given by the largest eigenvalue; *radial diffusivity* (RD), assessing the diffusivity perpendicular to the main diffusion axis as the average of the two smallest eigenvalues; and *mean diffusivity* (MD), given by the average over all three eigenvalues and thus providing an estimate for the total level of diffusion. Although the exact relationship between these diffusion tensor-derived measures and the micro-structural architecture of the underlying tissue is not yet completely understood (Beaulieu, 2002), evidence so far tends to suggest that (changes in) FA and AD are positively, and (changes in) RD and MD are negatively related to (changes in) the myelination level, axonal density, and axonal diameter of the white matter fibers in a voxel (Budde et al., 2007; Kochunov et al., 2012; Mädler et al., 2008; Song et al., 2003; Song et al., 2005). As a result, the described measures have become popular *in vivo* estimates for the white matter integrity or "quality" of these fibers (Collin et al., 2014; Gong et al., 2011; Hagmann et al., 2010; Madden et al., 2012; Marsteller et al., 2015; Verstraete et al., 2011).

Distortion correction and parcellation

In the preceding overview of the techniques and concepts involved in determining and interpreting the diffusion tensor, we have conveniently skipped some steps that, in our connectome reconstruction framework, are actually performed before the whole tensor-fitting machinery is put to work. The reason for not elaborately discussing these “preprocessing” steps is that they all involve their own particular area of expertise and are therefore carried out using specialized third-party software. Furthermore, it typically depends on the available data which steps are appropriate, making it difficult to present a general “recipe”.

First, there is the issue of correcting the acquired DWI data. Inhomogeneities in the main magnetic field of the MRI scanner due to so-called eddy currents (electric currents in the scanner coils induced by the diffusion gradients) and variations in magnetic susceptibility (for instance, between air and brain tissue) cause geometric distortions in the diffusion-weighted images produced by the scanner (Andersson and Skare, 2002; Andersson et al., 2003). In addition, distortions may also arise as a consequence of subject movement. The FMRIB Software Library (FSL) (Jenkinson et al., 2012) features several tools to correct for such distortions, which are most effective if an additional DTI set was obtained with reversed k -space readout (basically resulting in opposite susceptibility distortions) (Andersson et al., 2003).

Second, successful connectome reconstruction requires identification of different tissue classes and brain regions. Although this information could be added during later stages of the reconstruction process, it is most convenient to have it available from the start, allowing, for instance, to restrict the estimation of diffusion tensors to voxels comprising brain tissue. As will be further discussed in **chapter 3**, delineation of tissues and brain regions is usually carried out on the basis of a separate T1-weighted MRI scan. For each voxel of this T1-weighted scan, it should then be determined whether the voxel is part of the brain and, if so, to which tissue class or brain region it belongs. A particularly nice way to accomplish this is given by the FreeSurfer software suite, which provides a fully

automated segmentation and parcellation procedure involving a reconstruction of the cortical surface and surface-based registration methods which take local shape features such as cortical folding into account (Fischl et al., 2004). By registering the T1-weighted scan to the unweighted (i.e., $b = 0$) scan of the DWI set, the segmentation and parcellation results can be translated to diffusion space and used in subsequent processing steps. For the remainder of the chapter, we assume that such a procedure has been carried out and that all voxels of the DWI volumes have been labeled according to their tissue class or brain region.

Tracking of white matter fibers

Having established the main diffusion axis for each voxel, the brain's white matter fibers can be reconstructed by "knitting" the local information from individual voxels together; a procedure more formally known as *fiber tracking*. The idea behind fiber tracking is relatively straightforward. Since the main diffusion axes of voxels along the course of a large-scale bundle of nerve fibers will align with the bundle, the presence of such a bundle is expressed through sequences of neighboring voxels whose main diffusion axes are more or less attuned to each other. Proposed by Mori et al. (1999) as *fiber assignment by continuous tracking* (FACT), white matter fibers can therefore be reconstructed by following the main diffusion axis from voxel to voxel (Figure 2.1c).

First, at a chosen seed point, a *streamline* is initiated and this streamline is propagated in one direction along the main diffusion axis of the voxel containing the seed. Each time the tip of the streamline enters a new voxel, the direction in which it is propagated is updated to match the main diffusion axis of the newly entered voxel. This process continues until one of the *stopping criteria* is matched. To prevent biologically unrealistic fibers, streamline propagation is terminated if the newly entered voxel was not classified as brain tissue by the segmentation and parcellation procedure or if the diffusion profile of the newly entered voxel is not clearly elongated around the main axis (usually implemented by $FA < 0.1$), reflecting the absence of a dominant diffusion direction

and often indicating that the gray matter has been reached. Moreover, because the trajectories of large-scale white matter fibers are believed to be relatively smooth, streamline propagation is also terminated if the angle between the tip of the streamline and the main diffusion axis of the newly entered voxel is larger than a certain threshold (usually 45°), preventing streamlines to cross over from one bundle of nerve fibers to another. Second, going back to the seed point, the same procedure is used to propagate the streamline in the direction opposite to the initial extension, so that the streamline is extended in both ways along the main diffusion axis of the voxel containing the seed (appearing to run through the seed point, instead of emerging from it). In practice, it is easy to carry out the propagation from the seed in the “forward” and “backward” direction and the propagation of streamlines initiated from other seed points in parallel, making the tracking procedure very efficient. Because the trajectories of the streamlines are completely determined by the fitted diffusion tensors and chosen seeds points (e.g., placing one or more evenly distributed seeds in each voxel of the white matter), FACT is an example of *deterministic* fiber tracking.

Connectome reconstruction

In its simplest form, a macroscale connectome map lists for every pair of brain regions whether or not these brain region are connected. Combining the output of the segmentation and parcellation procedure with the output of the tracking procedure, such a map can be established by declaring two brain regions i and j connected if there exists a reconstructed fiber streamline that touches both a voxel from region i and a voxel from region j . However, in many connectome analyses, especially those involving comparisons between two or more groups of subjects, it is desirable to not only have information about the presence of connections, but also about the strength and quality of connections. Such information can be stored in a multi-weighted connectivity matrix; a three-dimensional matrix W , with information about a connection between brain region i and j placed in row i and column j of the “layers”, each layer containing data on one connection characteristic. Commonly used connection characteristics include: (1) the number of streamlines (NOS) interconnecting two brain regions,

(2) the average length of all interconnecting streamlines, (3-6) the average FA/AD/RD/MD of all interconnecting streamlines, and (7-8) the surface or volume density of the interconnecting streamlines (i.e., the number of streamlines per unit area or per unit volume).

A convenient practical recipe to obtain a multi-weighted connectivity matrix W comprising these characteristics is to start out with a three-dimensional matrix filled with zeros and to add information from one streamline at a time. For each streamline, it is first established which brain regions are touched by the streamline. Next, for each pair of touched regions i and j , the corresponding NOS entry of W is increased with one and the corresponding projection length entry of W is increased with the length of the shortest portion of the streamline that spans between a voxel from region i and a voxel from region j . The average FA/AD/RD/MD values are computed over the same portion of the streamline by taking the weighted average over the FA/AD/RD/MD values of all voxels touched by the portion, excluding the first and last (that is, the voxels from brain region i and j) and using the length of the streamline within each voxel as weight. Also these average FA/AD/RD/MD values are added to the corresponding entries of the multi-weighted connectivity matrix. Optionally, all contributions of the streamline portion between region i and j can be canceled if the length of the portion does not exceed an *a priori* set minimum fiber length threshold. After all streamlines have been processed in this fashion, all layers of W – except for the NOS layer itself – are divided by the NOS layer to turn the sums created by constantly adding values into averages. Finally, using information about the surface area (for cortical regions only) and volume of the brain regions as given by the segmentation and parcellation procedure, a streamline surface and volume density layer can be added to W by dividing the entries of the NOS layer by, respectively, the average surface area or the average volume of the endpoints of each connection (Hagmann et al., 2008).

Discussion

In this chapter, we have given a detailed overview of the processing steps involved in reconstructing the macroscale human connectome from a suitable set of magnetic resonance images. The resulting connectome map is given by a multi-weighted connectivity matrix, containing information about the presence (expressed through $NOS \geq 1$) and length of connections between brain regions, as well as information related to the strength and quality of connections. Except for some preprocessing steps that may need to be adjusted to the protocols used to acquire the MR images, the reconstruction procedure for macroscale connectome maps presented here is completely generic, forming the basis for the fast and standardized connectome mapping offered by our connectome reconstruction software (Baggio et al., 2015; Mallio et al., 2015; Marqués-Iturria et al., 2015; Peper et al., 2015).

Although it is safe to say that the techniques and methods reviewed here have revolutionized human (structural) connectomics, they are unfortunately not perfect. Reconstruction of white matter fibers via diffusion-weighted imaging is based on indirect measurements, inferring the course of white matter pathways from the movement of water molecules rather than revealing them directly. As nicely reviewed by Jbabdi and Johansen-Berg (2011), it has been noted that several problems may occur because of this indirect assessment. From a connectome perspective, such problems can essentially lead to three types of inaccuracies: placement of edges between brain regions which are not anatomically connected (false positives), absence of edges between brain regions which are in fact linked by a white matter pathway (false negatives, also see **chapter 4**), and inaccurate strength or quality estimates. In relation to the last type of inaccuracies, it has, for instance, been remarked that the number of reconstructed streamlines between two brain regions is methodologically influenced by the length of the interconnecting white matter fibers in at least two different ways. On the one hand, if streamline seeds are uniformly distributed over all white matter voxels, there will be generally more streamline seeds on the track of longer pathways and all those seeds have the potential of becoming interconnecting

streamlines (Hagmann et al., 2008). On the other hand, streamlines following longer pathways have a larger probability of encountering a noisy or otherwise problematic voxel (see below) and are therefore more likely to be terminated before reaching the gray matter (van den Heuvel et al., 2012; Johansen-Berg and Rushworth, 2009; Jones, 2010).

Another potential source of inaccuracies is the presence of *crossing fibers* in the brain. While the diffusion tensor formalism assumes that there is always at most one axis along which the diffusion of water molecules “peaks”, there are certain locations in the brain where two or more bundles of nerve fibers may cross or run closely past each other (Wiegell et al., 2000), resulting in voxels whose diffusion profile cannot be accurately described by a tensor. A possible solution to allow the recovery of multiple diffusion peaks per voxel, and thus the reconstruction of crossing fibers, is to fit more complex models (Tournier et al., 2007; Tuch et al., 2002) to the diffusion-weighted measurements or to use model-free approaches (Descoteaux et al., 2011; Tuch, 2004; Wedeen et al., 2005; Yeh et al., 2010). However, to function properly, these methods typically need many more, and sometimes also different (e.g., requiring multiple b -values), diffusion-weighted measurements than DTI, making them unsuitable for studies involving already existing DTI datasets or for (clinical) studies in which the allowable scan duration or choice of scan protocol is limited. In such cases, compressed sensing approaches like CFARI may be promising (Landman et al., 2012), allowing the recovery of multiple diffusion peaks per voxel using standard DTI measurements by assuming that these measurements may be described by a sparse collection of fixed-shaped tensors (with each tensor reflecting a major diffusion axis). Other possible solutions include the use of global or probabilistic fiber tracking techniques (Aganj et al., 2011; Behrens et al., 2003; Jones and Pierpaoli, 2005; Reisert et al., 2011), basically allowing reconstructed fibers to locally deviate from the path prescribed by the fitted diffusion tensors and therefore to “jump” over voxels with incompatible main diffusion axes.

Even though we have implemented some approaches that allow the reconstruc-

tion of crossing fibers in our connectome reconstruction software, we believe that – considering the almost continuous stream of proposals for new methods or improvements – there is also a strong case to make for the continued use of methods that have been around for a long time and whose strengths and weaknesses are well-known, creating a more stable and standardized framework for connectome reconstruction. As underscored by their use in many successful connectome studies, methods such as diffusion tensor imaging and deterministic tractography are still very suitable for connectome investigation, having the additional advantage of being considerably faster and relatively simpler than most more recently proposed methods. Indeed, in a recent review of literature on structural connectomics in brain diseases, Griffa et al. (2013) note that "currently DTI and deterministic streamline tractography are by far the most widely applied methods in clinical research, mainly for their simplicity, robustness and speed". Interestingly, validation studies comparing diffusion tractography results in the macaque brain with gold-standard neuronal tract-tracing findings have reported substantial, but certainly not perfect, overlap between the two techniques, both for simple deterministic (Dauguet et al., 2007; van den Heuvel et al., 2015) and super high-resolution probabilistic approaches (Azadbakht et al., 2015). Although large differences in study design make it difficult to compare the level of observed overlap between these studies, the reported overlap scores at least appear to be in the same ballpark and future studies providing more direct comparisons of different diffusion tractography approaches in relation to tract-tracing results would be of high relevance. Finally, coming back to the methodological influences of fiber length on the number of reconstructed streamlines between two brain regions, one of the validation studies found a reassuring significant positive relationship between NOS and connectivity strength derived from tract-tracing data (van den Heuvel et al., 2015), providing support for the common interpretation of NOS as an *in vivo* estimate of connectivity strength – all ultimately made possible by the curiosity of Robert Brown and his "simple microscope ... made ... by Mr. Dollond" (Brown, 1829).

References

- Aganj, I., Lenglet, C., Jahanshad, N., Yacoub, E., Harrel, N., Thompson, P.M., Sapiro, G., 2011. A Hough transform global probabilistic approach to multiple-subject diffusion MRI tractography. *Medical Image Analysis* 15, 414-425.
- Andersson, J.L.R., Skare, S., 2002. A Model-Based Method for Retrospective Correction of Geometric Distortions in Diffusion-Weighted EPI. *NeuroImage* 16, 177-199.
- Andersson, J.L.R., Skare, S., Ashburner, J., 2003. How to correct susceptibility distortions in spin-echo echo-planar images: application to diffusion tensor imaging. *NeuroImage* 20, 870-888.
- Azadbaht, H., Parkes, L.M., Haroon, H.A., Augath, M., Logothetis, N.K., de Crespigny, A., D'Arceuil, H.E., Parker, G.J.M., 2015. Validation of High-Resolution Tractography Against In Vivo Tracing in the Macaque Visual Cortex. *Cerebral Cortex*, epub ahead of print.
- Baggio, H.C., Segura, B., Junque, C., de Reus, M.A., Sala-Llonch, R., Van den Heuvel, M.P., 2015. Rich Club Organization and Cognitive Performance in Healthy Older Participants. *Journal of Cognitive Neuroscience*, epub ahead of print.
- Basser, P.J., Mattiello, J., LeBihan, D., 1994b. Estimation of the Effective Self-Diffusion Tensor from the NMR Spin Echo. *Journal of Magnetic Resonance, Series B* 103, 247-254.
- Basser, P.J., Mattiello, J., LeBihan, D., 1994a. MR diffusion tensor spectroscopy and imaging. *Biophysical Journal* 66, 259-267.
- Basser, P.J., Pierpaoli, C., 2011. Microstructural and physiological features of tissues elucidated by quantitative-diffusion-tensor MRI. *Journal of Magnetic Resonance* 213, 560-570.
- Beaulieu, C., 2002. The basis of anisotropic water diffusion in the nervous system – a technical review. *NMR in Biomedicine* 15, 435-455.
- Behrens, T.E.J., Woolrich, M.W., Jenkinson, M., Johansen-Berg, H., Nunes, R.G., Clare, S., Matthews, P.M., Brady, J.M., Smith, S.M., 2003. Characterization and propagation of uncertainty in diffusion-weighted MR imaging. *Magnetic Resonance in Medicine* 50, 1077-1088.
- Brown, R., 1828. On the particles contained in the pollen of plants; and on the general existence of active molecules in organic and inorganic bodies. *Edinburgh New Philosophical Journal* 5, 358-371.
- Brown, R., 1829. XXIV. Additional remarks on active molecules. *The Philosophical Magazine, or Annals of Chemistry, Mathematics, Astronomy, Natural History, and General Science* 6, 161-166.
- Budde, M.D., Kim, J.H., Liang, H.F., Schmidt, R.E., Russell, J.H., Cross, A.H., Song, S.K., 2007. Toward accurate diagnosis of white matter pathology using diffusion tensor imaging. *Magnetic Resonance in Medicine* 57, 688-695.
- Chang, L.C., Jones, D.K., Pierpaoli, C., 2005. RESTORE: Robust estimation of tensors by outlier rejection. *Magnetic Resonance in Medicine* 53, 1088-1095.
- Chang, L.C., Walker, L., Pierpaoli, C., 2012. Informed RESTORE: A method for robust estimation of diffusion tensor from low redundancy datasets in the presence of physiological noise artifacts. *Magnetic Resonance in Medicine* 68, 1654-1663.
- Collin, G., Sporns, O., Mandl, R.C.W., van den Heuvel, M.P., 2014. Structural and Functional Aspects Relating to Cost and Benefit of Rich Club Organization in the Human Cerebral Cortex. *Cerebral Cortex* 24, 2258-2267.
- Dauguet, J., Peled, S., Beregovskii, V., Delzescaux, T., Warfield, S.K., Born, R., Westin, C.F., 2007. Comparison of fiber tracts derived from in-vivo DTI tractography with 3D histological neural tract tracer reconstruction on a macaque brain. *NeuroImage* 37, 530-538.
- Descoteaux, M., Deriche, R., Le Bihan, D., Mangin, J.F., Poupon, C., 2011. Multiple q-shell diffusion propagator imaging. *Medical Image Analysis* 15, 603-621.
- Einstein, A., 1905. Über die von der molekularkinetischen Theorie der Wärme geforderte Bewegung von in ruhenden Flüssigkeiten suspendierten Teilchen. *Annales de Physique* 322, 549-560.
- Fischl, B. et al., 2004. Automatically Parcellating the Human Cerebral Cortex. *Cerebral Cortex* 14, 11-22.
- Gavin, H., 2011. The Levenberg-Marquardt method for nonlinear least squares curve-fitting problems. Unpublished. Source: <http://people.duke.edu/~hp-gavin/ce281/lm.pdf>.
- Gong, G., He, Y., Evans, A.C., 2011. Brain Connectivity: Gender Makes a Difference. *The Neuroscientist* 17, 575-591.

- Griffa, A., Baumann, P.S., Thiran, J.P., Hagmann, P., 2013. Structural connectomics in brain diseases. *NeuroImage* 80, 515-526.
- Hagmann, P., Cammoun, L., Gigandet, X., Meuli, R., Honey, C.J., Wedeen, V.J., Sporns, O., 2008. Mapping the Structural Core of Human Cerebral Cortex. *PLoS Biology* 6, e159.
- Hagmann, P., Jonasson, L., Maeder, P., Thiran, J.P., Wedeen, V.J., Meuli, R., 2006. Understanding Diffusion MR Imaging Techniques: From Scalar Diffusion-weighted Imaging to Diffusion Tensor Imaging and Beyond. *Radiographics* 26, S205-S223.
- Hagmann, P., Sporns, O., Madan, N., Cammoun, L., Pienaar, R., Wedeen, V.J., Meuli, R., Thiran, J.P., Grant, P.E., 2010. White matter maturation reshapes structural connectivity in the late developing human brain. *Proceedings of the National Academy of Sciences* 107, 19067-19072.
- Hahn, E.L., 1950. Spin Echoes. *Physical Review* 80, 580-594.
- van den Heuvel, M.P., Kahn, R.S., Goñi, J., Sporns, O., 2012. High-cost, high-capacity backbone for global brain communication. *Proceedings of the National Academy of Sciences* 109, 11372-11377.
- van den Heuvel, M.P., de Reus, M.A., Barrett, L.F., Scholtens, L.H., Coopmans, F.M.T., Schmidt, R., Preuss, T.M., Rilling, J.K., Li, L., 2015. Comparison of diffusion tractography and tract-tracing measures of connectivity strength in rhesus macaque connectome. *Human Brain Mapping*, epub ahead of print.
- Jbabdi, S., Johansen-Berg, H., 2011. Tractography: Where Do We Go from Here? *Brain Connectivity* 1, 169-183.
- Jenkinson, M., Beckmann, C.F., Behrens, T.E.J., Woolrich, M.W., Smith, S.M., 2012. FSL. *NeuroImage* 62, 782-790.
- Johansen-Berg, H., Rushworth, M.F.S., 2009. Using Diffusion Imaging to Study Human Connectional Anatomy. *Annual Review of Neuroscience* 32, 75-94.
- Jones, D.K., 2010. Challenges and limitations of quantifying brain connectivity *in vivo* with diffusion MRI. *Imaging in Medicine* 2, 341-355.
- Jones, D.K., Pierpaoli, C., 2005. Confidence mapping in diffusion tensor magnetic resonance imaging tractography using a bootstrap approach. *Magnetic Resonance in Medicine* 53, 1143-1149.
- Kingsley, P.B., 2006. Introduction to diffusion tensor imaging mathematics: Part III. Tensor calculation, noise, simulations, and optimization. *Concepts in Magnetic Resonance* 28A, 155-179.
- Koay, C.G., Carew, J.D., Alexander, A.L., Basser, P.J., Meyerand, M.E., 2006. Investigation of anomalous estimates of tensor-derived quantities in diffusion tensor imaging. *Magnetic Resonance in Medicine* 55, 930-936.
- Kochunov, P., Williamson, D.E., Lancaster, J., Fox, P., Cornell, J., Blangero, J., Glahn, D.C., 2012. Fractional anisotropy of water diffusion in cerebral white matter across the lifespan. *Neurobiology of Aging* 33, 9-20.
- Landman, B.A., Bogovic, J.A., Wan, H., ElShahaby, F.E.Z., Bazin, P.L., Prince, J.L., 2012. Resolution of crossing fibers with constrained compressed sensing using diffusion tensor MRI. *NeuroImage* 59, 2175-2186.
- Le Bihan, D., 2014. Diffusion MRI: what water tells us about the brain. *EMBO Molecular Medicine* 6, 569-573.
- Le Bihan, D., Breton, E., Lallemand, D., Grenier, P., Cabanis, E., Laval-Jeantet, M., 1986. MR imaging of intravoxel incoherent motions: application to diffusion and perfusion in neurologic disorders. *Radiology* 161, 401-407.
- Madden, D.J., Bennett, I.J., Burzynska, A., Potter, G.G., Chen, N.K., Song, A.W., 2012. Diffusion tensor imaging of cerebral white matter integrity in cognitive aging. *Biochimica et Biophysica Acta (BBA) – Molecular Basis of Disease* 1822, 386-400.
- Mädler, B., Drabycz, S.A., Kolind, S.H., Whittall, K.P., MacKay, A.L., 2008. Is diffusion anisotropy an accurate monitor of myelination?: Correlation of multicomponent T2 relaxation and diffusion tensor anisotropy in human brain. *Magnetic Resonance Imaging* 26, 874-888.
- Mallio, C.A., Schmidt, R., de Reus, M.A., Vernieri, F., Quintiliani, L., Curcio, G., Zobel, B.B., Quattrocchi, C.C., van den Heuvel, M.P., 2015. Epicentral Disruption of Structural Connectivity in Alzheimer's Disease. *CNS Neuroscience & Therapeutics*, epub ahead of print.
- Marquardt, D., 1963. An Algorithm for Least-Squares Estimation of Nonlinear Parameters. *Journal of the Society for Industrial and Applied Mathematics* 11, 431-441.
- Marqués-Iturria, I. et al., 2015. Affected connectivity organization of the reward system structure in obesity. *NeuroImage* 111, 100-106.

CHAPTER 2

- Marsteller, L., Williams, M., Rich, A., Savage, G., Burianová, H., 2015. Aging and large-scale functional networks: White matter integrity, gray matter volume, and functional connectivity in the resting state. *Neuroscience* 290, 369-378.
- Mori, S., 2007. Introduction to Diffusion Tensor Imaging. Elsevier, Amsterdam.
- Mori, S., Crain, B.J., Chacko, V.P., Van Zijl, P.C.M., 1999. Three-dimensional tracking of axonal projections in the brain by magnetic resonance imaging. *Annals of Neurology* 45, 265-269.
- Moseley, M.E., Cohen, Y., Kucharczyk, J., Mintorovitch, J., Asgari, H.S., Wendland, M.F., Tsuruda, J., Norman, D., 1990. Diffusion-weighted MR imaging of anisotropic water diffusion in cat central nervous system. *Radiology* 176, 439-445.
- Peper, J.S., de Reus, M.A., van den Heuvel, M.P., Schutter, D.J.L.G., 2015. Short fused? associations between white matter connections, sex steroids, and aggression across adolescence. *Human Brain Mapping* 36, 1043-1052.
- Reisert, M., Mader, I., Anastasopoulos, C., Weigel, M., Schnell, S., Kiselev, V., 2011. Global fiber reconstruction becomes practical. *NeuroImage* 54, 955-962.
- Song, S.K., Sun, S.W., Ju, W.K., Lin, S.J., Cross, A.H., Neufeld, A.H., 2003. Diffusion tensor imaging detects and differentiates axon and myelin degeneration in mouse optic nerve after retinal ischemia. *NeuroImage* 20, 1714-1722.
- Song, S.K., Yoshino, J., Le, T.Q., Lin, S.J., Sun, S.W., Cross, A.H., Armstrong, R.C., 2005. Demyelination increases radial diffusivity in corpus callosum of mouse brain. *NeuroImage* 26, 132-140.
- Sporns, O., Tononi, G., Kötter, R., 2005. The Human Connectome: A Structural Description of the Human Brain. *PLoS Computational Biology* 1, e42.
- Stejskal, E.O., Tanner, J.E., 1965. Spin Diffusion Measurements: Spin Echoes in the Presence of a Time-Dependent Field Gradient. *The Journal of Chemical Physics* 42, 288-292.
- Tournier, J.D., Calamante, F., Connelly, A., 2007. Robust determination of the fibre orientation distribution in diffusion MRI: Non-negativity constrained super-resolved spherical deconvolution. *NeuroImage* 35, 1459-1472.
- Tuch, D.S., Reese, T.G., Wiegell, M.R., Makris, N., Belliveau, J.W., Wedeen, V.J., 2002. High angular resolution diffusion imaging reveals intravoxel white matter fiber heterogeneity. *Magnetic Resonance in Medicine* 48, 577-582.
- Verstraete, E., Veldink, J.H., Mandl, R.C.W., van den Berg, L.H., van den Heuvel, M.P., 2011. Impaired Structural Motor Connectome in Amyotrophic Lateral Sclerosis. *PLoS ONE* 6, e24239.
- Wedgeen, V.J., Hagmann, P., Tseng, W.Y.I., Reese, T.G., Weisskoff, R.M., 2005. Mapping complex tissue architecture with diffusion spectrum magnetic resonance imaging. *Magnetic Resonance in Medicine* 54, 1377-1386.
- Wiegell, M.R., Larsson, H.B.W., Wedeen, V.J., 2000. Fiber Crossing in Human Brain Depicted with Diffusion Tensor MR Imaging. *Radiology* 217, 897-903.
- Yeh, F.C., Wedeen, V.J., Tseng, W.Y.I., 2010. Generalized q-Sampling Imaging. *IEEE Transactions on Medical Imaging* 29, 1626-1635.



Chapter 3

The parcellation-based connectome: Limitations and extensions

*Based on a publication (NeuroImage, vol. 80, 2013, pp. 397-404) by
Marcel A. de Reus and Martijn P. van den Heuvel*

Abstract

The human connectome is an intricate system of interconnected elements, providing the basis for integrative brain function. An essential step in the macroscopic mapping and examination of this network of structural and functional interactions is the subdivision of the brain into large-scale regions. Parcellation approaches used for the formation of macroscopic brain networks include application of predefined anatomical templates, randomly generated templates, and voxel-based divisions. In this chapter, we discuss the use of such parcellation approaches for the examination of connectome characteristics. We specifically address the impact of the choice of parcellation scheme and resolution on the estimation of the brain's topological and spatial network features. Although organizational principles of functional and structural brain networks appear to be largely independent of the adopted parcellation approach, quantitative measures of these principles may be significantly modulated. Future parcellation-based connectome studies might benefit from the adoption of novel network tools and promising advances in connectivity-based parcellation approaches.

Introduction

The brain is a complex network of structurally and functionally interlinked regions. Integrative brain function does not solely depend on the activation or influence of a single element of this network, but rather emerges from the system of interactions as a whole, the human connectome (Sporns et al., 2005). Inspired by pioneering work on the structure of animal connectomes, such as those of the nematode *Caenorhabditis elegans* (White et al., 1986), cat (Scannell et al., 1999; Scannell et al., 1995), and primate (Felleman and Van Essen, 1991; Young, 1993), recent advances in neuroimaging techniques (Basser et al., 2000; Lowe et al., 2000; Tuch, 2004; Wedeen et al., 2005) are utilized to map the brain's functional and structural connections in ever increasing detail (Cammoun et al., 2012; Gong et al., 2009; Hagmann et al., 2007; Toga et al., 2012; Tuch, 2004; Wedeen et al., 2005). Studies examining the spatial and topological organization

of these connectome maps have revealed several characteristics of an efficient network architecture, including aspects of economic wiring (Bassett et al., 2010; Bullmore and Sporns, 2012), the presence of clustered functional communities, indicative of information segregation (Bullmore and Sporns, 2009; Damoiseaux et al., 2006; van den Heuvel et al., 2009a; Hilgetag et al., 2000; Hilgetag and Kaiser, 2004; Salvador et al., 2005), short communication relays (Hagmann et al., 2007; van den Heuvel et al., 2012; van den Heuvel et al., 2009b; Kaiser and Hilgetag, 2006; Sporns and Zwi, 2004; Varshney et al., 2011), and the formation of a small set of densely connected and centrally placed hub nodes, playing a crucial role in global brain communication (Achard et al., 2006; Collin et al., 2014; Hagmann et al., 2008; van den Heuvel et al., 2012; van den Heuvel and Sporns, 2011; Sporns et al., 2007).

Macroscopic instead of microscopic

Due to the vast amounts of neurons and the small measurement scale, reconstructing an entire connectome on the neuronal level, be it of a simple life form as the *Drosophila* fly (Chiang et al., 2011; Chklovskii et al., 2010) or zebrafish (Stobb et al., 2012), let alone that of mammalian species, is an ambitious and challenging task. According to estimates, the human brain consists of circa 100 billion neurons, their soma varying between 4 and 100 µm in diameter, and a thousandfold connections (Azevedo et al., 2009; Williams and Herrup, 1988). For the mapping and analysis of this microscopic connectome, further advances in both imaging techniques (e.g., higher spatial resolutions and shorter acquisition times) and computer systems (increasing data storage and computational power) are required. Today, a complete connectome map on the microscopic scale is only available for the simple nematode *C. elegans*, with a nervous system consisting of just 302 neurons (Varshney et al., 2011; White et al., 1986). Connectome maps of the human brain are instead formed on a macroscopic scale, mapping structural and functional connections between large-scale brain regions rather than interactions between single neurons.

Parcellating the brain

To allow a rescaling of the connectome from a microscopic to a macroscopic scale, a definition of the brain's large-scale regions and connections is required. The process of dividing the brain into such macroscopic regions is usually referred to as *parcellation*. In particular when it comes to the delineation of structurally or functionally distinct regions in the cerebral cortex, there is a long research tradition (see Zilles and Amunts (2010) and Geyer et al. (2011) for an overview), going back more than a century to the seminal work of Penfield (Penfield, 1950; Penfield and Boldrey, 1937) and Brodmann (Brodmann, 1909; Brodmann, 1914). Through the ages, cortical areas have been distinguished on the basis of, e.g., cytoarchitecture (Brodmann, 1909; von Economo and Koskinas, 1925; Schleicher et al., 1999), myeloarchitecture (Vogt and Vogt, 1919), electrophysiological observations (Lim et al., 1994; Penfield and Boldrey, 1937), immunohistochemistry (Baleydier et al., 1997), and receptor autoradiography (Zilles et al., 2002). In recent years, novel techniques based on magnetic resonance imaging (MRI) have extended this list, exploiting cortical curvature patterns (Desikan et al., 2006; Van Essen, 2005), *in vivo* mappings of myelin content (Glasser and Van Essen, 2011), and similarities in structural and functional connectivity profiles (Craddock et al., 2012; Johansen-Berg et al., 2004). Results from these different parcellation criteria have been brought together in multiple three-dimensional brain atlases, also referred to as anatomical templates, which can be used to parcellate a subject's brain on the basis of an MRI scan (Collins et al., 1995; Fischl et al., 2004; Tzourio-Mazoyer et al., 2002). Together with high-resolution parcellation approaches that subdivide the brain into voxels (Eguíluz et al., 2005; van den Heuvel et al., 2008a) or randomly generated parcels (Hagmann et al., 2007; van den Heuvel and Sporns, 2011), these brain atlases are at the heart of parcellation-based connectome analysis, providing the large-scale brain regions whose structural and functional connections are the topic of investigation.

A formal representation of brain networks

For the examination of topological and spatial features of the brain's wiring pattern, a formal description of the system as a whole is needed. To this end, a connectome (map) is often represented as a graph; a mathematical notion of a network, describing elements (nodes) and their interactions (edges) in an abstract manner (Bullmore and Sporns, 2009), allowing a systematic study of the network's topology through computation of so-called graph metrics (Figure 3.1) (van den Heuvel and Hulshoff Pol, 2010; Rubinov and Sporns, 2010). In the graph

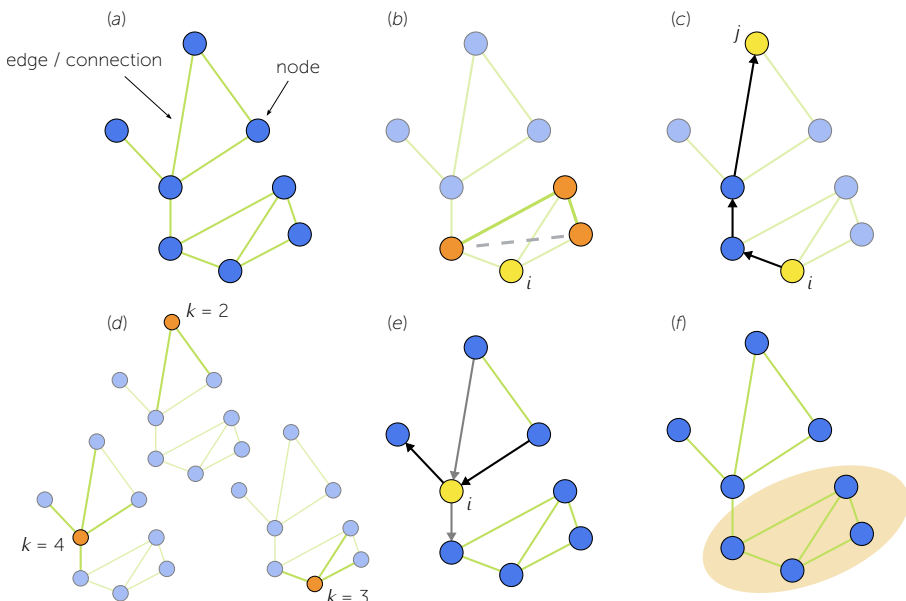


Figure 3.1. Commonly used graph metrics. (a) Parcellation-based connectomes can be represented as a graph; an abstract description of elements (nodes) and their interactions (edges or connections). In macroscopic brain networks, the nodes and edges correspond to large-scale brain regions and their structural or functional connections, respectively. (b) The clustering coefficient of a single node *i* is given by the fraction of connected neighbor pairs. The clustering coefficient of the entire graph is subsequently computed as the average over all nodes. (c) The characteristic path length of a graph is defined as the average number of steps required to travel between two nodes of the graph. (d) The number of connections of a node is known as its degree. The graph's degree distribution expresses how often each degree occurs in the graph. (e) The betweenness centrality of a node *i* reflects the (relative) number of shortest paths between all node pairs that pass through node *i*. (f) The modularity of a graph describes the extent to which the graph can be subdivided into weakly linked clusters of densely connected nodes.

Figure adapted from van den Heuvel and Hulshoff Pol (2010) with permission from Elsevier.

representation of a parcellation-based connectome, each node of the graph corresponds to a brain region from the template that was used to subdivide the brain. In turn, the edges of the graph correspond to structural or functional connections between these brain regions, depending on the utilized imaging modality. Since the boundaries and amount of distinguished regions, ranging in size from single voxels to large-scale parcels of hundreds of voxels, vary considerably between templates, the adopted parcellation approach directly implicates the (number of) nodes and therefore also the number and placement of edges. That is, the formal representation of a parcellation-based connectome depends on the choice of parcellation scheme.

Here, we review the application of parcellation templates for brain networks established by diffusion tractography (Basser et al., 2000; Hagmann et al., 2006; Mori et al., 1999; Wedeen et al., 2005) and resting-state functional magnetic resonance imaging (fMRI) (Biswal et al., 1995; Fox et al., 2005; Lowe et al., 2000) and discuss their impact on the estimation and examination of connectome characteristics. Special attention will be paid to the effect of parcellation resolution (i.e., the number of regions in a template), which has recently been suggested to play an important role in the assessment of network features. Following the main discussion on the use and impact of parcellation templates, we briefly touch upon the exciting field of connectivity-based parcellation, which aims to discern the fundamental functional and structural elements of the human brain on the basis of the connectivity profile of brain regions (Anwander et al., 2007; Johansen-Berg et al., 2004).

Use and impact of parcellation templates

Predefined anatomical templates

A common approach to select the nodes of a macroscopic brain network is to parcellate the brain of a given subject using a predefined anatomical template or brain atlas. Typically, the subject's anatomical images are registered to a template brain whose regions have been labeled using one or more manually

parcellated subjects from a fixed training set. The labels of this template brain are then propagated onto the registered anatomical images, thus subdividing the subject's gray matter into labeled brain regions. Successfully applied atlases for the formation of macroscopic brain networks include, among others, the Automated Anatomical Labeling (AAL) toolbox (Tzourio-Mazoyer et al., 2002), the Automated Non-linear Image Matching and Anatomical Labeling (ANIMAL) algorithm (Collins et al., 1995), FMRIB Software Library's Harvard-Oxford (HO) atlas (<http://fsl.fmrib.ox.ac.uk/fsl/fslwiki/Atlases>), FreeSurfer's Desikan-Killiany atlas (Desikan et al., 2006; Fischl et al., 2004), and the LONI (Laboratory of Neuro Imaging) Probabilistic Brain Atlas (LPBA40) (Shattuck et al., 2008). These atlases all aim to cover and parcellate the same system, but differ from each other on several aspects, including the number and spatial location of brain regions, as well as the used registration technique (ranging from affine transformations to surface-based registration methods that take local shape features such as cortical folding into consideration) (Bohland et al., 2009). In what follows, we discuss findings related to the effect of such differences between parcellation schemes on the mapping and examination of the human connectome.

Impact of anatomical templates

Two recent studies have investigated the impact of anatomical template choice on the spatial and topological organization of the resulting macroscopic brain networks (Bassett et al., 2011; Wang et al., 2009). Based on recordings of spontaneous brain activity through means of resting-state fMRI, Wang et al. (2009) compared the use of the AAL and ANIMAL anatomical parcellation template for the reconstruction of functional interactions between brain regions. Independent of parcellation scheme, functional brain networks displayed a small-world topology (Watts and Strogatz, 1998) with a truncated power-law degree distribution (Amaral et al., 2000). In a comparable study, Bassett et al. (2011) examined the impact of template use on connectome maps resulting from diffusion-weighted imaging. Overlapping the findings of Wang and colleagues, organizational principles such as sparsity, small-worldness, efficient embedding in physical space (Bassett et al., 2010; Christie and Stroobandt, 2000) and hierarchy (Ravasz and

Barabási, 2003) were all found to be conserved across three different anatomical templates (AAL, HO, and LPBA40). Both studies demonstrated, however, that precise numerical values of the underlying network metrics, including traditional (characteristic path length and clustering coefficient, see Figure 3.1) and efficiency-based (global and local efficiency) small-world measures (Latora and Marchiori, 2001; Rubinov and Sporns, 2010; Watts and Strogatz, 1998), as well as fitting parameters capturing the behavior of the degree distribution, differed significantly between brain atlases. Furthermore, the spatial location of highly connected brain regions (Bassett et al., 2011) and the relation between nodal properties and region size (Wang et al., 2009) were shown to be dependent on the atlas used. These findings therefore suggest that although large-scale organizational aspects are preserved across templates, important characteristics of individual regions and quantitative network measures can differ significantly between brain atlases, limiting a direct comparison of results across atlases and thus across studies.

Random templates

Besides the use of predefined parcellation templates that incorporate anatomically motivated regions, also randomly generated templates (Fornito et al., 2010; Hagmann et al., 2008; van den Heuvel and Sporns, 2011) and voxel-based parcellations (Buckner et al., 2009; Cecchi et al., 2007; Eguiluz et al., 2005; van den Heuvel et al., 2009a; van den Heuvel et al., 2008a; Zalesky et al., 2012) are regularly used to define the nodes of macroscopic brain networks. Since algorithms employed for random parcellation (Echtermeyer et al., 2011a; Hagmann et al., 2007; van den Heuvel and Sporns, 2011; Zalesky et al., 2010) are designed to produce parcels of roughly equal size, both non-anatomical approaches feature (approximately) uniformly sized brain regions. Whether this is an actual advantage over anatomical templates is open for debate and may depend on the research question. On the one hand, the usage of equally sized nodes, or a rescaling of connectivity by region size (Hagmann et al., 2008; van den Heuvel and Sporns, 2011), may highlight effects of spatial and topological location that otherwise might be obfuscated by size-related differences

in connectivity strength (Bassett et al., 2011; Wang et al., 2009). On the other hand, volumetric heterogeneity might be a natural and intrinsic property of the brain (Van Essen et al., 2012), possibly driven by connectivity differences between brain regions. A second feature of non-anatomical parcellation schemes is that they allow investigation of connectome characteristics at higher spatial resolutions: where anatomical templates vary in size between ~50 and ~120 regions, connectome analyses based on random parcels or voxels have been performed with thousands of nodes (Eguíluz et al., 2005; Hagmann et al., 2007). Such high-resolution connectome maps could potentially reveal characteristics that are concealed when coarser templates are used and may improve power to detect differences between (groups of) subjects.

Effects of spatial resolution

Influence on network metrics

The influence of spatial scale on macroscopic connectome characteristics has been addressed in several studies. Most importantly, all show a strong impact of network resolution on graph metrics. Bassett et al. (2011) repeatedly bisected the regions of the AAL, HO, and LPBA40 atlases, obtaining templates of two, four, and eight times the original resolutions. Similar to the comparison between anatomical templates, architectural principles were found to be robust across spatial scales, but network metrics varied substantially. A comparison between region- and voxel-based functional brain networks provides further support for this observation (Hayasaka and Laurienti, 2010). Although both types of functional networks appeared to fall within the small-world regime and displayed exponentially truncated power-law degree distributions, the computed small-world organization was consistently more clustered in the voxel-based networks (Eguíluz et al., 2005; Hayasaka and Laurienti, 2010; van den Heuvel et al., 2008a). Moreover, differences in decay parameters of the degree distributions revealed a possible underrepresentation of low degree nodes in the region-based networks (Hayasaka and Laurienti, 2010).

Also studies examining structural (Zalesky et al., 2010) and functional (Fornito et al., 2010) brain networks across random subdivisions of the AAL template (ranging from ~100 to ~4000 nodes) show that organizational properties of macroscopic brain networks are largely independent of the parcellation scheme, while the quantification of these properties is highly susceptible to changes in network resolution. To separate effects of spatial scale and choice of parcellation template, multiple random parcellations were generated for each resolution. Whereas relative differences in the small-world index (Humphries et al., 2006) were found to be as large as 95% between low- and high-resolution templates, differences between graph metrics computed on structural brain networks of the same scale never exceeded 3%. These findings indicate that graph metrics are particularly sensitive to the resolution of a parcellation scheme and not so much to varying regional boundaries (Zalesky et al., 2010). Furthermore, by computing correlation coefficients between metric outcomes of distinct parcellation templates, differences between individuals were shown to be generally preserved across spatial scales of more than ~200 nodes (Fornito et al., 2010).

Intrinsic dependence of metrics on network size

The question rises whether the prominent effect of spatial resolution on graph metrics reflects true characteristics of the human connectome, having different topological aspects across spatial scales, or can be attributed to methodological issues. Consistent with analytical derivations (Albert and Barabási, 2002) and earlier reports (Anderson et al., 1999), recent simulation studies (Good et al., 2010; Litvak and van der Hofstad, 2013; van Wijk et al., 2010) confirm that independent of the modeled system, the number of nodes of a graph (also known as the graph's *order*) has a clear impact on typical network metrics like the clustering coefficient, characteristic path length, small-world index (van Wijk et al., 2010), degree assortativity (Litvak and van der Hofstad, 2013), and modularity (Good et al., 2010). Considering this intrinsic dependence on the number of nodes, it is likely that the observed variation in graph metrics across human connectome maps of different spatial scales is at least to some degree attributable to the associated fluctuations in network order. Since the extent of the influence of

the number of nodes on graph metrics is only known for some simple network models, it is rather difficult to correct for this methodological effect, which thus limits the direct comparison of graph characteristics between brain networks of different order.

Extensions of network metrics

The comparability of topological features of large-scale brain networks acquired at different spatial resolutions might be improved by the development and application of new network tools that may be less susceptible to variations in network order. Examples of such tools, extending the computation of traditional graph metrics, include the application of *exponential random graph models* (Simpson et al., 2011; van Wijk et al., 2010) and *single node motifs* (Costa et al., 2009; Echtermeyer et al., 2011b; Kaiser, 2011). Exponential random graph models (ERGMs) are a class of statistical network models that can be used to study the influence of graph metrics on the overall organization of a network. After a long history in social sciences (see Robins et al. (2007) for an introduction), ERGMs have recently also been employed for the analysis and modeling of brain networks (Simpson et al., 2011; Simpson et al., 2012). To estimate the extent to which graph metrics, combined in a vector $g(y) = (g_1(y), \dots, g_m(y))$, contribute to the topology of an observed network y , the probability

$$P(Y = y) = \kappa(\theta)^{-1} \exp(\theta \cdot g(y)) \quad (3.1)$$

that y matches a randomly drawn network from the class of ERGMs defined by the parameters $\theta = (\theta_1, \dots, \theta_m)$ is maximized using a fitting procedure (Simpson et al., 2011). The resulting values for the fitting parameters $\theta_1, \dots, \theta_m$ then quantify the contribution of the corresponding graph metrics to the global organization of the observed network, and as such, they can be compared between networks. Whether the values of these fitting parameters provide a better assessment of organizational aspects of macroscopic brain networks across spatial scales than ordinary graph metrics remains to be determined in future studies.

Another network feature that might be useful to compare parcellation-based

connectome maps of different resolutions is the distribution of so-called single node motifs (Costa et al., 2009; Echtermeyer et al., 2011b; Kaiser, 2011). Single node motifs, not to be confused with network motifs (Sporns and Kötter, 2004) or path motifs (van den Heuvel et al., 2012), are nodal characteristics that are extracted from a multitude of local topological and spatial features of a node, such as its clustering coefficient and the average (fiber) distance to its neighbors. First, these local network features are computed for each node and combined into node specific feature vectors. On the basis of two-dimensional projections of these feature vectors, obtained by removing interdependencies between the features with principal component analysis, outlier nodes are then identified and assigned to a motif-group, characterized by a specific pattern of over- and under-expression of the local network features. Finally, the distribution of outlier nodes among the motif-groups gives a fingerprint of the network that can be compared with such fingerprints of other networks (Costa et al., 2009; Echtermeyer et al., 2011b).

In a study on the effect of spatial scale on single node motifs in structural brain networks, the number of expressed motif-groups was found to be similar for all considered parcellation schemes, while the number of outlier nodes and their distribution among these motif-groups depended strongly on the adopted resolution (Echtermeyer et al., 2011a). Because the detection of single node motifs is based on relative patterns of local network features rather than on their absolute values, such differences are less likely to be driven by intrinsic effects of network order and may therefore provide insight in true organizational differences between spatial scales.

Reproducibility and individual variation

The choice of spatial resolution may also have implications for the reproducibility and displayed individual variation of connectome characteristics. To provide insight in the variability of structural connectome maps, two studies obtained multiple sets of diffusion-weighted images and processed these at different spatial scales with streamline tractography (Bassett et al., 2011; Cammoun et al.,

2012). As a measure of the consistency of the resulting macroscopic brain networks, correlations between the associated weighted connectivity matrices – storing the measured connectivity between brain region i and j in the j th entry of the i th row – were computed. Both studies demonstrate that the results of the mapping procedure are highly reproducible and also rather consistent between different subjects. Correlations between different scans of the same subjects were found to be somewhat stronger than those calculated between connectivity matrices of different subjects, suggesting biological fluctuations on top of a solid common basis for the brain's macroscopic wiring.

All types of variation, either resulting from reprocessing scans (an additional analysis to assess the stability of the processing pipeline), repeatedly scanning the same subject, or comparing different subjects, were found to increase with increasing spatial resolution (i.e., when subdividing the brain into smaller parcels) (Cammoun et al., 2012). In agreement with these findings, the reproducibility of graph metrics dropped significantly with increasing parcellation resolution (Bassett et al., 2011). As illustrated in Figure 3.2, a possible explanation for this decreasing consistency at finer spatial scales might be that for smaller brain

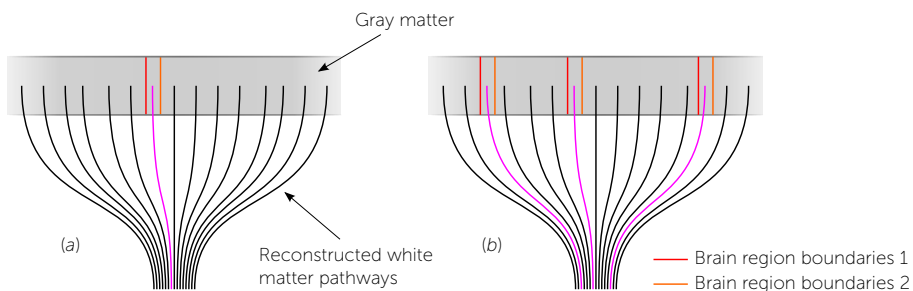


Figure 3.2. Schematic impression of the effect of varying brain region boundaries. (a) Due to measurement noise, registration difficulties, or biological variation, the location of regional boundaries may vary between subjects and between different scans of the same subject. Due to such discrepancies in brain region boundaries, similar positioned white matter pathways may be assigned to different brain regions (e.g., the pink fiber in the figure), inducing variation in the observed connectome maps and their associated connectivity matrices. (b) At finer spatial scales, brain regions become smaller and the total number and area of regional boundaries become larger. As a result, variation attributable to differently assigned white matter pathways increases with spatial resolution.

regions, variation in the location of region boundaries, caused either by registration difficulties or biological differences, is more likely to change the assigned source and target region of a reconstructed white matter fiber tract. Likewise, a reported reduction of mean functional connectivity at higher spatial resolutions also suggests that smaller brain regions introduce greater measurement uncertainties (Fornito et al., 2010). A potential problem of high-resolution connectome analyses is therefore that noise inherent to the mapping procedure might overshadow differences between (groups of) subjects (Cammoun et al., 2012).

Connectivity-based parcellation

Connectivity-based parcellation approaches are an exciting and upcoming class of parcellation techniques that aim to delineate large-scale brain regions by exploiting similarities in structural or functional connectivity patterns (Cloutman and Lambon Ralph, 2012). Similar to connectome research, connectivity-based parcellation is motivated by the idea that brain function may be understood from the underlying wiring pattern (Johansen-Berg et al., 2004; Sporns et al., 2005). Rather than independent elements, brain regions are part of a complex system of structural and functional interactions. In this system, the connections of a brain region, encoded by its “connectivity profile”, determine both the information that is available as input, as well as the potential recipients of the region’s output (Johansen-Berg et al., 2004). The premise of connectivity-based parcellation is that regions with a similar connectivity profile are involved in the same information streams and exhibit analogous functional roles. According to this premise, a large collection of small seed regions can be partitioned into a coarser collection of functionally homogeneous brain regions by clustering seeds with similar connectivity profiles.

Refinement of anatomical templates

Current applications of connectivity-based parcellation approaches mainly focus on the subdivision of selected large-scale anatomical structures (Cloutman and Lambon Ralph, 2012), delineating areas in, for example, the medial (Jbabdi

et al., 2009; Johansen-Berg et al., 2004; Klein et al., 2007) and inferior (Anwander et al., 2007; Gorbach et al., 2011; Klein et al., 2007) frontal cortex and the thalamus (Elias et al., 2012; Johansen-Berg et al., 2005). Within these approaches, starting seed regions can be voxels (Anwander et al., 2007) or surface vertices (Roca et al., 2009) of the anatomical structure, which are then clustered into larger parcels based on their functional (Kim et al., 2010) or structural (Klein et al., 2007) projections towards a collection of chosen target regions. Seeds with overlapping connectivity profiles with respect to these target regions are grouped together, while seeds with mostly disjoint profiles are placed into distinct groups, resulting in a subdivision of the original anatomical structure into regions of homogeneous connectivity and thus supposedly of homogeneous function. As such, insights from connectivity-based parcellation studies can be used to refine brain atlases and anatomical templates that are currently used for parcellation-based connectome studies, indirectly enhancing the investigation of macroscopic connectome features.

Whole-brain parcellation

Connectivity-based parcellation results depend on several parameters (e.g., the selected seed and target regions and the adopted clustering method) that are likely to introduce methodological variation between studies and complicate the construction of a single refined template. For the mapping of macroscopic brain networks, it might therefore be advantageous to subdivide the brain as a whole into regions of homogeneous connectivity. By selecting seed vertices from the entire brain, essentially the same procedure as outlined above could be used to obtain whole-brain connectivity-based parcellations (Craddock et al., 2012; Roca et al., 2009; Roca et al., 2010). However, especially for fMRI recordings, other data-driven subdivision approaches are also available, most notably the application of independent component analysis (ICA) (Beckmann et al., 2005) and traditional clustering approaches (van den Heuvel et al., 2008b), providing a subdivision of the brain into functional subnetworks. For example, hierarchical clustering methods and ICA have been used to select resting-state networks of interest (Damoiseaux et al., 2006) and examine the underlying anatomical

infrastructure of these networks (Greicius et al., 2009; van den Heuvel et al., 2009a; Salvador et al., 2005). Furthermore, advanced high-dimensional spatial ICA approaches (Smith, 2012) are currently used to create data-driven subdivisions of the human brain into homogeneous subparts, exploring their use both in the examination of intrinsic properties of the healthy brain, as well as potential disconnectivity in patients (Yu et al., 2013).

Conclusions

An important aspect of the mapping and analysis of parcellation-based connectomes is the choice of parcellation scheme, which directly implicates the nodes and edges of a macroscopic brain network. In this chapter, we have reflected upon the use and impact of several parcellation approaches, most prominently the application of predefined anatomical templates and random high-resolution templates. Studies examining the influence of parcellation schemes all support the same conclusion: organizational principles of functional and structural brain networks are largely independent of the adopted parcellation template, but the quantification of these principles may be significantly influenced by the parcellation. Therefore, care should be taken when collating results of studies that employ different parcellation schemes, as graph metrics expressing the connectome's spatial and topological features might not be directly comparable.

For the assessment of network characteristics of macroscopic brain networks, the number of brain regions in the utilized parcellation template appears to have a considerable influence (Bassett et al., 2011; Zalesky et al., 2010). This dependence of graph metrics on the number of nodes is also present in theoretical network models and simulations (Albert and Barabási, 2002; Anderson et al., 1999; Good et al., 2010; van Wijk et al., 2010). Some studies have suggested that the use of medium- and high-resolution templates (exceeding 200 nodes) may positively impact the consistency of some graph characteristics (Fornito et al., 2010), an effect that may be related to a relatively lower influence of network order at these resolutions (van Wijk et al., 2010). Unfortunately, others have shown

that the price for a finer spatial sampling might include an increasing impact of measurement and processing noise (Bassett et al., 2011; Cammoun et al., 2012; van den Heuvel et al., 2008a), possibly limiting the current usability of high-resolution approaches in case-control studies. In a near future, the development and adoption of novel network tools and whole-brain connectivity-based parcellation approaches might perhaps reduce undesirable methodological effects of arbitrary boundaries and high spatial resolutions, further increasing the utility of parcellation-based connectomes.

References

- Achard, S., Salvador, R., Whitcher, B., Suckling, J., Bullmore, E., 2006. A Resilient, Low-Frequency, Small-World Human Brain Functional Network with Highly Connected Association Cortical Hubs. *The Journal of Neuroscience* 26, 63-72.
- Albert, R., Barabási, A.L., 2002. Statistical mechanics of complex networks. *Reviews of Modern Physics* 74, 47-97.
- Amaral, L.A.N., Scala, A., Barthélémy, M., Stanley, H.E., 2000. Classes of small-world networks. *Proceedings of the National Academy of Sciences* 97, 11149-11152.
- Anderson, B.S., Butts, C., Carley, K., 1999. The interaction of size and density with graph-level indices. *Social Networks* 21, 239-267.
- Anwander, A., Tittgemeyer, M., von Cramon, D.Y., Friederici, A.D., Knösche, T.R., 2007. Connectivity-Based Parcellation of Broca's Area. *Cerebral Cortex* 17, 816-825.
- Azevedo, F.A.C., Carvalho, L.R.B., Grinberg, L.T., Farfel, J.M., Ferretti, R.E.L., Leite, R.E.P., Filho, W.J., Lent, R., Herculano-Houzel, S., 2009. Equal numbers of neuronal and nonneuronal cells make the human brain an isometrically scaled-up primate brain. *Journal of Comparative Neurology* 513, 532-541.
- Baleydier, C., Achache, P., Froment, J.C., 1997. Neurofilament architecture of superior and mesial premotor cortex in the human brain. *Neuroreport* 8, 1691-1696.
- Basser, P.J., Pajevic, S., Pierpaoli, C., Duda, J., Aldroubi, A., 2000. In vivo fiber tractography using DT-MRI data. *Magnetic Resonance in Medicine* 44, 625-632.
- Bassett, D.S., Brown, J.A., Deshpande, V., Carlson, J.M., Grafton, S.T., 2011. Conserved and variable architecture of human white matter connectivity. *NeuroImage* 54, 1262-1279.
- Bassett, D.S., Greenfield, D.L., Meyer-Lindenberg, A., Weinberger, D.R., Moore, S.W., Bullmore, E.T., 2010. Efficient Physical Embedding of Topologically Complex Information Processing Networks in Brains and Computer Circuits. *PLoS Computational Biology* 6, e1000748.
- Beckmann, C.F., DeLuca, M., Devlin, J.T., Smith, S.M., 2005. Investigations into resting-state connectivity using independent component analysis. *Philosophical Transactions of the Royal Society of London B: Biological Sciences* 360, 1001-1013.
- Biswal, B., Yetkin, F.Z., Haughton, V.M., Hyde, J.S., 1995. Functional connectivity in the motor cortex of resting human brain using echo-planar MRI. *Magnetic Resonance in Medicine* 34, 537-541.
- Bohland, J.W., Bokil, H., Allen, C.B., Mitra, P.P., 2009. The Brain Atlas Concordance Problem: Quantitative Comparison of Anatomical Parcellations. *PLoS ONE* 4, e7200.
- Brodmann, K., 1909. *Vergleichende Lokalisationslehre der Grosshirnrinde*. Johann Ambrosius Barth Verlag, Leipzig.
- Brodmann, K., 1914. *Physiologie des Gehirns*. Union Deutsche Verlagsgesellschaft, Stuttgart.
- Buckner, R.L., Sepulcre, J., Talukdar, T., Krienen, F.M., Liu, H., Hedden, T., Andrews Hanna, J.R., Sperling, R.A., Johnson, K.A., 2009. Cortical Hubs Revealed by Intrinsic Functional Connectivity: Mapping, Assessment of Stability, and Relation to Alzheimer's Disease. *The Journal of Neuroscience* 29, 1860-1873.
- Bullmore, E., Sporns, O., 2009. Complex brain networks: graph theoretical analysis of structural and functional systems. *Nature Reviews Neuroscience* 10, 186-198.
- Bullmore, E., Sporns, O., 2012. The economy of brain network organization. *Nature Reviews Neuroscience* 13, 336-349.
- Cammoun, L., Gigandet, X., Meskaldji, D., Thiran, J.P., Sporns, O., Do, K.Q., Maeder, P., Meuli, R., Haggmann, P., 2012. Mapping the human connectome at multiple scales with diffusion spectrum MRI. *Journal of Neuroscience Methods* 203, 386-397.
- Cecchi, G., Rao, A.R., Centeno, M., Baliki, M., Apkarian, A.V., Chialvo, D., 2007. Identifying directed links in large scale functional networks: application to brain fMRI. *BMC Cell Biology* 8, S5.
- Chiang, A.S. et al., 2011. Three-Dimensional Reconstruction of Brain-wide Wiring Networks in *Drosophila* at Single-Cell Resolution. *Current Biology* 21, 1-11.

- Chklovskii, D.B., Vitaladevuni, S., Scheffer, L.K., 2010. Semi-automated reconstruction of neural circuits using electron microscopy. *Current Opinion in Neurobiology* 20, 667-675.
- Christie, P., Stroobandt, D., 2000. The interpretation and application of Rent's rule. *IEEE Transactions on Very Large Scale Integration (VLSI) Systems* 8, 639-648.
- Cloutman, L.L., Lambon Ralph, M.A., 2012. Connectivity-based structural and functional parcellation of the human cortex using diffusion imaging and tractography. *Frontiers in Neuroanatomy* 6, 34.
- Collin, G., Kahn, R.S., de Reus, M.A., Cahn, W., van den Heuvel, M.P., 2014. Impaired Rich Club Connectivity in Unaffected Siblings of Schizophrenia Patients. *Schizophrenia Bulletin* 40, 438-448.
- Collins, D.L., Holmes, C.J., Peters, T.M., Evans, A.C., 1995. Automatic 3-D model-based neuroanatomical segmentation. *Human Brain Mapping* 3, 190-208.
- Costa, L.D.F., Rodrigues, F.A., Hilgetag, C.C., Kaiser, M., 2009. Beyond the average: Detecting global singular nodes from local features in complex networks. *Europhysics Letters* 87, 18008.
- Craddock, R.C., James, G., Holtzheimer, P.E., Hu, X.P., Mayberg, H.S., 2012. A whole brain fMRI atlas generated via spatially constrained spectral clustering. *Human Brain Mapping* 33, 1914-1928.
- Damoiseaux, J.S., Rombouts, S.A.R.B., Barkhof, F., Scheltens, P., Stam, C.J., Smith, S.M., Beckmann, C.F., 2006. Consistent resting-state networks across healthy subjects. *Proceedings of the National Academy of Sciences* 103, 13848-13853.
- Desikan, R.S. et al., 2006. An automated labeling system for subdividing the human cerebral cortex on MRI scans into gyral based regions of interest. *NeuroImage* 31, 968-980.
- Echtermeyer, C., Costa, L.D.F., Rodrigues, F.A., Kaiser, M., 2011b. Automatic Network Fingerprinting through Single-Node Motifs. *PLoS ONE* 6, e15765.
- Echtermeyer, C., Han, C.E., Rotarska-Jagiela, A., Mohr, H., Uhlhaas, P.J., Kaiser, M., 2011a. Integrating temporal and spatial scales: Human structural network motifs across age and region-of-interest size. *Frontiers in Neuroinformatics* 5, 10.
- von Economo, C., Koskinas, G.N., 1925. Die Cytoarchitektonik der Hirnrinde des erwachsenen Menschen. Springer, Berlin.
- Eguiluz, V.M., Chialvo, D.R., Cecchi, G.A., Baliki, M., Apkarian, A.V., 2005. Scale-Free Brain Functional Networks. *Physical Review Letters* 94, 018102.
- Elias, W.J., Zheng, Z.A., Dorner, P., Quigg, M., Pouratian, N., 2012. Validation of connectivity-based thalamic segmentation with direct electrophysiologic recordings from human sensory thalamus. *NeuroImage* 59, 2025-2034.
- Felleman, D.J., Van Essen, D.C., 1991. Distributed hierarchical processing in the primate cerebral cortex. *Cerebral Cortex* 1, 1-47.
- Fischl, B. et al., 2004. Automatically Parcellating the Human Cerebral Cortex. *Cerebral Cortex* 14, 11-22.
- Fornito, A., Zalesky, A., Bullmore, E.T., 2010. Network scaling effects in graph analytic studies of human resting-state fMRI data. *Frontiers in Systems Neuroscience* 4, 22.
- Fox, M.D., Snyder, A.Z., Vincent, J.L., Corbetta, M., Van Essen, D.C., Raichle, M.E., 2005. The human brain is intrinsically organized into dynamic, anti-correlated functional networks. *Proceedings of the National Academy of Sciences of the United States of America* 102, 9673-9678.
- Geyer, S., Weiss, M., Reimann, K., Lohmann, G., Turner, R., 2011. Microstructural parcellation of the human cerebral cortex – from Brodmann's post-mortem map to *in vivo* mapping with high-field magnetic resonance imaging. *Frontiers in Human Neuroscience* 5, 19.
- Glasser, M.F., Van Essen, D.C., 2011. Mapping Human Cortical Areas *In Vivo* Based on Myelin Content as Revealed by T1- and T2-Weighted MRI. *The Journal of Neuroscience* 31, 11597-11616.
- Gong, G., He, Y., Concha, L., Lebel, C., Gross, D.W., Evans, A.C., Beaulieu, C., 2009. Mapping Anatomical Connectivity Patterns of Human Cerebral Cortex Using *In Vivo* Diffusion Tensor Imaging Tractography. *Cerebral Cortex* 19, 524-536.
- Good, B.H., de Montjoye, Y.A., Clauset, A., 2010. Performance of modularity maximization in practical contexts. *Physical Review E* 81, 046106.
- Gorbach, N.S., Schütte, C., Melzer, C., Goldau, M., Sujazow, O., Jitsev, J., Douglas, T., Tittgemeyer, M., 2011. Hierarchical Information-based Clustering for Connectivity-based Cortex Parcellation. *Frontiers in Neuroinformatics* 5, 18.
- Greicius, M.D., Supekar, K., Menon, V., Dougherty, R.F., 2009. Resting-State Functional Connectivity Reflects Structural Connectivity in the Default Mode Network. *Cerebral Cortex* 19, 72-78.
- Hagmann, P., Cammoun, L., Gigandet, X., Meuli, R., Honey, C.J., Wedeen, V.J., Sporns, O., 2008. Mapping the Structural Core of Human Cerebral Cortex. *PLoS Biology* 6, e159.

CHAPTER 3

- Hagmann, P., Jonasson, L., Maeder, P., Thiran, J.P., Wedeen, V.J., Meuli, R., 2006. Understanding Diffusion MR Imaging Techniques: From Scalar Diffusion-weighted Imaging to Diffusion Tensor Imaging and Beyond. *Radiographics* 26, S205-S223.
- Hagmann, P., Kurant, M., Gigandet, X., Thiran, P., Wedeen, V.J., Meuli, R., Thiran, J.P., 2007. Mapping Human Whole-Brain Structural Networks with Diffusion MRI. *PLoS ONE* 2, e597.
- Hayasaka, S., Laurienti, P.J., 2010. Comparison of characteristics between region-and voxel-based network analyses in resting-state fMRI data. *NeuroImage* 50, 499-508.
- van den Heuvel, M.P., Hulshoff Pol, H.E., 2010. Exploring the brain network: A review on resting-state fMRI functional connectivity. *European Neuropsychopharmacology* 20, 519-534.
- van den Heuvel, M.P., Kahn, R.S., Goñi, J., Sporns, O., 2012. High-cost, high-capacity backbone for global brain communication. *Proceedings of the National Academy of Sciences* 109, 11372-11377.
- van den Heuvel, M.P., Mandl, R.C.W., Hulshoff Pol, H.E., 2008b. Normalized Cut Group Clustering of Resting-State fMRI Data. *PLoS ONE* 3, e2001.
- van den Heuvel, M.P., Mandl, R.C.W., Kahn, R.S., Hulshoff Pol, H.E., 2009a. Functionally linked resting-state networks reflect the underlying structural connectivity architecture of the human brain. *Human Brain Mapping* 30, 3127-3141.
- van den Heuvel, M.P., Sporns, O., 2011. Rich-Club Organization of the Human Connectome. *The Journal of Neuroscience* 31, 15775-15786.
- van den Heuvel, M.P., Stam, C.J., Boersma, M., Hulshoff Pol, H.E., 2008a. Small-world and scale-free organization of voxel-based resting-state functional connectivity in the human brain. *NeuroImage* 43, 528-539.
- van den Heuvel, M.P., Stam, C.J., Kahn, R.S., Hulshoff Pol, H.E., 2009b. Efficiency of Functional Brain Networks and Intellectual Performance. *The Journal of Neuroscience* 29, 7619-7624.
- Hilgetag, C.C., Burns, G.A., O'Neill, M.A., Scannell, J.W., Young, M.P., 2000. Anatomical connectivity defines the organization of clusters of cortical areas in the macaque monkey and the cat. *Philosophical Transactions of the Royal Society of London B: Biological Sciences* 355, 91-110.
- Hilgetag, C.C., Kaiser, M., 2004. Clustered organization of cortical connectivity. *Neuroinformatics* 2, 353-360.
- Humphries, M.D., Gurney, K., Prescott, T.J., 2006. The brainstem reticular formation is a small-world, not scale-free, network. *Proceedings of the Royal Society B: Biological Sciences* 273, 503-511.
- Jbabdi, S., Woolrich, M.W., Behrens, T.E.J., 2009. Multiple-subjects connectivity-based parcellation using hierarchical Dirichlet process mixture models. *NeuroImage* 44, 373-384.
- Johansen-Berg, H., Behrens, T.E.J., Robson, M.D., Drobniak, I., Rushworth, M.F.S., Brady, J.M., Smith, S.M., Higham, D.J., Matthews, P.M., 2004. Changes in connectivity profiles define functionally distinct regions in human medial frontal cortex. *Proceedings of the National Academy of Sciences of the United States of America* 101, 13335-13340.
- Johansen-Berg, H., Behrens, T.E.J., Sillery, E., Ciccarelli, O., Thompson, A.J., Smith, S.M., Matthews, P.M., 2005. Functional-Anatomical Validation and Individual Variation of Diffusion Tractography-based Segmentation of the Human Thalamus. *Cerebral Cortex* 15, 31-39.
- Kaiser, M., 2011. A tutorial in connectome analysis: Topological and spatial features of brain networks. *NeuroImage* 57, 892-907.
- Kaiser, M., Hilgetag, C.C., 2006. Nonoptimal Component Placement, but Short Processing Paths, due to Long-Distance Projections in Neural Systems. *PLoS Computational Biology* 2, e95.
- Kim, J.H. et al., 2010. Defining functional SMA and pre-SMA subregions in human MFC using resting state fMRI: Functional connectivity-based parcellation method. *NeuroImage* 49, 2375-2386.
- Klein, J.C., Behrens, T.E.J., Robson, M.D., Mackay, C.E., Higham, D.J., Johansen-Berg, H., 2007. Connectivity-based parcellation of human cortex using diffusion MRI: Establishing reproducibility, validity and observer independence in BA 44/45 and SMA/pre-SMA. *NeuroImage* 34, 204-211.
- Latora, V., Marchiori, M., 2001. Efficient Behavior of Small-World Networks. *Physical Review Letters* 87, 198701.
- Lim, S.H., Dinner, D.S., Pillay, P.K., Lüders, H., Morris, H.H., Klem, G., Wyllie, E., Awad, I.A., 1994. Functional anatomy of the human supplementary sensorimotor area: results of extraoperative electrical stimulation. *Electroencephalography and Clinical Neurophysiology* 91, 179-193.
- Litvak, N., van der Hofstad, R., 2013. Uncovering disassortativity in large scale-free networks. *Physical Review E* 87, 022801.

- Lowe, M.J., Dzemidzic, M., Lurito, J.T., Mathews, V.P., Phillips, M.D., 2000. Correlations in Low-Frequency BOLD Fluctuations Reflect Cortico-Cortical Connections. *NeuroImage* 12, 582-587.
- Mori, S., Crain, B.J., Chacko, V.P., Van Zijl, P.C.M., 1999. Three-dimensional tracking of axonal projections in the brain by magnetic resonance imaging. *Annals of Neurology* 45, 265-269.
- Penfield, W., 1950. The cerebral cortex of man: a clinical study of localization of function. Macmillan, New York.
- Penfield, W., Boldrey, E., 1937. Somatic motor and sensory representation in the cerebral cortex of man as studied by electrical stimulation. *Brain: A Journal of Neurology* 60, 389-443.
- Ravasz, E., Barabási, A.L., 2003. Hierarchical organization in complex networks. *Physical Review E* 67, 026112.
- Robins, G., Pattison, P., Kalish, Y., Lusher, D., 2007. An introduction to exponential random graph (p^*) models for social networks. *Social Networks* 29, 173-191.
- Roca, P., Rivière, D., Guevara, P., Poupon, C., Mangin, J.F., 2009. Tractography-Based Parcellation of the Cortex Using a Spatially-Informed Dimension Reduction of the Connectivity Matrix. Proceedings of the 12th International Conference on Medical Image Computing and Computer-Assisted Intervention: Part I, 935-942.
- Roca, P., Tucholka, A., Rivière, D., Guevara, P., Poupon, C., Mangin, J.F., 2010. Inter-subject connectivity-based parcellation of a patch of cerebral cortex. Proceedings of the 13th International Conference on Medical Image Computing and Computer-Assisted Intervention: Part II, 347-354.
- Rubinov, M., Sporns, O., 2010. Complex network measures of brain connectivity: Uses and interpretations. *NeuroImage* 52, 1059-1069.
- Salvador, R., Suckling, J., Coleman, M.R., Pickard, J.D., Menon, D., Bullmore, E., 2005. Neurophysiological Architecture of Functional Magnetic Resonance Images of Human Brain. *Cerebral Cortex* 15, 1332-1342.
- Scannell, J., Burns, G., Hilgetag, C., O'Neil, M., Young, M., 1999. The Connectional Organization of the Cortico-thalamic System of the Cat. *Cerebral Cortex* 9, 277-299.
- Scannell, J.W., Blakemore, C., Young, M.P., 1995. Analysis of connectivity in the cat cerebral cortex. *The Journal of Neuroscience* 15, 1463-1483.
- Schleicher, A., Amunts, K., Geyer, S., Morosan, P., Zilles, K., 1999. Observer-Independent Method for Microstructural Parcellation of Cerebral Cortex: A Quantitative Approach to Cytoarchitectonics. *NeuroImage* 9, 165-177.
- Shattuck, D.W., Mirza, M., Adisetiyo, V., Hojatkashani, C., Salamon, G., Narr, K.L., Poldrack, R.A., Bilder, R.M., Toga, A.W., 2008. Construction of a 3D probabilistic atlas of human cortical structures. *NeuroImage* 39, 1064-1080.
- Simpson, S.L., Hayasaka, S., Laurienti, P.J., 2011. Exponential Random Graph Modeling for Complex Brain Networks. *PLoS ONE* 6, e20039.
- Simpson, S.L., Moussa, M.N., Laurienti, P.J., 2012. An exponential random graph modeling approach to creating group-based representative whole-brain connectivity networks. *NeuroImage* 60, 1117-1126.
- Smith, S.M., 2012. The future of FMRI connectivity. *NeuroImage* 62, 1257-1266.
- Sporns, O., Honey, C.J., Kötter, R., 2007. Identification and Classification of Hubs in Brain Networks. *PLoS ONE* 2, e1049.
- Sporns, O., Kötter, R., 2004. Motifs in Brain Networks. *PLoS Biology* 2, e369.
- Sporns, O., Tononi, G., Kötter, R., 2005. The Human Connectome: A Structural Description of the Human Brain. *PLoS Computational Biology* 1, e42.
- Sporns, O., Zwi, J., 2004. The small world of the cerebral cortex. *Neuroinformatics* 2, 145-162.
- Stobb, M., Peterson, J.M., Mazzag, B., Gahtan, E., 2012. Graph Theoretical Model of a Sensorimotor Connectome in Zebrafish. *PLoS ONE* 7, e37292.
- Toga, A.W., Clark, K.A., Thompson, P.M., Shattuck, D.W., Van Horn, J.D., 2012. Mapping the Human Connectome. *Neurosurgery* 71, 1-5.
- Tuch, D.S., 2004. Q-ball imaging. *Magnetic Resonance in Medicine* 52, 1358-1372.
- Tzourio-Mazoyer, N., Landeau, B., Papathanassiou, D., Crivello, F., Etard, O., Delcroix, N., Mazoyer, B., Joliot, M., 2002. Automated Anatomical Labeling of Activations in SPM Using a Macroscopic Anatomical Parcellation of the MNI MRI Single-Subject Brain. *NeuroImage* 15, 273-289.
- Van Essen, D.C., 2005. A Population-Average, Landmark- and Surface-based (PALS) atlas of human cerebral cortex. *NeuroImage* 28, 635-662.

CHAPTER 3

- Van Essen, D.C., Glasser, M.F., Dierker, D.L., Harwell, J., Coalson, T., 2012. Parcellations and Hemispheric Asymmetries of Human Cerebral Cortex Analyzed on Surface-Based Atlases. *Cerebral Cortex* 22, 2241-2262.
- Varshney, L.R., Chen, B.L., Paniagua, E., Hall, D.H., Chklovskii, D.B., 2011. Structural Properties of the *Caenorhabditis elegans* Neuronal Network. *PLoS Computational Biology* 7, e1001066.
- Vogt, C., Vogt, O., 1919. Allgemeine Ergebnisse unserer Hirnforschung. Johann Ambrosius Barth Verlag, Leipzig.
- Wang, J., Wang, L., Zang, Y., Yang, H., Tang, H., Gong, Q., Chen, Z., Zhu, C., He, Y., 2009. Parcellation-dependent small-world brain functional networks: A resting-state fMRI study. *Human Brain Mapping* 30, 1511-1523.
- Watts, D.J., Strogatz, S.H., 1998. Collective dynamics of 'small-world' networks. *Nature* 393, 440-442.
- Wedeen, V.J., Hagmann, P., Tseng, W.Y.I., Reese, T.G., Weisskoff, R.M., 2005. Mapping complex tissue architecture with diffusion spectrum magnetic resonance imaging. *Magnetic Resonance in Medicine* 54, 1377-1386.
- White, J.G., Southgate, E., Thomson, J.N., Brenner, S., 1986. The Structure of the Nervous System of the Nematode *Caenorhabditis elegans*. *Philosophical Transactions of the Royal Society of London B: Biological Sciences* 314, 1-340.
- van Wijk, B.C.M., Stam, C.J., Daffertshofer, A., 2010. Comparing Brain Networks of Different Size and Connectivity Density Using Graph Theory. *PLoS ONE* 5, e13701.
- Williams, R.W., Herrup, K., 1988. The Control of Neuron Number. *Annual Review of Neuroscience* 11, 423-453.
- Young, M.P., 1993. The Organization of Neural Systems in the Primate Cerebral Cortex. *Proceedings of the Royal Society of London B: Biological Sciences* 252, 13-18.
- Yu, Q., Sui, J., Liu, J., Plis, S.M., Kiehl, K.A., Pearlson, G., Calhoun, V.D., 2013. Disrupted correlation between low frequency power and connectivity strength of resting state brain networks in schizophrenia. *Schizophrenia Research* 143, 165-171.
- Zalesky, A., Fornito, A., Harding, I.H., Cocchi, L., Yücel, M., Pantelis, C., Bullmore, E.T., 2010. Whole-brain anatomical networks: Does the choice of nodes matter? *NeuroImage* 50, 970-983.
- Zalesky, A. et al., 2012. Effect of long-term cannabis use on axonal fibre connectivity. *Brain* 135, 2245-2255.
- Zilles, K., Amunts, K., 2010. Centenary of Brodmann's map – conception and fate. *Nature Reviews Neuroscience* 11, 139-145.
- Zilles, K., Palomero-Gallagher, N., Grefkes, C., Scheperjans, F., Boy, C., Amunts, K., Schleicher, A., 2002. Architectonics of the human cerebral cortex and transmitter receptor fingerprints: reconciling functional neuroanatomy and neurochemistry. *European Neuropsychopharmacology* 12, 587-599.



Chapter 4

Estimating false positives and negatives in brain networks

*Based on a publication (NeuroImage, vol. 70, 2013, pp. 402-409) by
Marcel A. de Reus and Martijn P. van den Heuvel*

Abstract

The human brain is a complex network of anatomically segregated regions interconnected by white matter pathways, known as the human connectome. Diffusion tensor imaging can be used to reconstruct this structural brain network *in vivo* and noninvasively. However, due to a wide variety of influences, both false positive and false negative connections may occur. By choosing a *group threshold*, brain networks of multiple subjects can be combined into a single reconstruction, affecting the occurrence of these false positives and negatives. In this case, only connections that are detected in a large enough percentage of the subjects, specified by the group threshold, are considered to be present. Although this group threshold has a substantial impact on the resulting reconstruction and subsequent analyses, it is often chosen intuitively. Here, we introduce a model to estimate how the choice of group threshold influences the presence of false positives and negatives. Based on our findings, group thresholds should preferably be chosen between 30 and 90%. Our results further suggest that a group threshold of circa 60% is a suitable setting, providing a good balance between the elimination of false positives and false negatives.

Introduction

The human brain is a complex system. On a macroscopic scale, anatomically segregated brain regions and bundles of axonal fibers constitute a network (Bullmore and Sporns, 2009; van den Heuvel et al., 2010), known as the structural human connectome (Sporns, 2011; Sporns et al., 2005). By tracing white matter pathways (Conturo et al., 1999; Mori et al., 1999), diffusion tensor imaging (DTI) tractography allows *in vivo* and noninvasive reconstruction of this structural brain network (Gong et al., 2009; Hagmann et al., 2007). However, due to a variety of influences and technical limitations, not all fiber pathways can be traced with equal accuracy (Dauguet et al., 2007; Jbabdi and Johansen-Berg, 2011). From a network perspective, there are two types of errors that may occur in the reconstruction. Brain regions which are erroneously connected give rise to false positives, while existing connections between brain regions that are absent in

the reconstruction result in false negatives.

When studying the network characteristics of the healthy human brain (Bassett et al., 2011; Gong et al., 2009; Hagmann et al., 2008; van den Heuvel et al., 2012) or differences between groups (Brown et al., 2011; van den Heuvel et al., 2010; Lynall et al., 2010; Stam et al., 2007; Zalesky et al., 2012; Zalesky et al., 2011), it is often desirable to make a combined reconstruction across a group of subjects, influencing the occurrence of false positives and negatives. One commonly applied method to create such a combined reconstruction is to set a so-called *group threshold*, reflecting the number of subjects (usually expressed as a percentage of the total group) that have to share a connection before it is included. The combined reconstruction then consists of those connections whose prevalence (i.e., detection count) equals or exceeds this group threshold (Hagmann et al., 2008; van den Heuvel and Sporns, 2011; Honey et al., 2009).

The choice of group threshold, which will be shown to have a substantial impact on the network properties of the reconstruction, is subject to a conflict between eliminating false positives and preventing false negatives. High group thresholds require a connection to be present in many subjects, improving the accuracy of reported connections and thus eliminating false positives, while low group thresholds allow the inclusion of existing connections that are difficult to reconstruct and therefore prevent false negatives. This choice of setting a particular group threshold is typically based on the researcher's intuition, which may introduce a bias and reduce the comparability of group-based results across studies. Here, we aim to provide systematic insight into the influence of the group threshold on connectome reconstruction. First, we examine the effect of the group threshold on overall network organization. Second, we introduce a computational model to quantify the influence of the group threshold on the occurrence of false positives and negatives in the combined reconstruction.

Materials and methods

Data acquisition

Analyses were performed on a collection of reconstructed structural brain networks of 50 healthy subjects. The reconstructions reflect the connectivity of 68 cortical brain areas and were obtained at the University Medical Center Utrecht using diffusion tensor imaging and deterministic streamline tractography as described previously (van den Heuvel et al., 2010; van den Heuvel and Sporns, 2011).

For each subject, two high-angular DTI sets with opposite k -space readouts (Andersson et al., 2003) were obtained to find the preferred diffusion direction in $2 \times 2 \times 2$ mm voxels using a robust tensor fitting method (Chang et al., 2005). Fiber pathways were reconstructed by following this preferred diffusion direction from voxel to voxel as prescribed by the FACT algorithm (Mori et al., 1999). Moreover, on the basis of a T1-weighted image, the cortical surface was automatically parcellated (Fischl et al., 2004) into 68 anatomically distinct brain regions using the FreeSurfer software suite (<http://surfer.nmr.mgh.harvard.edu>). A structural connection between two such brain regions was considered to be detected, and thus included in the subject's brain network reconstruction, if at least one traced fiber pathway touched both regions. A more elaborate description of the reconstruction procedure is provided in a section with Supplementary Information (SI) at the end of the chapter.

An independent set of 30 reconstructed networks of healthy individuals (Brown et al., 2011) was retrieved from the UCLA Multimodal Connectivity Database to replicate findings and to assess the influence of acquisition parameters and the included number of subjects. Like the reconstructions in the principal data collection, these additional reconstructions were obtained using DTI and the FACT tractography algorithm. However, the Harvard-Oxford probabilistic cortical atlas, as distributed with the FMRIB Software Library (<http://fsl.fmrib.ox.ac.uk>), was used for cortical parcellation, resulting in 96 instead of 68 different brain regions.

In addition, there were several more subtle differences between the reconstruction procedures. Most notably, Brown et al. (2011) required the existence of at least three traced fibers between two brain regions before declaring them connected.

Combined reconstructions

Combined reconstructions were created by including only those connections whose prevalence equaled or exceeded a chosen group threshold. To be precise, given a group threshold t (expressed as a percentage) and a sample of m reconstructed brain networks, a connection was taken to be present in the combined reconstruction if it existed in at least $(t/100) \times m$ individual reconstructions.

Impact on network metrics

Using several commonly used network metrics, the impact of the group threshold on network organization was examined. Combined reconstructions were created for each group threshold and their network density, normalized characteristic path length, normalized clustering coefficient, and degree assortativity (Newman, 2002) were computed using the Brain Connectivity Toolbox (Rubinov and Sporns, 2010). For the normalization of clustering coefficient and path length, null distributions were obtained by randomizing each combined reconstruction 250 times while preserving the degree sequence (van den Heuvel et al., 2012; van den Heuvel and Sporns, 2011; Maslov and Sneppen, 2002; Rubinov and Sporns, 2010).

Next, the above procedure was repeated with group thresholds of 20, 40, 60, and 80% for 1000 groups of 25 reconstructions that were randomly drawn from the original set of 50 reconstructions. For each metric, the four resulting distributions – corresponding to the mentioned thresholds – were subsequently compared using t -tests to determine whether differences between group thresholds were significant.

Proposed model

To estimate the impact of the group threshold on false positives and negatives, we propose a model based on the rationale that connections that are consistently detected in a large percentage of the subjects are more likely to exist than connections that are only detected in a few subjects. A central role in our model is reserved for the prevalence distribution $p(k)$, which assigns to every integer k between zero and the sample size the number of connections with prevalence k (i.e., the number of connections that were detected precisely k times).

Assuming little biological variation in the presence of connections across subjects, it is in theory possible to classify connections as existing or non-existing. As a result, the prevalence distribution can be decomposed into a distribution $p_{\text{ex}}(k)$, counting existing connections, and a distribution $p_{\text{non}}(k)$, counting non-existing connections. By approximating this theoretical decomposition, the impact of the group threshold on false positives and false negatives may be estimated as follows.

If t denotes the group threshold and m the sample size, a connection is present in the combined reconstruction if its prevalence is greater than or equal to $(t/100) \times m$. Because false positives are non-existing connections that are nevertheless present in the reconstruction, the number of false positives in the combined reconstruction is given by

$$n_{\text{fp}}(t) = \sum_{k=\lceil(t/100)m\rceil}^m p_{\text{non}}(k). \quad (4.1)$$

Similarly, false negatives are existing connections that are not present in the reconstruction, so the number of false negatives in the combined reconstruction is given by

$$n_{\text{fn}}(t) = \sum_{k=0}^{\lceil(t/100)m\rceil-1} p_{\text{ex}}(k). \quad (4.2)$$

To approximate $p_{\text{ex}}(k)$ and $p_{\text{non}}(k)$, the sum of two model functions is fitted to the prevalence distribution. Since connections that are (almost) never detected are unlikely to exist and connections that are (almost) always detected are likely to exist, it should hold that $p(k) \approx p_{\text{non}}(k)$ for values of k near zero and $p(k) \approx p_{\text{ex}}(k)$ for values of k near the sample size. In other words, the left and right hand side of the prevalence distribution provide a preview of $p_{\text{non}}(k)$ and $p_{\text{ex}}(k)$, respectively. These previews can be used to find model functions for $p_{\text{ex}}(k)$ and $p_{\text{non}}(k)$ and because the sum of $p_{\text{ex}}(k)$ and $p_{\text{non}}(k)$ has to be equal to $p(k)$, fitting the sum of these model functions to the prevalence distribution gives the desired approximations.

Implementation

Based on the previews offered by the prevalence distribution (Figure 4.1a),

$$f_{\text{non}}(c, x) = \frac{c_1}{m^{-c_2} + c_3} - \frac{c_1}{x^{-c_2} + c_3} \quad (4.3)$$

and

$$f_{\text{ex}}(d, x) = \frac{d_1}{m^{-d_2} + d_3} - \frac{d_1}{(m - x)^{-d_2} + d_3} \quad (4.4)$$

were taken as model functions for $p_{\text{non}}(k)$ and $p_{\text{ex}}(k)$ respectively. In these equations, m denotes the sample size, $c = (c_1, c_2, c_3)$ and $d = (d_1, d_2, d_3)$ are the fitting parameters, and x is the continuous version of k ; a one-dimensional variable ranging between 0 and m . When the fitting parameters c and d are chosen appropriately, these model functions closely resemble the prevalence distribution on, respectively, the start and end of its domain, outperforming other candidates such as exponential and scale-free functions. The model functions are of the same functional form, only reflected in the line $k = m/2$, and are chosen such that $f_{\text{non}}(c, m) = 0$ and $f_{\text{ex}}(d, 0) = 0$ (i.e., consistently detected connections are assumed to exist and connections that are never detected are assumed to be absent).

A fitting approach dedicated to this specific situation was used to determine the

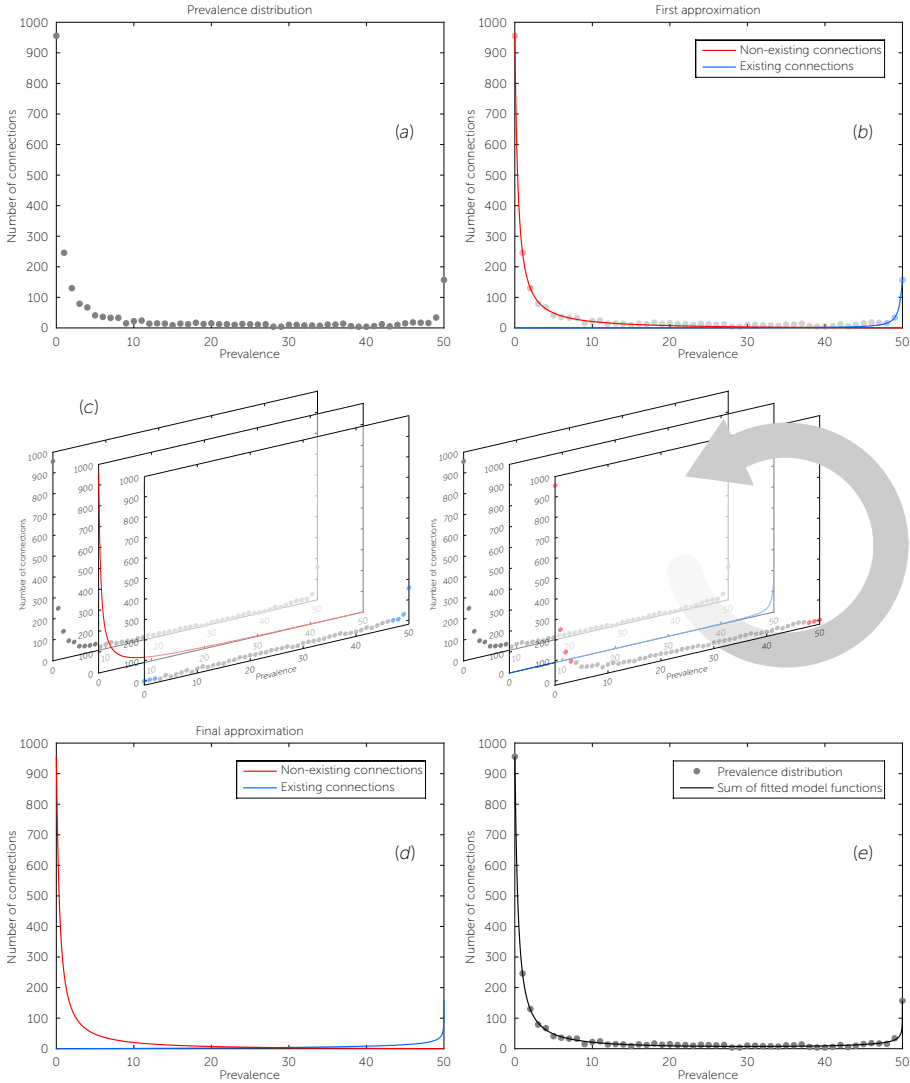


Figure 4.1. Decomposition of the prevalence distribution. (a) Based on the prevalence distribution, model functions were chosen for the components p_{non} and p_{ex} , which respectively count the non-existing and existing connections. (b) By fitting these model functions to the data points near $k = 0$ and $k = m$, first estimates of the contributions of p_{non} and p_{ex} were obtained. (c) After correcting the prevalence distribution for the estimated contribution of their complement, improved estimates were obtained by refitting the model functions to a larger number of data points. (d) Repeated application of the previous step resulted in a final approximation of the decomposition. (e) By design, the sum of the approximated components is a good fit for the prevalence distribution.

optimal values of c and d . Rather than fitting the sum $f_{\text{non}}(c, x) + f_{\text{ex}}(d, x)$ directly to $p(k)$, which does not take into account that $f_{\text{non}}(c, x)$ and $f_{\text{ex}}(d, x)$ should fit almost perfectly to the data points near $k = 0$ and $k = m$ respectively, the components $f_{\text{non}}(c, x)$ and $f_{\text{ex}}(d, x)$ were iteratively fitted to prevalence data corrected for the contribution of their complement (Figure 4.1). After establishing the optimal values of c and d , estimated numbers of false positives and negatives were obtained by replacing $p_{\text{non}}(k)$ and $p_{\text{ex}}(k)$ in equations (4.1) and (4.2) by their approximations $f_{\text{non}}(c, k)$ and $f_{\text{ex}}(d, k)$. Details of the fitting approach are provided in the SI section.

Error rates

From the estimated numbers of false positives and negatives, the associated error rates were derived. Using the same notation as above, the false positive rate α is given by

$$\alpha(t) = \frac{n_{\text{fp}}(t)}{\sum_{k=\lceil(t/100)m\rceil}^m p(k)}. \quad (4.5)$$

That is, the number of false positives divided by the total number of connections in the combined reconstruction. Analogously, the false negative rate β is obtained by dividing the number of false negatives by the total number of non-existing connections in the combined reconstruction and thus given by

$$\beta(t) = \frac{n_{\text{fn}}(t)}{\sum_{k=0}^{\lceil(t/100)m\rceil-1} p(k)}. \quad (4.6)$$

Model validation

Due to the absence of ground truth, it is difficult to validate the proposed model (i.e., to check if estimated numbers of false positives and negatives are accurate). Yet, to some extent, the model and its underlying ideas can be tested indirectly. In the context of the model, the total number of existing connections is estimated by

$$\sum_{k=0}^m f_{\text{ex}}(d, k). \quad (4.7)$$

Like the actual number of existing connections, this estimate should be independent of the sample size. To verify this, the number of existing connections was estimated in 10,000 bootstrap samples (i.e., samples randomly drawn from the original collection of 50 reconstructions) for each sample size between 15 and 35 subjects.

Another possibility to circumvent the absence of ground truth, is to test the proposed model on a collection of simulated networks. To this end, we have developed a preliminary method that approximately reproduced the variation witnessed in the collection of reconstructed brain networks by making changes to fifty copies of a randomly chosen blueprint. Rather than modifying connections according to uniformly distributed probabilities, which resulted in an entirely different prevalence pattern (Supplementary Figure 4.1a), preferential attachment was employed to match the characteristic shape of the prevalence distribution (Supplementary Figure 4.1b). Using the ground truth provided by the blueprint, an assessment of the proposed model's accuracy was made. A detailed description of all the steps involved can be found in the SI section.

Replication dataset

The proposed model was also used to estimate the impact of the group threshold on reconstruction errors in the independent collection of brain networks from the UCLA Multimodal Connectivity Database.

Results

Impact on network metrics

All tested network metrics displayed significantly different values between the selected group thresholds of 20, 40, 60, and 80% ($p < 0.001$, Bonferroni corrected, Figure 4.2b), underscoring the importance of good insight in the choice of the group threshold t . As can be seen from Figure 4.2a, the combined reconstruction did not exhibit a small-world topology, characterized by a high normalized clustering coefficient and a low normalized path length (Watts and

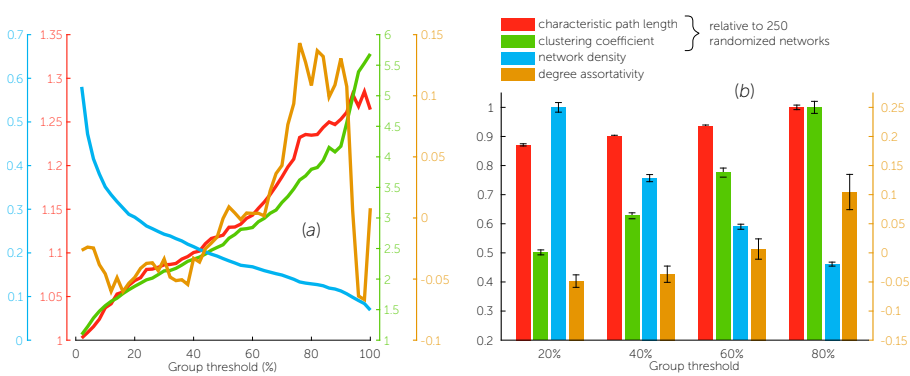


Figure 4.2. Influence of group threshold on commonly used network metrics. (a) Network density, normalized characteristic path length, normalized clustering coefficient, and degree assortativity as function of group threshold. (b) Normalized values of previously described network metrics, averaged over 1000 bootstrap samples. The error bars indicate the standard deviation. Because of the change of sign, degree assortativity values are presented on a separate axis.

Strogatz, 1998), if all measured connections were included (i.e., $t = 1\%$). When larger group thresholds were taken, the normalized clustering coefficient increased more rapidly than the normalized path length and the commonly reported small-world topology (Gong et al., 2009; Hagmann et al., 2007; He et al., 2007; van den Heuvel et al., 2008; Stam, 2004) emerged. Taken together, these findings confirm the intuition of a clear impact of the group threshold on network organizational properties.

Impact on false positives and negatives

The modeled impact of the group threshold on the number of false positives and negatives in the combined reconstruction is shown in Figure 4.3a. As expected, the estimates show that increasing the group threshold causes a decrease in false positives and an increase in false negatives. In addition, Figure 4.3a shows that also the rates of these changes (corresponding to the slopes of the curves) increase and decrease respectively. At low settings of t ($t < 30\%$), the number of false positives decreases rapidly and the number of false negatives stays relatively stable. At high group threshold settings ($t > 90\%$), this effect is reversed (although less pronounced), with an almost stable number of false positives and a quickly increasing number of false negatives. At intermittent levels ($30\% \leq t \leq 90\%$), the decrease in false positives is about the same size as the increase in false negatives, indicating a fair trade-off between the two types of errors.

As a result, the total number of errors (i.e., false positives plus false negatives) decreases during the first part of the threshold range and then increases again towards the end. This effect is visualized by the error decrease rate (Figure 4.3b), computed as the difference in total number of errors between each two subsequent group thresholds.

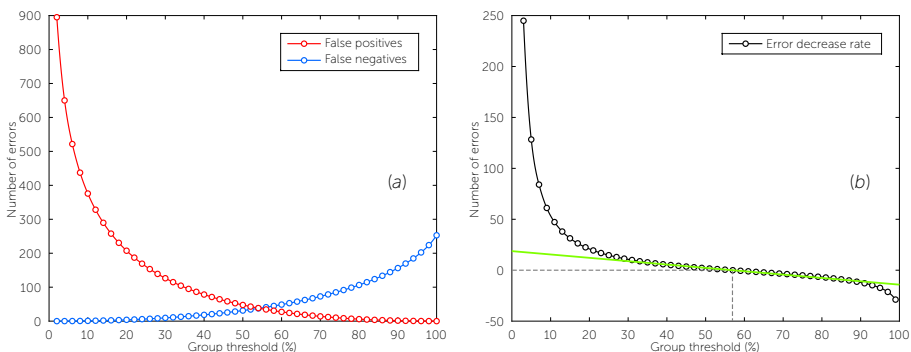


Figure 4.3. Estimated impact of the group threshold on false positives and negatives. (a) Number of false positives and negatives in the combined reconstruction for each group threshold as estimated by the proposed model. (b) Error decrease rate as function of group threshold. Data points represent the difference in total number of errors (i.e., false positives plus false negatives) between two subsequent group thresholds. If raising the group threshold increased the number of errors, the difference is negative. The straight line provides a visual aid to identify regions of rapid decay.

quent group thresholds. The turning point, at which the total number of errors is minimal, was found to be located around a group threshold of 57% (Figure 4.3b). Moreover, the change in the error decrease rate was revealed to be stable on a large portion of the threshold range. Only when the group threshold ranges between 1 and 30% and between 90 and 100%, the error decrease rate was found to change more rapidly (Figure 4.3b).

Impact on error rates

The estimated impact of the group threshold on the false positive error rate and the false negative error rate shown in Figure 4.4 is very similar to the impact on the absolute number of false positives and negatives. The most notable difference is a shift towards the right of the equilibrium, related to the effect of the group threshold on network density. While the number of false positives and false negatives are estimated to be equal at a group threshold of circa 54%, the associated error rates are equal at a group threshold of approximately 71%. Overall, (the slopes of) the error rates (Figure 4.4) tend to change more gently than (the slopes of) the absolute number of false positives and negatives (Figure 4.3a).

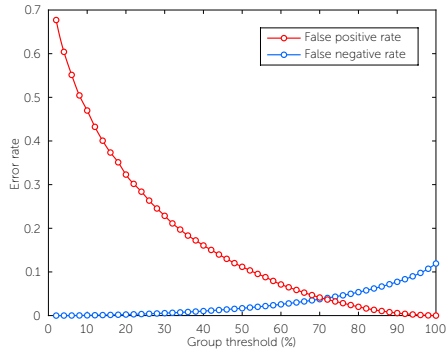


Figure 4.4. Estimated false positive and false negative rates as functions of the group threshold.

Model validation

Figure 4.5 shows the relationship between the estimated number of existing connections and the sample size (see Materials and methods). As expected, the two variables are independent. On average, the number of existing connections was estimated to be equal to 420.7 (corresponding to a network density of 18.5%) and there was only a 3.5 connection difference between the sample size

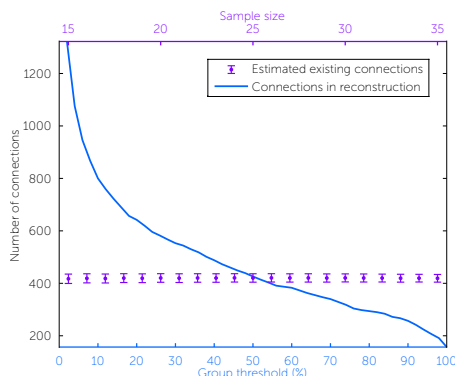


Figure 4.5 Estimated number of existing connections as function of sample size. For each sample size between 15 and 35 subjects, the mean and standard deviation of the number of existing connections as estimated for 10,000 bootstrap samples are displayed. In addition, the number of connections in the combined reconstruction is shown for each group threshold.

root mean square error of 2.5 connections, demonstrating a high level of accuracy in this simulated context. With a root mean square error of 12 connections, the estimated numbers of false positives and false negatives were found to be somewhat less accurate, though still within an acceptable range. Supplementary Figure 4.1c shows that the estimated false positive and false negative curves are also qualitatively similar to the ground truth.

Replication dataset

Similar results were found for the independent set of reconstructed brain networks from the UCLA Multimodal Connectivity Database (Supplementary Figure 4.2). Since the cerebral cortex was divided in 96 rather than 68 regions, resulting in a larger number of possibly connected brain regions, the absolute numbers of estimated connections and errors are higher than in the principal data collection. Apart from this scaling effect, the estimates for the two datasets are largely in agreement. Specific group thresholds, such as the one that minimizes the total number of errors, differ by at most seven percentage points.

with the highest and lowest mean. At a group threshold of about 51%, the average estimated number of existing connections was found to coincide with the number of connections in the combined reconstruction.

When applied to the collection of simulated networks associated with the prevalence distribution shown in Supplementary Figure 4.1b, the proposed model approximated the decomposition of the prevalence distribution with a

Discussion

Based on the quantifications provided by our model (Figure 4.3 and Figure 4.4), the most informative combined connectome reconstructions, balancing elimination of false positives and prevention of false negatives, are formed using a group threshold within the range of 30 to 90%. The results of our study further show that the group threshold – reflecting the number of subjects that have to share a connection before it is included in the reconstruction – has a substantial impact on commonly used network metrics (Figure 4.2), underlining the importance of systematic insight in the choice of this parameter.

The trade-off between false positives and false negatives inherent to the choice of group threshold is quantified by the error decrease rate (measuring change in the total amount of errors, Figure 4.3b) and (the slopes of) the false positive and false negative curves (Figure 4.3a). According to the estimates of our model, this trade-off is best balanced and most stable when the group threshold is set within the range of 30 to 90%. On this interval, changes in estimated numbers of false positives and negatives are of comparable size (Figure 4.3a), and the error decrease rate attains its smallest (absolute) values and decays linearly (Figure 4.3b). In contrast, Figure 4.3a shows that a decrease of the group threshold from 30 to 1% prevents only about 10 false negatives at the cost of more than 700 false positives. Similarly, increasing the group threshold from 90 to 100% eliminates only one false positive, while the number of false negatives increases by approximately 100. This suggests a non-optimal situation at these low and high group thresholds.

As shown by Figure 4.2 and Figure 4.3, the combined reconstruction still changes substantially between a group threshold of 30 and 90%. Within this range, group threshold settings that optimize one specific aspect of the reconstruction provide important markers for which setting could be regarded as generally optimal. First, the number of false positives and false negatives were found to be equal at a group threshold of 54% (Figure 4.3a). Second, their corresponding error rates were in balance at a threshold of 71% (Figure 4.4). Third, the total

number of errors was found to be minimal at 57% (Figure 4.3b). And, fourth, the number of connections in the combined reconstruction best approximated the estimated number of existing connections at 51% (Figure 4.5). Although some applications may specifically require strong elimination of false positives (i.e., a higher threshold) or false negatives (i.e., a lower threshold), these markers suggest that in most situations a group threshold of about 60% is a suitable choice.

The model-free measurements of the normalized path length and clustering coefficient (Figure 4.2) show that the more than seven hundred connections that were present at a threshold of 1%, but not at a threshold of 30%, caused the combined reconstruction to lose its small-world characteristics. As it is likely that brain networks exhibit a small-world topology (Hagmann et al., 2007; He et al., 2007; van den Heuvel et al., 2008; Hilgetag et al., 2000; Micheloyannis et al., 2006; Salvador et al., 2005; Stam, 2004), the inclusion of these connections presumably made the combined reconstruction less accurate. As a consequence, the majority of these connections are likely to be false positives, which is consistent with the above mentioned estimate of ten prevented false negatives at the cost of more than 700 false positives. Like the results (Figure 4.5 and Supplementary Figure 4.1) of the indirect validation tests described in the *Model validation* sections, this observation adds credibility to the model.

Despite differences in reconstruction procedure, our model produced similar estimates for the data collection that was retrieved from the UCLA Multimodal Connectivity Database (Supplementary Figure 4.2). The adoption of a different parcellation scheme unavoidably led to different quantitative estimates due to an increase in brain region pairs, but conclusions and qualitative descriptions were found to be the same for both datasets. An interesting question, to be addressed in future work, is how more substantial shifts in location and number of cortical parcels would affect our model. One might speculate that higher spatial resolutions cause an increase of the observed inter-subject variation, possibly diminishing the peak at the right hand side of the prevalence distribution. If this is indeed the case, the proposed model may have to be adapted before being

applicable to collections of high-resolution reconstructions.

Recently, Simpson et al. (2012) introduced a promising novel approach to create group-based representatives of functional brain networks by utilizing exponential random graph models, extending their excellent work on the use of these models for analysis and simulation of individual brain networks (Simpson et al., 2011). Even though this method has not yet been tested on structural brain networks, it would be interesting to compare the approach proposed by Simpson and colleagues with group threshold-based reconstruction. Considering the different nature of the two approaches, they might be able to complement each other. Another topic that can be of possible interest is the exploitation of connection weights (number of detected streamlines, mean fractional anisotropy, etc.) typically available for structural brain network reconstructions. The use of such weights to discriminate between reliable and spurious connections was briefly investigated, but it is not yet clear whether this could contribute to the method presented here.

One of the advantages of making group-based reconstructions lies in the examination of network properties that cannot be captured by a simple numeric measure. While scalar-valued network metrics, like those in the *Impact on network metrics* sections, could also be averaged over individual reconstructions, information about, e.g., community structure, (path) motifs and dynamic flow patterns is hard to combine. And even for scalar-valued network measures, computing values on a group-based reconstruction might be advantageous over averaging subject values. Indeed, combining reconstructions through application of a carefully chosen group threshold may reduce the influence of the noise known to be present in diffusion tractography reconstructions (Bassett et al., 2011; Cammoun et al., 2012; Jones and Pierpaoli, 2005), giving more reliable network estimates and increasing power to detect differences between groups. A simple post-hoc analysis, comparing bootstrap distributions of metric values in combined reconstructions (see Impact on network metrics) with subject specific outcomes, showed that metrics of the combined reconstruction at

the preferred group threshold of 60% lay within circa three standard deviations of averaged subject metrics while differing significantly from them ($p < 0.001$, Bonferroni corrected).

Assumptions

Our proposed model is based on two assumptions, which should be regarded as potential limitations and need to be taken into account when interpreting the estimated group threshold effects. The first one, being the assumption of little biological variation in the presence of connections across subjects, is implicitly present in many studies on brain networks. For example, network studies of the brain of nonhuman mammals typically use connectivity data obtained from a multitude of tracer studies, originating from numerous different animals, to create a reconstructed brain network (Felleman and Van Essen, 1991; Honey et al., 2007; Scannell and Young, 1993; Young, 1993). Especially on the macroscopic scale of interest, it may be argued that individual variation is more likely to affect strength and quality rather than presence of connections.

If biological variation in presence of connections would be negligible, the characteristic spread of the prevalence distribution would be predominantly the result of reconstruction errors. Although test-retest studies indicate that such reconstruction errors indeed play an important role (Bassett et al., 2011; Cammoun et al., 2012; Jones and Pierpaoli, 2005), correlations between binary network measures and cognitive performance reported in literature (Li et al., 2009; Zalesky et al., 2011) suggest that the observed variation also contains biologically relevant information. The characteristic prevalence pattern is therefore likely to originate from a combination of biological variation and reconstruction errors. For the proposed model, it suffices if the biological variation is small enough to admit a common substrate for structural brain networks. Combining individual reconstructions through the setting of a group threshold should then be viewed as an attempt to extract this common substrate from the observed data and the proposed model estimates how well the combined reconstruction resembles the common substrate.

The second assumption behind our proposed model is that connections that are consistently detected in a large percentage of the subjects are more likely to exist (in an underlying common substrate) than connections that are detected in only a few subjects. In particular, the model functions displayed in equations (4.3) and (4.4) classify connections that are detected in all subjects as existing and connections that are never detected as non-existing. In view of the difficulty of tracing long-distance fibers with diffusion tractography (Jbabdi and Johansen-Berg, 2011), the classification of connections that are never detected as non-existing might be too rigid. However, with the large sample used in this study, this discrepancy is believed to be small.

Conclusion

Quantifying the effect of the group threshold on connectome reconstruction and organization, our findings indicate that the best group thresholds for structural brain network reconstruction lie within the range of 30 to 90%. Our results further suggest that, for most applications, a group threshold of circa 60% is a suitable choice.

Supplementary information

Brain network reconstruction

Analyses were performed on a collection of reconstructed structural brain networks of 50 healthy subjects (mean age [std]: 29.2 [7.9] years; 32 males, 18 females) with no history of neurological or psychiatric disorders. The reconstructions were obtained at the University Medical Center Utrecht using diffusion tensor imaging (DTI) (Basser et al., 1994) and deterministic streamline tractography (Mori et al., 1999) and reflect the connectivity of 68 cortical brain areas, identified by the FreeSurfer software suite (<http://surfer.nmr.mgh.harvard.edu>). All subjects gave written informed consent and acquisition of the data was conducted in line with the Declaration of Helsinki and approved by the medical ethics committee for research in humans of the University Medical Center Utrecht (Utrecht, The Netherlands). Details of the reconstruction procedure, successfully applied before (van den Heuvel et al., 2009; van den Heuvel et al., 2010; van den Heuvel and Sporns, 2011; Mandl et al., 2010; de Weijer et al., 2011), are discussed below.

Data acquisition and correction

For each subject, two high-angular DTI sets with opposite k -space readouts, each consisting of diffusion-weighted scans for 30 different gradient directions (Jones, 2004; Jones et al., 1999) and 5 unweighted $b = 0$ scans, were made on a 3-Tesla Philips Achieva clinical scanner at the University Medical Center Utrecht, using an 8-channel SENSE receiver head coil and the following acquisition parameters: parallel imaging (SENSE) with a p reduction of 3; TR/TE, 7035/68 ms; 2 mm isotropic voxels; 75 slices covering the whole brain; b -weighting of 1000 s/mm². To correct for possible susceptibility distortions, a field distortion map, based on the $b = 0$ images, was applied to the two sets of 30 diffusion-weighted images, resulting in a single set of 30 weighted images and one $b = 0$ image (Andersson et al., 2003). The diffusion images of this single set were subsequently corrected for eddy-current distortions (Andersson and Skare, 2002) and realigned to the

$b = 0$ image. For anatomical reference, a T1-weighted image (3D fast field echo using parallel imaging; TR/TE, 10/4.6 ms; FOV, 240 × 240 mm; 0.75 mm isotropic voxels; 200 slices covering the whole brain) was acquired directly after the diffusion-weighted images and a brain mask was created.

Reconstruction of white matter fibers

Together, the 30 acquired and corrected diffusion images form a diffusion profile. Within each 2 × 2 × 2 mm voxel of the brain mask, a tensor was fitted to this diffusion profile using a robust tensor fitting method (Chang et al., 2005). From the eigenvalue decomposition of this tensor, the preferred diffusion direction within the voxel, taken to be the direction of the principal eigenvector, and fractional anisotropy (FA), measuring the level of preferred diffusion (Beaulieu and Allen, 1994), were extracted. Next, streamlines were started from eight evenly distributed seeds in each voxel, following the main diffusion direction from voxel to voxel, hence reconstructing the white matter fibers. The propagation of streamlines in this deterministic fiber tracking procedure was carried out using the FACT (fiber assignment by continuous tracking) algorithm (Mori et al., 1999; Mori and van Zijl, 2002). A streamline was stopped when it reached a voxel with an FA value < 0.1, when the trajectory of the traced fiber left the brain mask, or when the fiber tract made a sharp turn of > 45°.

Cerebral cortex parcellation

On the basis of the T1-weighted image, the cortical surface was automatically parcellated (Fischl et al., 2004) into 68 anatomically distinct brain regions using the FreeSurfer software suite (<http://surfer.nmr.mgh.harvard.edu>) according to the Desikan-Killiany cortical brain atlas (Desikan et al., 2006).

Reconstruction of individual brain networks

By combining the parcellation of the cerebral cortex with the collection F of reconstructed white matter fiber tracts, the cortical brain network of each subject was reconstructed. The 68 anatomically segregated brain regions from the

parcellation were defined to be the nodes of the network and, for each pair of brain regions i and j , a connection was placed between the corresponding nodes if the collection F contained a reconstructed fiber that touched both region i and j . The reconstructions obtained in this way only contain information about the presence of connections between brain regions, without making inferences on their strength, and are therefore known as *binary* or *unweighted* reconstructions.

Fitting approach

The sum of the model functions $f_{\text{non}}(c, x)$ and $f_{\text{ex}}(d, x)$ was fitted to the prevalence distribution $p(k)$ using the following approach. First, data points near $k = 0$ and $k = m$ were used to obtain initial fits for $f_{\text{non}}(c, x)$ and $f_{\text{ex}}(d, x)$, giving rough estimates of the contributions of $p_{\text{non}}(k)$ and $p_{\text{ex}}(k)$ to the prevalence distribution. Next, $f_{\text{non}}(c, x)$ was fitted to selected data points of $p(k)$ from which the estimated contribution of $p_{\text{ex}}(k)$ was removed and, similarly, $f_{\text{ex}}(d, x)$ was fitted to selected data points of $p(k)$ from which the estimated contribution of $p_{\text{non}}(k)$ was removed, giving improved estimates of the contributions of $p_{\text{non}}(k)$ and $p_{\text{ex}}(k)$. This procedure was repeated until the selected data points, which were extended step by step to the middle from the initial data points near $k = 0$ and $k = m$ on the sides, covered the entire range from $k = 0$ to $k = m$.

The pseudo-code below outlines the used MATLAB implementation of this algorithm. The parameter q controls the number of data points used for the first estimates. Like the shown initial guesses, it was empirically established that $q = 2$ (corresponding to three data points on each side) is a suitable choice. A non-linear least-squares method was used as fit function.

Pseudo-code

% Collect input.

get $\{p(k) \mid 0 \leq k \leq m\}$, q

% Use the $q + 1$ most left and right points of p ...

$D_{\text{non}} = \{(k, p(k)) \mid 0 \leq k \leq q\}$

$D_{\text{ex}} = \{(k, p(k)) \mid m - q \leq k \leq m\}$

% ... and the following initial guesses ...

$c_0 = (p(0), 1, 0)$

$d_0 = (p(m), 1, 0)$

% ... for the first estimates of p_{non} and p_{ex} .

$c_0 = \text{fit}(f_{\text{non}}(c, x), D_{\text{non}}, c_0)$

$d_0 = \text{fit}(f_{\text{ex}}(d, x), D_{\text{ex}}, d_0)$

% Obtain increasingly accurate estimates of p_{non} and p_{ex} by fitting $f_{\text{non}}(c, x)$ and

% $f_{\text{ex}}(d, x)$ iteratively to prevalence data corrected for the contribution of their

% complement.

$i = 1$

while $|D_{\text{non}}| < m + 1$

$D_{\text{non}} = \{(k, p(k) - f_{\text{ex}}(d_0, k)) \mid 0 \leq k \leq q + i, m - (q + i - 1) \leq k \leq m\}$

$D_{\text{ex}} = \{(k, p(k) - f_{\text{non}}(c_0, k)) \mid 0 \leq k \leq q + i - 1, m - (q + i) \leq k \leq m\}$

$c_0 = \text{fit}(f_{\text{non}}(c, x), D_{\text{non}}, c_0)$

$d_0 = \text{fit}(f_{\text{ex}}(d, x), D_{\text{ex}}, d_0)$

$i = i + 1$

end

% Return the estimated fitting parameters.

return c_0, d_0

Simulated networks

The absence of ground truth poses an important limitation for extensive assessment of the proposed model's accuracy. An interesting possibility to circumvent this issue, is to test the model on a collection of simulated networks for which the ground truth is known. To this end, we have developed a preliminary method that approximately reproduces the variation witnessed in the collection of reconstructed brain networks by making changes to fifty copies of a randomly chosen blueprint. The details of this simulation method and its utility for the validation of our model are discussed below.

Rationale

An important assumption behind the proposed false positives and negatives model is that (human) structural brain networks admit a common substrate. This common substrate is then regarded as a blueprint for structural brain networks, from which observed reconstructions might differ due to reconstruction errors and biological variation. Combining individual reconstructions by setting a group threshold can be explained as an attempt to recover this common substrate and the proposed model estimates how well the common substrate is resembled by the combined reconstruction. In other words, in the real setting, individual reconstructions are given and the blueprint is to be obtained. The idea behind our simulation approach is to turn this around; i.e., start with a blueprint and create "individual reconstructions" from it. Then the ground truth is available and the accuracy of the proposed model can be examined.

Reproducing variation

Suppose for a moment that a blueprint network has already been selected. Since the proposed model was created with the prevalence pattern of reconstructed structural brain networks (Figure 4.1a and Supplementary Figure 4.2a) in mind, the true accuracy of the model (i.e., the accuracy when applied to brain networks) is most faithfully estimated on a collection of simulated networks with a similar prevalence pattern. To create such a collection, the blueprint network is

first copied fifty times, matching the number of reconstructed brain networks in the principal dataset. Next, in each copy of the blueprint, connections are added and removed according to a probability model, resulting in a collection of fifty different simulated brain network reconstructions.

The variation displayed by the collection of simulated networks heavily depends on the chosen probability model. The simplest probability models are uniform ones, giving each connection the same probability to be removed and each pair of unconnected network nodes equal probability to become connected. However, these uniform models produce entirely different patterns of variation than the one observed in structural brain networks (Supplementary Figure 4.1a). Instead, a probability model was used in which simulated subjects have probability distributions that depend on the outcome of their predecessors. More specifically, the probability that connection k from the blueprint is removed in simulated subject i is proportional to

$$(n_k + u_r)^{s_r} \quad (4.8)$$

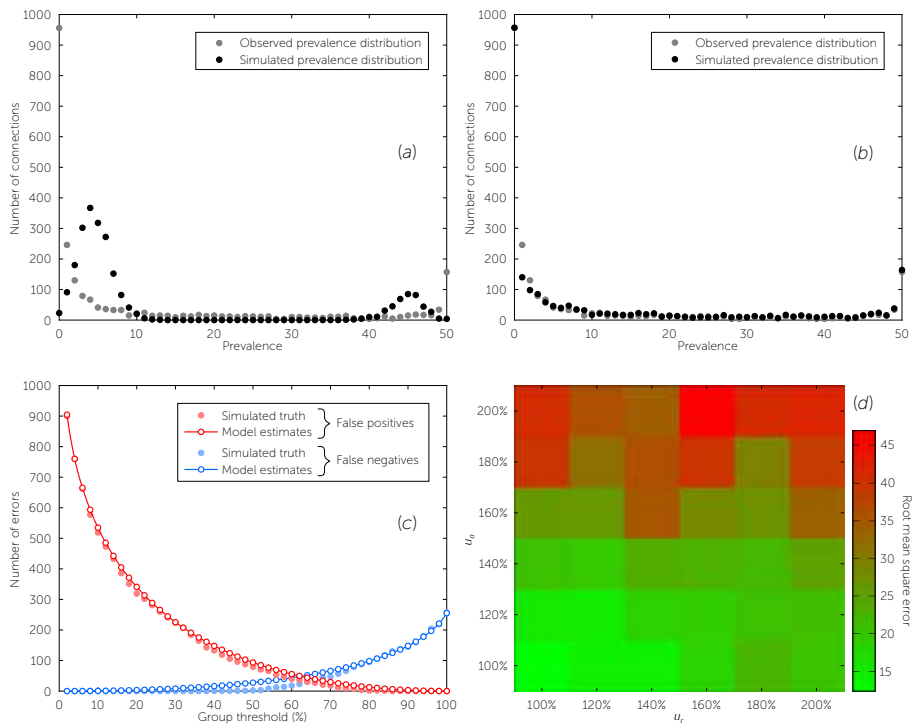
in this probability model, where u_r and s_r are global simulation parameters and n_k is the number of times that connection k has been removed in simulated subjects 1, 2, ..., $i - 1$. Similarly, the probability that a connection is placed between a pair of unconnected network nodes l is proportional to

$$(m_l + u_a)^{s_a}, \quad (4.9)$$

with m_l the number of simulated subjects in which this pair of nodes has previously been connected. In this process, probabilities are normalized such that, on average, p_r percent of the blueprint's connections are removed and p_a percent of the blueprint's unconnected node pairs become connected.

After a crude manual search for suitable initial values for the simulation parameters (u_r, s_r, p_r) and (u_a, s_a, p_a) , a collection of simulated networks was obtained by optimizing these parameters using MATLAB's *fminsearch* routine. Since the placement of connections is irrelevant for the simulation procedure outlined

above, a randomly chosen network with 68 nodes and a network density of 18.5% (see the main text) was used as blueprint. As shown by Supplementary Figure 4.1b, the prevalence distribution associated with the simulated networks resembles the prevalence distribution of the principal collection of 50 structural brain network reconstructions quite closely, thus providing a suitable environment for an accuracy test of the proposed model.



Supplementary Figure 4.1. Simulated networks. (a) Example of a prevalence distribution that emerged from modification of connections according to uniformly distributed probabilities in fifty copies of a randomly chosen blueprint. Also shown is the prevalence distribution as observed in the principal dataset of fifty structural brain network reconstructions. (b) Prevalence distribution of the collection of simulated brain networks produced by our preliminary simulation method. (c) False positive and negative curve for the collection of simulated brain networks as estimated by the proposed model, together with the corresponding values provided by the ground truth (i.e., blueprint) of the simulated collection. (d) Effect of increasing the simulation method's uniformity parameters on the accuracy of the estimated false positive and negative curve. All other simulation parameters were kept equal to those used for the collection of simulated brain networks.

Accuracy of estimates

All analyses in the main text are based on the approximated decomposition of the prevalence distribution in a component counting existing and a component counting non-existing connections. For the collection of simulated networks, it is revealed by the blueprint which connections should be regarded as existing and which as non-existing, giving rise to a true and exact decomposition of the prevalence distribution. In other words, using the terminology from the main text, $p_{\text{non}}(k)$ and $p_{\text{ex}}(k)$ are known in the simulated setting. The accuracy of their approximations $f_{\text{non}}(c, k)$ and $f_{\text{ex}}(d, k)$, obtained by applying the proposed model to the collection of simulated networks, is quantified by the combined root mean square error:

$$\sqrt{\frac{\sum_{k=0}^m (p_{\text{non}}(k) - f_{\text{non}}(c, k))^2 + (p_{\text{ex}}(k) - f_{\text{ex}}(d, k))^2}{2(m+1)}}. \quad (4.10)$$

Similarly, employing equations (4.1) and (4.2) from the main text, the combined accuracy of the estimated false positive and false negative curve is quantified by:

$$\sqrt{\frac{\sum_{k'=1}^m (\sum_{k=k'}^m p_{\text{non}}(k) - f_{\text{non}}(c, k))^2 + \left(\sum_{k=0}^{k'-1} p_{\text{ex}}(k) - f_{\text{ex}}(d, k)\right)^2}{2m}}. \quad (4.11)$$

Preferential attachment

The simulation procedure described by equations (4.8) and (4.9) above, is an example of a (non-linear) preferential attachment process, also referred to as “the rich get richer”. In such a process, the distribution of a quantity of interest (here, modified connectivity) among several objects (here, node pairs) depends positively on the quantity already received. The simulation parameters (s_r, u_r), respectively (s_o, u_o), which were all required to be positive, together control the strength of this feedback. That variation in a collection of structural brain network reconstructions appears to be explicable by a preferential attachment process is in itself an interesting finding. It shows that variation, whether intrinsic and biologically relevant or attributable to reconstruction noise, tends to aggregate.

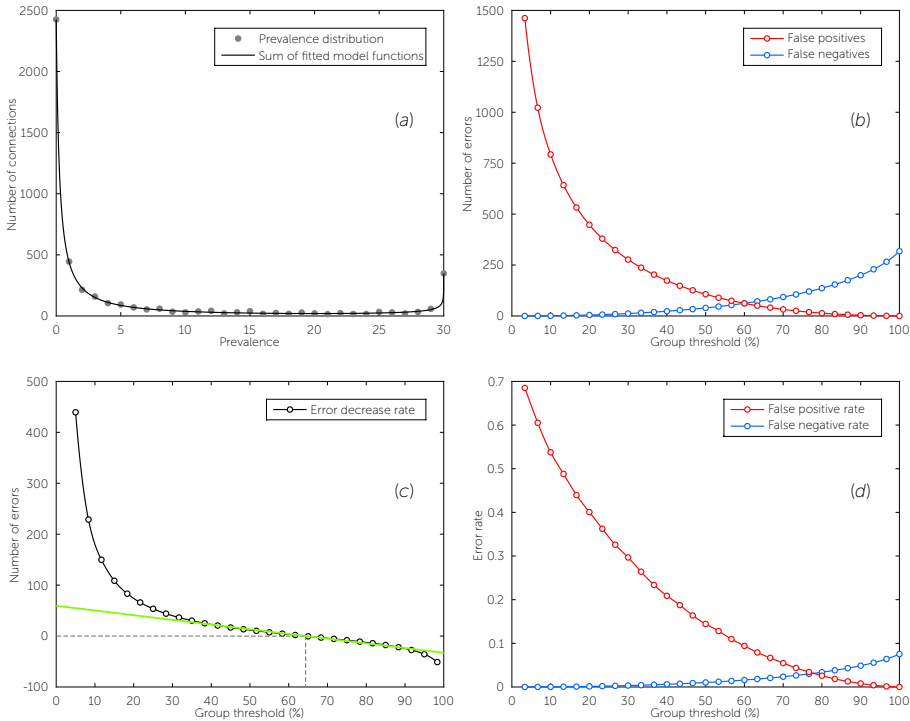
Of course, this is not entirely surprising; for example, connections that are difficult to reconstruct in one subject are probably also difficult to reconstruct in other subjects.

Limitations

Although simulated networks are an interesting tool to test the proposed model, some reservations should be made. When validating a model with another model, the uncertainty associated with modeling builds up, making it difficult to judge whether the results contain meaningful information about the original research questions. For example, the observation that our simulation method is able to produce a collection of simulations that resembles the original prevalence pattern, does not prove that the mechanisms underlying the real data are the same as those in the simulation. It is very well possible that other mechanisms also provide faithful simulations. Moreover, the simulation procedure presented here should be regarded as preliminary. It was added as an extra feature, supporting the false positives and negatives model introduced in the main text, and was not investigated as intensively as the main model.

Other applications

The availability of a simulation method offers interesting possibilities to quickly investigate research questions. For example, in the discussion section of the main text, we suggest that the use of finer-grained parcellation schemes might cause more inter-subject variation. In the simulation procedure, this could be incorporated by increasing the uniformity parameters u_r and $u_{r'}$, the effect of which can simply be computed by rerunning the simulation (see Supplementary Figure 4.1d).



Supplementary Figure 4.2. Results for the replication dataset. Due to a different parcellation scheme, dividing the cerebral cortex in 96 rather than 68 regions, absolute numbers of connections and errors are higher than in the principal data collection. (a) Prevalence distribution and sum of the approximated components. (b) Number of false positives and negatives in the combined reconstruction for each group threshold as estimated by the proposed model. (c) Error decrease rate as function of group threshold. (d) Estimated false positive and false negative rates as functions of group threshold.

References

- Andersson, J.L.R., Skare, S., 2002. A Model-Based Method for Retrospective Correction of Geometric Distortions in Diffusion-Weighted EPI. *NeuroImage* 16, 177-199.
- Andersson, J.L.R., Skare, S., Ashburner, J., 2003. How to correct susceptibility distortions in spin-echo echo-planar images: application to diffusion tensor imaging. *NeuroImage* 20, 870-888.
- Basser, P.J., Mattiello, J., LeBihan, D., 1994. MR diffusion tensor spectroscopy and imaging. *Biophysical Journal* 66, 259-267.
- Bassett, D.S., Brown, J.A., Deshpande, V., Carlson, J.M., Grafton, S.T., 2011. Conserved and variable architecture of human white matter connectivity. *NeuroImage* 54, 1262-1279.
- Beaulieu, C., Allen, P.S., 1994. Determinants of anisotropic water diffusion in nerves. *Magnetic Resonance in Medicine* 31, 394-400.
- Brown, J.A., Terashima, K.H., Burggren, A.C., Ercoli, L.M., Miller, K.J., Small, G.W., Bookheimer, S.Y., 2011. Brain network local interconnectivity loss in aging APOE-4 allele carriers. *Proceedings of the National Academy of Sciences* 108, 20760-20765.
- Bullmore, E., Sporns, O., 2009. Complex brain networks: graph theoretical analysis of structural and functional systems. *Nature Reviews Neuroscience* 10, 186-198.
- Cammoun, L., Gigandet, X., Meskaldji, D., Thiran, J.P., Sporns, O., Do, K.Q., Maeder, P., Meuli, R., Hagmann, P., 2012. Mapping the human connectome at multiple scales with diffusion spectrum MRI. *Journal of Neuroscience Methods* 203, 386-397.
- Chang, L.C., Jones, D.K., Pierpaoli, C., 2005. RESTORE: Robust estimation of tensors by outlier rejection. *Magnetic Resonance in Medicine* 53, 1088-1095.
- Conturo, T.E., Lori, N.F., Cull, T.S., Akbudak, E., Snyder, A.Z., Shimony, J.S., McKinstry, R.C., Burton, H., Raichle, M.E., 1999. Tracking neuronal fiber pathways in the living human brain. *Proceedings of the National Academy of Sciences* 96, 10422-10427.
- Dauguet, J., Peled, S., Berezovskii, V., Delzescaux, T., Warfield, S.K., Born, R., Westin, C.F., 2007. Comparison of fiber tracts derived from in-vivo DTI tractography with 3D histological neural tract tracer reconstruction on a macaque brain. *NeuroImage* 37, 530-538.
- Desikan, R.S. et al., 2006. An automated labeling system for subdividing the human cerebral cortex on MRI scans into gyral based regions of interest. *NeuroImage* 31, 968-980.
- Felleman, D.J., Van Essen, D.C., 1991. Distributed hierarchical processing in the primate cerebral cortex. *Cerebral Cortex* 1, 1-47.
- Fischl, B. et al., 2004. Automatically Parcellating the Human Cerebral Cortex. *Cerebral Cortex* 14, 11-22.
- Gong, G., He, Y., Concha, L., Lebel, C., Gross, D.W., Evans, A.C., Beaulieu, C., 2009. Mapping Anatomical Connectivity Patterns of Human Cerebral Cortex Using In Vivo Diffusion Tensor Imaging Tractography. *Cerebral Cortex* 19, 524-536.
- Hagmann, P., Cammoun, L., Gigandet, X., Meuli, R., Honey, C.J., Wedeen, V.J., Sporns, O., 2008. Mapping the Structural Core of Human Cerebral Cortex. *PLoS Biology* 6, e159.
- Hagmann, P., Kurant, M., Gigandet, X., Thiran, P., Wedeen, V.J., Meuli, R., Thiran, J.P., 2007. Mapping Human Whole-Brain Structural Networks with Diffusion MRI. *PLoS ONE* 2, e597.
- He, Y., Chen, Z.J., Evans, A.C., 2007. Small-World Anatomical Networks in the Human Brain Revealed by Cortical Thickness from MRI. *Cerebral Cortex* 17, 2407-2419.
- van den Heuvel, M.P., Kahn, R.S., Goñi, J., Sporns, O., 2012. High-cost, high-capacity backbone for global brain communication. *Proceedings of the National Academy of Sciences* 109, 11372-11377.
- van den Heuvel, M.P., Mandl, R.C.W., Kahn, R.S., Hulshoff Pol, H.E., 2009. Functionally linked resting-state networks reflect the underlying structural connectivity architecture of the human brain. *Human Brain Mapping* 30, 3127-3141.
- van den Heuvel, M.P., Mandl, R.C.W., Stam, C.J., Kahn, R.S., Hulshoff Pol, H.E., 2010. Aberrant Frontal and Temporal Complex Network Structure in Schizophrenia: A Graph Theoretical Analysis. *The Journal of Neuroscience* 30, 15915-15926.
- van den Heuvel, M.P., Sporns, O., 2011. Rich-Club Organization of the Human Connectome. *The Journal of Neuroscience* 31, 15775-15786.

- van den Heuvel, M.P., Stam, C.J., Boersma, M., Hulshoff Pol, H.E., 2008. Small-world and scale-free organization of voxel-based resting-state functional connectivity in the human brain. *NeuroImage* 43, 528-539.
- Hilgetag, C.C., Burns, G.A., O'Neill, M.A., Scannell, J.W., Young, M.P., 2000. Anatomical connectivity defines the organization of clusters of cortical areas in the macaque monkey and the cat. *Philosophical Transactions of the Royal Society of London B: Biological Sciences* 355, 91-110.
- Honey, C.J., Kotter, R., Breakspear, M., Sporns, O., 2007. Network structure of cerebral cortex shapes functional connectivity on multiple time scales. *Proceedings of the National Academy of Sciences* 104, 10240-10245.
- Honey, C.J., Sporns, O., Cammoun, L., Gigandet, X., Thiran, J.P., Meuli, R., Hagmann, P., 2009. Predicting human resting-state functional connectivity from structural connectivity. *Proceedings of the National Academy of Sciences* 106, 2035-2040.
- Jbabdi, S., Johansen-Berg, H., 2011. Tractography: Where Do We Go from Here? *Brain Connectivity* 1, 169-183.
- Jones, D.K., 2004. The effect of gradient sampling schemes on measures derived from diffusion tensor MRI: A Monte Carlo study. *Magnetic Resonance in Medicine* 51, 807-815.
- Jones, D.K., Horsfield, M.A., Simmons, A., 1999. Optimal strategies for measuring diffusion in anisotropic systems by magnetic resonance imaging. *Magnetic Resonance in Medicine* 42, 515-525.
- Jones, D.K., Pierpaoli, C., 2005. Confidence mapping in diffusion tensor magnetic resonance imaging tractography using a bootstrap approach. *Magnetic Resonance in Medicine* 53, 1143-1149.
- Li, Y., Liu, Y., Li, J., Qin, W., Li, K., Yu, C., Jiang, T., 2009. Brain Anatomical Network and Intelligence. *PLoS Computational Biology* 5, e1000395.
- Lynall, M.E., Bassett, D.S., Kerwin, R., McKenna, P.J., Kitzbichler, M., Muller, U., Bullmore, E., 2010. Functional Connectivity and Brain Networks in Schizophrenia. *The Journal of Neuroscience* 30, 9477-9487.
- Mandl, R.C.W., Schnack, H.G., Luiges, J., van den Heuvel, M.P., Cahn, W., Kahn, R.S., Hulshoff Pol, H.E., 2010. Tract-based Analysis of Magnetization Transfer Ratio and Diffusion Tensor Imaging of the Frontal and Frontotemporal Connections in Schizophrenia. *Schizophrenia Bulletin* 36, 778-787.
- Maslov, S., Sneppen, K., 2002. Specificity and Stability in Topology of Protein Networks. *Science* 296, 910-913.
- Micheloyannis, S., Pachou, E., Stam, C.J., Vourkas, M., Erimaki, S., Tsirka, V., 2006. Using graph theoretical analysis of multi channel EEG to evaluate the neural efficiency hypothesis. *Neuroscience Letters* 402, 273-277.
- Mori, S., Crain, B.J., Chacko, V.P., Van Zijl, P.C.M., 1999. Three-dimensional tracking of axonal projections in the brain by magnetic resonance imaging. *Annals of Neurology* 45, 265-269.
- Mori, S., van Zijl, P.C.M., 2002. Fiber tracking: principles and strategies – a technical review. *NMR in Biomedicine* 15, 468-480.
- Newman, M.E.J., 2002. Assortative Mixing in Networks. *Physical Review Letters* 89, 208701.
- Rubinov, M., Sporns, O., 2010. Complex network measures of brain connectivity: Uses and interpretations. *NeuroImage* 52, 1059-1069.
- Salvador, R., Suckling, J., Coleman, M.R., Pickard, J.D., Menon, D., Bullmore, E., 2005. Neurophysiological Architecture of Functional Magnetic Resonance Images of Human Brain. *Cerebral Cortex* 15, 1332-1342.
- Scannell, J.W., Young, M.P., 1993. The connectional organization of neural systems in the cat cerebral cortex. *Current Biology* 3, 191-200.
- Simpson, S.L., Hayasaka, S., Laurienti, P.J., 2011. Exponential Random Graph Modeling for Complex Brain Networks. *PLoS ONE* 6, e20039.
- Simpson, S.L., Moussa, M.N., Laurienti, P.J., 2012. An exponential random graph modeling approach to creating group-based representative whole-brain connectivity networks. *NeuroImage* 60, 1117-1126.
- Sporns, O., 2011. The human connectome: a complex network. *Annals of the New York Academy of Sciences* 1224, 109-125.
- Sporns, O., Tononi, G., Kotter, R., 2005. The Human Connectome: A Structural Description of the Human Brain. *PLoS Computational Biology* 1, e42.
- Stam, C.J., 2004. Functional connectivity patterns of human magnetoencephalographic recordings: a 'small-world' network? *Neuroscience Letters* 355, 25-28.
- Stam, C.J., Jones, B.F., Nolte, G., Breakspear, M., Scheltens, P., 2007. Small-World Networks and Functional Connectivity in Alzheimer's Disease. *Cerebral Cortex* 17, 92-99.

CHAPTER 4

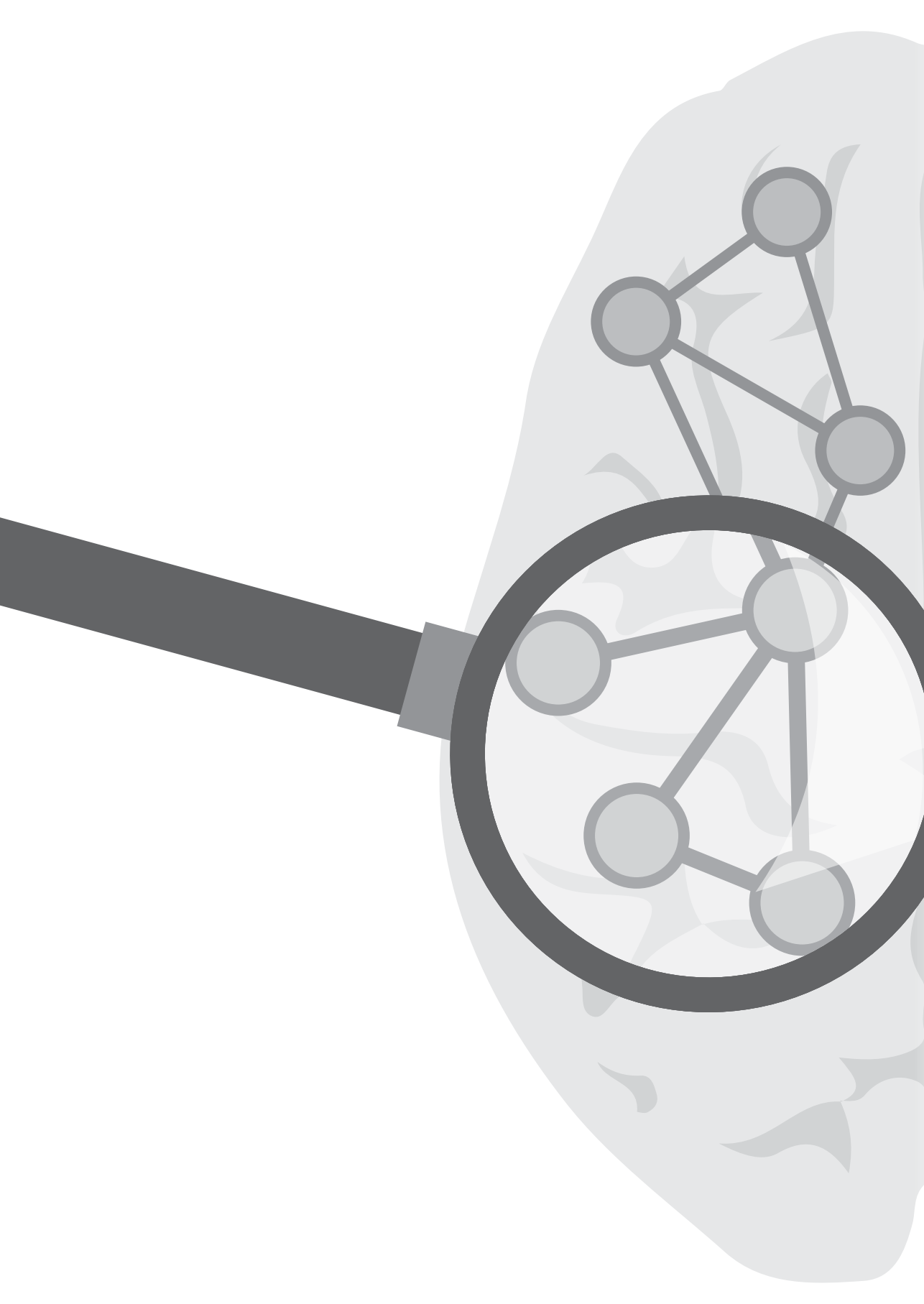
Watts, D.J., Strogatz, S.H., 1998. Collective dynamics of 'small-world' networks. *Nature* 393, 440-442.

de Weijer, A.D., Mandl, R.C.W., Diederend, K.M.J., Neggers, S.F.W., Kahn, R.S., Hulshoff Pol, H.E., Sommer, I.E.C., 2011. Microstructural alterations of the arcuate fasciculus in schizophrenia patients with frequent auditory verbal hallucinations. *Schizophrenia Research* 130, 68-77.

Young, M.P., 1993. The Organization of Neural Systems in the Primate Cerebral Cortex. *Proceedings of the Royal Society of London B: Biological Sciences* 252, 13-18.

Zalesky, A., Cocchi, L., Fornito, A., Murray, M.M., Bullmore, E., 2012. Connectivity differences in brain networks. *NeuroImage* 60, 1055-1062.

Zalesky, A., Fornito, A., Seal, M.L., Cocchi, L., Westin, C.F., Bullmore, E.T., Egan, G.F., Pantelis, C., 2011. Disrupted Axonal Fiber Connectivity in Schizophrenia. *Biological Psychiatry* 69, 80-89.



Chapter 5

Rich club organization and intermodule communication in the cat connectome

Based on a publication (The Journal of Neuroscience, vol. 33, 2013, pp. 12929-12939) by Marcel A. de Reus and Martijn P. van den Heuvel

Abstract

Macroscopic brain networks have been shown to display several properties of an efficient communication architecture. In light of global communication, the formation of a densely connected neural *rich club* of hubs is of particular interest, because brain hubs have been suggested to play a key role in enabling short communication pathways within neural networks. Here, analyzing the cat connectome as reconstructed from neuronal tract-tracing data (Scannell et al., 1995), we provide several lines of evidence for an important role of the structural rich club in interlinking functional domains. First, rich club hub nodes were found to be mostly located at the boundaries between functional communities and were well-represented among intermodule hubs, displaying a diverse connectivity profile. Second, rich club connections – linking nodes of the rich club – and feeder connections – linking non-rich club nodes to rich club nodes – were found to comprise 86% of the intermodule connections, whereas local connections between peripheral nodes mostly spanned between nodes of the same functional community. Third, almost 90% of all intermodule communication paths were found to follow a sequence or *path motif* involving rich club or feeder edges and thus traversed a rich club node. Together, our findings provide evidence for the structural rich club to form a central infrastructure for intermodule communication in the brain.

Introduction

Brain function depends on efficient processing and integration of information within a complex network of neuronal interactions. Studies examining the macroscopic architecture of neural networks have suggested that the mammalian brain, and likely neural systems in general, are organized according to a *small-world modular* architecture, combining high levels of local clustering and a community structure with short global communication pathways (Bullmore and Sporns, 2009; Hagmann et al., 2008; van den Heuvel and Hulshoff Pol, 2010). It has been hypothesized that local clustered communities may ensure segregation and local specialization of the brain, whereas the presence of short

communication relays may provide an infrastructure for global integration of information (Sporns, 2011; Sporns et al., 2005). Studies have further noted the existence of a relatively small but crucial set of highly connected regions that play a central role in the overall architecture of brain networks (Buckner et al., 2009; Hagmann et al., 2008; van den Heuvel et al., 2012; Sepulcre et al., 2012; Tomasi and Volkow, 2010). Besides being comprised of regions which are individually "rich" in connectivity, this set of putative hubs also shows a dense level of interconnectivity, suggesting the formation of a core or *rich club* in the cat, macaque, and human brain (Harriger et al., 2012; van den Heuvel et al., 2012; van den Heuvel and Sporns, 2011; Zamora-López et al., 2010), as well as in the neural system of the nematode *Caenorhabditis elegans* (Towlson et al., 2013). From the perspective of information integration, the formation of a centrally connected rich club is of particular interest, because it may act as a central backbone for global brain communication (Bullmore and Sporns, 2012; Collin et al., 2014; van den Heuvel et al., 2012; Zamora-López et al., 2010).

Animal studies allow for a detailed reconstruction of white matter pathways through means of neural tracing of axonal connections (Felleman and Van Essen, 1991; Scannell et al., 1995; Selemon and Goldman-Rakic, 1988). The cat connectome dataset, as presented by Scannell et al. (1995), involves detailed tract-tracing reconstructions of the cat's white matter pathways, including information about the directionality of white matter projections, a property that remains out of reach of present day *in vivo* neuroimaging techniques. Moreover, in the case of the cat connectome, *a priori* neurophysiological information about the functional role of each included brain area facilitates the description of four distinct functional communities, independent of the spatial or topological organization of the underlying structural network (Scannell et al., 1995; Scannell and Young, 1993; Young, 1993). Here, reanalyzing this connectivity dataset with network analysis tools, combining information on the functional organization of the cat brain with information about the cat's structural white matter pathways, we show an important role for the structural rich club in forming a central infrastructure that interlinks all communities and shapes intermodule communica-

tion pathways in the cat brain.

Materials and methods

Connectivity dataset

The cat connectivity dataset comprises a description of corticocortical connections in the cat brain as published by Scannell et al. (1995); a connectivity set resulting from a comprehensive literature search of anatomical tract-tracing studies in the cat cortex. No specific information on the sex of the included animals was available, suggesting that the dataset includes combined information on connectivity of male as well as female cats (Scannell et al., 1995). The parcellation scheme used by Scannell and colleagues, dividing the cat cortex into 65 distinct, non-overlapping regions, was based on previous work considering the cytoarchitecture and physiology of cortical regions and did not involve clear information on subcortical regions of the cat brain. Detailed information on the delineated regions, including information on the used parcellation scheme, abbreviations, and possible overlap with other parcellation schemes, as well as information on the physiological characteristics of these regions, is given in the appendix of the original study by Scannell et al. (1995). The connectivity dataset incorporates data of one hemisphere, including 65 regions and 1139 interregional macroscopic axonal projections, with the strength of the connections measured in three levels: 1, reflecting a weak connection; 2, reflecting a medium strength connection; and 3, reflecting a strong connection. The connectivity dataset was transformed to a binary connectivity matrix, including all connections independent of their strength, and interpreted as an unweighted graph $G = (V, E)$, with V describing the nodes of the network taken as the collection of 65 cortical regions and E the collection of macroscopic projections between nodes V in the network.

Functional modules

The cat connectivity dataset included a classification of the cortical regions (i.e., nodes in the network) into four categories (Scannell et al., 1995), being (1) visual regions (18 regions), (2) auditory regions (10 regions), (3) somatomotor regions (18 regions), and (4) frontolimbic regions (19 regions). This subdivision was based on neurophysiological information about the functional role of each included brain area. The four categories were taken and interpreted as an *a priori* classification of the nodes of the cat connectome into four functional communities, as originally proposed by Scannell et al. (1995). Verifying this *a priori* definition on the basis of the connectivity structure of the network itself (Hagmann et al., 2008; Harriger et al., 2012), Newman's directed community detection algorithm (1000 runs, taking the solution with the highest modularity score) revealed a highly similar community pattern (Newman, 2006), with the only clear difference being that the somatomotor community was further subdivided into two separate modules (one module involving regions 17, 18, 19, PMLS, AMLS, 21a, 21b, ALG, 7, and region SVA, and the other module involving regions PLLS, ALLS, VLS, DLS, and 20a).

Rich club organization

Rich club organization of a network describes the phenomenon that high-degree nodes of the network are more densely connected than one would expect on the basis of their individual degree alone (Colizza et al., 2006; van den Heuvel and Sporns, 2011; Zamora-López et al., 2010). In short, for each node of the cat connectome, its individual in-degree (i.e., the number of incoming connections) and out-degree (i.e., the number of outgoing connections) was computed. For each level of k , the subgraph S_k consisting of $N_{>k}$ nodes with a combined in-degree and out-degree larger than k was selected. The rich club coefficient $\Phi(k)$ of level k was computed as the ratio between the number of connections $E_{>k}$ present within this subgraph S_k and the total number of possible connections in S_k (i.e., $N_{>k} \times (N_{>k} - 1)$), formally given by Colizza et al. (2006):

$$\Phi(k) = \frac{E_{>k}}{N_{>k}(N_{>k} - 1)}. \quad (5.1)$$

To compensate for the fact that in randomized networks higher-degree nodes also have a higher probability of becoming interconnected, the cat rich club coefficient $\Phi(k)$ was compared with the rich club coefficient of a set of randomized graphs with a similar degree sequence in which the overall global topology was destroyed. To this end, 1000 random graphs were formed, randomly rewiring the connections of the directed connectivity matrix of the cat connectome while preserving the in-degree and out-degree of each node in the network (i.e., hubs remain hubs), and the rich club coefficient $\Phi_{\text{random}}(k)$ of these random graphs was computed to obtain a null distribution. For each level of k , $\Phi(k)$ was assigned a p -value as the percentage of the null distribution that exceeded the rich club coefficient as observed in the original network. A network is said to display a rich club organization if, for a range of k , $\Phi(k) > \Phi_{\text{random}}(k)$, or, expressed differently, if the ratio $\Phi_{\text{norm}}(k)$ between $\Phi(k)$ and $\Phi_{\text{random}}(k)$ exceeds 1.

Rich club selection

In this study, the cat rich club was taken as the top 15 highest-degree nodes in the network, effectively selecting a rich club threshold of $k > 45$ from the range in which $\Phi(k)$ significantly exceeded $\Phi_{\text{random}}(k)$. Previous studies have demonstrated that very consistent results are found across threshold choices and across rich club selection criteria (Harriger et al., 2012; van den Heuvel et al., 2013). In this context, it could be noted that, like the small-world phenomenon, the presence or absence of rich club organization should be regarded as a topological property of the network as a whole, rather than a property of a single subset of nodes. The existence of a rich club organization in a network is most often displayed by the presence of a “rich club regime” – an interval on the degree range for which $\Phi_{\text{norm}}(k)$ significantly exceeds 1 – and not only by the presence of a single rich club.

Participation of nodes in functional modules

Distinct roles can be assigned to the nodes of a network depending on their intermodule and intramodule connectivity profile (Fornito et al., 2012; Guimerà and Amaral, 2005; Sporns et al., 2007). To this end, two metrics were examined in detail: (1) the within-module degree z -score, and (2) the between-module participation coefficient.

Within-module degree z -score. Taking the functional communities as defined by Scannell et al. (1995) as module classification, the within-module degree z -score of node i was computed as follows (Guimerà and Amaral, 2005):

$$z_i = \frac{\kappa_{iS} - \kappa_S}{\sigma_S}, \quad (5.2)$$

where κ_{iS} is the number of connections of node i to other nodes in the same module S , and κ_S and σ_S , respectively, represent the mean and standard deviation of the within-module degree over all nodes in S . As such, z_i describes how well connected (on the structural level) node i is to the other nodes in its (functional) module. High within-module degree z -scores thus reflect a high level of intramodule connectivity of node i (Guimerà and Amaral, 2005). For each node, both an in-degree z_i^{in} and out-degree z_i^{out} score were computed, based, respectively, on its incoming and outgoing connections.

Between-module participation coefficient. In addition to the within-module degree z -score, providing information on the level of intramodule connectivity, the between-module participation coefficient quantifies the extent to which the connections of a node are evenly distributed across the different functional modules (Guimerà and Amaral, 2005). It is given by:

$$P_i = 1 - \sum_S \left(\frac{\kappa_{iS}}{k_i} \right)^2, \quad (5.3)$$

where κ_{iS} is the number of structural links from node i to nodes in functional

module S , and k_i is the total degree of node i . As such, P_i expresses the role of node i in interconnecting different modules. For each node, both an in-degree P_i^{in} and out-degree P_i^{out} score were computed, based, respectively, on its incoming and outgoing connections.

Nodes were classified according to their in-degree and out-degree z_i and P_i scores using a ranking procedure. First, for each of the four metrics separately, node values were ranked according to their metric levels. Second, across metrics, each node was given a rank score ranging from 0 to 4, expressing the number of times it ranked among the top 15 nodes of one of the four metrics. Third, inspired by the concept of Guimerà and Amaral (2005) and Sporns et al. (2007) of labeling nodes that display a high z_i (originally defined as > 2.5) and high P_i (originally defined as > 0.3) as *connector hubs*, nodes that displayed a high rank score (≥ 3) were interpreted as *intermodule hubs* to underscore their central character and involvement in linking different functional modules.

Centrality

For each node, the betweenness centrality B_i and level of PageRank centrality PageRank_i (Page et al., 1999) were computed. The betweenness centrality of node i expresses the proportion of all shortest paths between node j and node h in the network that travel through node i , summed over all combinations of j and h in the network with $j \neq h$, and provides an estimate of the role of node i in global network communication. The PageRank centrality of node i reflects how frequently that node is visited by a (infinite) random walk (Rubinov and Sporns, 2010); a type of analysis that has been suggested to provide insight into diffusion-like communication processes in a graph (Goñi et al., 2013). Higher levels of PageRank_i reflect a more central role of node i in the overall network topology.

Overlapping node communities

To detect regions of overlap between the four *a priori* defined functional modules of the cat brain, a “fuzzy” overlapping community approach, driven by efficient encoding of random walk trajectories, was applied to the structural connectivity network (for technical details, see Esquivel and Rosvall (2011)). This algorithm allows nodes of the network to participate in multiple communities on top of their original community assignment, extending the initial division of the network (i.e., into four non-overlapping functional modules) to an overlapping community pattern in which nodes are allowed to participate in other communities besides their original assignment. Nodes that participate in multiple communities can be interpreted to be on the boundary between modules, taking on a mediating role between the two (or more) communities to which they are assigned (Esquivel and Rosvall, 2011).

Node and connection classes

Rich club definition allowed for a classification of the nodes of the cat network into rich club and non-rich club nodes. Furthermore, based on this node classification, the connections of the cat connectome were divided into the following three connection classes: (1) *rich club* connections, linking rich club members; (2) *feeder* connections, linking non-rich club nodes to rich club nodes; and (3) *local* connections, linking non-rich club nodes (van den Heuvel et al., 2012). Including information on the directionality of the connections, feeder connections were further subdivided into *feeder-in* connections, projecting from non-rich club to rich club nodes, and *feeder-out* connections, projecting from rich club nodes to non-rich club nodes. In addition, combining connectivity information with information on the functional modules, connections were labeled as *intramodular* if they connected nodes located in the same functional community and as *intermodular* if they connected nodes of different functional communities. Finally, using information on the directionality of the edges, connections were labeled as *bidirectional* or *unidirectional*.

Structural homogeneity of connections

For each connection c , the structural homogeneity was computed as the overlap O between the neighbors of its endpoints i and j (i.e., the nodes connected by c), formally given by

$$O = \frac{|n_i \cap n_j|}{|n_i \cup n_j|}, \quad (5.4)$$

where n_i and n_j are the collections of neighbors of node i and node j , respectively. Higher O values indicate that node i and j have similar neighbors, suggesting that c links nodes with a comparable role in the network.

Module diversity of connections

The module diversity of a connection c between nodes i and j was defined as the product $p_i \times p_j$, where p_i and p_j are equal to the fraction of functional modules that were directly connected to, respectively, node i and node j . As such, a high module diversity score reflects that a connection is embedded between two regions in which information from many functional modules might merge, whereas a low diversity score suggests that a connection facilitates the communication of more unimodal information.

Statistical analyses

Permutation testing was used to assess statistical significance of group differences on node and connection metrics. First, for a given metric (e.g., node metrics such as P_i^{in} , P_i^{out} , or B_i), the difference between the mean of two groups (e.g., rich club vs. non-rich club) was computed. Second, for N permutations, the metric values were randomly assigned to two random groups of the same size as the two original classes, and, for each permutation, their group difference was computed (in this study, N was set to 10,000 in all tests). This resulted in a distribution of differences one can expect under the null hypothesis that no statistical difference is present between the two groups. On the basis of this null distribution, the original difference between the two groups was assigned a

(one-tailed) p -value as the proportion of the null-distribution values that exceeded the observed original difference. Note that, because the cat dataset involves a reconstruction of the cat connectome based on the aggregation of connectivity data across a large number of studies, the permutation tests do not take into account intersubject variability. The degrees of freedom in all statistical tests thus come from the dimensions of the network and not from the number of subjects.

Path motifs

The previously introduced concept of *path motifs* (van den Heuvel et al., 2012) was applied and extended. A path motif of a communication path expresses the order in which the rich club (RC), feeder (F) and local (L) edge categories are traversed and thus defines “groups of paths”. To this end, all shortest communication paths in the network were computed and labeled with the categories of connections passed, and the prevalence of each unique sequence was computed (van den Heuvel et al., 2012). Especially within an unweighted network, multiple paths may achieve the minimum length between two nodes, all of which were included as “shortest” paths. The prevalence of each path motif (L-L, F-F, F-RC-F, etc.) was computed as the ratio between the number of times a path motif was present and the total number of examined paths. Extending previous studies on path motifs in the human (van den Heuvel et al., 2012) and macaque (Harriger et al., 2012) brain, and in the nematode *Caenorhabditis elegans* (Towlson et al., 2013), path motifs were examined in more detail with edges now labeled not only according to their primary connection class (rich club, feeder, local), but also according to their directional character and their intermodular versus intramodular role.

Because studies have emphasized the importance of proper normalization of network metrics (Bialonski et al., 2011; Zalesky et al., 2012), the pattern of path motif counts was compared with the pattern of motifs occurring in an ensemble of random networks (van den Heuvel et al., 2012). As for the computation of the normalized rich club coefficient, a set of 1000 random networks was generated, randomly rewiring the connections of the cat dataset while preserving the

in-degree and out-degree of each node (Maslov and Sneppen, 2002). Because the in- and out-degree of each node kept the same values as in the original dataset, node labels (i.e., rich club/non-rich club) also remained the same, and connections in the random networks were labeled as rich club, feeder, and local connections according to this node classification. Next, of each of the labeled random networks, motif counts (given as proportions of the total number of examined paths) of each of the path motifs as observed in the original cat dataset were computed, providing a null distribution of path motif prevalence at chance level. Based on this null distribution, each path motif count as observed in the original dataset was assigned a *p*-value as the number of entries in the null distribution that exceeded the path motif count in the original dataset.

Results

Rich club nodes and non-rich club nodes

As shown in Figure 5.1a, structural connectivity of the cat connectome showed a clear rich club organization, with a normalized rich club coefficient $\Phi_{\text{norm}}(k) > 1$ for the range from $k = 15$ to $k = 49$ (i.e., the rich club regime; $p < 0.05$, Bonferroni corrected), a finding consistent with a previous report on rich club organization in the cat connectome by Zamora-López et al. (2010). From the rich club regime, the rich club was selected as the top 15 (23%) highest-degree nodes (in-degree and out-degree combined), corresponding to a rich club level of $k > 45$. Consistent results were found when the rich club was selected at different levels (for instance, $k > 43$, being the peak of the $\Phi_{\text{norm}}(k)$ curve, or $k > 47$). At $k > 45$, the rich club comprised the regions 20a, 7, AES, SSF, EPp, 6m, 5al, PFCdl, 1a, Ig, CGa, CGp, LA, 35, and 36. The density (i.e., the percentage of the total possible number of connections that was present) between these 15 rich club hub nodes was found to be 77% (1.14 times higher than in the 1000 random networks used for normalization, $p < 0.001$). Schematic drawings of the regions of the cat cortex indicating the four functional modules (i.e., visual, auditory, somatomotor, and frontolimbic) and rich club regions are shown in Figure 5.1b and Figure 5.1c, respectively.

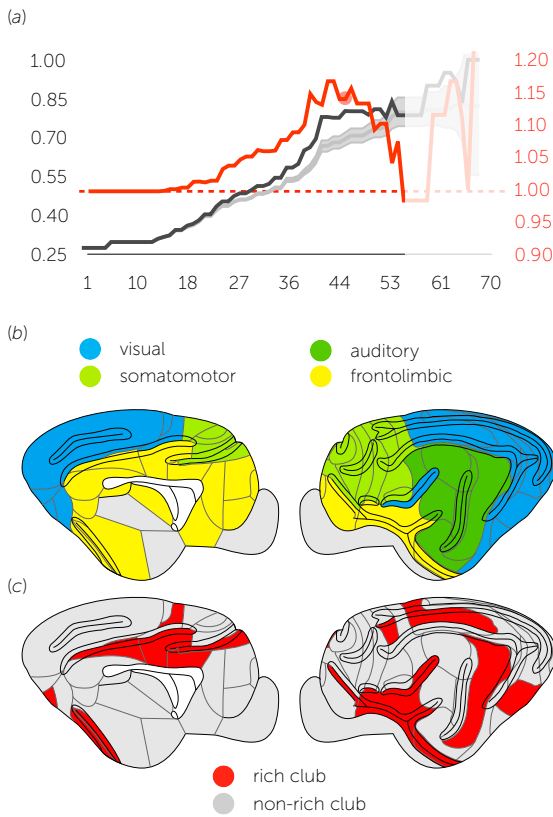


Figure 5.1. (a) Rich club curve. The plot shows the unweighted rich club coefficient $\Phi(k)$ of the cat connectome (black line) for a range from $k = 1$ to $k = 68$, the mean rich club curve $\Phi_{\text{random}}(k)$ of a set of 1000 comparable random graphs (gray line, randomizing the connections of the cat network while preserving its degree sequence), and their ratio (red line). Top and bottom gray lines mark the standard deviation of the rich club coefficient over the 1000 random networks. The red circle indicates the $k > 45$ level. (b) Schematic figure of the cat cortex (adapted from Scannell et al. (1995)) with regions colored according to their functional community: somatomotor, visual, auditory, and frontolimbic. (c) Regional plot with the rich club members depicted in red and non-rich club nodes depicted in gray.

Information on the directionality of the connections allowed for an additional generalization of the rich club concept to a specific in-degree and out-degree rich club. Over the network, nodal in-degree and out-degree showed a strong correlation ($r = 0.72$, $p < 0.001$, linear regression), indicating that (on average) high in-degree nodes also show a high out-degree. As a result, defining a rich club on the basis of in-degree or out-degree only (selected as the top 15 nodes with highest in-degree or out-degree, respectively) revealed high overlap with the rich club as defined on the combined degree, with 14 of the 15 nodes overlapping (20a, 7, AES, EPp, 6m, 5al, PFCdl, Ia, Ig, CGa, CGp, LA, 35, and 36) when considering in-degree and 11 of the 15 nodes overlapping (20a, 7, AES, EPp, 6m, Ia, Ig, CGa, CGp, 35, and 36) when considering out-degree. Ten of the 15 rich club nodes (66%) were revealed to have a higher in-degree than out-degree, the same being true for only 33% of the non-rich club nodes.

Participation of rich club nodes in functional modules

Rich club members were found to be present in all functional modules (Figure 5.2a and Figure 5.2b), suggesting a diverse connectivity profile of the rich club as a whole. Rich club nodes showed a significantly higher within-module degree z_i^{in} score (mean [std]; rich club nodes, 0.43 [0.76]; non-rich club nodes, -0.13 [1.00]; $p = 0.044$, 10,000 permutations) but not a different z_i^{out} score (rich club, 0.028 [0.79]; non-rich club, -0.01 [1.03]; $p = 0.907$) compared with non-rich club nodes. Furthermore, both the in-degree participation coefficient P_i^{in} (rich club, 0.68 [0.0337]; non-rich club, 0.3352 [0.22]; $p < 0.001$) and the out-degree participation coefficient P_i^{out} (rich club, 0.65 [0.0611]; non-rich club, 0.3936 [0.21]; $p < 0.001$) were found to be higher for rich club nodes compared with non-rich club nodes, indicating a diverse connectivity character of rich club nodes.

Obtaining for each node an overall rank score, expressing the number of times a node ranked among the top 15 highest in-degree and out-degree z_i and P_i values, rich club nodes displayed a significantly higher rank score than non-rich club nodes (mean [std]; rich club nodes, 2.13 [0.83]; non-rich club nodes, 0.56 [0.58]; $p < 0.001$, 10,000 permutations). The distribution of rank scores across the classes of rich club and non-rich club nodes is shown in Figure 5.2c, showing that all nodes with a rank score of 3 (which is the highest rank score in the network, no nodes showed a score of 4) were found to be rich club nodes, including 6 of the 15 rich club members. To reflect both their high degree and their intermodular character (all six scored among the top 15 on P_i^{in} and P_i^{out}), these nodes are referred to as intermodule hubs. The density (i.e., percentage of possible connections present) between these six intermodule hubs was found to be 87%. In addition, 11 (73%) of the 15 rich club nodes showed a score of 2 or more, in contrast to only 5 (10%) of the 50 non-rich club nodes.

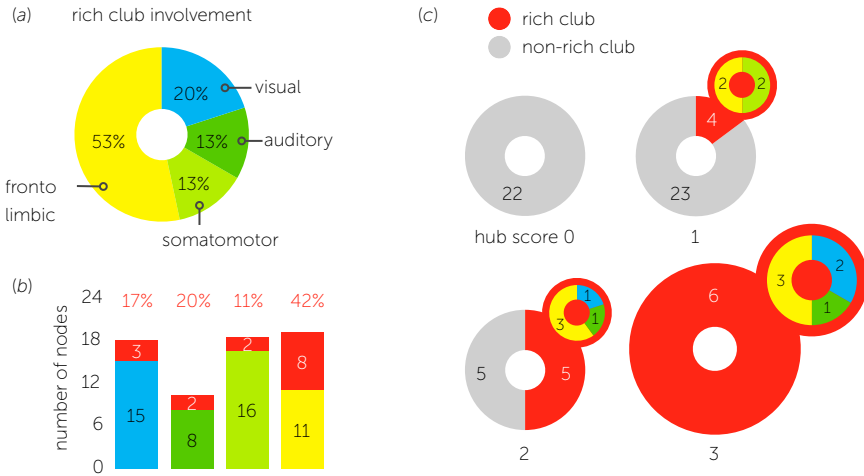


Figure 5.2. (a) Rich club nodes were found to be present in all four functional modules. The pie chart shows how the 15 rich club nodes were distributed across the four modules. (b) Number of nodes involved in the rich club per functional module. (c) Distribution of rich club nodes (red) and non-rich club nodes (gray) across rank scores (ranging from 0 to 3, top left to bottom right), expressing the number of times a node scored among the top 15 nodes on in-degree and out-degree z_i and P_i in the network. Rich club nodes were found to be well-represented among the highest scoring nodes (class 3, labeled intermodule hubs), underscoring the central role of rich club hubs in linking all four functional communities of the network.

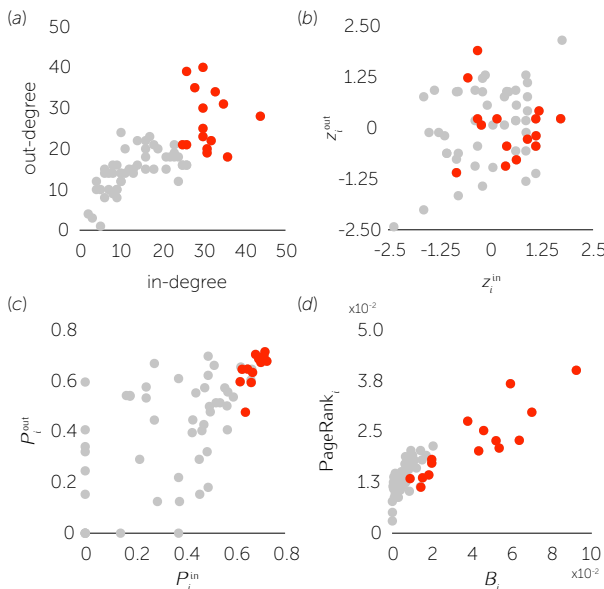


Figure 5.3. Node values and interactions of: (a) in-degree and out-degree, (b) in-degree and out-degree z_i , (c) in-degree and out-degree P_i , and (d) B_i and PageRank $_i$. Non-rich club nodes are shown in gray, and rich club nodes are shown in red.

Rich club centrality

Rich club nodes showed a significantly higher betweenness centrality B_i (mean [std]: 0.041 [0.025]) compared with the group of non-rich club nodes (mean [std]: 0.006 [0.0049], $p < 0.001$, 10,000 permutations), and also a significantly higher PageRank centrality (rich club, 0.02 [0.0085]; non-rich club, 0.013 [0.0038]; $p < 0.01$), indicating a central role of rich club nodes in the overall network structure. Betweenness and PageRank centrality values and their interaction are shown in Figure 5.3.

Rich club involvement in overlapping communities

Using an information-theoretic fuzzy community approach (Esquivel and Rosvall, 2011), regions of possible overlap between the four functional modules were identified by allowing nodes to participate in multiple communities while preserving their original module assignment. In the overlapping community pattern (Figure 5.4a), rich club nodes were on average involved in 1.87 communities (std: 1.06), whereas non-rich club nodes were on average involved in 1.16 communities (std: 0.37), significantly less than rich club regions ($p = 0.0014$, 10,000 permutations). Furthermore, 7 (46%) of the 15 rich club nodes (including areas from all four functional domains) were involved in multiple communities (13% participating in two communities, 27% in three communities, and 6% in all four communities), in contrast to only 16% of the non-rich club nodes. Such a diverse community involvement of rich club regions, and their specific representation in areas in which multiple functional domains may fuse together, emphasizes the potential role of the rich club in interlinking different functional communities of the brain. Indeed, examining for each node the number of functional communities to which it was directly connected (referred to as the *functional neighborhood* of a node), revealed that all rich club nodes are directly connected to nodes in all four functional communities (mean [std]: 4 [0]), thus showing a significantly more diverse functional neighborhood in comparison with non-rich club nodes (mean [std]: 3 [0.9], $p < 0.001$, 10,000 permutations) (Figure 5.4b).

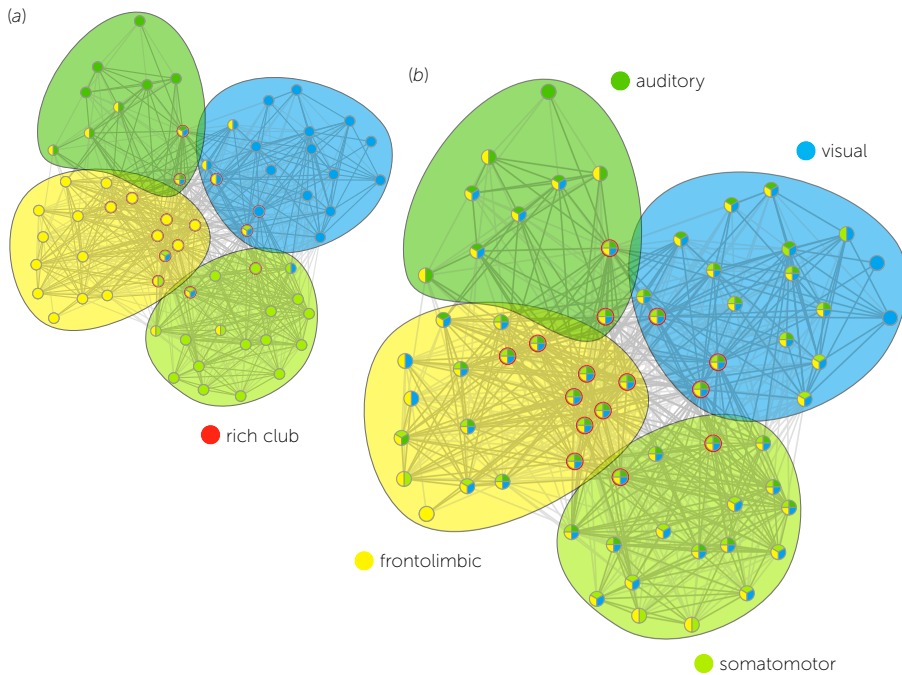


Figure 5.4. (a) Overlap between the four functional domains of the cat brain as revealed by an information-theoretic fuzzy community approach, allowing nodes of the network to participate in multiple communities while preserving their original community assignment (see Materials and methods). The figure illustrates that rich club nodes are well-represented among nodes that participate in multiple communities. (b) Functional neighborhood score of each node of the cat connectome, reflecting the number of functional communities to which a node is directly connected. All rich club nodes comprised connections to all four functional domains. Interestingly, although scoring significantly lower than rich club members, non-rich club nodes still displayed a remarkably high functional neighborhood score, with most of the nodes showing direct connections to multiple functional communities.

Characterization of rich club, feeder, and local connections

Figure 5.5a shows the (weighted) connectivity matrix of the cat connectome, as adopted from Scannell et al. (1995). Classification of the nodes into rich club and non-rich club nodes allowed for the categorization of the connections of the network into three classes: (1) *rich club* connections, linking rich club members; (2) *feeder* connections, linking non-rich club nodes to rich club nodes; and (3) *local* connections, linking non-rich club nodes (Figure 5.5b). Furthermore, information on the direction of projection pathways allowed for an additional classification of the feeder connections into *feeder-in* connections (those con-

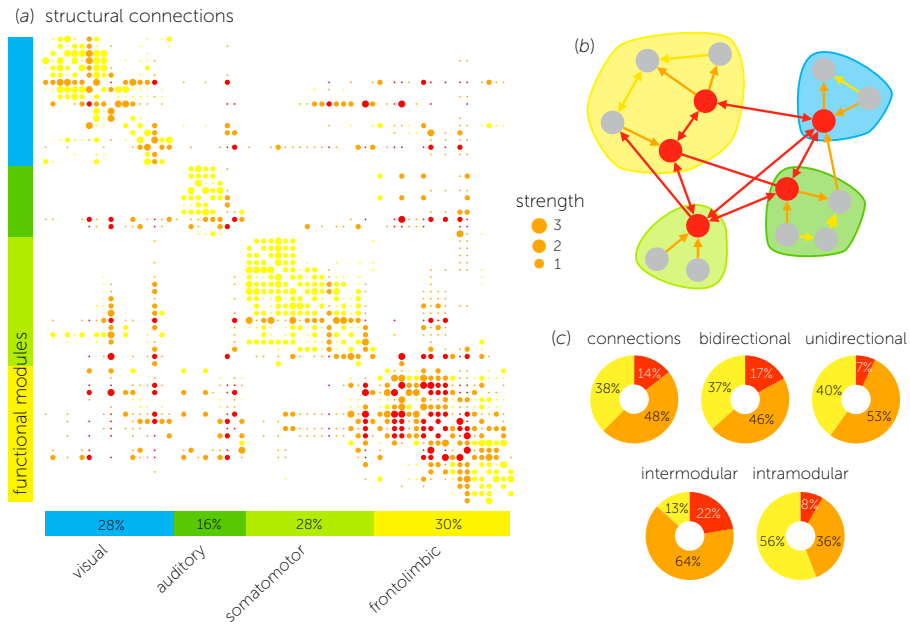


Figure 5.5. (a) Connectivity matrix of the cat connectome, with nodes ordered according to participation in the four functional modules. Connections are color coded according to their connection class: rich club (red), feeder (orange), or local (yellow). (b) Schematic figure of rich club (red) and non-rich club (gray) nodes, and directional rich club (red), feeder (orange), and local (yellow) connections. (c) Metrics of interest for the three classes of connections. The figure shows how connections are distributed over the three connection classes and how this distribution is modulated by considering only bi/unidirectional connections or inter/intramodule connections.

nections that project from non-rich club to rich club nodes) and *feeder-out* connections (projections from rich club nodes to non-rich club nodes). A circular graph representation of the cat connectome showing rich club (red), feeder (orange), and local (yellow) connections is given in Figure 5.6. Rich club connections accounted for 14% of all traced connections of the cat cortex, feeder-in and feeder-out connections for 27% and 21%, respectively (together 48%), and local connections accounted for the remaining 38% of the total number of connections (Figure 5.5c).

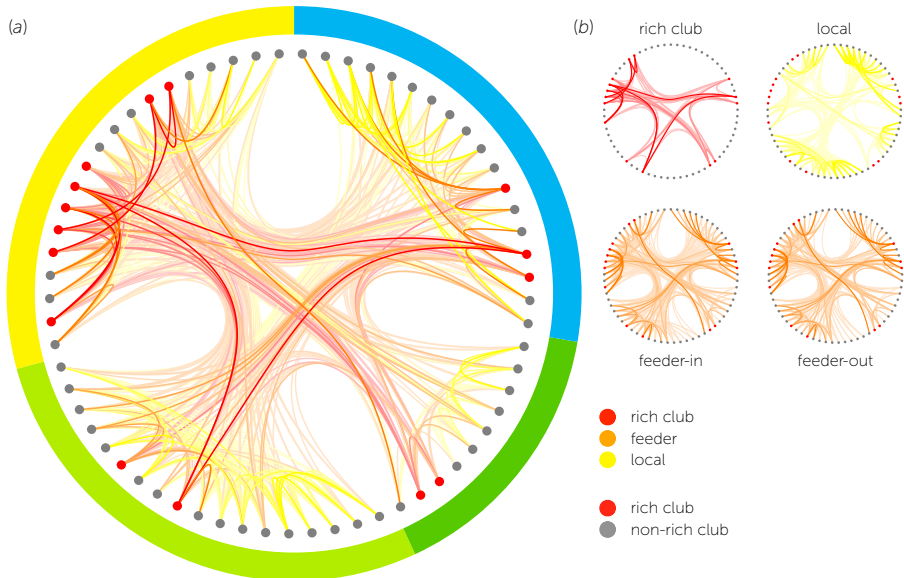


Figure 5.6. (a) Ring plot of the cat connectome. Nodes of the cat brain are ordered on a ring according to their module participation. Connections are colored according to their connection class. (b) Connections of the network split into rich club, local, feeder-in, and feeder-out connections. Nodes in the plots of panel b are arranged in the same order as in panel a. The plots show a clear intermodular character of rich club and feeder connections, whereas local connections mostly connect nodes within the same module.

Intermodule and intramodule connections

A total of 43% of the connections were found to be intermodular, linking nodes of different functional modules, and 57% were found to be intramodular, linking nodes of the same module. Of all intermodule connections, 86% were classified as either rich club (22%) or feeder (64%) connections, underscoring an important role for these connections in intermodule communication (Figure 5.5c). Indeed, 67% of the rich club connections and 57% of the feeder connections were found to link nodes of different modules, compared to only 15% of the local connections (Figure 5.7a). When examining the number of connections per node, on average almost 39% of the connections of a node were found to be intermodular. For rich club nodes, this percentage was much higher, ranging from 38 to 90% and reaching an average of 60%. For non-rich club nodes, on average 32% of the connections were intermodular (ranging from 0 to 80%), with over 60% of all non-rich club nodes having more than 33% intermodule connections.

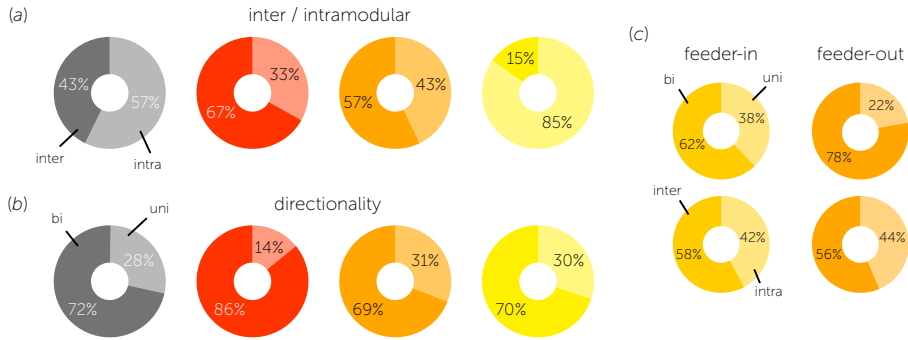


Figure 5.7. (a) Percentage of intermodule and intramodule connections across the group of all connections (gray) and across the class of rich club (red), feeder (orange), and local (yellow) connections. (b) Percentage of bidirectional (bi) and unidirectional (uni) connections across all connections, and across the three subclasses of connections. (c) Percentage of bidirectional (bi) and unidirectional (uni) connections and intermodule and intramodule connections across feeder-in (light orange) and feeder-out (dark orange) connections.

Directionality

Of the total amount of connections, 72% were found to be bidirectional and 28% unidirectional (Figure 5.7b). The majority of rich club connections were found to be bidirectional projections (86% bidirectional vs. 14% unidirectional), more than feeder (69 vs. 31%) and local (70 vs. 30%) connections. In addition, feeder-out edges were found to be more often bidirectional (78% bidirectional vs. 22% unidirectional) than feeder-in edges (62 vs. 38%) (Figure 5.7c). Intramodule connections were found to be predominantly bidirectional (79% bidirectional vs. 21% unidirectional), while intermodule connections showed a somewhat more balanced ratio (62 vs. 38%).

Structural homogeneity of connections

Measuring the structural homogeneity of each connection in the network, expressed as the overlap between the (one-step) connection neighborhoods of the two nodes joined by the connection, revealed a significantly lower overlap in the connection neighborhoods of feeder connections (mean [std]: 0.37 [0.13]) compared with rich club (mean [std]: 0.49 [0.11], $p < 0.001$) and local (mean [std]: 0.49 [0.16], $p < 0.001$, 10,000 permutations) connections. No differences

in structural homogeneity between feeder-in and feeder-out connections were observed.

Module diversity of connections

In addition to the structural homogeneity, the module diversity of each connection was computed, examining the richness of the functional neighborhoods of its endpoints (see Materials and methods). Rich club connections (mean [std]: 1 [0]) showed a higher module diversity than both feeder (mean [std]: 0.82 [0.19], $p < 0.001$) and local (mean [std]: 0.66 [0.24], $p < 0.001$) connections. Bidirectional links (mean [std]: 0.80 [0.23]) were found to have a higher diversity score than unidirectional links, but this effect was only marginally significant (mean [std]: 0.77 [0.23], $p = 0.05$, 10,000 permutations).

Path motifs

Tracing all shortest communication paths in the network spanning between two non-rich club nodes of different functional communities, revealed that 89.5% of all paths traveled through a rich club node (significantly more than in randomized networks, $p < 0.001$), with 24.2% ($p < 0.001$) traveling through at least one rich club connection. These values were found to be much higher than in a set of comparable random networks, in which 65% of the intermodule communication paths crossed a rich club node (std: 1.4%) and 8.9% of the paths crossed at least one rich club connection (std: 1.1%) (1000 random networks examined). As shown in Figure 5.8b, examining the ordered sequence of connections – referred to as path motifs – passed when traveling along these shortest communication paths in the network, revealed a strong prevalence of paths following a F-RC-F path motif (23% of all shortest paths, 2.6 \times higher than random, $p < 0.001$, 1000 random networks). Note that, because of a relatively low spatial resolution, the overall shortest path length in the cat dataset is low (97% of all intermodule paths comprise just two or three links, and paths of length five are entirely absent), making long motifs, such as the L-F-RC-F-L motif reported for the human (van den Heuvel et al., 2012) and macaque (Harriger et al., 2012) brain, impossi-

ble to occur. For intermodule paths between non-rich club nodes as examined here, the F-RC-F motif is the only submotif of L-F-RC-F-L of less than four steps and therefore its natural analog in the cat connectome. In contrast, paths that followed an F-F motif were found to be less prevalent in the cat brain compared with random networks (22.3% vs. 38.7% in random networks). Also note the relatively high occurrence of paths following a L-F-F motif ($p < 0.001$, Figure 5.8b), representing paths that directly pass through a rich club node when traveling between nodes of different modules without traversing a rich club connection, indicating an important role for feeder connections in intermodule communication.

Further delineating paths that followed the most prevalent F-RC-F path motif, now including information on the intermodular and intramodular character of the connections of the network (Figure 5.8c), revealed an above-chance level occurrence of paths that followed a “intramodule feeder-in to intermodule rich club to intramodule feeder-out” motif (15 times higher than random, $p < 0.001$). These paths were more prevalent than, for example, paths following a “intermodule feeder-in to intermodule rich club to intramodule feeder-out” (4.7 \times more than random, $p < 0.001$) or a “intermodule feeder-in to intramodule rich club to intramodule feeder-out” motif (not significantly different from random, Figure 5.8c). Interestingly, consistent with the results shown in Figure 5.8b, paths following a “intramodule local to intermodule feeder-in to intramodule feeder-out” motif were found to be among the most prevalent paths in the network ($p < 0.001$, Figure 5.8c), suggesting that, besides intermodule rich club connections, intermodule feeder connections (linking non-rich club nodes to rich club nodes) play an important role in maintaining short communication pathways between different functional modules in the cat brain.

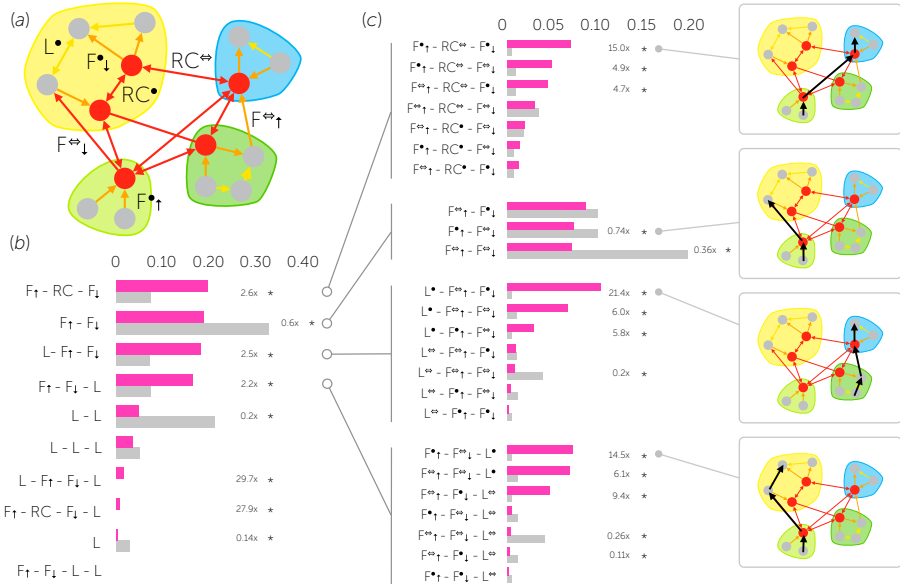


Figure 5.8. (a) Schematic figure of a network with rich club organization, indicating eight classes of connections: RC \leftrightarrow , rich club intermodular; RC \bullet , rich club intramodular; F \leftrightarrow , feeder-out intermodular; F \leftrightarrow_1 , feeder-in intermodular; F \bullet \downarrow , feeder-out intramodular; F \bullet \uparrow , feeder-in intramodular; L \leftrightarrow , local intermodular; L \bullet , local intramodular. (b) Distribution of path motifs across all shortest paths between local nodes in different functional communities, taking into account information on rich club, feeder-in, feeder-out, and local connections. Path motif counts of the cat dataset are depicted in pink, and path motif counts in a random situation (average across 1000 random networks) are depicted in gray. The figure illustrates that the F-RC-F motif occurs 2.6x more in the cat dataset than in the random model ($p < 0.001$). (c) Distribution of path motifs as shown in panel b now further specified using information on the intramodular or intermodular character of the traversed connections. Only the path motif counts of the four highest scoring path motifs from panel b are shown. Significant differences between the cat dataset and random situation are marked with an asterisk ($p < 0.05$, Bonferroni corrected).

Discussion

This study provides additional support for the notion that the rich club of the brain may form an infrastructure for communication between different functional domains. Extending recent reports on rich club formation in the *C. elegans* (Towlson et al., 2013), cat (Zamora-López et al., 2010), macaque (Harriger et al., 2012), and human (Collin et al., 2014; van den Heuvel and Sporns, 2011) cortex, our findings provide six lines of evidence to pinpoint the rich club as a

central anatomical infrastructure that interconnects functional domains of the mammalian brain.

First, analyzing data of the macroscopic cat connectome as presented in the seminal work of Scannell et al. (1995) almost 20 years ago, rich club nodes were found to be present in all four functional modules of the cat brain. This observation indicates that the rich club involves regions from all functional domains, including not only frontolimbic, but also primary visual, auditory, and somatomotor networks. Second, rich club nodes were found to show a particularly diverse connectivity profile, being well-represented among the so-called intermodule hubs of the network. Third, more than two-thirds of all rich club and more than half of all feeder connections were found to span between different functional modules, indicating a clear relevance of these types of connections for bridging different functional communities. This stands in contrast to local connections, the vast majority of which (85%) connected nodes of the same module. Fourth, all rich club nodes were found to be directly connected to nodes across all four functional domains. Fifth, an information-theoretic approach to detect possible overlap between the four functional modules (Esquivel and Rosvall, 2011) revealed a clear multimodal character of rich club nodes, suggesting that rich club nodes operate at the topological “border zones” of functional subsystems (Figure 5.4). Sixth, examination of the sequence of connection classes along communication paths in the brain showed a clear participation of the rich club in intermodule paths, suggesting an important role of rich club and feeder connections in intermodule communication (Figure 5.8).

Connections linked to rich club members were found to be well-represented among intermodule connections. Although, split up by connection class, rich club connections showed the highest proportion of intermodule connections (Figure 5.7), both feeder-in and feeder-out connections were also found to be well-represented among intermodule connections and intermodule paths. More than half of all feeder connections were found to link nodes of different functional modules (Figure 5.7), and paths involving feeder connections were found

to be among the most occurring path motifs in the network (see Figure 5.8). This suggests that feeder connections are likely to play a crucial role in maintaining high levels of direct connectivity between functional domains and that rich club connections may not necessarily be designed to only facilitate quick global communication routes. Rich club nodes and connections showed a particularly high level of module diversity, suggesting that they are positioned in areas in which information from many functional modules passes and merges. With communication in neural systems involving continuous transformation and integration, the diverse character of rich club nodes and their edges thus leaves room for the hypothesis that the rich club does not only facilitate a set of global communication pathways, but may constitute, as a core system, a central place for global integration of information. Theories of consciousness and cognition have suggested that global integration of information may take place in a "global workspace", hypothesized as a dynamical core in which segregated functional systems can share their information through neuronal interaction (Dehaene and Naccache, 2001). The rich club system connects a large portion of all central hubs of the network and participates in a large portion of all global communication pathways, making it an ideal candidate for a neural substrate of such an integrative global workspace in the mammalian brain (Harriger et al., 2012).

The observed rich club topology of the cat cortex is consistent with recently reported rich club organization of the macaque and human cortex (Harriger et al., 2012; van den Heuvel et al., 2012; Shen et al., 2012). Although caution is needed when directly comparing brain regions across species (Sereno and Tootell, 2005), the macaque and human rich club have also been suggested to involve occipital and parietal visual and sensory regions, temporofrontal insular regions, frontal motor and premotor regions, and medioparietal and mediofrontal regions (Figure 5.9). The spatial and topological overlap of rich club systems across the cat, macaque, and human cortex proposes a strong preservation of this subsystem across species, suggesting high value of retaining a neural substrate for integration of information between separated systems in the brain.

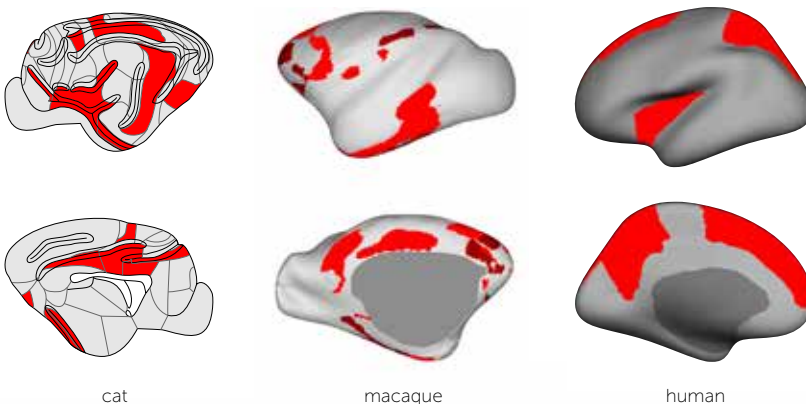


Figure 5.9. Cortical rich clubs across species. From left to right, the figures shows rich club regions (color coded in red) of the cat cortex (as presented in this chapter and by Zamora-López et al. (2010)), macaque cortex (figure adapted from Harriger et al. (2012)), and human cortex (low resolution, 34 cortical nodes per hemisphere, data from van den Heuvel and Sporns (2011)). Overlapping with rich club involvement in the cat cortex as presented in this chapter, the macaque (Harriger et al., 2012) and human (van den Heuvel et al., 2012) rich club have also been reported to involve occipital and parietal visual and sensory regions, temporal auditory regions, frontal (pre)motor regions, as well as insular, medioparietal, and mediofrontal regions overlapping the limbic system.

At least one additional observation stood out and deserves a more detailed discussion. Besides nodes of the rich club, the rest of the cat brain network was also found to show a distinct intermodular character. Indeed, almost half of all macroscopic white matter projections in the cat brain were found to link nodes of different functional modules. Examining the placement of connections per node, on average 30% of the edges of non-rich club nodes were found to directly connect to a node in one of the other functional domains, among which a large proportion of feeder connections. More than 60% of all peripheral non-rich club nodes were found to show an even more diverse character, having more than 33% of their connections projecting to or from other functional domains. These observations tend to suggest that the mammalian brain on the macroscopic level has a less modular and perhaps more integrative organization than commonly argued. Such a diverse character of the majority of regions in the brain is supported by functional studies of the human brain, suggesting a dynamic participation of cortical areas into multiple communities (Bassett et al.,

2006), and by the observation that most cortical areas show involvement in a wide variety of cognitive tasks (Anderson and Pessoa, 2011).

Some comments are in place when interpreting the findings of this study. First, in the main analysis of the study, no information on the strength of corticocortical projections was taken into account. Including information from the original classification of connections into *weak*, *medium*, and *strong* connections did not change the nature of our findings, nor did it reveal clear distinctions in connectivity strength between connection classes. However, the available information on the strength of corticocortical projections in the cat connectome dataset is coarse (Scannell et al., 1995), and future studies examining the architecture of tract-tracing based connectomes including more direct and extensive information on connectivity strength (Markov et al., 2014) would be of high interest. Second, in contrast to aforementioned reports of rich club formation in the human brain, the cat dataset comprises information from a single hemisphere only, which is likely to have an impact on the path motif analysis as only intrahemispheric paths can be examined. However, the considerable overlap between the rich club in the human brain and the cat and macaque brain (Harriger et al., 2012) (with the latter also based on single hemisphere data) further supports the notion that the rich club does not merely relate to bridging the two hemispheres, but rather to linking functional domains in general. Third, the here adopted reconstruction of the cat connectome, as well as macaque connectome reconstructions based on the CoCoMac (for Collation of Connectivity Data on the Macaque Brain) database (Stephan et al., 2001) and the original reconstruction of the connectome of the *Caenorhabditis elegans* (White et al., 1986), are not the result of connectivity mapping within a single animal. Instead, these connectome reconstructions involve the aggregation of connectivity data from multiple animals, obtained (in case of the cat and macaque connectome) through a large number of (mostly) single injection site and single connection studies. This in contrast to *in vivo* diffusion-based studies of the human connectome, which do allow for the examination of brain networks as reconstructed from single individuals (Fornito et al., 2011; Hagmann et al.,

2008; van den Heuvel and Sporns, 2011; Iturria-Medina et al., 2008; Zalesky et al., 2011). Fourth, a number of analyses in this chapter assume an important role for shortest paths in interactions between brain regions. However, as noted previously (van den Heuvel et al., 2012), the human brain is likely a system in which elements only have access to information about the local structure of the network, while selecting shortest paths requires knowledge about the global architecture of the network. Recent studies have proposed a number of interesting metrics that express communication in networks in terms of diffusion-like processes (Esquivel and Rosvall, 2011; Goñi et al., 2013), and studies examining the notion of, for instance, path motifs in combination with such diffusion-based metrics would be of particular interest.

In conclusion, our findings show an important role for the rich club to cross-link different functional communities in the cat brain. A central bridge function of rich club and feeder connections further supports the theory that the rich club forms a key system for global communication and integration in the mammalian brain.

References

- Anderson, M.L., Pessoa, L., 2011. Quantifying the diversity of neural activations in individual brain regions. Proceedings of the 33rd annual conference of the cognitive science society, 2421-2426.
- Bassett, D.S., Meyer-Lindenberg, A., Achard, S., Duke, T., Bullmore, E., 2006. Adaptive reconfiguration of fractal small-world human brain functional networks. *Proceedings of the National Academy of Sciences* 103, 19518-19523.
- Bialonski, S., Wendler, M., Lehnhertz, K., 2011. Unraveling Spurious Properties of Interaction Networks with Tailored Random Networks. *PLoS ONE* 6, e22826.
- Buckner, R.L., Sepulcre, J., Talukdar, T., Krienen, F.M., Liu, H., Hedden, T., Andrews Hanna, J.R., Sperling, R.A., Johnson, K.A., 2009. Cortical Hubs Revealed by Intrinsic Functional Connectivity: Mapping, Assessment of Stability, and Relation to Alzheimer's Disease. *The Journal of Neuroscience* 29, 1860-1873.
- Bullmore, E., Sporns, O., 2009. Complex brain networks: graph theoretical analysis of structural and functional systems. *Nature Reviews Neuroscience* 10, 186-198.
- Bullmore, E., Sporns, O., 2012. The economy of brain network organization. *Nature Reviews Neuroscience* 13, 336-349.
- Colizza, V., Flammini, A., Serrano, M.A., Vespignani, A., 2006. Detecting rich-club ordering in complex networks. *Nature Physics* 2, 110-115.
- Collin, G., Sporns, O., Mandl, R.C.W., van den Heuvel, M.P., 2014. Structural and Functional Aspects Relating to Cost and Benefit of Rich Club Organization in the Human Cerebral Cortex. *Cerebral Cortex* 24, 2258-2267.
- Dehaene, S., Naccache, L., 2001. Towards a cognitive neuroscience of consciousness: basic evidence and a workspace framework. *Cognition* 79, 1-37.
- Esquivel, A.V., Rosvall, M., 2011. Compression of Flow Can Reveal Overlapping-Module Organization in Networks. *Physical Review X* 1, 021025.
- Felleman, D.J., Van Essen, D.C., 1991. Distributed hierarchical processing in the primate cerebral cortex. *Cerebral Cortex* 1, 1-47.
- Fornito, A., Harrison, B.J., Zalesky, A., Simons, J.S., 2012. Competitive and cooperative dynamics of large-scale brain functional networks supporting recollection. *Proceedings of the National Academy of Sciences* 109, 12788-12793.
- Fornito, A. et al., 2011. Genetic Influences on Cost-Efficient Organization of Human Cortical Functional Networks. *The Journal of Neuroscience* 31, 3261-3270.
- Goñi, J., Avena-Koenigsberger, A., de Mendizabal, N.V., van den Heuvel, M.P., Betzel, R.F., Sporns, O., 2013. Exploring the Morphospace of Communication Efficiency in Complex Networks. *PLoS ONE* 8, e58070.
- Guimerà, R., Amaral, L.A.N., 2005. Functional cartography of complex metabolic networks. *Nature* 433, 895-900.
- Hagmann, P., Cammoun, L., Gigandet, X., Meuli, R., Honey, C.J., Wedeen, V.J., Sporns, O., 2008. Mapping the Structural Core of Human Cerebral Cortex. *PLoS Biology* 6, e159.
- Harriger, L., van den Heuvel, M.P., Sporns, O., 2012. Rich Club Organization of Macaque Cerebral Cortex and Its Role in Network Communication. *PLoS ONE* 7, e46497.
- van den Heuvel, M.P., Hulshoff Pol, H.E., 2010. Exploring the brain network: A review on resting-state fMRI functional connectivity. *European Neuropsychopharmacology* 20, 519-534.
- van den Heuvel, M.P., Kahn, R.S., Goñi, J., Sporns, O., 2012. High-cost, high-capacity backbone for global brain communication. *Proceedings of the National Academy of Sciences* 109, 11372-11377.
- van den Heuvel, M.P., Sporns, O., 2011. Rich-Club Organization of the Human Connectome. *The Journal of Neuroscience* 31, 15775-15786.
- van den Heuvel, M.P., Sporns, O., Collin, G., Scheewe, T., Mandl, R.C.W., Cahn, W., Goñi, J., Hulshoff Pol, H.E., Kahn, R.S., 2013. Abnormal rich club organization and functional brain dynamics in schizophrenia. *JAMA Psychiatry* 70, 783-792.
- Iturria-Medina, Y., Sotero, R.C., Canales-Rodríguez, E.J., Alemán-Gómez, Y., Melie-García, L., 2008. Studying the human brain anatomical network via diffusion-weighted MRI and Graph Theory. *NeuroImage* 40, 1064-1076.

CHAPTER 5

- Markov, N.T. et al., 2014. A Weighted and Directed Interareal Connectivity Matrix for Macaque Cerebral Cortex. *Cerebral Cortex* 24, 17-36.
- Maslov, S., Sneppen, K., 2002. Specificity and Stability in Topology of Protein Networks. *Science* 296, 910-913.
- Newman, M.E.J., 2006. Modularity and community structure in networks. *Proceedings of the National Academy of Sciences* 103, 8577-8582.
- Page, L., Brin, S., Motwani, R., Winograd, T., 1999. The PageRank Citation Ranking: Bringing Order to the Web. Technical Report. Stanford InfoLab, 1999-66.
- Rubinov, M., Sporns, O., 2010. Complex network measures of brain connectivity: Uses and interpretations. *NeuroImage* 52, 1059-1069.
- Scannell, J.W., Blakemore, C., Young, M.P., 1995. Analysis of connectivity in the cat cerebral cortex. *The Journal of Neuroscience* 15, 1463-1483.
- Scannell, J.W., Young, M.P., 1993. The connectional organization of neural systems in the cat cerebral cortex. *Current Biology* 3, 191-200.
- Selemon, L.D., Goldman-Rakic, P.S., 1988. Common cortical and subcortical targets of the dorsolateral prefrontal and posterior parietal cortices in the rhesus monkey: evidence for a distributed neural network subserving spatially guided behavior. *The Journal of Neuroscience* 8, 4049-4068.
- Sepulcre, J., Sabuncu, M.R., Johnson, K.A., 2012. Network assemblies in the functional brain. *Current Opinion in Neurology* 25, 384.
- Sereno, M.I., Tootell, R.B.H., 2005. From monkeys to humans: what do we now know about brain homologies? *Current Opinion in Neurobiology* 15, 135-144.
- Shen, K., Bezgin, G., Hutchison, R.M., Gati, J.S., Menon, R.S., Everling, S., McIntosh, A.R., 2012. Information Processing Architecture of Functionally Defined Clusters in the Macaque Cortex. *The Journal of Neuroscience* 32, 17465-17476.
- Sporns, O., 2011. The human connectome: a complex network. *Annals of the New York Academy of Sciences* 1224, 109-125.
- Sporns, O., Honey, C.J., Kötter, R., 2007. Identification and Classification of Hubs in Brain Networks. *PLoS ONE* 2, e1049.
- Sporns, O., Tononi, G., Kötter, R., 2005. The Human Connectome: A Structural Description of the Human Brain. *PLoS Computational Biology* 1, e42.
- Stephan, K.E., Kamper, L., Bozkurt, A., Burns, G.A.P.C., Young, M.P., Kötter, R., 2001. Advanced database methodology for the Collation of Connectivity data on the Macaque brain (CoCoMac). *Philosophical Transactions of the Royal Society of London B: Biological Sciences* 356, 1159-1186.
- Tomasi, D., Volkow, N.D., 2010. Functional connectivity density mapping. *Proceedings of the National Academy of Sciences* 107, 9885-9890.
- Towlson, E.K., Vértes, P.E., Ahnert, S.E., Schafer, W.R., Bullmore, E.T., 2013. The Rich Club of the *C. elegans* Neuronal Connectome. *The Journal of Neuroscience* 33, 6380-6387.
- White, J.G., Southgate, E., Thomson, J.N., Brenner, S., 1986. The Structure of the Nervous System of the Nematode *Caenorhabditis elegans*. *Philosophical Transactions of the Royal Society of London B: Biological Sciences* 314, 1-340.
- Young, M.P., 1993. The Organization of Neural Systems in the Primate Cerebral Cortex. *Proceedings of the Royal Society of London B: Biological Sciences* 252, 13-18.
- Zalesky, A., Fornito, A., Bullmore, E., 2012. On the use of correlation as a measure of network connectivity. *NeuroImage* 60, 2096-2106.
- Zalesky, A., Fornito, A., Seal, M.L., Cocchi, L., Westin, C.F., Bullmore, E.T., Egan, G.F., Pantelis, C., 2011. Disrupted Axonal Fiber Connectivity in Schizophrenia. *Biological Psychiatry* 69, 80-89.
- Zamora-López, G., Zhou, C., Kurths, J., 2010. Cortical hubs form a module for multisensory integration on top of the hierarchy of cortical networks. *Frontiers in Neuroinformatics* 4, 1.



Chapter 6

Simulated rich club lesioning in brain networks: a scaffold for communication and integration?

*Based on a publication (Frontiers in Human Neuroscience, vol. 8, 2014)
by Marcel A. de Reus and Martijn P. van den Heuvel*

Abstract

Brain function depends on effective neural communication and integration across different domains. This exchange of information is facilitated by the *connectome*; the complex network of all neural elements and neural connections of an organism that provides the anatomical foundation for emerging functional dynamics. How the complex wiring of the connectome relates to the demands and constraints placed upon the brain is an important question in neuroscience, receiving attention from a rapidly increasing number of researchers.

One potential aspect of macroscale connectome architecture related to global communication and integration is the existence of *neural hubs*, referring to brain regions that display many connections and thus exhibit a topologically central position in the overall network. In addition to being individually rich in connectivity, hubs in neural systems tend to be also densely interconnected, together forming a central *rich club* (van den Heuvel and Sporns, 2011). Over the past years, several reports on a number of different species (including human, macaque, cat, and nematode) have consistently suggested that brain hubs and their rich club connections play an important role in enabling efficient neural communication and integration, constituting a central communication backbone that boosts the functional repertoire of the system (Crossley et al., 2013; Grayson et al., 2014; van den Heuvel and Sporns, 2013; Mišić et al., 2014; Senden et al., 2014; Towlson et al., 2013; Zamora-López et al., 2010) (also see **chapter 5**). Since brain hubs have been shown to be implicated in both neurological (Buckner et al., 2009; Stam et al., 2007) and psychiatric (Collin et al., 2014; van den Heuvel et al., 2013) diseases, it is the general hope that a better fundamental understanding of their role in connectome organization may eventually provide insight in the pathology and effects of brain disorders.

In an interesting article recently published in *Frontiers in Human Neuroscience*, Andrei Irimia and John Van Horn aimed to further elucidate healthy brain network architecture by pinpointing those neural connections that are critical for the overall organization of the human connectome (Irimia and Van Horn, 2014).

Simulating the effects of white matter lesions by removing individual connections from the connectome, the authors report on a scaffold of white matter connections whose disruption is suggested to have significant global-level effects on the brain. However, quite contrary to our expectations, the authors note that "connections between rich club nodes in the human brain overlap only very moderately – and even then, perhaps accidentally – with the core scaffold" (Irimia and Van Horn, 2014).

In this chapter, we discuss the apparent incongruity between Irimia and Van Horn's lesioning scaffold and the growing amount of studies suggesting that neural hubs and their connections may form a fundamental architecture for shaping global neural processes. Analyzing new data, we show that the importance of connections assessed by simulated lesioning largely depends on the measures chosen to evaluate the outcome. We further demonstrate that lesioning connections between rich club regions has pronounced effects on two specific measures of communication and integration, both in the human and animal brain.

6

Lesioning connections

We concur with Irimia and Van Horn that while much research is geared toward understanding the network features of brain regions (i.e., the nodes of the connectome), network properties of the edges between brain regions – representing white matter connections – may contain important additional information (**chapter 1**). The strategy adopted by Irimia and Van Horn to quantify how lesioning an individual connection affects the global network structure is an elegant way to shift focus from nodes to edges and provides insight in the role or importance of the disrupted connection (also see **chapter 7** and **chapter 8**).

In Irimia and Van Horn's paper, individual white matter edges were removed, one at a time, across reconstructed brain networks of 110 individuals. Brain networks were derived using diffusion tractography and comprised 165 regions.

The effect of the removal of each edge was quantified by comparing four graph measures, being assortativity, characteristic path length, density, and transitivity (see Rubinov and Sporns (2010) for an overview), before and after removal of the edge. Next, the observed differences with respect to these four metrics were combined into a single test statistic for each connection, expressing the significance of the effects caused by its removal. After evaluating the effects across all edges of the connectome, the authors found a diverse scaffold of white matter connections with a significant combined effect on the examined global network metrics, presenting (somewhat surprisingly) only little overlap with hub-to-hub rich club connections.

Choosing metrics

An essential ingredient of the adopted simulated lesioning approach are the network metrics chosen to assess the consequences of the simulated lesions. Unfortunately, it is generally difficult to judge which network metrics reflect "key" features of the brain and are suitable to capture lesion effects. For instance, since it is not always beneficial for a network to be assortative (Zhou et al., 2012), it is unclear whether changes in assortativity (e.g., due to lesions) are relevant for the functioning of brain networks.

In addition, there is a somewhat more attestable issue regarding the effectiveness of the mean shortest (i.e., characteristic) path length to assess changes upon connection lesioning. If the hypothesized disruption of a connection does eliminate some but not all shortest paths between two brain regions, the shortest path length between those regions does not change, while their mutual communication is still likely to be affected (Figure 6.1a). This issue is related to the observation by Rubinov and Sporns (2010) that "measures such as the characteristic path length ... do not incorporate multiple and longer paths" and is especially relevant because of the high incidence of parallel processing paths in the brain (Alexander and Crutcher, 1990; Goldman-Rakic, 1988). A generalization of shortest path length that takes all possible paths between brain regions

into account is the *communicability* metric of Estrada and Hatano (2008). This metric assigns higher weights to shorter paths (an explicit definition is given in the Supplementary Information (SI) section at the end of the chapter), which elegantly aligns with a recent report showing that shorter communication paths are associated with higher functional connectivity between brain regions (Goñi et al., 2014). Combined with some interesting applications of communicability in neuroscience (Duarte-Carvajalino et al., 2012; Mantzaris et al., 2013), especially as a tool to measure effects of actual (non-simulated) lesions in the brain (Crofts and Higham, 2009; Crofts et al., 2011), we believe that communicability may be a promising metric for simulated lesioning approaches.

Role of rich club connections

To offer quantitative insight on this matter, we made a connectome map of the human cerebral cortex on the basis of high-quality diffusion-weighted MRI data from 215 subjects as provided by the Q3 data release of the Human Connectome Project (Glasser et al., 2013; Van Essen et al., 2012). White matter fibers were traced using generalized *q*-sampling imaging (GQI; allowing for the reconstruction of crossing fibers) and streamline tractography (Yeh et al., 2010) and the cortex was parcellated into 219 distinct regions on the basis of a high-resolution subdivision of FreeSurfer's Desikan-Killiany atlas (Cammoun et al., 2012). Combining data from all 215 subjects, a group-averaged connectome map was formed by placing an edge between two brain regions if those regions were found to be connected in at least 60% of the subjects (see **chapter 4**). Rich club regions were taken to include the 15% highest degree nodes of this connectome map (van den Heuvel et al., 2012).

Impact on assortativity, transitivity and path length

As shown in Figure 6.1b, our analyses revealed that systematic removal of connections between rich club regions did have a (modestly) larger impact on the assortativity and transitivity of the network than removal of *feeder* and *local* connections – respectively reflecting edges between rich club hub regions and

peripheral non-hub regions and edges between peripheral regions (Figure 6.1c). However, in agreement with the report of Irimia and Van Horn, removal of rich club connections did not have an outspoken effect on the characteristic path length of the network (Figure 6.1b), explaining why rich club connections may not appear in a scaffold that is based on the combined effects on assortativity, transitivity, and path length.

Impact on communicability

Interestingly, the same lesioning approach did reveal a strong impact of rich club connections on the above-described communicability measure. In fact, removal of rich club connections (mean [std]: -3.8 [1.9]%) had a 2.4 times larger impact on the network's communicability than removal of feeder connections (mean [std]: -1.6 [1.3]%, $p < 10^{-4}$, permutation test) and a 9.5 times larger impact than removal of local connections (mean [std]: -0.4 [0.5]%, $p < 10^{-4}$) (Figure 6.1b).

Furthermore, going beyond the examination of rich club connections as a class, Figure 6.1d shows the communicability impact for each connection separately, confirming a strong concentration of high-impact edges around rich club nodes. Quantifying the overlap between rich club connections and potential communicability scaffolds, we found that the vast majority of rich club connections (86%) belonged to the 30% connections with the highest impact on communicability, with 79/63% of the rich club connections even scoring among the "best" 20/10%. Statistical evaluation through random reassignment of connection scores showed that these effects are highly unlikely to occur if the two phenomena are unrelated (all $p < 10^{-6}$), in which case the expected number of rich club connections among the 30, 20, and 10% connections with the highest impact on communicability would just be equal to, respectively, 30, 20, and 10%.

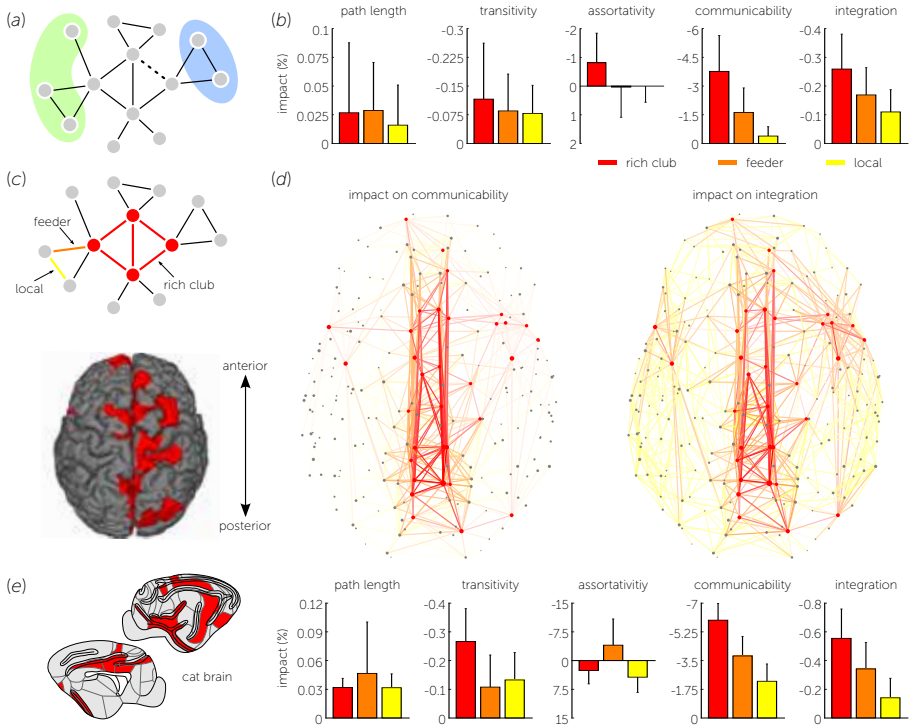


Figure 6.1. Effects of simulated connection lesioning. (a) A simple toy network shows that, due to the presence of parallel pathways, removal of the dashed connection does not alter the path length (i.e., minimum number of steps) between nodes in the green and blue zone. A change in communication capacity between the two zones is only detected if also the number of possible routes is taken into account, as is the case with Estrada and Hatano's communicability metric (Estrada and Hatano, 2008). (b) Impact of connection lesioning in the human brain as measured by five different network metrics. Connection scores were obtained by comparing a group-averaged connectome map, based on high-quality data of 215 subjects from the Human Connectome Project (Van Essen et al., 2012), before and after removing an individual edge. The bars and whiskers indicate the average score and standard deviation for the three connection classes illustrated in panel (c): *rich club* connections between (red) rich club nodes, *feeder* connections between rich club and (gray) non-rich club nodes, and *local* connections between non-rich club nodes. (d) Network plots showing the importance of individual connections for the network's communicability and functional integration. Removal scores are reflected by the transparency of connections, the most important connections being the most opaque. Underscoring the visual concentration of crucial edges around rich club nodes, the vast majority of rich club connections was found to belong to the 30% connections with the highest impact on communicability. (e) Validation on the basis of a tract-tracing reconstruction of the cat connectome revealed highly similar results, again showing a pronounced role of rich club connections in global communication and functional integration.

Impact on functional integration

Assessment of the effect of simulated connection disruption on a metric for the integration between 11 previously identified resting-state functional brain networks proposed by Tononi et al. (1994) (see the SI section for details) revealed a similar pattern. As shown in Figure 6.1b and Figure 6.1d, removal of rich club connections (mean [std]: -0.26 [0.12]%) resulted in a 1.5 times larger decrease of functional integration than removal of feeder connections (mean [std]: -0.17 [0.09]%, $p < 10^{-4}$) and a 2.4 times larger decrease than removal of local connections (mean [std]: -0.11 [0.08]%, $p < 10^{-4}$).

Validation

As described in more detail in the SI section, the elevated impact of rich club connections on the adopted communicability and integration metric was both confirmed using alternative group-averaged connectomes (constructed with group thresholds of 30, 45, 75, and 90%) and by simulated lesioning of individual connectome reconstructions (see Supplementary Figures 6.1 and 6.2). To further validate our findings, we additionally examined a tract-tracing based reconstruction of the cat connectome. Using the same cat rich club regions and functional domains as described in **chapter 5**, removal of rich club connections showed a distinct impact on the communicability of the cat connectome (mean [std]: -6.0 [1.0]%), significantly exceeding the removal effects of both feeder and local connections (both $p < 10^{-4}$, Figure 6.1e). Closely matching our findings on the human connectome, 62% of the rich club connections scored among the top 10% connections with the highest removal effect on communicability and almost all rich club connections (97%) belonged to the top 30%. Moreover, also the staircase relation for functional integration was clearly reproducible (all differences significant with $p < 10^{-4}$).

Discussion

The observed differences between simulated lesioning results assessed with characteristic path length, which is a conventional measure for communication and integration (Rubinov and Sporns, 2010), and simulated lesioning results assessed with Estrada's communicability or Tononi's integration metric, demonstrate that the answer to the question "which white matter connections cause large global-level effects when hypothetically lesioned?" largely depends on the metrics chosen to evaluate those effects, even if the metrics belong to the same "family". This is further underscored by a post-hoc analysis in which we computed the impact of connection disruption on a measure for diffusion-based communication, estimating the number of steps needed to send a "signal" from one brain region to another under the assumption that the signal moves randomly along the connections of the network (see the SI section for details). Simulated lesioning outcomes with respect to this diffusion-based communication metric qualitatively differed from both characteristic path length and communicability outcomes, showing a "reverse" staircase with a low impact for rich club connections and a prominent role for local connections (Supplementary Figure 6.3).

Taken together, our results extend the observations of Irimia and Van Horn by showing that although hub-to-hub rich club connections may not appear in an aggregated lesioning scaffold derived using characteristic path length as communication metric, they do have a high impact on two other specific measures for communication and integration, namely Estrada's communicability and Tononi's integration metric. Rich club connections may thus not be critical for establishing (unique) short paths between remote brain regions, but do appear to play an important role in providing diverse communication paths across the network and integration of information between different functional domains. These observations nicely align with a growing number of reports suggesting that neural hubs and their connections play a central role in neural networks (van den Heuvel and Sporns, 2014) and recent simulation studies suggesting that the presence of neural rich clubs enhances functional diversity (Senden et al., 2014).

The idea behind communicability that also parallel and longer paths may contribute to exchange of information between brain regions holds the middle between characteristic path length, assuming that signals only follow shortest paths, and diffusion-based metrics, assuming randomly moving signals (which actually tend to get “trapped” in densely connected zones such as the rich club (Rosvall and Bergstrom, 2008)). In our opinion, this could be a plausible regime for the brain, especially because brain networks do not appear to be specifically optimized for either shortest path-based or diffusion-based communication (Goñi et al., 2013). An important future challenge in the field of connectomics will be to examine the biological relevance of such communication principles and other network measures, making it possible to determine which metrics encode key features of the brain’s wiring architecture.

Acknowledgments

Human neuroimaging data for this study was provided by the Human Connectome Project, WU-Minn Consortium (Principal Investigators: David Van Essen and Kamil Ugurbil; 1U54MH091657) funded by the 16 NIH Institutes and Centers that support the NIH Blueprint for Neuroscience Research; and by the McDonnell Center for Systems Neuroscience at Washington University.

Supplementary information

Communicability and integration

Complementing standard network metrics such as characteristic path length, transitivity, and assortativity (see (Rubinov and Sporns, 2010) for an overview), we also used the following less well-known metrics to quantify the effects of simulated white matter lesions:

Communicability

Originally introduced by Estrada and Hatano (2008), communicability G_{ij} is a measure for the "ease of communication" between two nodes i and j of a network. Rather than taking only the shortest paths between i and j into account, G_{ij} incorporates all possible walks (i.e., paths that may visit the same edge multiple times) between the two nodes with appropriate weights, assigning lower weights to longer walks. It is formally given by:

$$G_{ij} = \sum_{k=0}^{\infty} \frac{(A^k)_{ij}}{k!} = \exp(A)_{ij}, \quad (6.1)$$

where A denotes the adjacency matrix of the network, satisfying $A_{ij} = 1$ if node i and j are connected and $A_{ij} = 0$ otherwise, and $(A^k)_{ij}$ equals the number of walks of length k from node i to node j . To measure the overall communicability G within the entire network, G_{ij} was averaged over all node pairs (i, j) (Benzi and Klymko, 2013). As such, G is a direct generalization of the characteristic path length, with the notable difference that also the number of shortest paths (i.e., parallel paths), as well as slightly longer paths, are assumed to contribute to information exchange between network nodes.

Integration

As proposed in the seminal paper of Tononi et al. (1994), the level of integration I between subnetworks X_1, X_2, \dots, X_m of a network X can be theoretically described by the formula:

$$I(X) = \sum_{i=1}^m H(X_i) - H(X), \quad (6.2)$$

where $H(X_i)$ is the entropy of subnetwork X_i considered as an isolated system and $H(X)$ is the joint entropy of the network as a whole. The idea behind this formula is that dependencies between the subnetworks reduce the "amount of freedom" in the network, causing the entropy of the entire system to be lower than the sum of isolated subnetwork entropies. By measuring the size of this discrepancy, $I(X)$ thus effectively measures the extent to which the subnetworks X_1, X_2, \dots, X_m depend on each other.

As described in detail by Zamora-López et al. (2010), the entropies required to compute $I(X)$ can be derived from the covariance matrix $\text{cov}(X)$ of the network. Using a simple linear model for network dynamics in which the nodes of the network are driven by Gaussian noise, this covariance matrix can be computed analytically from the adjacency matrix A and coupling factor g by $\text{cov}(X) = Q \cdot Q^t$, with matrix Q equal to $1/(1 - gA^t)$. The entropies $H(X), H(X_1), H(X_2), \dots, H(X_m)$, and thus $I(X)$, can then be computed using:

$$H(X_i) = \frac{1}{2} \log((2\pi e)^{n_i} |\text{cov}(X_i)|), \quad (6.3)$$

where n_i is the number of nodes in X_i and $|\text{cov}(X_i)|$ is the determinant of the submatrix of $\text{cov}(X)$ obtained by selecting the rows and columns that correspond to nodes in X_i .

For the present study, the subnetworks X_1, X_2, \dots, X_m were taken to reflect 11 previously identified resting-state functional brain networks (van den Heuvel et al., 2014; van den Heuvel and Sporns, 2013) and the coupling factor g was taken

to be $0.5/\lambda_{\max}$, with λ_{\max} equal to the largest eigenvalue of the intact adjacency matrix (Zamora-López et al., 2010).

Mean first-passage time

Next to characteristic path length and communicability, a different perspective on communication in complex networks is given by diffusion-based communication metrics such as the mean first-passage time (Goñi et al., 2013). The assumption behind these diffusion-based metrics is that network nodes do not have any information about each other's (topological) position and possible communication routes, implying that "signals" have to reach their destination by moving randomly along the connections of the network. The mean first-passage time T_{ij} estimates how many connections a randomly moving signal starting at node i on average has to traverse to reach node j .

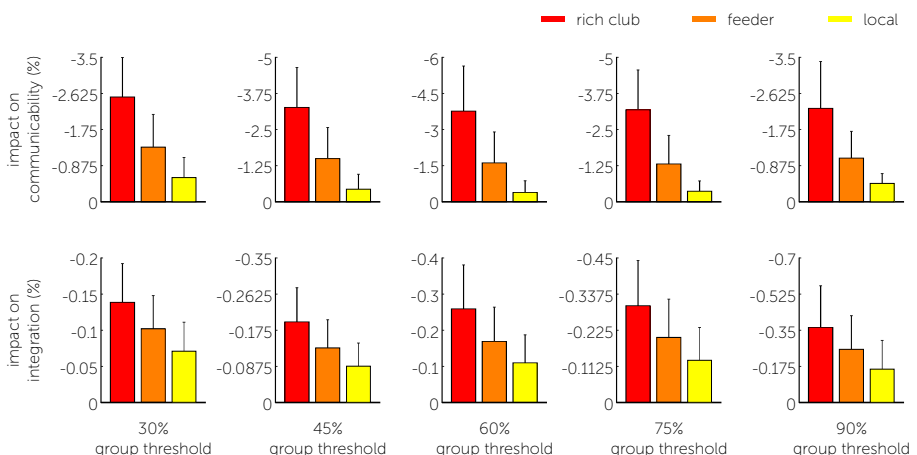
Mathematically, random signal movement is captured by the concept of a *random walk*, moving from one node in the network to the next by randomly selecting one of the node's neighbors. The probability that a random walk transits from node i to node j is therefore given by $P_{ij} = A_{ij}/d_i$, with A equal to the adjacency matrix of the network and d_i equal to the degree (i.e., number of connections) of node i . Together, these probabilities P_{ij} constitute the transition matrix P of the network and the mean first-passage time T_{ij} can be computed from P using:

$$T_{ij} = \frac{Z_{jj} - Z_{ij}}{\pi_j}, \quad (6.4)$$

where π is the left eigenvector of P corresponding to its largest eigenvalue (normalized such that $\sum_i \pi_i = 1$), describing the ergodic node visit frequencies of an infinitely long random walk, and $Z = (I - P + W)^{-1}$ is the fundamental matrix, with I equal to the identity matrix and W a square matrix with every row equal to π (Goñi et al., 2013; Zhang et al., 2011). Analogous to the approach for path length and communicability, a global estimate T for the mean first-passage time was obtained by averaging T_{ij} over all node pairs (i, j) .

Group threshold selection

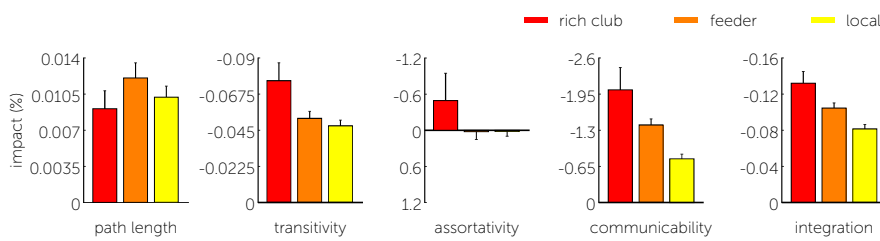
Simulated lesioning results were obtained by removing individual connections from a group-averaged connectome map, incorporating high-quality MRI data of 215 subjects as provided by the Human Connectome Project. The group-averaged connectome map was formed by placing an edge between two brain regions if those regions were found to be connected in at least 60% of the subjects. An extensive study concerning this averaging procedure and the associated choice of *group threshold* can be found in **chapter 4**. In that chapter, we conclude that the group threshold should preferable be chosen between 30 and 90% and that 60% appears to be an optimal choice, explaining our current setting. To eliminate the possibility that the here presented findings depend on the chosen group threshold, we additionally computed the impact of connection lesioning for group thresholds of 30, 45, 75, and 90%. The results obtained using these four additional group thresholds (Supplementary Figure 6.1) were found to be highly similar to the results presented in the main text, consistently showing that removal of rich club connections has a significantly larger impact on the above-described communicability and integration metric than removal of feeder and local connections.



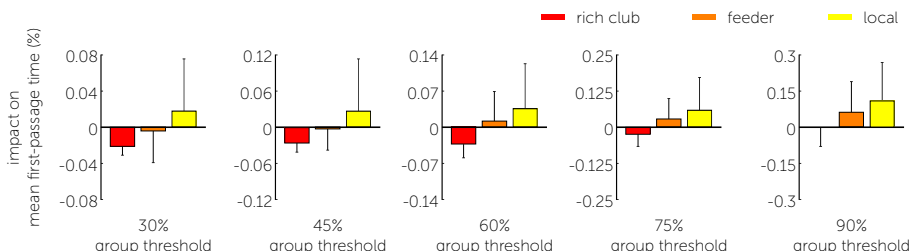
Supplementary Figure 6.1. Effects of simulated connection lesioning on communicability and integration for five different group-averaged connectomes, constructed with group thresholds of 30, 45, 60 (the setting used in the main text), 75, and 90%. For all thresholds, lesioning rich club connections had a significantly larger impact on communicability and integration than lesioning feeder or local connections ($p < 10^{-4}$).

Simulated lesioning in individual subjects

In addition to simulating lesions in group-averaged connectomes, we also quantified the effects of simulated lesioning on the basis of individual connectome reconstructions. To this end, the average impact of rich club, feeder, and local connections with respect to the adopted network metrics was computed for each individual subject and the three resulting distributions were tested for differences using permutation tests (Supplementary Figure 6.2). Consistent with our findings based on group-averaged connectomes, simulated lesioning of rich club connections had significantly larger impact on communicability and integration than removal of feeder and local connections ($p < 10^{-4}$).



Supplementary Figure 6.2. Effects of simulated connection lesioning based on individual connectome reconstructions. For each of the 215 subjects, the average impact of its rich club, feeder, and local connections was measured with respect to five different network metrics, resulting in 15 distributions of 215 values. The depicted bars and whiskers respectively reflect the mean and standard deviation of these distributions.

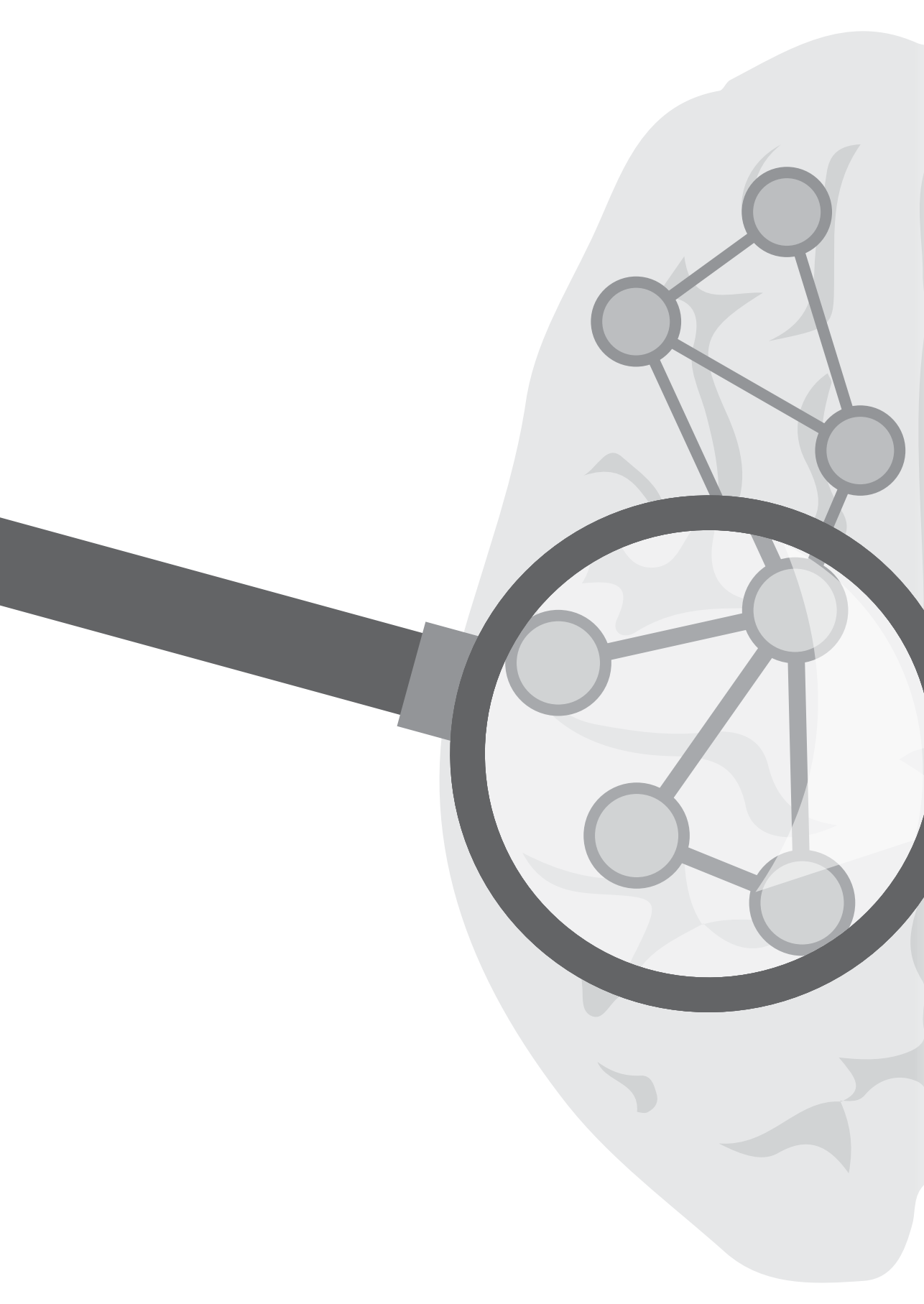


Supplementary Figure 6.3. Effects of simulated connection lesioning on the mean first-passage time. The mean first-passage time between two nodes i and j of the network is an estimate for the number of connections that a signal starting at node i traverses before it reaches node j when randomly moving along the connections of the network.

References

- Alexander, G.E., Crutcher, M.D., 1990. Functional architecture of basal ganglia circuits: neural substrates of parallel processing. *Trends in Neurosciences* 13, 266-271.
- Benzi, M., Klymko, C., 2013. Total communicability as a centrality measure. *Journal of Complex Networks* 1, 124-149.
- Buckner, R.L., Sepulcre, J., Talukdar, T., Krienen, F.M., Liu, H., Hedden, T., Andrews Hanna, J.R., Sperling, R.A., Johnson, K.A., 2009. Cortical Hubs Revealed by Intrinsic Functional Connectivity: Mapping, Assessment of Stability, and Relation to Alzheimer's Disease. *The Journal of Neuroscience* 29, 1860-1873.
- Cammoun, L., Gigandet, X., Meskaldji, D., Thiran, J.P., Sporns, O., Do, K.Q., Maeder, P., Meuli, R., Hagmann, P., 2012. Mapping the human connectome at multiple scales with diffusion spectrum MRI. *Journal of Neuroscience Methods* 203, 386-397.
- Collin, G., Kahn, R.S., de Reus, M.A., Cahn, W., van den Heuvel, M.P., 2014. Impaired Rich Club Connectivity in Unaffected Siblings of Schizophrenia Patients. *Schizophrenia Bulletin* 40, 438-448.
- Crofts, J.J., Higham, D.J., 2009. A weighted communicability measure applied to complex brain networks. *Journal of the Royal Society Interface* 6, 411-414.
- Crofts, J.J., Higham, D.J., Bosnell, R., Jbabdi, S., Matthews, P.M., Behrens, T.E.J., Johansen-Berg, H., 2011. Network analysis detects changes in the contralesional hemisphere following stroke. *NeuroImage* 54, 161-169.
- Crossley, N.A., Mechelli, A., Vértes, P.E., Winston-Brown, T.T., Patel, A.X., Ginestet, C.E., McGuire, P., Bullmore, E.T., 2013. Cognitive relevance of the community structure of the human brain functional coactivation network. *Proceedings of the National Academy of Sciences* 110, 11583-11588.
- Duarte-Carvajalino, J.M., Jahanshad, N., Lenglet, C., McMahon, K.L., de Zubicaray, G.I., Martin, N.G., Wright, M.J., Thompson, P.M., Sapiro, G., 2012. Hierarchical topological network analysis of anatomical human brain connectivity and differences related to sex and kinship. *NeuroImage* 59, 3784-3804.
- Estrada, E., Hatano, N., 2008. Communicability in complex networks. *Physical Review E* 77, 036111.
- Glasser, M.F. et al., 2013. The minimal preprocessing pipelines for the Human Connectome Project. *NeuroImage* 80, 105-124.
- Goldman-Rakic, P.S., 1988. Topography of Cognition: Parallel Distributed Networks in Primate Association Cortex. *Annual Review of Neuroscience* 11, 137-156.
- Goñi, J., Avena-Koenigsberger, A., de Mendizabal, N.V., van den Heuvel, M.P., Betzel, R.F., Sporns, O., 2013. Exploring the Morphospace of Communication Efficiency in Complex Networks. *PLoS ONE* 8, e58070.
- Goñi, J., van den Heuvel, M.P., Avena-Koenigsberger, A., de Mendizabal, N.V., Betzel, R.F., Griffa, A., Hagmann, P., Corominas-Murtra, B., Thiran, J.P., Sporns, O., 2014. Resting-brain functional connectivity predicted by analytic measures of network communication. *Proceedings of the National Academy of Sciences* 111, 833-838.
- Grayson, D.S., Ray, S., Carpenter, S., Iyer, S., Dias, T.G.C., Stevens, C., Nigg, J.T., Fair, D.A., 2014. Structural and Functional Rich Club Organization of the Brain in Children and Adults. *PLoS ONE* 9, e88297.
- van den Heuvel, M.P., Kahn, R.S., Goñi, J., Sporns, O., 2012. High-cost, high-capacity backbone for global brain communication. *Proceedings of the National Academy of Sciences* 109, 11372-11377.
- van den Heuvel, M.P., Kersbergen, K.J., de Reus, M.A., Keunen, K., Kahn, R.S., Groenendaal, F., de Vries, L.S., Binders, M.J.N.L., 2014. The Neonatal Connectome During Preterm Brain Development. *Cerebral Cortex*, epub ahead of print.
- van den Heuvel, M.P., Sporns, O., 2011. Rich-Club Organization of the Human Connectome. *The Journal of Neuroscience* 31, 15775-15786.
- van den Heuvel, M.P., Sporns, O., 2013. An Anatomical Substrate for Integration among Functional Networks in Human Cortex. *The Journal of Neuroscience* 33, 14489-14500.
- van den Heuvel, M.P., Sporns, O., 2014. Network hubs in the human brain. *Trends in Cognitive Sciences* 17, 683-696.
- van den Heuvel, M.P., Sporns, O., Collin, G., Scheewe, T., Mandl, R.C.W., Cahn, W., Goñi, J., Hulshoff Pol, H.E., Kahn, R.S., 2013. Abnormal rich club organization and functional brain dynamics in schizophrenia. *JAMA Psychiatry* 70, 783-792.

- Irimia, A., Van Horn, J.D., 2014. Systematic network lesioning reveals the core white matter scaffold of the human brain. *Frontiers in Human Neuroscience* 8, 51.
- Mantzaris, A.V., Bassett, D.S., Wymbs, N.F., Estrada, E., Porter, M.A., Mucha, P.J., Grafton, S.T., Higham, D.J., 2013. Dynamic network centrality summarizes learning in the human brain. *Journal of Complex Networks* 1, 83-92.
- Mišić, B., Sporns, O., McIntosh, A.R., 2014. Communication Efficiency and Congestion of Signal Traffic in Large-Scale Brain Networks. *PLoS Computational Biology* 10, e1003427.
- Rosvall, M., Bergstrom, C.T., 2008. Maps of random walks on complex networks reveal community structure. *Proceedings of the National Academy of Sciences* 105, 1118-1123.
- Rubinov, M., Sporns, O., 2010. Complex network measures of brain connectivity: Uses and interpretations. *NeuroImage* 52, 1059-1069.
- Senden, M., Deco, G., de Reus, M.A., Goebel, R., van den Heuvel, M., 2014. Rich club organization supports a diverse set of functional network configurations. *NeuroImage* 96, 174-182.
- Stam, C.J., Jones, B.F., Nolte, G., Breakspear, M., Scheltens, P., 2007. Small-World Networks and Functional Connectivity in Alzheimer's Disease. *Cerebral Cortex* 17, 92-99.
- Tononi, G., Sporns, O., Edelman, G.M., 1994. A measure for brain complexity: relating functional segregation and integration in the nervous system. *Proceedings of the National Academy of Sciences* 91, 5033-5037.
- Towlson, E.K., Vértes, P.E., Ahnert, S.E., Schafer, W.R., Bullmore, E.T., 2013. The Rich Club of the *C. elegans* Neuronal Connectome. *The Journal of Neuroscience* 33, 6380-6387.
- Van Essen, D.C. et al., 2012. The Human Connectome Project: A data acquisition perspective. *NeuroImage* 62, 2222-2231.
- Yeh, F.C., Wedeen, V.J., Tseng, W.Y.I., 2010. Generalized q-Sampling Imaging. *IEEE Transactions on Medical Imaging* 29, 1626-1635.
- Zamora-López, G., Zhou, C., Kurths, J., 2010. Cortical hubs form a module for multisensory integration on top of the hierarchy of cortical networks. *Frontiers in Neuroinformatics* 4, 1.
- Zhang, Z., Julaiti, A., Hou, B., Zhang, H., Chen, G., 2011. Mean first-passage time for random walks on undirected networks. *The European Physical Journal B* 84, 691-697.
- Zhou, D., Stanley, H.E., D'Agostino, G., Scala, A., 2012. Assortativity decreases the robustness of interdependent networks. *Physical Review E* 86, 066103.



Chapter 7

Mapping and examining the rodent connectome

Part I: Based on a publication (ACS Chemical Neuroscience, vol. 5, 2014, pp. 491-493) by Martijn P. van den Heuvel and Marcel A. de Reus

Part II: Based on a publication (Brain Structure and Function, 2015, doi:10.1007/s00429-015-0999-6) by Martijn P. van den Heuvel, Lianne H. Scholtens and Marcel A. de Reus

Abstract

The mammalian brain is a complex network of anatomically interconnected regions. Animal studies allow for an invasive measurement of the connections of this network by means of neuronal tracing of axonal projections, providing a unique opportunity for the formation of detailed connectome maps. In the first part of this chapter, we discuss a recently published connectome map of the mouse brain. We underscore the map's high spatial resolution and discuss key organizational network attributes of the presented connectome, its potential impact on neuroscience, and the general importance of connectome maps to obtain insight in the workings of the brain at a systems level. In the second part of the chapter, we present an analysis of the macroscale connectome of the rat brain as provided by the high-quality, open-access BAMS-II database on rat brain anatomical projections, focusing in particular on the non-uniform distribution of projection strength across pathways.

Part I: Chasing the dreams of early connectionists

Dating as far back as to the earliest days of neuroscience, anatomists have always been fascinated by creating maps of the brain's white matter. One of the early pioneers, Niels Stensen (1638-1686), envisioned in his 1665 essay that a fruitful way of studying the brain's white matter might be to follow "the nerve threads through the substance of the brain to find out where they go and where they end" (cited in Schmahmann and Pandya (2006, p. 11)). Today, inspired by their vision, neuroscience is standing at the frontier of state-of-the-art technology capable of making a map of not just a subset, but all nerve threads that comprise the brain.

In a recent *Nature* paper (Oh et al., 2014), the team of Hongkui Zeng from the Allen Institute for Brain Science describes the results of a high-throughput data acquisition and processing platform to systematically map and document the anatomical wiring of the adult mouse brain. Connection mapping involved the administration of anterograde recombinant adeno-associated virus (AAV) tracers to 295 non-overlapping anatomical regions, providing a complete coverage of the mouse brain, with axonal projections systematically traced from the (cell bodies at the) injection site to the synaptic termination sites of the infected axons using two-photon microscopy. With this technology, Zeng and colleagues provide a first brain-wide *connectome* map (Bullmore and Sporns, 2009) of the neural wiring of a mammalian brain at a mesoscopic scale. Previous studies have provided macroscale wiring diagrams of, for example, the macaque and cat cortex, but all these maps have been based on a collation of tract-tracing data across a large number of studies, resulting in relatively coarse and often not entirely complete connectome maps. Besides an unprecedented mesoscale resolution, the Allen Brain mouse connectome map (Figure 7.1.1a) thus provides one of the first reconstructions performed by a single group following a standardized mapping protocol, which is another strong improvement over earlier pioneering endeavors.

Interestingly, going beyond “just” mapping connections, Zeng and colleagues also performed a first examination of the topological architecture of the presented mouse connectome. Several features of mammalian brain organization are reported. The wiring density ranged up to 38% between ipsilateral and 35% between contralateral regions, suggesting a remarkably high level of interhemispheric connectivity. Furthermore, connectivity strength – expressing the level of axonal connectivity between brain sites – is noted to span a 10^5 -fold range, leading the authors to conclude that not only the presence of long-range neural projections, but also the variation in strength of connection pathways forms a fundamental aspect of neural network architecture. Embracing network science as a mathematical tool for examining the topological organization of the presented neural network (Figure 7.1.2), the mouse connectome further revealed significantly elevated levels of local clustering (over 7 times higher than in a set of 1000 random networks) and community structure (showing six large-scale communities, Figure 7.1.1b). These local organizational features are combined with short global paths between brain regions, which are just a fraction longer than the very short routes that appear in random networks, together indicating a *small-world* organization of the mouse connectome (Bullmore and Sporns, 2009) (Figure 7.1.1c).

The authors further note that the number of afferent and efferent white matter projections per brain site tends to follow a fat-tailed distribution, reflecting the presence of a set of high-degree regions with an above-average level of connectivity. Sparse additional examination reveals that these putative neural *hubs* (van den Heuvel and Sporns, 2014) are widely distributed across the mouse brain (Figure 7.1.1b, red dots), cover the majority of anatomical communities, and have a significantly denser level of mutual connectivity than expected based on their degree ($p < 0.001$). Interestingly, connections spanning between hub nodes tend to involve (on average) relatively long anatomical pathways ($p < 0.001$, as compared to other connections), a high number of bidirectional connections (67% in contrast to 37% for other connections), and higher ranked weights ($p < 0.001$), supporting the notion that neural hubs and their connections form a central

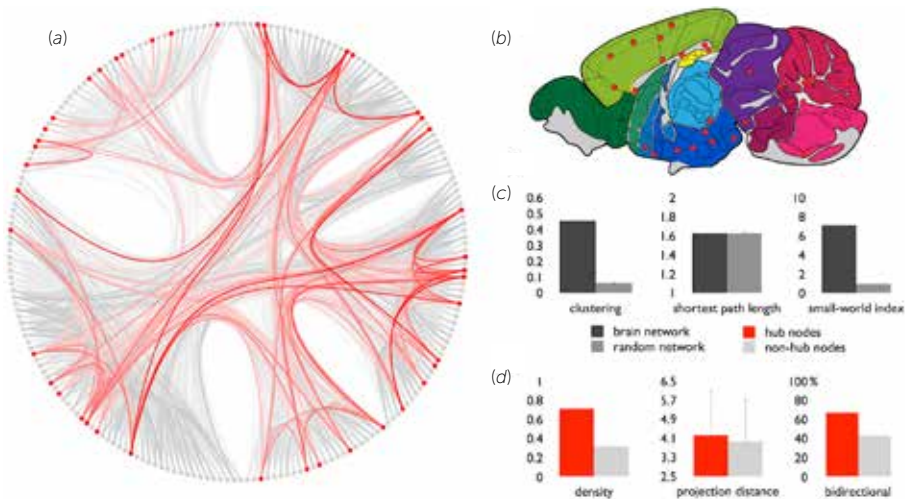


Figure 7.1.1. (a) Circular representation of the 25% strongest intrahemispheric connections of the mouse connectome as mapped by Zeng and colleagues, with nodes arranged according to community participation (six main communities are observed). Hub-to-hub connections (red) are shown on top. (b) Schematic figure of a sagittal slice of the mouse brain taken from the Allen Brain atlas (<http://connectivity.brain-map.org>). (c) The mouse connectome reveals a high level of topological clustering (> random level) and short communication pathways (~ random level), indicative of a small-world organization. (d) Preliminary findings suggest the presence of densely interconnected hub nodes (red points in panel a and panel b, left bar diagram) with hub-to-hub connections (red edges in panel a) that span on average longer physical distances (middle diagram), comprise higher ranked weights, and are more often part of a bidirectional pathway (right diagram) compared to the other pathways in the network (gray edges in panel a).



Figure 7.1.2. Neural networks can be described and examined as a set of nodes (e.g., neurons or mesoscale brain regions) and a collection of connections between nodes (e.g., reconstructed anatomical pathways) (most left panel). Within this mathematical framework, information on the local organization of the network can, for example, be provided by the level of network clustering, reflecting how strong the neighbors of a node are connected (left panel, orange), and by the extent to which nodes form local subnetworks or communities (left panel, blue). Information on the global organization of a network can, among other measures, be given by the average number of steps that is needed to travel from one place to another place in the network (right panel, green). Due to their high level of connectivity and central embedding in the network, hub nodes and their connections often form a prominent structure within the overall network (most right panel, red).

high-capacity, high-cost *rich club* in the mammalian brain (van den Heuvel et al., 2012). All together, the described network examinations provide converging evidence that the mammalian brain has a complex, nonrandom network architecture. However, as nicely put forward by Zeng and colleagues, neither a small-world nor a scale-free model could fully explain the topological organization of the mouse connectome, suggesting that the complexity of neural networks goes beyond that of simple wiring models.

After the presentation of such an unprecedentedly detailed connectome map, what is next? Given the still growing interest in brain connectivity, it is certain that the open-access Allen Brain map will be heavily used in the most exciting years of connectomics yet to come. Among many other purposes, it may serve as a gold standard for studies elucidating key organizational features of anatomical neural systems, provide an anatomical reference for studies that use the mouse as animal model for brain disorders, or function as dataset for more computationally driven studies. However, despite its high spatial and sampling resolution, the presented map cannot provide answers to all connectome questions. For instance, similar to previously reconstructed connectome maps of other species, the adopted techniques do not allow the reconstruction of connectome wiring on the individual level. Data from a large number of different animals is required to obtain a complete connectome map, thus limiting the examination of potential individual variation in connectome wiring. Intriguingly, in a small subset of overlapping injection experiments, Zeng and colleagues report high consistency of connectivity across tested animal specimens, while connectome studies in human samples – with connectivity estimates derived from *in vivo* magnetic resonance imaging – often report individual differences in brain wiring to be related to individual variation in cognitive performance or aspects of personality. It therefore remains an open challenge for future studies to clarify on which scale, and to what extent, variation in brain wiring is linked to individual differences in behavior. And while connectome mapping is undeniably a crucial step in improving our understanding of the workings of the mammalian brain, Zeng and colleagues rightfully mention that obtaining detailed insight into the

functioning of neural networks may require a different approach. Providing a sneak preview of new advances to come, Zeng and colleagues discuss an extension of their framework to viral vectors that actively monitor and manipulate synaptic processes, potentially bridging the gap between anatomical connectivity and functional circuitry.

Pioneering anatomist Niels Stensen concluded: "To say that the white matter is but a uniform substance like wax in which there is no hidden contrivance, would be too low an opinion of nature's finest masterpiece. We are assured that wherever in the body there are fibers, they everywhere adopt a certain arrangement among themselves, created more or less according to the functions for which they are intended. If the substance is everywhere of fibers, as, in fact, it appears to be in several places, you must admit that these fibers have been arranged with great skill, since all the diversity of our sensation and our movements depends upon this." (cited in Schmahmann and Pandya (2006, p. 11)). With the presented mesoscale brain map (<http://connectivity.brain-map.org>), the researchers of the Allen Institute for Brain Science have brought neuroscience one step closer to fulfilling the dreams of these early connectionists. And for that matter, those of today's connectomists.

Part II: Topological organization of connectivity strength in the rat connectome

Below, we present our analysis of the macroscale connectome of the rat brain, including detailed information on large-scale interregional pathways between 67 cortical and subcortical regions as provided by the high-quality, open-access BAMS-II database. First, network analysis confirmed a small-world, modular, and rich club organization of the rat connectome; findings in clear support of previous studies on connectome organization in other mammalian species. More importantly, we show that pathways with different topological roles have significantly different levels of connectivity strength. Among other findings, intramodule connections are shown to display a higher connectivity strength than intermodule connections and hub-to-hub rich club connections are shown to include significantly stronger pathways than connections spanning between peripheral nodes. Furthermore, analyzing network properties of different connection weight classes, we show evidence indicating that edges of different weight classes display different topological characteristics, potentially suggesting varying roles and origins of pathways in the mammalian brain network.

Introduction

Neural systems comprise complex networks of structurally and functionally linked elements. Studies examining the architecture of neural networks of mammalian and non-mammalian species – including the macroscale network of the human, macaque, and cat brain, but also microscale neural systems of lower order nematode species – have provided ample evidence indicating that the wiring diagram of organisms, their *connectome* (Sporns et al., 2005), shows several features of an efficient communication network (Bullmore and Sporns, 2009; van den Heuvel and Hulshoff Pol, 2010a; Sporns, 2011). A fundamental attribute of an organism’s connectome appears to be its combined ability to process specialized information and to efficiently integrate neural information across different domains (Sporns, 2013). It has been hypothesized that the

formation of local, densely clustered communities may ensure segregation of information and specialization, while the presence of global shortcuts may provide the infrastructure for global communication between remote regions (Bullmore and Sporns, 2009). Indeed, embracing network science as a theoretical framework to examine the wiring of neural networks, computational studies have consistently shown brain networks to display cost-effective wiring and a small-world modular organization, including high levels of local clustering and pronounced community structure, combined with short pathways ensuring efficient global communication (Bassett and Bullmore, 2006; Hagmann et al., 2008; van den Heuvel et al., 2008). It has been suggested that an important role in the formation of short communication routes may be occupied by a relatively small number of highly connected hub nodes (Hagmann et al., 2008; van den Heuvel et al., 2012). As a set of densely interlinked regions, hub nodes have been noted to form a *rich club* or *core*, constituting a spatially diffuse, but topologically central system, suggested to be important for global neural communication and thus integration of information between otherwise segregated functional systems (Cole et al., 2010; van den Heuvel and Sporns, 2014; Tomasi and Volkow, 2010) (also see **chapter 5** and **chapter 6**).

In humans, most of the connectome work is based on *in vivo* neuroimaging data, with macroscale pathways and indirect measures of anatomical connectivity strength derived from diffusion-weighted imaging (**chapter 2**). In contrast, animal studies allow for a detailed reconstruction of macroscale white matter pathways by means of neuronal tracing of axonal projections (Goldman-Rakic, 1988; Scannell et al., 1995). By collecting data across a large number of tract-tracing experiments, detailed reconstructions of the connectomes of (among other species) the macaque, cat, rat, and mouse have been made (Bota and Swanson, 2007; Markov et al., 2011; Oh et al., 2014; Scannell et al., 1995; Stephan et al., 2001), and examinations of the topology of these networks have shown ample evidence of global organizational principles similar to those observed in the human brain (Goulas et al., 2014; Hagmann et al., 2008; Harriger et al., 2012; Li et al., 2013; Sporns et al., 2007). An advantage of tract-tracing data

is that it allows for assessment of the directionality of the brain's white matter projections, providing important information that is out of the scope of current *in vivo* imaging-based reconstructions of the human connectome. Moreover, in case of animal connectomes, some reconstructions provide detailed information on the connectivity strength of axonal projections, allowing examination of the effect of the presence of weaker and stronger pathways on global network properties. Here, analyzing the directed and weighted macroscale connectome reconstruction of the rat brain as provided by the BAMS-II project (Bota and Swanson, 2007) – a detailed dataset with information on the connectivity of cortical and subcortical regions, including direction as well as connectivity strength of pathways – we provide new insights into the architectural attributes of the mammalian connectome. We first show that the rat connectome has similar topological features as previously shown for the human, macaque, cat, and mouse connectome, including a modular structure, short communication pathways, and a dense central rich club. Next, extending previous observations, we show distinct network characteristics of weak versus strong network connections, suggesting varying network roles of edges of different connectivity strength in the rat connectome.

Materials and methods

Connectivity dataset

Data on large-scale white matter pathways of the rat brain was taken from the open-access BAMS-II connectivity database (<http://brancusi1.usc.edu/connectome>), involving a comprehensive collection of tract-tracing experiments on the nervous system of the rat (Bota and Swanson, 2007). The BAMS-II database includes information on white matter pathways between 71 non-overlapping regions covering one hemisphere of the rat cerebrum, including a number of subcortical regions, providing a relatively fine-grained parcellation of the rat brain. The BAMS-II database has been used and described in several studies (French and Pavlidis, 2011; Leergaard et al., 2012; Wolf et al., 2011), with one of the most recent releases described in detail by Bota et al. (2012).

Binary connectivity

The BAMS-II database includes information on the presence of 1,424 directed connections between the 71 cortical and subcortical regions, and experimental reports on the absence of an anatomical projection between another 1,955 region pairs. This level of coverage is comparable to previous studies examining connectome reconstructions of the macaque (Modha and Singh, 2010) and cat cortex (Scannell et al., 1995). Four regions (AOB (accessory olfactory bulb), DG (hippocampal region, dentate gyrus), IG (hippocampal region, indusium griseum) and FC (hippocampal region, fasciola cinerea)) were found to have no (weighted) outgoing projections and were discarded from the graph theoretical analysis. Using this information, a directed binary adjacency matrix A of size $n \times n$ ($n = 67$) was constructed, including anatomical projections that were found to be present as a 1 and absent and non-reported connections as a 0. This matrix corresponded to a graph $G = (V, E)$, with V being a collection of 67 nodes, reflecting the included cortical and subcortical regions, and E a collection of 1,397 directed edges, reflecting the directed anatomical pathways between the regions.

Connectivity strength

Besides information on the absence or presence of connection pathways between regions of the rat brain, the BAMS-II database also provides information on the strength of the white matter pathways as directly derived from the tract-tracing experiments. Connections are categorized in 7 strength classes, ranging from 1 (very weak) to 7 (very strong). Data on projection strength was available for 1,337 connections (95.7 % of all reported binary connections). In this study, the 64 connections for which the projection strength was unknown were excluded from analyses in which weight information was examined (i.e., in binary analyses these connections were included). Information on the weights of the projections was collected in a directed weighted connectivity matrix W , with information on the connectivity strength of a white matter pathway projecting from region j to region i appearing as entry W_{ij} . Figure 7.2.1 depicts the directed weighted connectivity matrix derived from the BAMS-II database.

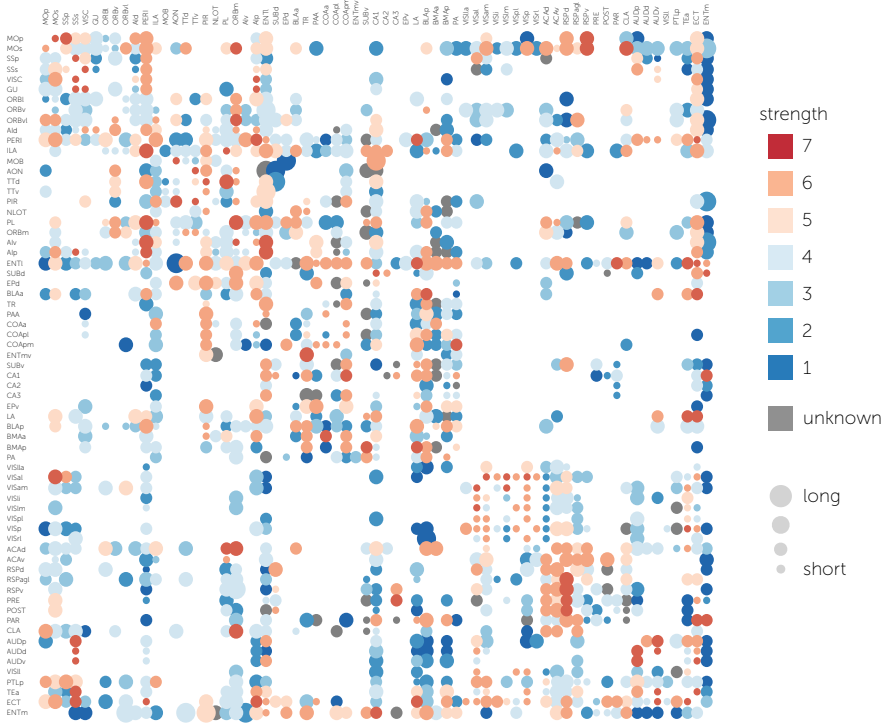


Figure 7.2.1. Connectivity matrix of the BAMS-II rat connectome dataset. Matrix entries reflect the reported presence of an anatomical projection between brain regions, with the level of connectivity strength varying between very weak (strength 1) and very strong (strength 7).

Standard network metrics

Graph theoretical analysis of the rat connectome included examination of several commonly used network metrics, including assessment of the: *characteristic path length*, indicative of the global efficiency of the network; *clustering coefficient*, measuring the level of local connectedness of the network; and *modularity*, expressing the extent to which the network can be subdivided into sparsely connected modules of densely interconnected nodes by algorithmically searching for an optimal partition (Leicht and Newman, 2008). Normalization of these metrics was carried out by dividing them by the average value observed in a set of 1000 randomized reference networks, formed by randomly rewiring the edges of the rat connectome while preserving the degree sequence (Maslov and Sneppen, 2002). A small-world organization was said to be present if the

ratio γ/λ , known as the *small-world index*, of the normalized clustering coefficient γ and the normalized path length λ exceeded 1. All network metrics were computed on the basis of the binary directed network. More information about these commonly used metrics can be found in **chapter 1** and in the overview by Rubinov and Sporns (2010).

Hubs and rich club organization

Hub nodes are nodes that play a central role in the overall network structure (van den Heuvel and Sporns, 2014). Hub nodes were selected on the basis of a cumulative *centrality* or *hub score* (Bassett et al., 2008; van den Heuvel et al., 2010) given by the number of times a node scored among the top 30% of highest ranking nodes on in-degree (number of incoming projections), out-degree (number of outgoing projections), betweenness centrality (average fraction of shortest paths passing through the node), and participation coefficient (diversity of projections relative to modules, see **chapter 5**), and among the top 30% of nodes with the shortest average path length to all other nodes in the network (all computed on the binary network). The cumulative hub score could vary from 0 – representing completely non-central nodes – to 5 – representing the most centrally situated nodes in the network. Nodes belonging to the subset H of nodes with a cumulative hub score of 4 or more were classified as hub nodes; all other nodes were classified as peripheral non-hub nodes.

Rich club organization of a network describes the phenomenon of high-degree nodes of a network expressing high levels of mutual connectivity, being more densely connected among each other than expected based on their degree alone. A network is said to show a rich club organization if, for a range of degree k , the density of connections between the subset of nodes with a degree larger than k is higher than in comparable random networks (Colizza et al., 2006). For each level of degree k , the subgraph S_k consisting of $N_{>k}$ nodes that displayed a combined in- and out-degree higher than k was selected, with the rich club coefficient $\Phi(k)$ computed as the ratio between the number of connections $E_{>k}$ present in subgraph S_k and the total number of possible connections in S_k .

(see **chapter 5**). To compensate for the fact that higher degree nodes in random networks also show a higher probability of being interconnected, $\Phi(k)$ was compared to the average rich club coefficient $\Phi_{\text{random}}(k)$ of the above-described set of 1000 randomized graphs (Colizza et al., 2006). The rich club coefficients of these random graphs formed a null distribution of the level of connectivity appearing among nodes with degree larger than k . For each level of k , $\Phi(k)$ was then assigned a p -value as the percentage of the null-distribution values that exceeded $\Phi(k)$. A rich club organization can thus be noted when, for a range of k , $\Phi(k)$ significantly exceeds $\Phi_{\text{random}}(k)$, or, put differently, when the ratio $\Phi_{\text{norm}}(k)$ between $\Phi(k)$ and $\Phi_{\text{random}}(k)$ exceeds 1 (Colizza et al., 2006; van den Heuvel and Sporns, 2011). Previous studies have noted a rich club organization for the human (Grayson et al., 2014; van den Heuvel and Sporns, 2011), macaque (Harriger et al., 2012), cat (Zamora-López et al., 2010) (**chapter 5**), and avian (Shanahan et al., 2013) brain, as well as for the neural systems of nematodes (Towlson et al., 2013).

After establishing the existence of a rich club organization, the rich club of the rat connectome was selected as the set of high-degree and highly central hub nodes H defined above. The rich club coefficient $\Phi(H)$ of this set of hub nodes was computed as the ratio between the number of existing edges and the total number of possible edges between the nodes of H , which amounts to replacing S_k by H . Similarly, $\Phi_{\text{norm}}(H)$ was computed by comparing $\Phi(H)$ to the average density $\Phi_{\text{random}}(H)$ between nodes of H as observed in the set of randomized networks.

Connection classes

Based on the identified modules during the modularity assessment, the selected rich club hub nodes, and the reported directionality of connections in the rat connectome dataset, the same connection classes as previously examined in the cat connectome (**chapter 5**) were formed. In short, connections were subdivided in three different ways, namely: (1) into *rich club* (spanning between hub nodes), *feeder-in* (projecting from peripheral to hub nodes), *feeder-out* (pro-

jection from hub to peripheral nodes), and *local* (spanning between peripheral nodes) connections; (2) into *intramodule* (connecting nodes of the same module) and *intermodule* (connecting nodes of different modules) connections; and (3) into *bidirectional* (i.e., being part of a two-way projection) and *unidirectional* (i.e., non-reciprocal) connections.

Connection classes were examined by assessment of the overlap between classes resulting from different subdivisions (e.g., describing the percentage of bidirectional rich club connections) and by comparing average connection characteristics between classes, including projection distance, connectivity strength, wiring cost, and a previously introduced measure of *module diversity*. In short, the module diversity of a connection c interlinking nodes i and j was defined as the product $p_i \times p_j$, with p_i representing the fraction of modules to which node i was connected (see **chapter 5**). High levels of module diversity indicate that connection c spans between two nodes which may have access to many different types of information, while a low module diversity expresses that connection c may be involved in the exchange of more unimodal information.

Topological organization of weight classes

Another natural subdivision of the edges of the rat connectome was given by the categorization into 7 strength or weight classes, with weights ranging from 1 (very weak) to 7 (very strong). To explore the existence of potential organizational differences between the network's weak and strong connections, we investigated the topological network organization of each weight class separately by examining graph characteristics of the subgraphs G^w of edges of strength w , represented by the connectivity matrix:

$$A_{ij}^w = \begin{cases} 1 & \text{if } W_{ij} = w \\ 0 & \text{otherwise} \end{cases} \quad (7.1)$$

with W the weighted adjacency matrix of the rat connectome and w ranging between 1 and 7. Although general caution is needed when interpreting sub-

networks as independent networks with metrics of organization now computed and analyzed in isolation of other connections, this type of analysis could provide insight into the distribution of connections of a certain strength over the total network. Examined metrics of the subnetworks G^w included: (1-2) global clustering and modularity, providing information on the local organization of a connectivity strength class, and (3-4) global efficiency (reciprocal of the harmonic mean topological distance over all node pairs, used instead of path length to avoid effects of disconnected nodes, see Latora and Marchiori (2001)) and diameter (maximum topological distance over all node pairs, ignoring pairs of nodes with no path between them), providing insight into the global organization of a subnetwork.

Edge perturbation

The various connection classes (including the ones based on connection strength) were further examined by estimating the importance of each individual connection for several network metrics and aggregating these scores per connection class, providing insight in the role in the network of connections from different classes. The importance of a connection with respect to a chosen network metric was estimated by computing this network metric both before and after removing the connection from the network (see **chapter 6**). The percentage of change caused by the removal was then taken as an indication of the relevance of that connection for the examined network metric. Four metrics were considered, being the impact of a connection on (1) the characteristic path length, (2) the global clustering coefficient, (3) the average (i.e., global) communicability between all nodes of the network, and (4) the local communicability between the endpoints of the connection. The communicability measure is a weighted sum (computed as the matrix exponent of the adjacency matrix) that includes paths of all possible lengths between nodes i and j in the network, assigning higher weights to shorter paths, and is indicative of the level of theoretical network communication between nodes (Estrada and Hatano, 2008) (**chapter 6**). All computations involved in the assessment of connection relevance were based on the binary directed connectivity matrix of the rat brain and

thus completely independent of the strength of connections.

Results

Clustering, path length, small-world

Consistent with previous reports on connectome organization of the mammalian brain, the reconstructed rat connectome (Figure 7.2.1) revealed a density of 31.6%, a right-tailed degree distribution, above-chance levels of clustering ($1.18\times$ higher than in 1000 randomized networks), a short path length ($1.02\times$ random) and a small-world index larger than 1 ($1.16, p < 0.001$). The rat connectome further revealed a hierarchical modular organization with a top split of the network into 3 modules (modularity $2.57\times$ higher than random), which themselves consisted of respectively 1, 2, and 3 submodules (Figure 7.2.2).

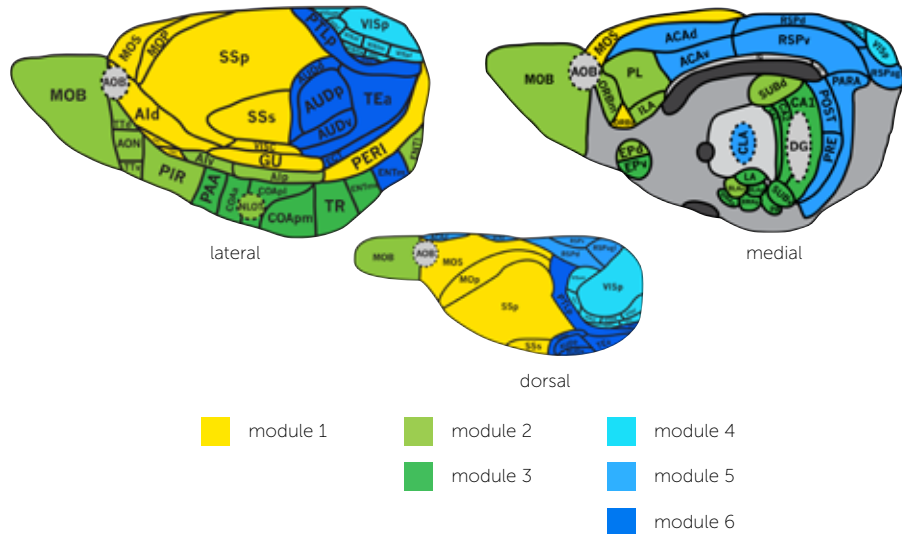
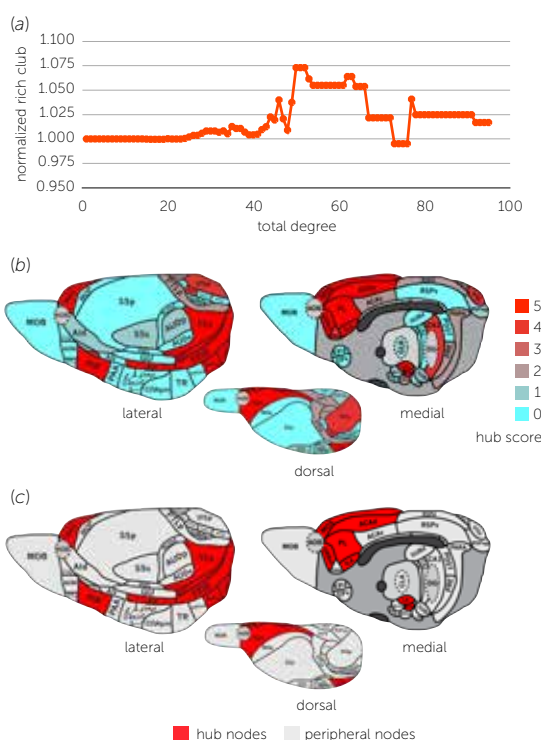


Figure 7.2.2. Module partitioning of the rat brain. The regions of the rat connectome were found to form three main modules (yellow, green, and blue) and six submodules (respectively 1, 2, and 3 submodules), indicated by color shades varying from light to dark). Lateral, medial, and dorsal views are artist renderings of figures presented by Palomero-Gallagher and Zilles (2004).

Hubs and rich club organization

The rat connectome also displayed a rich club organization. Across the range $50 \leq k \leq 52$, $\Phi(k)$ significantly exceeded $\Phi_{\text{random}}(k)$ (i.e., $\Phi_{\text{norm}}(k) > 1$; $p < 0.01$, 1000 random networks, Figure 7.2.3a), an observation consistent with reports on rich club organization in other species. Assessment of the cumulative hub score – computed as the number of times a node ranked among the 30% highest ranking nodes on five nodal centrality metrics – revealed the existence of 14 potential hub nodes, all showing a cumulative hub score ≥ 4 (Figure 7.2.3b). This set H of hub nodes included the following regions: MOs (secondary motor cortex), ILA (infralimbic area), PIR (piriform area), ACAd (dorsal part of the anterior cingulate area), PL (prelimbic area), ORBm (medial orbital area), Alp (posterior agranular insular cortex), TEa (temporal association areas), ECT (ectorhinal area), PERI (perirhinal area), ENTL (entorhinal area, lateral part), ENTm (entorhinal area, medial part, dorsal zone), LA (lateral amygdalar nucleus), and BLAp (baso-

Figure 7.2.3. (a) Rich club curve of the rat connectome. The x-axis shows the total degree k (always having integer values) and the y-axis shows the corresponding normalized rich club coefficient, reflecting the normalized density between nodes with degree $> k$. Rich club organization was found to be present for several levels of k , as indicated by a normalized rich club coefficient > 1 . (b) Centrality or hub score per brain region, ranging from 0 (not central) to 5 (highly central). (c) Hub nodes were taken to be nodes with a centrality score of 4 or more. Hub nodes are depicted in red, non-hub nodes are depicted in gray.



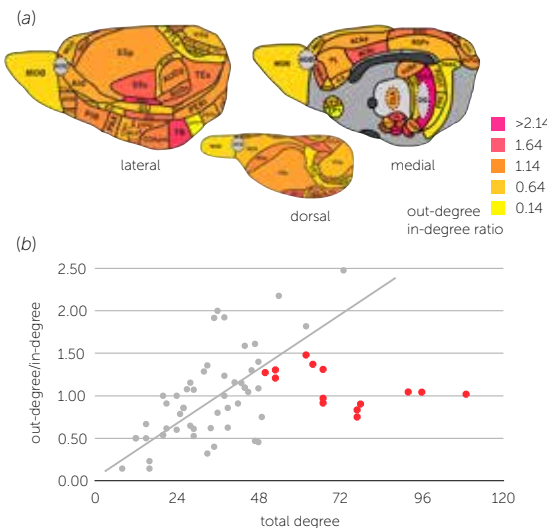


Figure 7.2.4. (a) Ratio between nodal out-degree and nodal in-degree. Nodes with a low out-degree/in-degree ratio form *neural sinks* (having more incoming than outgoing connections) and nodes with a high out-degree/in-degree ratio form *neural sources* (reflecting nodes with more outgoing than incoming connections). (b) The out-degree/in-degree ratio correlated significantly with total degree, although hub nodes (red points) appear to be outliers to this relationship.

lateral amygdalar nucleus, posterior part) (Figure 7.2.3c). Together, these hubs formed a significant rich club, with $\Phi(H)$ being significantly higher than $\Phi_{\text{random}}(H)$ ($p = 0.001$). Moreover, hubs were found to be present in five of the six 2-step modules, underscoring the importance of hub nodes in interlinking modules.

Neural sinks and sources

Examining potential differences between the out- and in-degree of brain regions, the ratio between nodal out-degree and in-degree displayed a right-tailed distribution, with the majority of nodes showing a ratio around 1 (73% scoring between 0.5 and 1.5), suggesting a relative overall balance in the number of efferent and afferent connections of brain regions (Figure 7.2.4a). Only a small set of nodes revealed an imbalance, showing more afferent than efferent connections (thus forming “neural sinks”, ratio < 0.5 , regions: VISll (laterolateral visual area), ORBvl (ventrolateral orbital area), PTLp (posterior parietal association areas), ENTmv (entorhinal area, medial part, ventral zone), PRE (presubiculum), PAR (parasubiculum), EPv (endopiriform nucleus, ventral part); yellow colored regions in Figure 7.2.4a) or more efferent than afferent connections (thus forming “neural sources”, ratio > 1.5 , regions: SSs (secondary somatosensory cortex), VISC (visceral area), TR (postpiriform transition area), ACAv (ventral part of

the anterior cingulate area), CA1 (hippocampal region CA1), LA (lateral amygdalar nucleus), BMAp (basomedial amygdalar nucleus, posterior part), PA (posterior amygdalar nucleus); magenta colored regions in Figure 7.2.4a).

The out-degree/in-degree ratio of brain regions was found to be positively correlated to their total degree (Figure 7.2.4b), indicating that connections of regions with a higher total number of pathways are on average more often efferent (linear regression, $r = 0.40$, $p = 0.007$). Interestingly, hub nodes appeared to form potential outliers to this organizational rule (red nodes in Figure 7.2.4b), showing a relatively balanced number of afferent and efferent connections (out-degree/in-degree ratio, mean [std]: 1.14 [0.29]; not different from the ratio of peripheral nodes, $p = 0.22$, 10,000 permutations), likely due to the strong bidirectional character of most of their pathways (see below).

Characterization of rich club, feeder, and local connections

As in our study of the cat connectome presented in **chapter 5**, the edges of the rat connectome were subdivided into rich club, feeder-in, feeder-out, and local connections, and several connection characteristics were compared across these classes to provide insight in the type of connections that they involve. The class of rich club connections comprised 11% of all edges, the class of feeder-out connections 27%, the class of feeder-in connections 24%, and the class of local connections 38%.

Intermodular vs. intramodular

Seventy-five percent of all rich club connections were intermodular, compared to 72, 76 and 53% of all feeder-out, feeder-in, and local connections, respectively. Thus, only 25% of the rich club edges were intramodule connections, in contrast to 47% of the local connections. Furthermore, rich club connections included 13% of all intermodule edges of the network, being 1.14x their overall share. Feeder-out connections and feeder-in connections included respectively 29 and 27% of all intermodule connections (1.09 and 1.13x their overall share). In

contrast, local connections were found to be less involved in interlinking different modules (including 39% of all intermodule connections, 0.80 \times their overall share) and appeared more frequently among intramodule connections (including 52% of them, 1.38 \times their overall share). Rich club, feeder-out, and feeder-in connections included respectively 8, 21, and 17% of all intramodule connections.

Bidirectional vs. unidirectional

Of the total collection of edges, 62% was found to be bidirectional (i.e., part of a two-way projection). Interestingly, the directionality of connections was found to interact with their inter- or intramodular role, with 56% of all intermodule connections and 75% of all intramodule connections being bidirectional. Rich club connections were found to predominantly include connections of bidirectional nature (94% bidirectional, with 92% of the intermodule rich club connections and 92% of the intramodule rich club connections being bidirectional), with feeder-in (70% bidirectional, 60% for intermodule) and feeder-out (62%, 57% for intermodule) connections coming in second and third place. Of all local projections, just 49% were found to be bidirectional, a percentage which became even lower when considering only intermodule local connections (35%).

Module diversity

Rich club edges were found to display a higher module diversity than local connections (1.26 \times higher, $p < 0.001$, permutation test), with feeder-out (1.12 \times , $p < 0.001$) and feeder-in (1.09 \times , $p < 0.001$) edges coming in second and third place.

Projection distance

Rich club connections spanned significantly longer distances (as approximated by Euclidean distances between estimated centers of mass for all regions) compared to local (1.25 \times longer, $p < 0.001$) and feeder connections (compared to feeder-out: $p = 0.002$; compared to feeder-in: $p = 0.002$). Furthermore, also feeder-out (1.10 \times , $p < 0.001$) and feeder-in (1.12 \times , $p < 0.001$) connections were

found to be (on average) longer than local connections.

Wiring cost

Rich club connections were found to display a significantly higher wiring cost (computed as physical distance times connectivity strength, see van den Heuvel et al. (2012)) than local connections (1.65 \times higher, $p < 0.001$, 10,000 permutations), as well as than feeder-out (1.36 \times , $p < 0.001$) and feeder-in (1.22 \times , $p = 0.004$) connections.

Distribution of connectivity strength

With the exception of the last statement about the wiring cost of rich club, feeder, and local connections, all results presented so far considered the organization of the rat connectome interpreted as a binary (directed) network. Examining the relationship between the network role of edges and their connectivity strength, intramodule connections were found to involve significantly higher connectivity weights (mean [std]: 4.57 [1.58]) than intermodule connections (mean [std]: 3.87 [1.66], $p = 0.002$, 10,000 permutations). Moreover, the class of rich club connections was found to show a higher average connectivity strength than the other classes, being 1.18 \times higher than the strength of local ($p < 0.001$), 1.23 \times higher than the strength of feeder-out ($p < 0.001$), and 1.16 \times higher than the strength of feeder-in ($p < 0.001$) connections. Of all strong connections (i.e., connections with weight ≥ 6), 16% were rich club connections (1.46 \times their overall share), while 34% belonged to the class of local connections (0.89 \times their overall share). Figure 7.2.5a shows the distribution of connectivity strength over the classes of rich club, feeder-out, feeder-in, and local connections.

Further categorizing the connections of the network in intermodule and intra-module connections, intermodule rich club connections were found to display a significantly higher connectivity strength (mean [std]: 4.73 [1.50]) as compared to intermodule feeder-out (3.59 [1.79], $p < 0.001$), feeder-in (4.09 [1.55], $p = 0.002$), and local (3.56 [1.52], $p < 0.001$, 10,000 permutations) connections

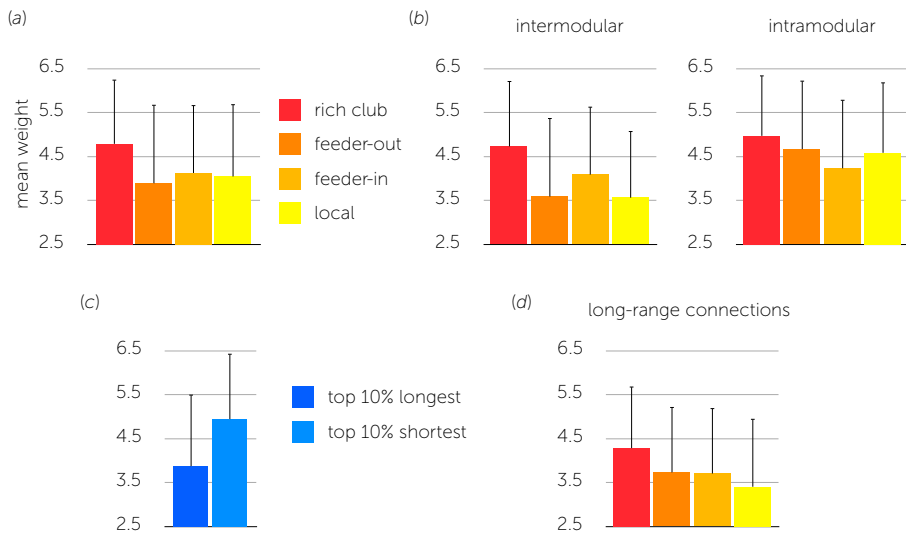


Figure 7.2.5. (a) Average connectivity strength of the class of rich club (red), feeder (feeder-out: dark orange, feeder-in: light orange), and local (yellow) connections. (b) Further subdivision of rich club, feeder, and local connections into intermodule and intramodule edges. Rich club connections display the highest connectivity strength in both classes. (c) Average edge weights of the 10% longest (dark blue) and 10% shortest (light blue) connections (as estimated on the basis of Euclidean distance). Consistent with previous observations, short connections have a higher average connectivity strength than long connections. (d) Subdivision of the top 10% longest network connections into rich club, feeder, and local edges.

(Figure 7.2.5b). Furthermore, of all strong intermodule connections (i.e., connections with weight ≥ 6 spanning between modules), 22% were rich club connections (1.96x their overall share) and only 19% were local connections (0.49x their overall share). For the class of very strong intermodule connections (i.e., having a weight of 7) these differences were even bigger, with 40% rich club connections (3.47x) and only 14% local connections (0.37x their overall share).

Considering a potential relationship between the length and strength of connections, the 10% shortest connections were found to show stronger projection strengths (mean [std]: 4.95 [1.64]) than the 10% longest connections (mean [std]: 3.88 [1.50], $p < 0.001$, Figure 7.2.5c). Furthermore, also a general correlation between projection length and connectivity strength was observed ($r = -0.21$, $p < 0.001$, linear regression). When exclusively looking at the subset of the top

10% longest connections, rich club edges were still found to display a higher connectivity strength (mean [std]: 4.29 [1.41]) than local edges (mean [std]: 3.41 [1.56], $p = 0.0318$, Figure 7.2.5d). Similar results were found when selecting the top 15% or top 20%.

Topological organization of weight classes

Next, we examined the topological organization of the connections within each weight class by interpreting the weight classes as subgraphs. Figure 7.2.6a shows how the edges are distributed over the different weight classes (weights ranging from 1 for very weak connections to 7 for very strong connections), with the classes of very weak (6.5% of total number of connections) and very strong (6.2%) edges including the smallest groups of edges and the class of edges of moderate strength (weight 4) including the largest set (26.4%). As a result, the density of the weight-based subgraphs varied between 2 and 8% (Figure 7.2.6b).

The different subgraphs were found to show distinct topological network features. First, examining metrics of local organization, weak edges (strength 1-2) were found to show low levels of normalized clustering (strength 1: 0.8, strength 2: 1.0, normalized to 1000 random networks) and low modularity (raw 0.37, 0.39; 1.04, 1.10 when normalized to random networks) (Figure 7.2.7). This in contrast to the strong edges of the network (strength 6-7), which showed high levels of normalized clustering (strength 6: 2.1, strength 7: 5.3) and high modularity (1.59 \times and 1.21 \times higher than random). Further examining metrics of global organization, weight classes 2 to 6 revealed relatively short communication paths (global efficiency 0.86 to 0.94 \times that of randomized networks), while the subgraph of very strong connections showed relatively long communication paths (global efficiency 0.55 \times that of randomized networks, indicating the subnetwork to be more locally and less globally oriented). Consistent with this observation, the subgraph diameter (reflecting the longest path length present, ignoring pairs of nodes without an interconnecting path) was found to be relatively small for very weak and weak connections (< 1 \times random level), and relatively large (1.28 \times random level) for very strong connections (Figure 7.2.7).



Figure 7.2.6 (a) Percentage of the total number of edges in the rat connectome dataset per weight class (1: very weak, 7: very strong). The percentage of edges per class varied between 6% (class 1 and 7) and 26% (class 4). (b) Corresponding density of each of the weight classes when interpreted as subgraph.

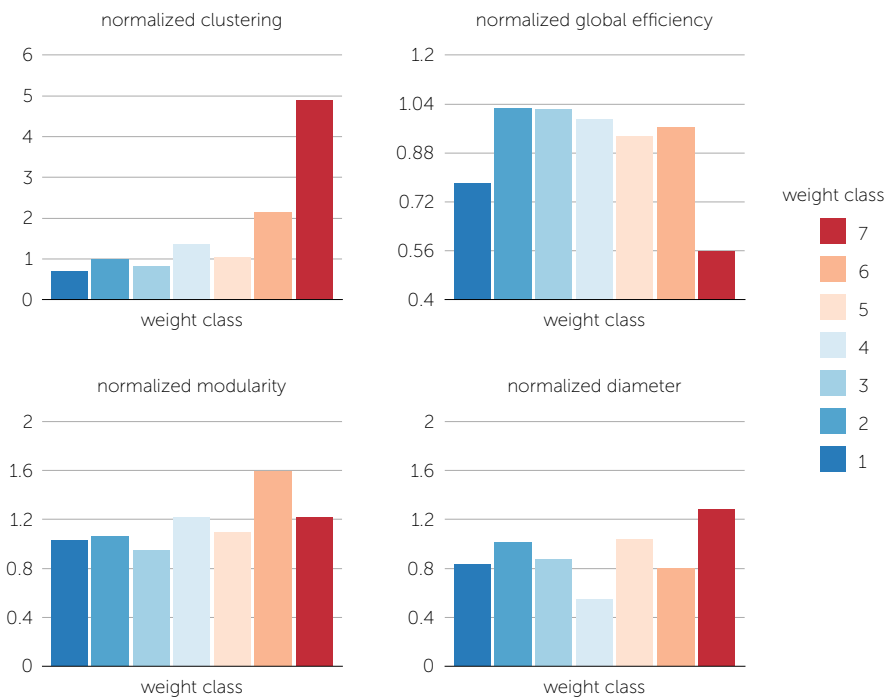


Figure 7.2.7. Values of graph metrics computed per weight class. For each weight class, graph metrics were computed for the binary subnetwork of edges belonging to that class. The panels show for each of the seven weight classes (depicted in different colors corresponding to Figure 7.2.1) the normalized clustering, normalized path length, normalized modularity, and normalized diameter (all compared to 1000 randomized networks), indicating different topological structures for different weight classes.

Edge perturbation

Underscoring a different topological role in the network for edges of different weight classes, removal of strong edges (weight ≥ 6 , removing one edge at a time) was found to have a significantly higher impact on binary global communicability than removal of weak connections (weight 2-3, $p = 0.0014$, 10,000

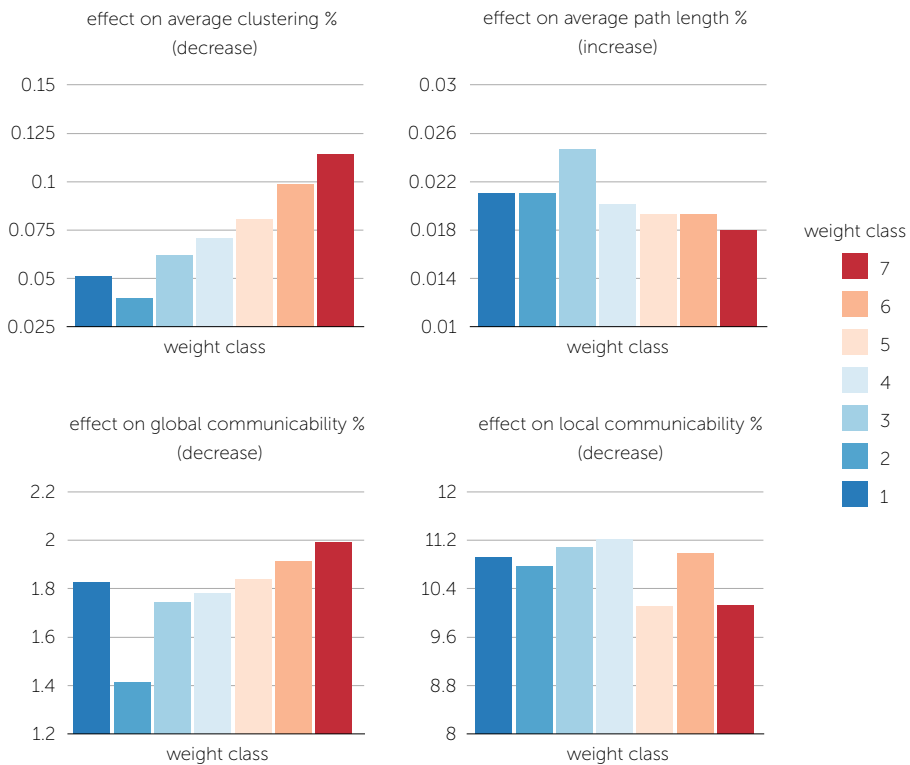


Figure 7.2.8 Edge removal scores for each of the connectivity weight classes. Figure shows the average effects of removing an edge on global clustering, global path length, global communicability, and local communicability, tested by removing one edge at a time and evaluating the effect on the graph metric of interest, with class values reflecting the average over all edges in a class. Effects are quantified as the percentage of change (resulting from removal) with respect to the values observed in the original non-damaged network. Note that effects on path length are positive (i.e., reflecting an increase in path length after removal of an edge), while effects on clustering, global communicability, and local communicability are negative (i.e., reflecting a decrease in these metrics after removal of an edge). All removal scores were computed on the basis of the binary rat network, with the weight of edges only used to categorize connections into the different connection classes. Reported removal effects thus reflect the relevance of connections for the topological organization of the network and do not incorporate connectivity strength.

permutations). More generally, the estimated relevance of connections for clustering and global communicability appeared to increase with connectivity strength in a staircase-like manner (Figure 7.2.8). Interestingly, weight class 1 formed an exception to this observation, showing a unique combination of a relatively high relevance for global communicability and a relatively low relevance for clustering. Considering the classes of intermodule and intramodule edges, the impact on global communicability was found to be 1.10x higher for intermodule connections as compared to intramodule connections ($p < 0.001$, 10,000 permutations). Furthermore, removal of a rich club connection led on average to a 4.76x stronger reduction in global communicability than removal of a local connection, findings consistent with those observed for the human and cat connectome (chapter 6) and in support of an important role of rich club connections in global network communication (van den Heuvel et al., 2012). Moreover, removal of an intermodule rich club connection on average had a 5.30x stronger impact on global communicability than removal of an intermodule local connection. Consistent with previous investigations on edge perturbations (chapter 6), less pronounced effects were observed when considering the impact of edge removal on the characteristic path length. Notably, the strongest increases in path length were found in the lower weight classes (class 1-3, Figure 7.2.8), suggesting that these edges may act as randomly placed global shortcuts in the overall network.

Discussion

Examining a detailed anatomical wiring diagram of the rat brain extracted from the BAMS-II connectivity database (Bota and Swanson, 2007), we revealed several organizational features of the rat's neural network architecture. Supporting findings of previous studies on macroscale connectome organization in other mammalian and non-mammalian species, the rat brain network showed a small-world, hierarchical modular organization and exhibited a small number of high-degree, high-strength hub regions. Furthermore, extending previous observations, our findings reveal potential interactions between network topology and the distribution of connectivity strength over the edges of the rat connectome.

First, general descriptives of neural network organization revealed several attributes of an efficient processing and communication architecture for the rat brain. Consistent with previous observations on structural and functional connectivity in the rat brain (Liang et al., 2011; Schmitt et al., 2012) and with observations made in other species (Chatterjee and Sinha, 2007; Hagmann et al., 2008; Kaiser and Hilgetag, 2006; Salvador et al., 2005; Sporns et al., 2007; Stephan et al., 2000), the examined rat connectome showed above-random levels of clustering and community structure, indicating the formation of anatomical communities. In addition to clustered anatomical communities, the network exhibited relatively short communication pathways with node pairs from different communities being no further apart than three consecutive steps, together indicative of an efficient small-world modular organization. Moreover, again confirming several previous observations, the rat neural network revealed the existence of a set of highly central, high-degree hub nodes forming a densely connected rich club (Grayson et al., 2014; Harriger et al., 2012; van den Heuvel and Sporns, 2011; Towlson et al., 2013; Zamora-López et al., 2010). Rich club hub nodes were found to be spatially distributed across the brain, including areas in almost all observed communities. Validating previous observations in the human (Collin et al., 2014; van den Heuvel et al., 2012; van den Heuvel and Sporns, 2013) and cat connectome (**chapter 5**), connections spanning between rich club nodes revealed several distinctive properties as compared to other classes of connections. Rich club connections (purely selected on the basis of topological properties of their endpoints) spanned significantly longer physical distances than connections attached to peripheral nodes, involved a large proportion of the total macroscale wiring cost, and were predominantly intermodular and bidirectional. Notably, the class of rich club connections also showed a significantly higher average connectivity strength than the classes of feeder and local connections.

Second, further exploring the relation between the topological role of connections and their connectivity strength, our results show evidence of a non-random distribution of connectivity strength over the connections of the rat brain

network. Subclasses of edges based on projection strength were found to show different topological properties, with edges of low strength (the class of weak connections) showing low levels of clustering and modularity, a small diameter, and – especially compared to very strong connections – relatively short communication paths. In contrast, high strength connections (the class of strong and very strong connections) showed high levels of clustering, relatively strong community formation, and long subgraph paths. Furthermore, weak connections were found to combine a relatively high importance for global communicability (measured in the binary network, not including information on connection strength) with a relatively low impact on global network clustering, indicating that these connections may appear in rather unique positions. Speculating on these findings, the observed characteristics seem to indicate that low strength edges are more widespread and scattered than high strength edges, suggesting a potentially random organization of weaker neural pathways and a relatively ordered organization of stronger connections in the mammalian brain. This suggestion coincides with observations from developmental studies, noting widespread – possibly somewhat random – termination zones of long-range corpus callosum tracts at birth (day 4, as observed in the visual system of the cat), followed by a relatively short period (days to weeks) in which rapid spatial specialization of corticocortical tracts and their termination zones occurs (Huttenlocher and Dabholkar, 1997). Such an initial overgrowth of macroscopic connectivity in the preterm developing brain is supported by empirical observations in the young rhesus monkey, revealing the highest axonal connection count of corpus callosum fibers at birth, followed by a decrease (up to 70%) in axonal number in the first postnatal weeks (LaMantia and Rakic, 1990). Linking these developmental findings to the suggested widespread and relatively random organization of weak macroscale projections in the adult mammalian brain, a speculative hypothesis may be that the class of weak connections includes pathways that are to some extent “left over” from a macroscale pruning period during brain development and that may thus be potentially non- or less-functional (Collin and van den Heuvel, 2013; van den Heuvel et al., 2014). Extending this hypothesis, the strongest connections observed in the rat brain may be those pathways that

have been subject to strong activation during later development, which may strengthen the functional role of anatomical pathways in the total system and could lead to stronger pathways in the adult brain.

As already mentioned, our current study of the tract-tracing based rat connectome confirmed several previous observations related to hub and rich club formation in mammalian brain networks, underscoring that neural hubs and their connections form a high-cost feature of brain network architecture (Bullmore and Sporns, 2012; van den Heuvel et al., 2012). Complementing the reported high connectivity strength and wiring cost of hub-to-hub rich club connections, a post-hoc analysis showed that the ratio of high strength (weight > 4) versus low strength (weight ≤ 4) connections (HL ratio) of brain regions was significantly correlated to their binary degree ($r = 0.33, p = 0.0056$), suggesting that nodes with a high binary high degree comprise on average more high strength connections than low strength connections. Also the inverse of the average path length of a node correlated significantly with the HL ratio ($r = 0.26, p = 0.0357$). Considering that both a high degree and a short average path length are indicators for a high centrality score, these findings suggest that neural hubs are not only “rich” in terms of the number of pathways, but also in terms of the projection strength of these pathways. Interestingly, extending observations of hub formation in cortical brain networks (Harriger et al., 2012; Sporns et al., 2007; Zamora-López et al., 2010) (also see **chapter 5** and **chapter 6**), the rat connectome dataset included information on anatomical connectivity of deeper gray matter structures, revealing an above-average number of connections and relatively high centrality scores for hippocampal (CA1, centrality score of 3) and amygdalar nuclei (LA, BMAp, centrality score of 3; BLAp, centrality score of 4). This tract-tracing based observation provides support for reports of rich club formation in the human brain, suggesting a high number of macroscale connections for subcortical structures such as the hippocampus and thalamus on the basis of *in vivo* diffusion imaging (van den Heuvel and Sporns, 2011). Of course, participation of subcortical regions in a central club of high-degree regions is also consistent with the critical role of these regions in memory and in the relay

and processing of neural information (Kandel et al., 2000).

Some points should be taken into consideration when interpreting the findings of this study. First, the BAMS-II rat brain dataset – similar to other pioneering endeavors concerning the mapping of the connectomes of the cat, macaque, mouse, and *Caenorhabditis elegans* – comprises data from a large number of experiments and does not constitute a macroscale connectome map of a single specimen (Bota et al., 2012; Scannell et al., 1995; Stephan et al., 2001). The examined connectome dataset therefore does not provide information on individual variation in brain wiring. In addition, the BAMS-II database does not yet include information on the presence or absence of connectivity between all region pairs, and database updates incorporating information for more region pairs are regularly made (Bota et al., 2012; Bota and Swanson, 2007). Second, it is important to note that the rat connectome dataset as extracted for this study only contains information on intrahemispheric connectivity (with tract-tracing data from the left and right hemisphere combined), and that the absence of information on corpus callosum tracts is likely to influence the graph theoretical analysis. Tracts running through the corpus callosum are known to constitute a large proportion of all white matter tracts (Schmahmann and Pandya, 2006) and play an important role in interhemispheric functional connectivity and communication (van den Heuvel and Hulshoff Pol, 2010b; LaMantia and Rakic, 1990; Lowe et al., 2008; Pandya et al., 1971; Verstraete et al., 2011; Wahl et al., 2007). Notably, the tract-tracing efforts by Oh et al. (2014) discussed in the first part of this chapter revealed an intriguingly high level of interhemispheric connectivity in the mouse brain, as well as a non-trivial organization of these projections, highlighting the important role of interhemispheric connectivity in global connectome structure.

In conclusion, our findings provide evidence supporting an efficient communication architecture of neural systems and suggest a non-random distribution of connectivity strength over the white matter pathways, with distinct network characteristics for weak and strong connections. Anatomical connections be-

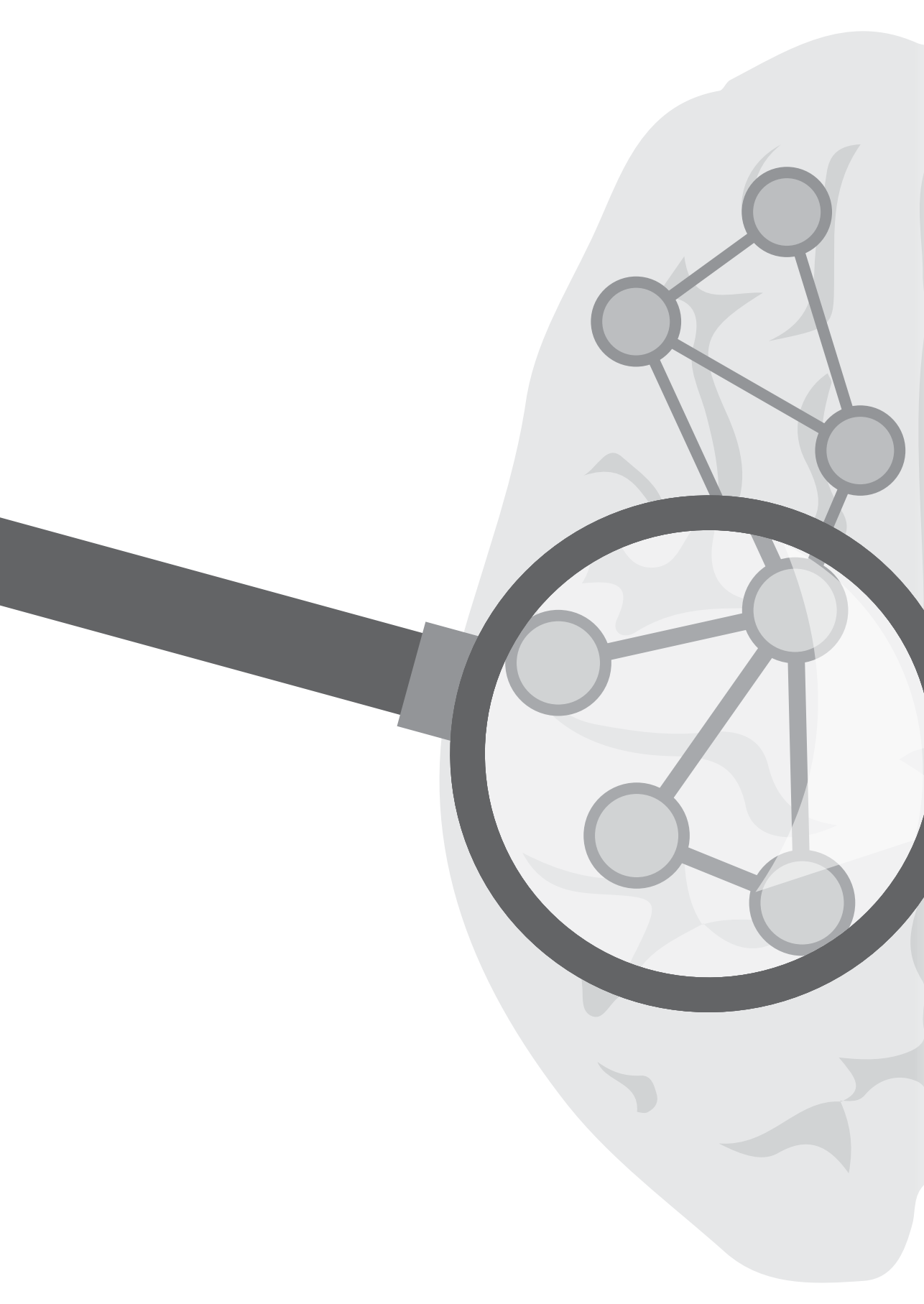
tween high-degree hub nodes were observed to show a higher connectivity strength as compared to other types of connections, further confirming the notion of neural hubs to form a high-cost infrastructure in the mammalian brain. Future studies examining whether weak and strong pathways might also differ in their microscale neuroarchitectonics would be of high interest and could provide important insight into the hypothesized disproportionate vulnerability of high-degree, high-strength hub regions and their connections in disease processes (Crossley et al., 2014; van den Heuvel and Sporns, 2014).

References

- Bassett, D.S., Bullmore, E., 2006. Small-World Brain Networks. *The Neuroscientist* 12, 512-523.
- Bassett, D.S., Bullmore, E., Verchinski, B.A., Mattay, V.S., Weinberger, D.R., Meyer-Lindenberg, A., 2008. Hierarchical Organization of Human Cortical Networks in Health and Schizophrenia. *The Journal of Neuroscience* 28, 9239-9248.
- Bota, M., Dong, H.W., Swanson, L.W., 2012. Combining collation and annotation efforts toward completion of the rat and mouse connectomes in BAMS. *Frontiers in Neuroinformatics* 6, 2.
- Bota, M., Swanson, L.W., 2007. Online workbenches for neural network connections. *Journal of Comparative Neurology* 500, 807-814.
- Bullmore, E., Sporns, O., 2009. Complex brain networks: graph theoretical analysis of structural and functional systems. *Nature Reviews Neuroscience* 10, 186-198.
- Bullmore, E., Sporns, O., 2012. The economy of brain network organization. *Nature Reviews Neuroscience* 13, 336-349.
- Chatterjee, N., Sinha, S., 2007. Understanding the mind of a worm: hierarchical network structure underlying nervous system function in *C. elegans*. In: Banerjee, R., Chakrabarti, B.K. (Ed.), *Models of Brain and Mind – Physical, Computational and Psychological Approaches*, 145-153. Elsevier.
- Cole, M.W., Pathak, S., Schneider, W., 2010. Identifying the brain's most globally connected regions. *NeuroImage* 49, 3132-3148.
- Colizza, V., Flammini, A., Serrano, M.A., Vespignani, A., 2006. Detecting rich-club ordering in complex networks. *Nature Physics* 2, 110-115.
- Collin, G., van den Heuvel, M.P., 2013. The Ontogeny of the Human Connectome: Development and Dynamic Changes of Brain Connectivity Across the Life Span. *The Neuroscientist* 19, 616-628.
- Collin, G., Sporns, O., Mandl, R.C.W., van den Heuvel, M.P., 2014. Structural and Functional Aspects Relating to Cost and Benefit of Rich Club Organization in the Human Cerebral Cortex. *Cerebral Cortex* 24, 2258-2267.
- Crossley, N.A., Mechelli, A., Scott, J., Carletti, F., Fox, P.T., McGuire, P., Bullmore, E.T., 2014. The hubs of the human connectome are generally implicated in the anatomy of brain disorders. *Brain*, epub ahead of print.
- Estrada, E., Hatano, N., 2008. Communicability in complex networks. *Physical Review E* 77, 036111.
- French, L., Pavlidis, P., 2011. Relationships between Gene Expression and Brain Wiring in the Adult Rodent Brain. *PLoS Computational Biology* 7, e1001049.
- Goldman-Rakic, P.S., 1988. Topography of Cognition: Parallel Distributed Networks in Primate Association Cortex. *Annual Review of Neuroscience* 11, 137-156.
- Goulas, A., Bastiani, M., Bezgin, G., Uylings, H.B.M., Roebroek, A., Stiers, P., 2014. Comparative Analysis of the Macroscale Structural Connectivity in the Macaque and Human Brain. *PLoS Computational Biology* 10, e1003529.
- Grayson, D.S., Ray, S., Carpenter, S., Iyer, S., Dias, T.G.C., Stevens, C., Nigg, J.T., Fair, D.A., 2014. Structural and Functional Rich Club Organization of the Brain in Children and Adults. *PLoS ONE* 9, e88297.
- Hagmann, P., Cammoun, L., Gigandet, X., Meuli, R., Honey, C.J., Wedeen, V.J., Sporns, O., 2008. Mapping the Structural Core of Human Cerebral Cortex. *PLoS Biology* 6, e159.
- Harriger, L., van den Heuvel, M.P., Sporns, O., 2012. Rich Club Organization of Macaque Cerebral Cortex and Its Role in Network Communication. *PLoS ONE* 7, e46497.
- van den Heuvel, M.P., Hulshoff Pol, H.E., 2010a. Exploring the brain network: A review on resting-state fMRI functional connectivity. *European Neuropsychopharmacology* 20, 519-534.
- van den Heuvel, M.P., Hulshoff Pol, H.E., 2010b. Specific somatotopic organization of functional connections of the primary motor network during resting state. *Human Brain mapping* 31, 631-644.
- van den Heuvel, M.P., Kahn, R.S., Goñi, J., Sporns, O., 2012. High-cost, high-capacity backbone for global brain communication. *Proceedings of the National Academy of Sciences* 109, 11372-11377.

- van den Heuvel, M.P., Kersbergen, K.J., de Reus, M.A., Keunen, K., Kahn, R.S., Groenendaal, F., de Vries, L.S., Binders, M.J.N.L., 2014. The Neonatal Connectome During Preterm Brain Development. *Cerebral Cortex*, epub ahead of print.
- van den Heuvel, M.P., Mandl, R.C.W., Stam, C.J., Kahn, R.S., Hulshoff Pol, H.E., 2010. Aberrant Frontal and Temporal Complex Network Structure in Schizophrenia: A Graph Theoretical Analysis. *The Journal of Neuroscience* 30, 15915-15926.
- van den Heuvel, M.P., Sporns, O., 2011. Rich-Club Organization of the Human Connectome. *The Journal of Neuroscience* 31, 15775-15786.
- van den Heuvel, M.P., Sporns, O., 2013. An Anatomical Substrate for Integration among Functional Networks in Human Cortex. *The Journal of Neuroscience* 33, 14489-14500.
- van den Heuvel, M.P., Sporns, O., 2014. Network hubs in the human brain. *Trends in Cognitive Sciences* 17, 683-696.
- van den Heuvel, M.P., Stam, C.J., Boersma, M., Hulshoff Pol, H.E., 2008. Small-world and scale-free organization of voxel-based resting-state functional connectivity in the human brain. *NeuroImage* 43, 528-539.
- Huttenlocher, P.R., Dabholkar, A.S., 1997. Regional differences in synaptogenesis in human cerebral cortex. *Journal of Comparative Neurology* 387, 167-178.
- Kaiser, M., Hilgetag, C.C., 2006. Nonoptimal Component Placement, but Short Processing Paths, due to Long-Distance Projections in Neural Systems. *PLoS Computational Biology* 2, e95.
- Kandel, E.R., Schwartz, J.H., Jessell, T.M., 2000. Principles of neural science. McGraw-Hill, New York.
- LaMantia, A.S., Rakic, P., 1990. Axon overproduction and elimination in the corpus callosum of the developing rhesus monkey. *The Journal of Neuroscience* 10, 2156-2175.
- Latora, V., Marchiori, M., 2001. Efficient Behavior of Small-World Networks. *Physical Review Letters* 87, 198701.
- Leergaard, T.B., Hilgetag, C.C., Sporns, O., 2012. Mapping the connectome: Multi-level analysis of brain connectivity. *Frontiers in Neuroinformatics* 6, 14.
- Leicht, E.A., Newman, M.E.J., 2008. Community Structure in Directed Networks. *Physical Review Letters* 100, 118703.
- Li, L., Hu, X., Preuss, T.M., Glasser, M.F., Damen, F.W., Qiu, Y., Rilling, J., 2013. Mapping putative hubs in human, chimpanzee and rhesus macaque connectomes via diffusion tractography. *NeuroImage* 80, 462-474.
- Liang, Z., King, J., Zhang, N., 2011. Uncovering Intrinsic Connectional Architecture of Functional Networks in Awake Rat Brain. *The Journal of Neuroscience* 31, 3776-3783.
- Lowe, M.J., Beall, E.B., Sakaie, K.E., Koenig, K.A., Stone, L., Marrie, R.A., Phillips, M.D., 2008. Resting state sensorimotor functional connectivity in multiple sclerosis inversely correlates with transcallosal motor pathway transverse diffusivity. *Human Brain Mapping* 29, 818-827.
- Markov, N.T. et al., 2011. Weight Consistency Specifies Regularities of Macaque Cortical Networks. *Cerebral Cortex* 21, 1254-1272.
- Maslov, S., Sneppen, K., 2002. Specificity and Stability in Topology of Protein Networks. *Science* 296, 910-913.
- Modha, D.S., Singh, R., 2010. Network architecture of the long-distance pathways in the macaque brain. *Proceedings of the National Academy of Sciences* 107, 13485-13490.
- Oh, S.W. et al., 2014. A mesoscale connectome of the mouse brain. *Nature* 508, 207-214.
- Palomero-Gallagher, N., Zilles, K., 2004. Isocortex. In: Paxinos, G. (Ed.), *The Rat Nervous System* (Third Edition), 729-757. Academic Press.
- Pandya, D., Karol, E., Heilbronn, D., 1971. The topographical distribution of interhemispheric projections in the corpus callosum of the rhesus monkey. *Brain Research* 32, 31-43.
- Rubinov, M., Sporns, O., 2010. Complex network measures of brain connectivity: Uses and interpretations. *NeuroImage* 52, 1059-1069.
- Salvador, R., Suckling, J., Coleman, M.R., Pickard, J.D., Menon, D., Bullmore, E., 2005. Neurophysiological Architecture of Functional Magnetic Resonance Images of Human Brain. *Cerebral Cortex* 15, 1332-1342.
- Scannell, J.W., Blakemore, C., Young, M.P., 1995. Analysis of connectivity in the cat cerebral cortex. *The Journal of Neuroscience* 15, 1463-1483.
- Schmahmann, J.D., Pandya, D.N., 2006. Fiber Pathways of the Brain. Oxford University Press, New York.

- Schmitt, O., Eipert, P., Philipp, K., Kettlitz, R., Fuellen, G., Wree, A., 2012. The intrinsic connectome of the rat amygdala. *Frontiers in Neural Circuits* 6, 81.
- Shanahan, M., Bingman, V.P., Shimizu, T., Wild, M., Güntürkün, O., 2013. Large-Scale Network Organization in the Avian Forebrain: A Connectivity Matrix and Theoretical Analysis. *Frontiers in Computational Neuroscience* 7, 89.
- Sporns, O., 2011. The human connectome: a complex network. *Annals of the New York Academy of Sciences* 1224, 109-125.
- Sporns, O., 2013. Network attributes for segregation and integration in the human brain. *Current Opinion in Neurobiology* 23, 162-171.
- Sporns, O., Honey, C.J., Kötter, R., 2007. Identification and Classification of Hubs in Brain Networks. *PLoS ONE* 2, e1049.
- Sporns, O., Tononi, G., Kötter, R., 2005. The Human Connectome: A Structural Description of the Human Brain. *PLoS Computational Biology* 1, e42.
- Stephan, K.E., Hilgetag, C.C., Burns, G.A.P.C., O'Neill, M.A., Young, M.P., Kötter, R., 2000. Computational analysis of functional connectivity between areas of primate cerebral cortex. *Philosophical Transactions of the Royal Society of London B: Biological Sciences* 355, 111-126.
- Stephan, K.E., Kamper, L., Bozkurt, A., Burns, G.A.P.C., Young, M.P., Kötter, R., 2001. Advanced database methodology for the Collation of Connectivity data on the Macaque brain (CoCoMac). *Philosophical Transactions of the Royal Society of London B: Biological Sciences* 356, 1159-1186.
- Tomasi, D., Volkow, N.D., 2010. Functional connectivity density mapping. *Proceedings of the National Academy of Sciences* 107, 9885-9890.
- Towlson, E.K., Vértes, P.E., Ahnert, S.E., Schafer, W.R., Bullmore, E.T., 2013. The Rich Club of the *C. elegans* Neuronal Connectome. *The Journal of Neuroscience* 33, 6380-6387.
- Verstraete, E., Veldink, J.H., Mandl, R.C.W., van den Berg, L.H., van den Heuvel, M.P., 2011. Impaired Structural Motor Connectome in Amyotrophic Lateral Sclerosis. *PLoS ONE* 6, e24239.
- Wahl, M., Lauterbach-Soon, B., Hattingen, E., Jung, P., Singer, O., Volz, S., Klein, J.C., Steinmetz, H., Ziemann, U., 2007. Human Motor Corpus Callosum: Topography, Somatotopy, and Link between Microstructure and Function. *The Journal of Neuroscience* 27, 12132-12138.
- Wolf, L., Goldberg, C., Manor, N., Sharan, R., Ruppin, E., 2011. Gene Expression in the Rodent Brain is Associated with Its Regional Connectivity. *PLoS Computational Biology* 7, e1002040.
- Zamora-López, G., Zhou, C., Kurths, J., 2010. Cortical hubs form a module for multisensory integration on top of the hierarchy of cortical networks. *Frontiers in Neuroinformatics* 4, 1.



Chapter 8

Link communities in the human brain

*Based on a publication (*Philosophical Transactions of the Royal Society B*, vol. 369, 2014) by Marcel A. de Reus, Victor M. Saenger, René S. Kahn and Martijn P. van den Heuvel*

Abstract

Brain function depends on efficient processing and integration of information within a complex network of neural interactions, known as the connectome. An important aspect of connectome architecture is the existence of community structure, providing an anatomical basis for the occurrence of functional specialization. Typically, communities are defined as groups of densely connected network nodes, representing clusters of brain regions. Looking at the connectome from a different perspective, instead focusing on the interconnecting links or edges, we find that the white matter pathways between brain regions also exhibit community structure. Eleven link communities were identified: five spanning through the midline fissure, three through the left hemisphere, and three through the right hemisphere. We show that these link communities are consistently identifiable and investigate the network characteristics of their underlying white matter pathways. Furthermore, examination of the relationship between link communities and brain regions revealed that the majority of brain regions participate in multiple link communities. In particular, the highly connected and central hub regions showed a rich level of community participation, supporting the notion that these hubs play a pivotal role as confluence zones in which neural information from different domains merges.

Introduction

The human brain is a complex network of neuronal interactions which facilitates efficient processing and integration of information. The macroscopic architecture of this intricate network, known as the human connectome (Sporns et al., 2005), can be studied using graph theory, providing a formal network description in which brain regions are represented by nodes and their interconnecting white matter pathways by links or edges (Bullmore and Sporns, 2009). An architectural feature of particular interest, the subject of a large number of recent studies (Alexander-Bloch et al., 2012; Chen et al., 2008; Crossley et al., 2013; Meunier et al., 2010; Wu et al., 2011), is the connectome's community structure, describing the existence of groups of nodes (i.e., brain regions) with high levels

of connectivity between members of the same group and low connectivity between groups (Girvan and Newman, 2002). These *communities* can be unveiled using specialized algorithms and typically reflect subsystems or building blocks of the network (Porter et al., 2009). For neural systems, the presence of groups of densely interconnected nodes has been demonstrated in both human and animal brain networks (Hagmann et al., 2008; Hilgetag et al., 2000; Power et al., 2011). The formation of neural communities has been suggested to be an important architectural attribute for functional specialization and segregation of information processing (Hilgetag et al., 2000; Sporns, 2013).

In addition to the traditional view on communities as groups of nodes, the community structure of complex networks may also be described from an edge-centric perspective, instead identifying groups of links or edges (Ahn et al., 2010; Evans and Lambiotte, 2009). Such link communities have been reported for several empirical networks, including metabolic networks, mobile phone networks, and social networks, and have been shown to highlight different subsystems than node-based communities (Ahn et al., 2010; Boldi and Rosa, 2012; Evans and Lambiotte, 2009; Kim and Jeong, 2011). Furthermore, link communities allow the examination of interaction between node and link properties in a network. This in particular includes the identification of “community hot spots” where links from multiple communities come together at a single node, reflecting the involvement of a node in multiple subsystems (Ahn et al., 2010; Evans and Lambiotte, 2009). Reported overlap of resting-state functional brain networks (Beckmann et al., 2005; van den Heuvel and Sporns, 2013) and overlap of communities in volumetric coupling networks (Wu et al., 2011) indicate that also brain network nodes are not always likely to belong to a single community, making an edge-centric perspective on community structure particularly suitable to provide further insight into the network organization of the brain.

In this chapter, we explore the link community structure of the brain’s white matter pathways using macroscopic connectome maps of the healthy adult brain derived from *in vivo* diffusion imaging measurements. We demonstrate

that the connectome exhibits multiple link communities and we assess their robustness to variations in the underlying connectome data. To provide support for a possible first interpretation of the identified link communities, we extend our edge-centric perspective from communities to individual white matter pathways. By monitoring the effect of the hypothetical removal of individual edges, several network properties are estimated for each of the connectome's connections, which are then compared across link communities. Furthermore, the relationship between link communities and network nodes is examined by assessing the overlap of link communities at brain regions. We report a pronounced role of a small collective of central hub regions (van den Heuvel and Sporns, 2011; Sporns et al., 2007) as "link community hot spots" in the brain, establishing a connection between the edge-centric perspective adopted here and node-based findings.

Connectome reconstruction

The brain's network of white matter pathways was represented by a group-averaged connectome map, including *in vivo* magnetic resonance imaging data of 50 healthy participants. In short, for each participant, two diffusion-weighted imaging sets with opposite k -space readouts were acquired at the University Medical Center Utrecht (van den Heuvel et al., 2010; van den Heuvel and Sporns, 2011). After correction for possible eddy-current (Andersson and Skare, 2002) and susceptibility (Andersson et al., 2003) distortions, the principal diffusion direction in each $2 \times 2 \times 2$ mm voxel was determined using a robust tensor fitting method (Chang et al., 2005). Fiber pathways were reconstructed by following these principal diffusion directions from voxel to voxel with the Fiber Assignment by Continuous Tracking algorithm (Mori et al., 1999). In addition, a T1-weighted image was acquired to parcellate the cortical surface into 68 anatomically segregated cortical brain regions (34 in each hemisphere) using the FreeSurfer software suite (<http://surfer.nmr.mgh.harvard.edu>).

The macroscopic anatomical brain network of each participant was reconstruct-

ed by combining the cortical parcellation with the estimated white matter fiber tracts. The 68 anatomically segregated cortical brain regions from the parcellation were defined to be the nodes of the network and, for each pair of regions i and j , an edge was placed between the corresponding nodes if a reconstructed fiber touched both regions i and j . The 50 resulting individual brain network reconstructions were put together to form a group-averaged connectome map by including only those edges that were found to be present in at least 60% (30) of the participants. More details about the outlined procedures and included participants can be found in **chapter 4**, which presents an extensive analysis concerning the group-averaging procedure based on the same collection of reconstructed brain networks. Basic statistics of the reconstructed brain networks are provided in a section with Supplementary Information (SI) at the end of the current chapter.

Link communities

Link communities of the group-averaged connectome map were identified using the network's associated line graph (Evans and Lambiotte, 2009). This line graph is formed by defining a "node" for every link in the connectome map and a "connection" between two of these nodes if the links that they represent share a common endpoint (Figure 8.1a). Subsequently, communities within the line graph, the link communities, are identified by applying a traditional (node-based) community detection method to the line graph. Since nodes of the line graph correspond to links of the original connectome map, detected communities of densely interconnected line graph nodes map one-to-one to link communities of the connectome (Figure 8.1b). For community detection on the line graph, we applied the Infomap algorithm of Rosvall and Bergstrom (2008), identifying network partitions that minimize the description length of an infinite random walk on the network (see the SI section for details).

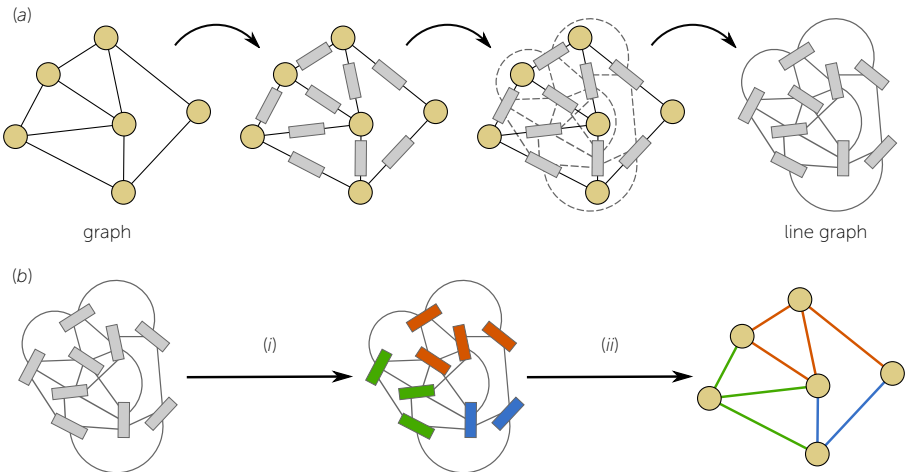


Figure 8.1. Identifying link communities. (a) First, the original graph (here, a simple toy network) is converted to its associated line graph. This line graph has a node (depicted as a rectangle) for every link in the original graph and a connection between two of these nodes if the links that they represent have a common endpoint (depicted as discs). (b) Next, a conventional node-based community detection technique is applied to the line graph (i), and the resulting communities of line graph nodes are mapped to link communities of the original graph (ii) (Evans and Lambiotte, 2009).

Using this approach, the group-averaged connectome map revealed 11 link communities (Figure 8.2). Five of the 11 identified communities spanned through the midline fissure, being (1) the precuneus/occipital (Pr/Oc) community, mostly spanning between brain regions from the occipital lobe, (2) the cingulate community, comprising anterior-posterior white matter connections that originate from the cingulum tract, (3) the medial frontal (medF) community of pathways between frontal and a few temporal regions, and (4,5) two homologous communities centered around the left and right paracentral (PC) lobule. The six other communities were found to be predominantly confined to a single hemisphere, forming three communities in the left hemisphere and three homologous communities in the right hemisphere. These link communities are: (6,7) the left and right middle frontal (midF) communities, comprising connections between frontal and insular regions, (8,9) the middle temporal (midT) communities, involving connections between temporal regions as well as connections between the temporal lobe and other lobes, and (10,11) the parahippocampal/entorhinal

(Ph/Er) communities, mainly involving projections from regions in the medial wall of the temporal lobe.

In the next sections, we examine the consistency of these link communities and the individual white matter pathways that constitute them.

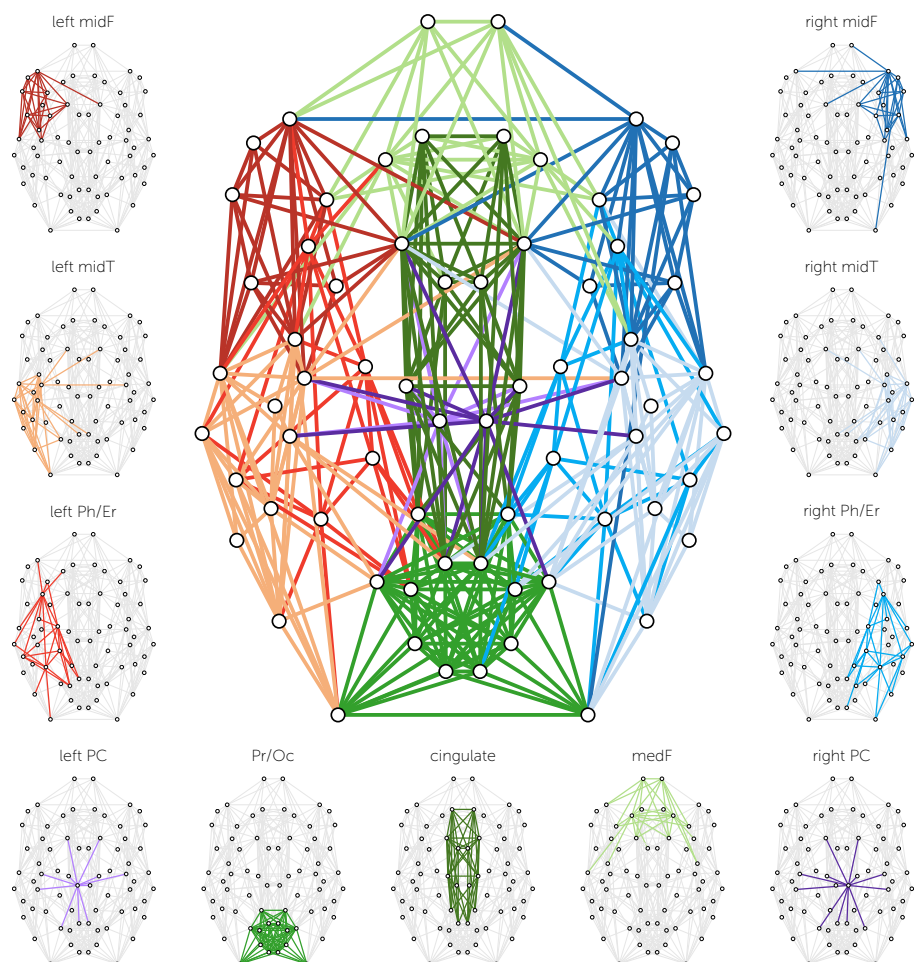


Figure 8.2. Link communities in the human brain. The 11 identified link communities are depicted in different colors according to their spatial location. Communities spanning the midline fissure are represented by green shades, left-lateralized communities by red shades, right-lateralized communities by blue shades, and the PC communities are depicted in purple. Pr/Oc, precuneus/occipital community; medF, medial frontal community; midF, middle frontal communities; midT, middle temporal communities; Ph/Er, parahippocampal/entorhinal communities; PC, paracentral communities.

Consistency

To examine the level of robustness of link communities to variations in the underlying connectome data, from the total sample of 50 participants, individual brain network reconstructions of 15 participants were randomly selected and averaged using a 60% group threshold. This process was repeated a thousand times, generating group-averaged brain networks for 1000 bootstrap samples, all exhibiting their own link community pattern. Next, for each pair of links from the original group-averaged connectome, it was assessed in how many of the bootstrap samples in which these links were simultaneously present, they also appeared in the same community. Outcomes were scaled between 0 and 100%, with 100% reflecting that the pair of links was consistently clustered together across bootstrap samples.

The collected clustering scores (shown in Figure 8.3a) were found to demonstrate a high consistency of the identified link communities. Across all 11 communities, connections that were assigned to the same link community in the group-averaged connectome (Figure 8.2) also shared their community assignment in 91% of the bootstrap samples. The most consistent communities were the Pr/Oc, cingulate, and both PC communities (all having an average score of 99%), reflected by the dark diagonal blocks in Figure 8.3a. The least consistent communities were the left Ph/Er and left midT community, still displaying consistency percentages of 76% and 77%, respectively. The somewhat lower consistency of these link communities appears to be caused by relatively “fuzzy” boundaries between bilaterally segregated communities in the same hemisphere. As reflected by the off-diagonal horizontal and vertical lines in Figure 8.3a, connections from the Ph/Er communities were in some bootstrap samples instead assigned to the ipsilateral midT or midF communities. A similar exchange of connections was observed between the midT and midF communities.

An additional comparison of link communities identified on individual brain network reconstructions revealed a highly similar consistency pattern ($r = 0.87$, Figure 8.3b), but with lower overall consistency values. Connections that were

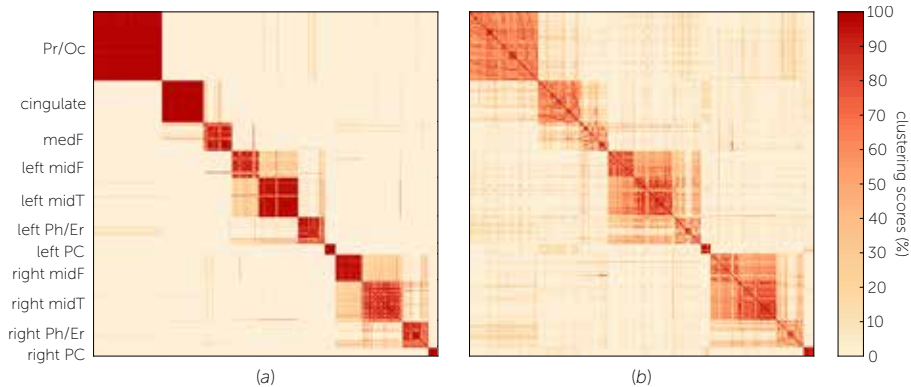


Figure 8.3. Consistency matrices. (a) The consistency of the identified link communities was verified by repeating community detection for 1000 bootstrap samples. The consistency matrix lists for every pair of links how often these links were clustered together (i.e., assigned to the same community) across bootstrap samples. As the rows and columns of the matrix are ordered according to the identified communities, the blocks on the diagonal reflect the consistency of a community, while off-diagonal stripes indicate exchange of connections between communities. (b) A similar matrix was formed by counting how often links were assigned to the same community when performing link community detection on individual brain network reconstructions. Although individual reconstructions are more susceptible to measurement errors and thus inevitably display more variability (see chapter 4), the pattern of clustering scores was found to be highly similar to the observed clustering across bootstrap samples ($r = 0.87$, Pearson's correlation coefficient).

assigned to the same link community in the group-averaged connectome also shared their community assignment in 63% of the participants, the most consistent communities being the PC communities (left 90% and right 93%). For comparison, connections from different link communities in the group-averaged connectome shared their community assignment in only 7% of the participants. Together, these scores indicate that link communities observed in individual participants are quite similar to those identified on the group level. Clustering between connections from ipsilateral midT and midF communities was again observed to be elevated, underscoring that the boundary between these communities is relatively fuzzy.

Comparing communities by connection features

In order to obtain more insight into the identified link communities, it would be of interest to explore the network characteristics of the underlying white matter pathways. However, most network metrics capture properties of (single) nodes or the entire network, overlooking properties of individual connections. A notable exception is a metric known as *edge betweenness*, which assigns to each connection the fraction of shortest paths in which it participates (Girvan and Newman, 2002). Although a very useful and commonly applied measure, computing this betweenness metric still covers only a single aspect of the role of a connection in the network.

Inspired by lesion models that assess the vulnerability of brain networks to simulated damage (He et al., 2008; He et al., 2009; van den Heuvel and Sporns, 2011; Kaiser and Hilgetag, 2004; Kaiser et al., 2007), we estimated several additional characteristics of the connectome's connections by monitoring the effect of their hypothetical removal. To this end, traditional network metrics of the intact group-averaged connectome map were compared with those of slightly modified maps, missing only the single connection whose features were to be estimated. Measuring the percentage change caused by the absence of a connection in the modified maps, traditional (node oriented) metrics were effectively mapped to edge-centric ones, estimating the relevance of a connection for the network properties assessed by the metrics. Figure 8.4 displays the results of four such *edge removal metrics*, measuring the relevance of the connections of the group-averaged connectome map for (1) the characteristic path length, (2) the clustering coefficient, (3) global communicability within the entire network, and (4) local communicability between the endpoints of a connection (details about the metrics are provided in the SI section). Together with edge betweenness (also displayed in Figure 8.4), a total of five different edge-centric measures were collected for each connection.

Aggregating the collected connection scores per link community (Figure 8.5), edge-centric metrics were found to vary strongly within communities, suggest-

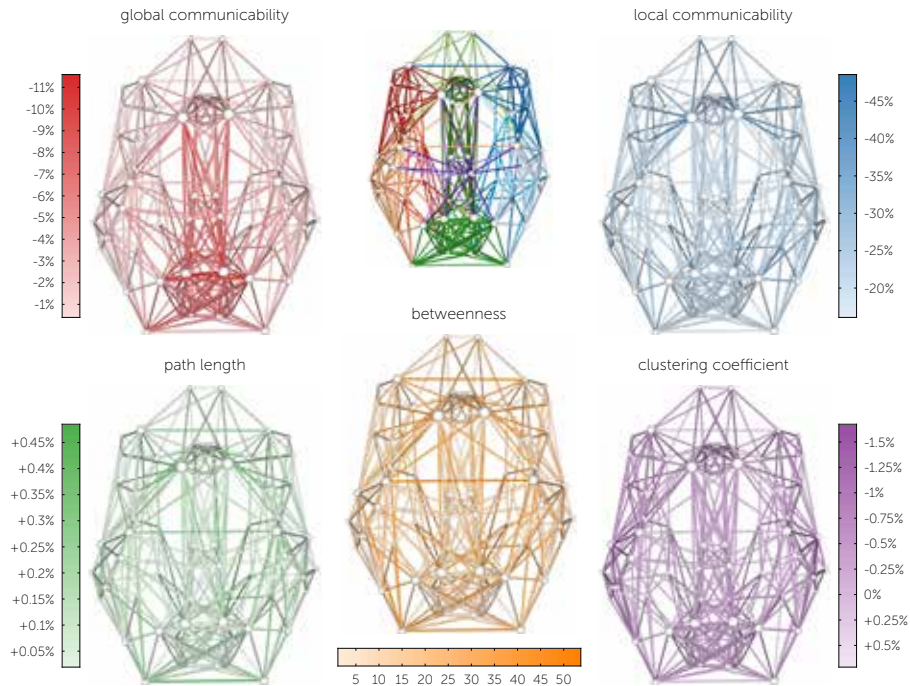


Figure 8.4. Relevance of white matter connections with respect to several network characteristics. Properties of individual white matter pathways were estimated by comparing network metrics of the intact connectome map with those of modified maps, missing only the single connection whose relevance was to be estimated. The shade of a connection reflects the percentage change caused by its hypothetical removal. As incorporated in the color scales, it depends on the metric whether connections causing the strongest increase (path length; long path lengths being disadvantageous for the network) or connections causing the strongest decrease (clustering coefficient, global/local communicability) should be considered the most relevant for that metric. For reference, the identified link communities are shown in the top middle. Conventional edge betweenness scores, representing the fraction of shortest paths a connection participates in, are shown in the bottom middle.

ing that link communities comprise a heterogeneous mixture of connections with varying roles in the network. As shown in Figure 8.5, the mean connection scores of link communities with respect to path length, clustering, local communicability, and betweenness fluctuated only marginally, with none of the communities differing significantly from the global mean (i.e., the average over all connections). Interestingly, edge removal scores with respect to global communicability formed an exception, displaying significantly higher values than the global mean in the Pr/Oc and cingulate community, while significantly lower

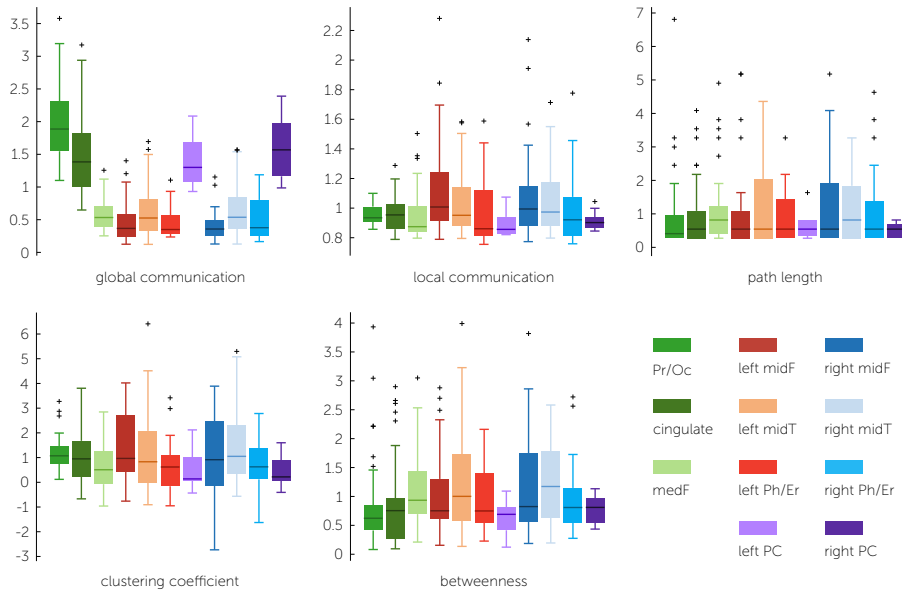


Figure 8.5. Connection scores per link community displayed as box plots. The outcomes of each edge-centric metric were first divided by the average over all connections, so that values above unity indicate a larger-than-average relevance and values below unity indicate a lower-than-average relevance.

levels were observed in the left midT and the left/right midF and Ph/Er communities ($p < 0.05$, Bonferroni corrected, permutation tests). Also the connections of the left and right PC communities displayed a substantially (but not significantly) higher average impact on global communicability (exceeding the global mean by, respectively, 41% and 60%), implying that the Pr/Oc, cingulate, and PC communities must comprise many connections with a pronounced relevance for communicability within the brain network.

Relationship with brain regions: community overlap

An important advantage of identifying communities of links instead of nodes is that community participation of brain regions is not limited to a single community. Instead, the white matter projections of a brain region may be divided over multiple link communities, indicating the involvement of this region in multiple subsystems (Ahn et al., 2010; Evans and Lambiotte, 2009). Investigating how

the presented edge-centric findings relate to the nodes of the network, we examined the number of communities coming together in each single node, providing a measure for the link diversity of brain regions. Figure 8.6 illustrates the distribution of these participation numbers over the brain regions. Approximately 56% of the brain regions (38 out of 68) were found to participate in multiple link communities, with their nodal participation numbers ranging from two to a maximum of eight communities per node. Such a relatively diverse link community participation of the nodes may be related to recent observations showing that many brain regions participate in multiple functional domains and thus are, to some extent, involved in multimodal neural processes (van den Heuvel and Sporns, 2013; Kinnison et al., 2012; Lancichinetti et al., 2009; Sepulcre et al., 2012).

Triggered by the findings depicted in Figure 8.6, showing that a select number of brain regions even participated in as many as five, seven, or eight of the 11 identified link communities, we specifically examined the community participation of previously reported *hub nodes*. Hub nodes are highly connected brain regions with a central position in the network (van den Heuvel and Sporns, 2014)

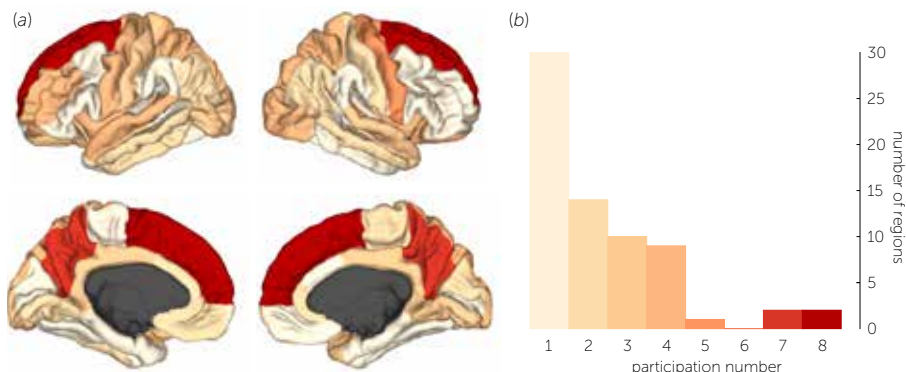


Figure 8.6. Overlap of link communities at brain regions. (a) The color of each brain region on the cortical surface indicates the number of link communities in which it was found to participate. The colors used on the cortical surface are identical to those in the histogram depicted in (b). The majority (56%) of the brain regions participated in multiple communities, their participation numbers ranging up to a maximum of eight of the 11 identified communities.

and have been noted to be involved in a variety of cognitive tasks and functions (Anderson et al., 2011; Crossley et al., 2013; Margulies et al., 2009). Together, the hubs of the brain form a densely connected *core* or *rich club* (Harriger et al., 2012; van den Heuvel and Sporns, 2011; Shanahan et al., 2013; Towlson et al., 2013) which has been suggested to play a role in the integration of information between functional domains (van den Heuvel and Sporns, 2013) (also see **chapter 5** and **chapter 6**). Considering these properties, we hypothesized a pronounced participation of rich club hubs in the identified link communities. In agreement with previous reports (Collin et al., 2014; van den Heuvel et al., 2012; van den Heuvel and Sporns, 2011), rich club hubs were taken to include the left/right superior frontal, superior parietal, precuneus, and insula, comprising the highest degree nodes of the group-averaged connectome map (i.e., the regions with the most connections). These hub regions also appeared most frequently among the highest degree nodes in the 50 individual network reconstructions, demonstrating a good consistency between hub selection on an individual basis and hub selection on the group level (see the SI section).

In line with our hypothesis, several observations indeed tend to suggest a strong and diverse link community participation of the selected hub nodes, both individually and as a collective. First, as a collective, the eight hub regions were attached to links from all 11 link communities, emphasizing their distributed nature. With the exception of the left Ph/Er community, all communities involved at least three different brain hubs (Figure 8.7a). Second, each hub individually participated in (on average) 5.8 (std: 1.9) communities, significantly exceeding the number of link communities in which non-hub nodes participated (mean [std]: 1.9 [1.1], $p < 0.001$, permutation test). This effect was even significant ($p = 0.02$) after performing a linear regression to compensate for the positive relationship between degree and community participation (more attached links generally giving access to more communities, Figure 8.7b), indicating that the high community participation of rich club hubs is not only attributable to their high degree, but also to their specific wiring pattern in the overall brain network. Third, although some non-hub nodes also presented high community parti-

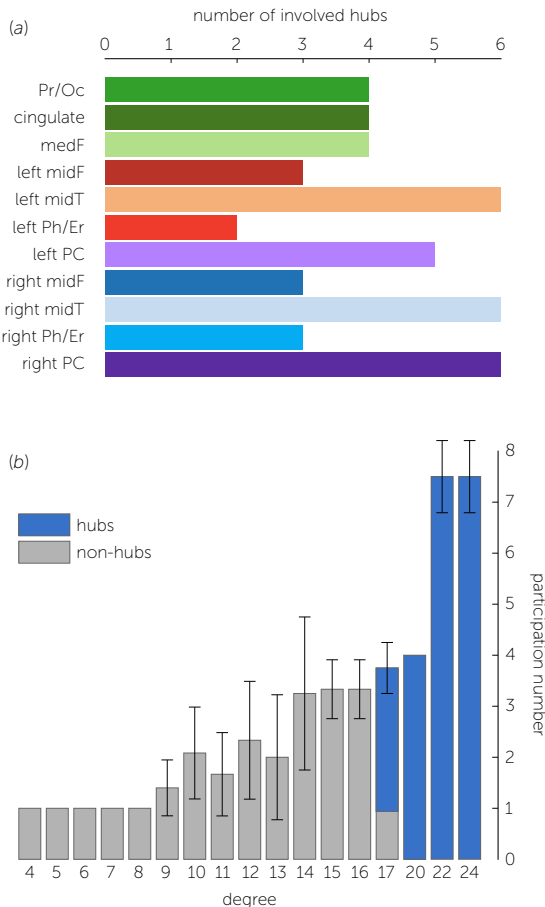


Figure 8.7. Community participation of hub regions. The relationship between hub regions and link communities was examined by selecting eight putative hub regions (left/right superior frontal, superior parietal, precuneus, and insula) on the basis of degree (i.e., number of connections) and previous reports (van den Heuvel et al., 2012; van den Heuvel and Sporns, 2011). (a) All identified communities involved at least two of these brain hubs, emphasizing their distributed nature. (b) Hub regions further displayed a significantly stronger community participation than non-hubs ($p < 0.001$), even after regressing out the positive relationship between degree and community participation ($p = 0.02$).

participation, reflecting a general heterogeneity of the nodes of the network (Kinnison et al., 2012), all hub regions scored among the top 14 nodes with a participation number of four or higher (Figure 8.7b). Taken together, our findings support previous suggestions that brain hubs operate on the boundaries between communities (van den Heuvel and Sporns, 2013) (**chapter 5**) and therefore form ideal candidates to facilitate integration of information and intermodule communication (van den Heuvel and Sporns, 2014; Margulies et al., 2009; Sporns et al., 2007) (**chapter 6**).

Discussion

Our study shows that the brain's white matter pathways display a rich and diverse community pattern. Examining the line graph of an anatomical brain network derived from diffusion imaging data, 11 link communities were observed, forming a Pr/Oc, cingulate, and medF community, and left and right PC, midF, midT, and Ph/Er communities (Figure 8.2). Moreover, the identified link communities were found to be highly consistent across bootstrap samples, indicating a good robustness to variations in the underlying connectome data (Figure 8.3).

The biological meaning of link communities in the brain is not immediately clear and very much open to scientific debate. In network literature, community detection is generally applied to uncover *a priori* unknown subsystems or building blocks of the network (Ahn et al., 2010; Girvan and Newman, 2002; Palla et al., 2005; Porter et al., 2009). This view on communities is also firmly anchored in the objective of community detection algorithms to find dense clusters of nodes or links that are relatively loosely attached to the rest of the network. Considering that functional brain networks are shaped by the underlying structural connections (Greicius et al., 2009; van den Heuvel et al., 2009; Honey et al., 2007), one could therefore speculate that link communities form an anatomical substrate for functionally specialized subsystems in the brain, as is also often suggested for node communities (Hilgetag et al., 2000; Sporns, 2013). In a first attempt to aid the interpretation of link communities using data-driven analyses, assessment of several network characteristics of individual white matter pathways showed that connection features vary strongly within link communities (Figure 8.5). This observation may indicate that link communities do not form collections of similar pathways, but rather comprise a mixture of connections with varying roles in the network. Future studies are needed to investigate the potential biological relevance of such an arrangement of white matter connections and the biological meaning of link communities in general.

An interesting feature of link communities is that links from multiple communities may come together at a single brain region, allowing the identification

of “community hot spots”. Among other regions, putative hub regions such as the insula, precuneus, and superior frontal cortex were found to be involved in a variety of communities (Figure 8.6). This diverse community participation of brain regions might reflect a multimodal internal organization emerging from different (functional) subparts. In favor of this hypothesis, the anterior part of the insula has been shown to project to the middle and inferior temporal cortex, to frontal regions, and to the anterior cingulate cortex, while the middle-posterior insula projects to premotor and sensorimotor regions, and the posterior mid-cingulate cortex (Cauda et al., 2011; Deen et al., 2011; Taylor et al., 2009). Similar functional specialization has been suggested for other regions with high community participation. For instance, examinations of the connectivity profile of the precuneus suggest the existence of structurally and functionally diverse anterior, posterior, and central parts (Cavanna and Trimble, 2006; Margulies et al., 2009; Zhang and Li, 2012), confirming our observation of both the left and right precuneus to participate in a large number of link communities (Figure 8.6). Also the superior frontal cortex, which showed the highest participation number, has been suggested to exhibit several functionally distinct subparts (Zhang et al., 2012), underscoring a possible relationship between link community involvement and internal heterogeneity of brain regions. It may therefore be relevant for future studies to investigate whether link communities could be used to create finer parcellation templates and to examine how link communities are affected by the adoption of such templates.

The marked involvement of hub regions in a wide variety of link communities also supports the idea that brain hubs may play a pivotal role as confluence zones in which neural information from different domains merges (van den Heuvel and Sporns, 2014). All link communities were found to be directly attached to at least two different regions from a central hub collective (Hagmann et al., 2008; van den Heuvel and Sporns, 2011) and participation levels of hub nodes significantly exceeded those of non-hubs. This distributed nature and diverse connectivity of hub regions with respect to link communities aligns with recent findings on the importance of hubs for the integration of functional subsys-

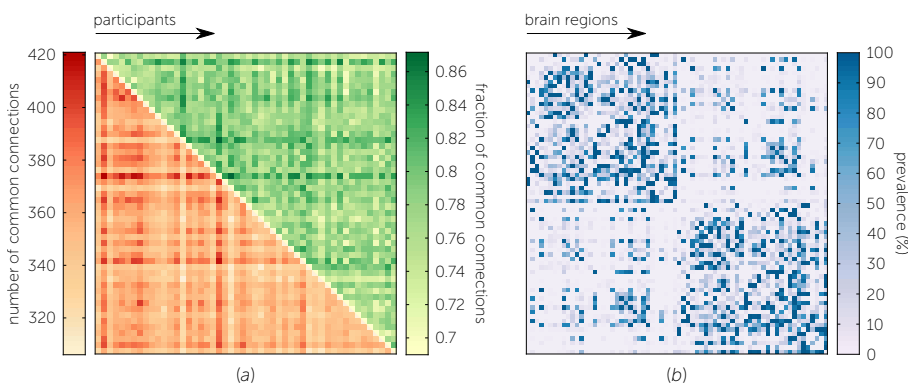
tems in the cat (**chapter 5**) and human (van den Heuvel and Sporns, 2013) brain and the similarly pronounced participation of hub regions in node communities (Kinnison et al., 2012; Meunier et al., 2010; Sporns et al., 2007). Moreover, a recent report by Crosley et al. (2013) based on a meta-analysis of task-related activation studies showed that brain hubs were coactivated by a diverse range of experimental tasks, suggesting that hubs facilitate a large functional repertoire. It would be of interest for future studies to examine whether connections of a link community may correspond to coactivations of a specific set of behavioural domains, potentially providing a connection between this diverse coactivation of hubs and their link community participation.

Finally, it should be noted that the link communities presented in this article were obtained using unweighted brain networks, considering only the presence or the absence of white matter connections between brain regions without making inferences on the quality or strength of these connections. Although it is, in principle, possible to generalize the adopted link community detection approach to weighted networks (Evans and Lambiotte, 2010), it is unclear whether a weighted approach is preferable and, if so, which choice of connection weights (fractional anisotropy, streamline count, streamline density, magnetization transfer ratio, etc.) would be most suitable. Instead, by keeping the results as general as possible, focusing on the topological structure of the network, the identified link communities can naturally serve as *link categories* to illuminate contrasts with respect to any type of connection weight. Considering recently reported connectivity deficits in schizophrenia patients found using link categories (van den Heuvel et al., 2013; Zalesky et al., 2011) and the tendency of neurodegenerative diseases to target subsystems of the brain (Seeley et al., 2009; Verstraete et al., 2011), link communities could prove to be a fruitful instrument for future case-control studies.

Supplementary information

Reconstructed brain networks

The brain's network of white matter pathways was represented by a group-averaged connectome map, based on reconstructed anatomical brain networks of 50 healthy participants. The reconstructed individual brain networks on average comprised 478 (std: 38) connections, corresponding to a network density of 21% (std: 1.7%). To check for possible outliers, overlap between individual brain networks was assessed by counting the number of common connections between each pair of participants (Supplementary Figure 8.1a). The average overlap of participants with the rest of the sample was found to be approximately normally distributed, with all participants scoring within three standard deviations of the mean (mean [std]: 353.5 [12.8] connections). Since participants with strongly deviating connectivity (e.g., due to technical problems) would either



Supplementary Figure 8.1. Inter-participant variability. (a) Similarity between reconstructed individual brain networks from our sample of 50 participants. The lower triangular part of the matrix shows how many white matter connections two participants (p, q) have in common, while the upper triangular part shows the corresponding fraction of common connections (i.e., the number of common connections divided by $\min(\#p, \#q)$, with $\#[\cdot]$ equal to the total number of connections in the participant's brain network). The rows and columns of the matrix correspond to the 50 participants. (b) Connection prevalence. For each possible pair of brain regions (i, j), the corresponding entry of the depicted matrix shows the percentage of participants for which brain region i and j were found to be connected. The rows and columns of the matrix correspond to the 68 anatomically segregated brain regions that were incorporated in the brain network reconstructions.

have abnormally low overlap scores or very high scores (in case of overabundant connectivity), no reason was found to exclude any of the participants. The group-averaged connectome map was formed by including only those connections that were found to be present in at least 60% (30) of the participants, resulting in an averaged brain network with 383 connections (corresponding to a network density of 16.8%). This connectome map on average shared 344 of its 383 connections (90%) with a given individual brain network, which is comparable to the mutual overlap between the (denser) individual networks. More information about the included participants and the brain network reconstruction procedure can be found in the SI section of **chapter 4**, which provides a thorough motivation for the 60% group threshold on the basis of the same sample of 50 healthy participants.

Link community detection

Following the approach proposed by Evans and Lambiotte (2009), the link communities of the group-averaged connectome map were identified using the network's associated *line graph*. This line graph is formed by defining a "node" for every link in the connectome map and a "connection" between two of these nodes if the links that they represent share a common endpoint. Subsequently, communities within the line graph are identified by applying a traditional (node-based) community detection method to the line graph. Since nodes of the line graph correspond to links of the original connectome map, detected communities of densely interconnected line graph nodes map one-to-one to link communities of the connectome.

Community detection on the line graph was performed with the Infomap algorithm of Rosvall and Bergstrom (2008). This algorithm searches for network partitions that minimize the description length of an infinite random walk on the network, hopping from node to node by randomly choosing connections with probability proportional to their weight. In order to establish a natural correspondence between random walks on the line graph and "link-node-link" transitions

on the original brain network, the connections of the line graph were weighted such that a random walk moved from one link (i.e., node of the line graph) to the next by first uniformly selecting one of the link's endpoints, followed by a link incident to that endpoint. As explained in detail in the aforementioned paper by Evans and Lambiotte (2009), this is achieved by giving each line graph connection weight $1/(k_i - 1)$, with k_i equal to the degree of the common endpoint that caused its existence.

Edge removal metrics

To aid the interpretation of the identified link communities, several network properties of the underlying white matter pathways were estimated by comparing the intact group-averaged connectome map with slightly modified versions, missing only the single connection whose features were to be assessed. By quantifying the change between the intact and modified networks with commonly used network metrics, traditional (node oriented) metrics were effectively mapped to edge-centric ones. Four of such *edge removal metrics* were considered, measuring the relevance of connections for the (1) characteristic path length, (2) clustering coefficient, (3) global communicability within the entire network, and (4) local communicability between the endpoints of a connection.

Characteristic path length

The characteristic path length L of a network is defined as the mean of the path lengths L_{ij} between all possible pairs (i, j) of the n nodes, where L_{ij} represents the minimum number of connections that needs to be traversed when traveling between nodes i and j (Rubinov and Sporns, 2010). The associated edge removal metric of a connection e is obtained by comparing the characteristic path length before and after hypothetically removing e . Expressed in formulas, if A represents the (adjacency matrix of the) intact network and $A[\neg e]$ represents the same network without e , the edge removal metric of e with respect to the characteristic path length L is given by:

$$\frac{L(A[\neg e]) - L(A)}{L(A)}, \quad (8.1)$$

estimating the relevance of connection e for maintaining short path lengths.

Clustering coefficient

Similarly, the edge removal metric of connection e that measures its relevance with respect to the clustering coefficient of the network is given by:

$$\frac{C(A[\neg e]) - C(A)}{C(A)}, \quad (8.2)$$

with $C(A)$ equal to the clustering coefficient of the intact network and $C(A[\neg e])$ equal to the clustering coefficient of the same network without e . The clustering coefficient C of a network was computed as the average of the local clustering coefficients of the nodes, measuring how many neighbors of a node are also neighbors of each other (Rubinov and Sporns, 2010).

Communicability

The communicability or “ease of communication” G_{ij} between two nodes i and j of a network was measured as proposed in the work of Estrada and Hatano (2008). Their metric takes not only the (length of the) shortest paths between node i and j into account, but rather includes all possible walks (i.e., paths that may visit the same edge multiple times) between the two nodes with appropriate weights, assigning lower weights to longer walks, formally given by:

$$G_{ij} = \sum_{k=0}^{\infty} \frac{(A^k)_{ij}}{k!} = \exp(A)_{ij}, \quad (8.3)$$

Here, A denotes the adjacency matrix of the network, satisfying $A_{ij} = 1$ if node i and j are connected and $A_{ij} = 0$ otherwise. To measure the overall communicability G within the entire network, G_{ij} was averaged over all node pairs (i, j) (Benzi and Klymko, 2013).

The relevance of connections with respect to the network's communicability was measured on two levels. The global relevance of a connection e for the communicability of the network as a whole was estimated with an edge removal metric of the same form as those for clustering and path length, given by:

$$\frac{G(A[\neg e]) - G(A)}{G(A)}. \quad (8.4)$$

The second measure is instead focused on the local relevance of connection e for the communicability between its endpoints i and j :

$$\frac{G(A[\neg e])_{ij} - G(A)_{ij}}{G(A)_{ij}}, \quad (8.5)$$

where $G(A)_{ij}$ represents the communicability between the endpoints i and j in the intact network and $G(A[\neg e])_{ij}$ represents the communicability between i and j after connection e has been removed.

Rich club regions

Motivated by the participation of a select number of brain regions in as many as five, seven, or eight of the eleven identified link communities, the community participation of previously reported *rich club regions* was examined (Collin et al., 2014; van den Heuvel et al., 2012; van den Heuvel and Sporns, 2011). In agreement with those previous reports (some of which consider overlapping samples (van den Heuvel et al., 2012; van den Heuvel and Sporns, 2011), some of which independent ones (Collin et al., 2014)), rich club hubs were taken to include the left/right superior frontal, superior parietal, precuneus, and insula. As expected, these eight regions were found to comprise the highest degree nodes of the group-averaged connectome map (i.e., the regions with the most connections). Since degree is the usual criterion for the selection of (rich club) hubs, this observation demonstrates that the previously reported rich club regions are also representative for our current sample. In addition, selecting the highest degree nodes in each individual participant (in principle the eight highest ones, but possibly more in case of ties) and counting the number of times each region was

selected, showed that the aforementioned rich club regions were also most frequently selected across participants, further confirming that these hubs are indeed appropriate for the sample.

References

- Ahn, Y.Y., Bagrow, J.P., Lehmann, S., 2010. Link communities reveal multiscale complexity in networks. *Nature* 466, 761-764.
- Alexander-Bloch, A., Lambiotte, R., Roberts, B., Giedd, J., Gogtay, N., Bullmore, E., 2012. The discovery of population differences in network community structure: New methods and applications to brain functional networks in schizophrenia. *NeuroImage* 59, 3889-3900.
- Anderson, J.S., Ferguson, M.A., Lopez-Larson, M., Yurgelun-Todd, D., 2011. Connectivity Gradients Between the Default Mode and Attention Control Networks. *Brain Connectivity* 1, 147-157.
- Andersson, J.L.R., Skare, S., 2002. A Model-Based Method for Retrospective Correction of Geometric Distortions in Diffusion-Weighted EPI. *NeuroImage* 16, 177-199.
- Andersson, J.L.R., Skare, S., Ashburner, J., 2003. How to correct susceptibility distortions in spin-echo echo-planar images: application to diffusion tensor imaging. *NeuroImage* 20, 870-888.
- Beckmann, C.F., DeLuca, M., Devlin, J.T., Smith, S.M., 2005. Investigations into resting-state connectivity using independent component analysis. *Philosophical Transactions of the Royal Society of London B: Biological Sciences* 360, 1001-1013.
- Benzi, M., Klymko, C., 2013. Total communicability as a centrality measure. *Journal of Complex Networks* 1, 124-149.
- Boldi, P., Rosa, M., 2012. Arc-Community Detection via Triangular Random Walks. *Proceedings of the 8th Latin American Web Congress*, 48-56.
- Bullmore, E., Sporns, O., 2009. Complex brain networks: graph theoretical analysis of structural and functional systems. *Nature Reviews Neuroscience* 10, 186-198.
- Cauda, F., D'Agata, F., Sacco, K., Duca, S., Geminiani, G., Vercelli, A., 2011. Functional connectivity of the insula in the resting brain. *NeuroImage* 55, 8-23.
- Cavanna, A.E., Trimble, M.R., 2006. The precuneus: a review of its functional anatomy and behavioural correlates. *Brain* 129, 564-583.
- Chang, L.C., Jones, D.K., Pierpaoli, C., 2005. RESTORE: Robust estimation of tensors by outlier rejection. *Magnetic Resonance in Medicine* 53, 1088-1095.
- Chen, Z.J., He, Y., Rosa-Neto, P., Germann, J., Evans, A.C., 2008. Revealing Modular Architecture of Human Brain Structural Networks by Using Cortical Thickness from MRI. *Cerebral Cortex* 18, 2374-2381.
- Collin, G., Kahn, R.S., de Reus, M.A., Cahn, W., van den Heuvel, M.P., 2014. Impaired Rich Club Connectivity in Unaffected Siblings of Schizophrenia Patients. *Schizophrenia Bulletin* 40, 438-448.
- Crossley, N.A., Mechelli, A., Vértes, P.E., Winter-Brown, T.T., Patel, A.X., Ginestet, C.E., McGuire, P., Bullmore, E.T., 2013. Cognitive relevance of the community structure of the human brain functional coactivation network. *Proceedings of the National Academy of Sciences* 110, 11583-11588.
- Deen, B., Pitskel, N.B., Pelpfrey, K.A., 2011. Three Systems of Insular Functional Connectivity Identified with Cluster Analysis. *Cerebral Cortex* 21, 1498-1506.
- Estrada, E., Hatano, N., 2008. Communicability in complex networks. *Physical Review E* 77, 036111.
- Evans, T.S., Lambiotte, R., 2009. Line graphs, link partitions, and overlapping communities. *Physical Review E* 80, 016105.
- Evans, T.S., Lambiotte, R., 2010. Line graphs of weighted networks for overlapping communities. *The European Physical Journal B* 77, 265-272.
- Girvan, M., Newman, M.E.J., 2002. Community structure in social and biological networks. *Proceedings of the National Academy of Sciences* 99, 7821-7826.
- Greicius, M.D., Supekar, K., Menon, V., Dougherty, R.F., 2009. Resting-State Functional Connectivity Reflects Structural Connectivity in the Default Mode Network. *Cerebral Cortex* 19, 72-78.
- Hagmann, P., Cammoun, L., Gigandet, X., Meuli, R., Honey, C.J., Wedeen, V.J., Sporns, O., 2008. Mapping the Structural Core of Human Cerebral Cortex. *PLoS Biology* 6, e159.
- Harriger, L., van den Heuvel, M.P., Sporns, O., 2012. Rich Club Organization of Macaque Cerebral Cortex and Its Role in Network Communication. *PLoS ONE* 7, e46497.
- He, Y., Chen, Z.J., Evans, A.C., 2008. Structural Insights into Aberrant Topological Patterns of Large-Scale Cortical Networks in Alzheimer's Disease. *The Journal of Neuroscience* 28, 4756-4766.

CHAPTER 8

- He, Y. et al., 2009. Uncovering Intrinsic Modular Organization of Spontaneous Brain Activity in Humans. *PLoS ONE* 4, e5226.
- van den Heuvel, M.P., Kahn, R.S., Goñi, J., Sporns, O., 2012. High-cost, high-capacity backbone for global brain communication. *Proceedings of the National Academy of Sciences* 109, 11372-11377.
- van den Heuvel, M.P., Mandl, R.C.W., Kahn, R.S., Hulshoff Pol, H.E., 2009. Functionally linked resting-state networks reflect the underlying structural connectivity architecture of the human brain. *Human Brain Mapping* 30, 3127-3141.
- van den Heuvel, M.P., Mandl, R.C.W., Stam, C.J., Kahn, R.S., Hulshoff Pol, H.E., 2010. Aberrant Frontal and Temporal Complex Network Structure in Schizophrenia: A Graph Theoretical Analysis. *The Journal of Neuroscience* 30, 15915-15926.
- van den Heuvel, M.P., Sporns, O., 2011. Rich-Club Organization of the Human Connectome. *The Journal of Neuroscience* 31, 15775-15786.
- van den Heuvel, M.P., Sporns, O., 2013. An Anatomical Substrate for Integration among Functional Networks in Human Cortex. *The Journal of Neuroscience* 33, 14489-14500.
- van den Heuvel, M.P., Sporns, O., 2014. Network hubs in the human brain. *Trends in Cognitive Sciences* 17, 683-696.
- van den Heuvel, M.P., Sporns, O., Collin, G., Scheewe, T., Mandl, R.C.W., Cahn, W., Goñi, J., Hulshoff Pol, H.E., Kahn, R.S., 2013. Abnormal rich club organization and functional brain dynamics in schizophrenia. *JAMA Psychiatry* 70, 783-792.
- Hilgetag, C.C., Burns, G.A., O'Neill, M.A., Scannell, J.W., Young, M.P., 2000. Anatomical connectivity defines the organization of clusters of cortical areas in the macaque monkey and the cat. *Philosophical Transactions of the Royal Society of London B: Biological Sciences* 355, 91-110.
- Honey, C.J., Kötter, R., Breakspear, M., Sporns, O., 2007. Network structure of cerebral cortex shapes functional connectivity on multiple time scales. *Proceedings of the National Academy of Sciences* 104, 10240-10245.
- Kaiser, M., Hilgetag, C.C., 2004. Edge vulnerability in neural and metabolic networks. *Biological Cybernetics* 90, 311-317.
- Kaiser, M., Martin, R., Andras, P., Young, M.P., 2007. Simulation of robustness against lesions of cortical networks. *European Journal of Neuroscience* 25, 3185-3192.
- Kim, Y., Jeong, H., 2011. Map equation for link communities. *Physical Review E* 84, 026110.
- Kinnison, J., Padmala, S., Choi, J.M., Pessoa, L., 2012. Network Analysis Reveals Increased Integration during Emotional and Motivational Processing. *The Journal of Neuroscience* 32, 8361-8372.
- Lancichinetti, A., Fortunato, S., Kertész, J., 2009. Detecting the overlapping and hierarchical community structure in complex networks. *New Journal of Physics* 11, 033015.
- Margulies, D.S., Vincent, J.L., Kelly, C., Lohmann, G., Uddin, L.Q., Biswal, B.B., Villringer, A., Castellanos, F.X., Milham, M.P., Petrides, M., 2009. Precuneus shares intrinsic functional architecture in humans and monkeys. *Proceedings of the National Academy of Sciences* 106, 20069-20074.
- Meunier, D., Lambiotte, R., Bullmore, E.T., 2010. Modular and hierarchically modular organization of brain networks. *Frontiers in Neuroscience* 4, 200.
- Mori, S., Crain, B.J., Chacko, V.P., Van Zijl, P.C.M., 1999. Three-dimensional tracking of axonal projections in the brain by magnetic resonance imaging. *Annals of Neurology* 45, 265-269.
- Palla, G., Derényi, I., Farkas, I., Vicsek, T., 2005. Uncovering the overlapping community structure of complex networks in nature and society. *Nature* 435, 814-818.
- Porter, M.A., Onnela, J.P., Mucha, P.J., 2009. Communities in networks. *Notices of the American Mathematical Society* 56, 1082-1097.
- Power, J. et al., 2011. Functional Network Organization of the Human Brain. *Neuron* 72, 665-678.
- Rosvall, M., Bergstrom, C.T., 2008. Maps of random walks on complex networks reveal community structure. *Proceedings of the National Academy of Sciences* 105, 1118-1123.
- Rubinov, M., Sporns, O., 2010. Complex network measures of brain connectivity: Uses and interpretations. *NeuroImage* 52, 1059-1069.
- Seeley, W.W., Crawford, R.K., Zhou, J., Miller, B.L., Greicius, M.D., 2009. Neurodegenerative Diseases Target Large-Scale Human Brain Networks. *Neuron* 62, 42-52.
- Sepulcre, J., Sabuncu, M.R., Yeo, T.B., Liu, H., Johnson, K.A., 2012. Stepwise Connectivity of the Modal Cortex Reveals the Multimodal Organization of the Human Brain. *The Journal of Neuroscience* 32, 10649-10661.

Shanahan, M., Bingman, V.P., Shimizu, T., Wild, M., Güntürkün, O., 2013. Large-Scale Network Organisation in the Avian Forebrain: A Connectivity Matrix and Theoretical Analysis. *Frontiers in Computational Neuroscience* 7, 89.

Sporns, O., 2013. Network attributes for segregation and integration in the human brain. *Current Opinion in Neurobiology* 23, 162-171.

Sporns, O., Honey, C.J., Kötter, R., 2007. Identification and Classification of Hubs in Brain Networks. *PLoS ONE* 2, e1049.

Sporns, O., Tononi, G., Kötter, R., 2005. The Human Connectome: A Structural Description of the Human Brain. *PLoS Computational Biology* 1, e42.

Taylor, K.S., Seminowicz, D.A., Davis, K.D., 2009. Two systems of resting state connectivity between the insula and cingulate cortex. *Human Brain Mapping* 30, 2731-2745.

Towlson, E.K., Vértes, P.E., Ahnert, S.E., Schafer, W.R., Bullmore, E.T., 2013. The Rich Club of the *C. elegans* Neuronal Connectome. *The Journal of Neuroscience* 33, 6380-6387.

Verstraete, E., Veldink, J.H., Mandl, R.C.W., van den Berg, L.H., van den Heuvel, M.P., 2011. Impaired Structural Motor Connectome in Amyotrophic Lateral Sclerosis. *PLoS ONE* 6, e24239.

Wu, K. et al., 2011. The Overlapping Community Structure of Structural Brain Network in Young Healthy Individuals. *PLoS ONE* 6, e19608.

Zalesky, A., Fornito, A., Seal, M.L., Cocchi, L., Westin, C.F., Bullmore, E.T., Egan, G.F., Pantelis, C., 2011. Disrupted Axonal Fiber Connectivity in Schizophrenia. *Biological Psychiatry* 69, 80-89.

Zhang, S., Ide, J.S., Li, C.R., 2012. Resting-State Functional Connectivity of the Medial Superior Frontal Cortex. *Cerebral Cortex* 22, 99-111.

Zhang, S., Li, C.R., 2012. Functional connectivity mapping of the human precuneus by resting state fMRI. *NeuroImage* 59, 3548-3562.



Chapter 9

Spectral fingerprints of neural networks

Part I: Based on a publication (Frontiers in Computational Neuroscience, vol. 7, 2014) by Siemon C. de Lange, Marcel A. de Reus and Martijn P. van den Heuvel

*Part II: Based on a manuscript submitted for publication by
Siemon C. de Lange, Martijn P. van den Heuvel and Marcel A. de Reus*

Part I: The Laplacian spectrum of neural networks

Abstract

The brain is a complex network of neural interactions, both at the microscopic and macroscopic level. Graph theory is well-suited to examine the global network architecture of these neural networks. Many popular graph metrics, however, encode average properties of individual network elements. Complementing these “conventional” graph metrics, the eigenvalue spectrum of the normalized Laplacian describes network structure directly at a systems level, without referring to individual nodes or connections. In the first part of this chapter, we examine the Laplacian spectra of the macroscopic brain networks of the macaque and cat, and the microscopic neuronal network of the nematode *Caenorhabditis elegans*. Consistent with conventional graph metrics, analysis of these Laplacian spectra revealed an integrative community structure in neural networks. Extending previous findings of overlapping network attributes across species, similarity of the Laplacian spectra of the cat, macaque, and *C. elegans* suggests a certain level of consistency in the overall architecture of the anatomical neural networks of these species. Our results further suggest a specific network class for neural networks, distinct from conceptual small-world and scale-free models, as well as from several non-neural empirical networks.

Introduction

The brain is a complex system of structurally and functionally interconnected elements. Within this system, healthy brain function depends on a constant interplay between local information processing and efficient global integration of information, facilitated by a large-scale network of structurally interconnected neurons and brain regions; a network known as the connectome (Bullmore and Sporns, 2009; Sporns et al., 2005). Neural interactions occur on multiple scales, ranging from the microscopic level of neuronal cells and their synaptic connections to the macroscopic level of neural projections between large-scale brain regions (Sporns et al., 2005). In the past decades, studies examining the

topological structure of neural systems, including those of mammalian species (Modha and Singh, 2010; Scannell et al., 1995) as well as those of nematode (Varshney et al., 2011) and diptera species (Pavlou and Goodwin, 2013), have reported several network attributes of an efficient communication architecture. Neural systems were shown to combine high levels of local clustering and community structure with short pathways and central hubs, suggested to facilitate efficient long-distance communication and global integration of information between subparts of the system (Bassett and Bullmore, 2006; Bullmore and Sporns, 2009; Hagmann et al., 2008; Harriger et al., 2012; van den Heuvel et al., 2012; Sporns and Zwi, 2004).

Mathematically, neural systems can be described as a graph $G = (V, E)$, comprising a collection of nodes V , representing neurons or brain regions, and a collection of interconnecting edges E (Boccaletti et al., 2006; Bullmore and Sporns, 2009; van den Heuvel and Hulshoff Pol, 2010; Reijneveld et al., 2007; Sporns, 2011). Commonly explored graph theoretical metrics often involve properties of the nodes of the network, including their level of local clustering, their degree (i.e., number of connections), their betweenness or closeness centrality, or their global or local communication efficiency (Boccaletti et al., 2006; Newman, 2003; Watts and Strogatz, 1998). For the examination of overall aspects of network organization, like small-world or scale-free features, these node properties are then typically aggregated across the individual nodes of the network (for example achieved by averaging), resulting in a global descriptive for the entire network.

Complementing “conventional” metrics composed of node properties, direct examination of the global structure of neural networks at a systems level may capture qualitative aspects of the network as a whole that otherwise remain out of sight (Atay et al., 2006; Banerjee, 2012; Banerjee and Jost, 2007; Varshney et al., 2011). In recent years, studies have started to utilize concepts from a mathematical discipline known as *spectral graph theory* to examine neural networks (Banerjee and Jost, 2007; Varshney et al., 2011), including metrics based on ei-

genvectors of network matrices, such as nodal centrality measures (Bonacich, 1972; Lohmann et al., 2010; Page et al., 1999) and community identification methods (Fortunato, 2010; Harriger et al., 2012; Liang et al., 2011; Newman, 2006). While eigenvectors are still closely related to properties of individual network elements, and are often used as such, the spectrum of the associated eigenvalues contains valuable information related to the global structure of a graph (Banerjee, 2012; Banerjee and Jost, 2007; McGraw and Menzinger, 2008; Vukadinović et al., 2002), potentially providing new insights in the workings of the brain as a system.

Here, we investigate the architecture of neural networks at a systems level by examining the so-called Laplacian eigenvalue spectrum for connectome maps of three different species: the macaque, cat, and *Caenorhabditis elegans*. The normalized Laplacian matrix, in short referred to as the *Laplacian*, is a transformation of the connectivity matrix of a network, with the Laplacian eigenvalues describing aspects related to global network structure and dynamic interactions between network parts (Banerjee, 2012; Chung, 1997). The spectrum of the normalized Laplacian of undirected networks has the advantage that all eigenvalues are found in the domain between 0 and 2, enabling the comparison of networks of different sizes (Banerjee, 2012). Furthermore, it has been noted that similarities between the spectra of networks can be used for the classification of networks (Banerjee and Jost, 2008a; Cetinkaya et al., 2012; Ipsen and Mikhailov, 2002; Vukadinović et al., 2002). The neural spectra are therefore specifically examined in the light of potential similarities which may reflect general organizational characteristics of neural networks across species.

Materials and methods

Connectome maps

The three connectome maps examined in this study are often used in the literature (Hilgetag et al., 2000; Kaiser, 2011; Sporns and Kötter, 2004; Zamora-López et al., 2011) and provide comprehensive information about the anatomical neu-

ral networks of the macaque, cat, and *C. elegans*. They describe the structural connectivity of, on the microscopic level, the whole neuronal system of the *C. elegans*, and, on the macroscopic level, the networks of long-range white matter projections of the cerebral cortex in the macaque and cat. To make the analysis of the Laplacian eigenvalues feasible, all connectome maps were transformed into undirected and unweighted graphs (i.e., all edges were transformed to reciprocal binary edges). A description of the three datasets is included below.

Macaque

The connectivity dataset of the macaque was based on tract-tracing studies collected in the online *Collation of Connectivity data on the Macaque brain* (CoCoMac) database (Kötter, 2004; Stephan et al., 2001), as previously analyzed by Modha and Singh (2010), and describes macroscopic white matter projections between regions of the macaque cortex. The connection matrix examined in this study was a subset of the matrix provided by Modha and Singh (2010) and was taken from a study of Harriger et al. (2012), excluding subcortical areas (thalamus, basal ganglia, and brainstem) and including only regions with at least one incoming and one outgoing connection. In all, the included macroscopic connectivity dataset comprised 242 cortical regions and 4,090 directed binary connections (Harriger et al., 2012). The density of the connectivity matrix, representing the number of connections divided by the total number of connections possible, was 7.0%. For the spectral analysis performed here, the directionality of the edges was removed, resulting in an undirected network with 3,054 connections and a density of 10.5%. More detailed information on the macroscopic macaque connectome map can be found in the papers by Modha and Singh (2010) and Harriger et al. (2012).

Cat

As in **chapter 5**, the macroscopic connectivity dataset of the cat cortex was taken from a paper by Scannell et al. (1995), as previously analyzed by, among others, Hilgetag et al. (2000), Sporns et al. (2004), and Zamora-López et al.

(2009). Similar to the macaque connectome map, the cat dataset resulted from a literature review, combining information from neuroanatomical literature and tract-tracing studies (Scannell et al., 1995). The dataset included 65 cortical areas, connected by 1,139 directed and weighted connections (all areas having at least one in- and one outgoing connection), giving a density of 27.4%. Three connections strengths were distinguished: weak connections having weight 1, medium strength connections having weight 2, and strong connections having weight 3. For our study, the dataset was converted to a binary, undirected network with a density of 35.1%, including 730 unweighted, undirected connections.

C. elegans

The microscopic connectivity dataset of the *C. elegans* was taken from a study by Varshney et al. (2011). The dataset was based on original data from White et al. (1986) and was further improved by Varshney and colleagues, adding new data from serial section electron microscopy reconstructions. The connectivity dataset described 279 neurons, of which 274 were included in this study. Five neurons (IL2DL, IL2DR, PLNR, DD06, and PVDR) were excluded as they had not at least one in- and one outgoing connection (Varshney et al., 2011). In total, the dataset contained 2,956 directed connections formed by gap junctions (always generating reciprocal connections) and chemical synapses, corresponding to a density of 3.95%. The transformed undirected and unweighted network used in our analyses had 2,253 connections and a density of 6.02%.

Model networks

The Laplacian spectra of the neural networks were compared to the spectra of three commonly used network models. First, the network model by Erdős and Rényi (1959) (ER) was examined, in which nodes are linked by randomly placed connections. Second, the Watts-Strogatz (WS) model was used to generate small-world networks, obtained by randomly rewiring 30% of the connections of a regular ring lattice with degree 16 for each node (Watts and Strogatz, 1998). Third, scale-free networks created with the Barabási-Albert (BA) model were ex-

amined. These BA networks were formed by a stochastic growth process on the basis of preferential attachment: starting with a clique (i.e., fully connected network) of 8 nodes, a new node was added to the network at every timestep and this node was connected to 8 already existing nodes with selection probabilities proportional to the degree of the old nodes (Barabási and Albert, 1999). All model networks had 274 nodes and a density close to 6%, comparable to the neural network of the *C. elegans* (5.86% density for the WS small-world networks, 6.02% for the ER networks, and 5.76% for the BA scale-free networks). For each of the three network models, a representative Laplacian spectrum was created by taking the average spectrum over 1000 model networks. It was verified that these spectra had roughly similar shapes if the number of nodes and density of the model networks were instead matched to the macaque or cat connectome map.

Empirical networks

In addition to the three neural networks and network models, also four non-neural empirical networks were examined, including a food web (source: <http://www.cbl.umces.edu/~atlss/ATLSS.html>), an email interchange network, a network of football games, and a power grid network (all obtained from <http://www.cise.ufl.edu/research/sparse/matrices>). The food web network described the food web of Florida Bay during wet season and consisted of 121 connected living compartments (Ulanowicz et al., 1998). After transformation to an undirected, unweighted network, the food web consisted of 1,763 connections, with a density of 23.9%. The email interchange network described email communication at Rovira i Virgili University and had 1,133 nodes, 5,451 undirected, unweighted connections and a density of 0.85% (Guimerá et al., 2003). The American football network described the games between Division I-A college teams in the year 2000 and had 115 nodes and 613 undirected, unweighted connections, resulting in a density of 9.35% (Girvan and Newman, 2002). Finally, the power grid network of the western United States had 4,941 nodes and 6,594 undirected, unweighted connections, with a density of 0.054% (Watts and Strogatz, 1998).

Reference networks

The eigenvalues of the Laplacian spectra of the examined neural networks were compared to average values of 1000 randomized reference networks. These reference networks were obtained by rewiring the connections of the original networks following a random switching algorithm, ensuring preservation of network size, network density, and the degree sequence, while destroying the overall topological structure (Maslov and Sneppen, 2002).

The normalized Laplacian matrix

The network spectra considered in this study were derived from the normalized Laplacian matrix L , which has the advantage that all eigenvalues are found in the domain between 0 and 2, enabling the comparison of networks of different sizes (Chung, 1997). It is defined by:

$$L_{ij} = \begin{cases} 1 & \text{if } i = j \\ -\frac{1}{k_i} & \text{if } i \text{ and } j \text{ are connected} \\ 0 & \text{otherwise} \end{cases} \quad (9.1)$$

with i and j representing two nodes of the network and k_i equal to the degree of node i . Alternatively, the normalized Laplacian can be expressed in terms of the adjacency matrix A as $L = I - D^{-1}A$, where I is the identity matrix and D is a diagonal matrix with $D_{ii} = k_i$. The normalized Laplacian spectrum of the network is then given by the collection of all eigenvalues of L ; that is, the collection of all scalars λ for which there exists a nonzero vector v (being the associated eigenvector) that satisfies the eigenvalue equation $Lv = \lambda v$.

The normalized Laplacian matrix is unitarily equivalent to the symmetric normalized Laplacian defined by Chung (1997), defined as $L = I - D^{-1/2}AD^{-1/2}$, showing that the eigenvalues of the normalized Laplacian are real. Furthermore, the smallest eigenvalue of the normalized Laplacian is always 0, as the constant eigenvector c , assigning the same value to each node and thus describing the stationary state of the network, satisfies $Lc = 0$. The number of eigenvalues equal to 0 (i.e., the multiplicity of $\lambda = 0$) matches the number of connected

components in the network, being the number of network parts that are not connected to each other (Chung, 1997). The largest eigenvalue is at most 2 and the eigenvalues are labeled and ordered as $0 = \lambda_1 \leq \dots \leq \lambda_n \leq 2$.

Spectral plots

Spectral plots were obtained from the smoothed eigenvalue distribution $\Gamma(x)$, convolving the eigenvalue frequencies with a Gaussian kernel:

$$\Gamma(x) = \sum_{i=1}^n \frac{1}{\sqrt{2\pi\sigma^2}} \exp\left(\frac{-|x - \lambda_i|^2}{2\sigma^2}\right), \quad (9.2)$$

with n being the number of eigenvalues (equal to the number of nodes) and σ being a smoothing factor of 0.015. For the plots, a discrete smoothed spectrum was used in which Γ had steps of 0.001. Furthermore, the distribution was normalized such that the total eigenvalue frequency was one.

Spectral distance

The similarity between spectra was quantified using a spectral distance measure, taken as the average Euclidean distance between two spectral plots Γ_1 and Γ_2 :

$$D(\Gamma_1, \Gamma_2) = \frac{1}{2|X|} \sum_{x \in X} \min_{y \in X} \left(\sqrt{(\Gamma_1(x) - \Gamma_2(y))^2 + (x - y)^2} \right) + \frac{1}{2|X|} \sum_{y \in X} \min_{x \in X} \left(\sqrt{(\Gamma_1(x) - \Gamma_2(y))^2 + (x - y)^2} \right), \quad (9.3)$$

where X is the discrete collection of points in the interval $[0, 2]$ for which the values of Γ_1 and Γ_2 were sampled (i.e., $X = \{i \times 0.001 \mid 0 \leq i \leq 2000\}$). As this distance function is dependent on the scaling of the axes, different scales result in different distances. Therefore, this measure of spectral distance is not an invariant distance measure between two networks, but only a tool to quantitatively underpin the visual results.

Robustness

To investigate the effect of (small) modifications to the neural datasets, reflecting the inclusion of noise in the connectome maps, we examined the spectra of “noise including neural networks”. In the noise including networks, a small proportion, respectively 1, 2, and 5%, of the edges of the original networks (i.e., macaque, cat, and *C. elegans*) were randomly rewired in such a way that the degree distributions of the networks were preserved (Maslov and Sneppen, 2002). The upper and lower eigenvalue boundary of 1000 generated noise including networks were plotted and the spectral similarity between the original network and the noise including networks was quantified by computing the average spectral distance between each of the noise including networks and the original network.

Results

Laplacian spectra of neural networks

The Laplacian spectra of the macaque, cat, and *C. elegans* revealed several characteristic properties that were observed for all three networks, see Figure 9.1.1. First, all the spectra, from micro- (*C. elegans*) to macroscale (cat and macaque), showed a left-skewed distribution in which the largest eigenvalue was closer to one than the smallest (nonzero) eigenvalue. Second, all spectra showed a peak around one. Third, the first (i.e., smallest) eigenvalues were scattered around a few small peaks at the beginning of the spectra. These similarities between the Laplacian spectra of the macaque, cat, and *C. elegans* suggest shared structural properties in the underlying connectomes. Before giving a more detailed description of the observed spectral properties, we first compare the neural spectra with spectra of commonly used network models and spectra of a number of non-neural empirical networks.

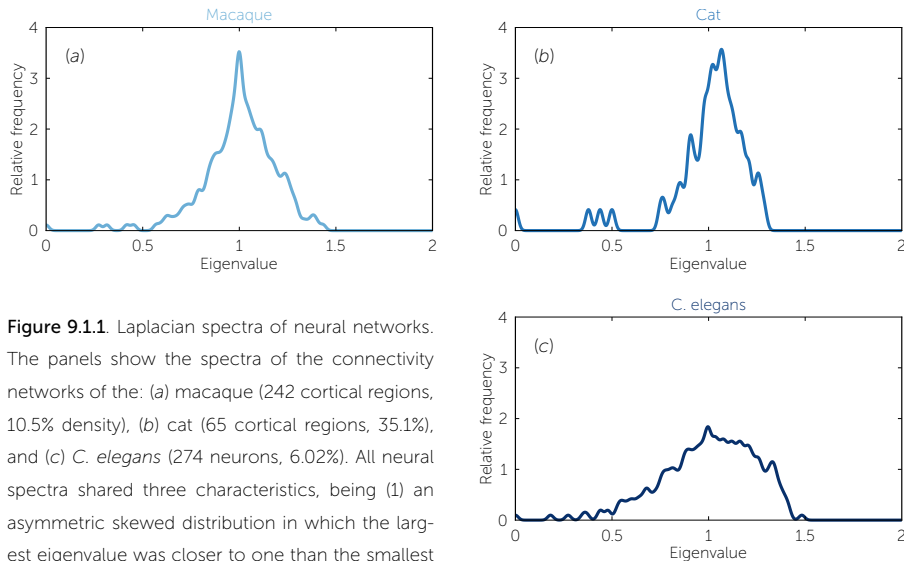


Figure 9.1.1 Laplacian spectra of neural networks. The panels show the spectra of the connectivity networks of the: (a) macaque (242 cortical regions, 10.5% density), (b) cat (65 cortical regions, 35.1%), and (c) *C. elegans* (274 neurons, 6.02%). All neural spectra shared three characteristics, being (1) an asymmetric skewed distribution in which the largest eigenvalue was closer to one than the smallest (nonzero) eigenvalue, (2) a peak around one, and (3) a few scattered small eigenvalues. The spectral overlap across the three neural datasets suggests a level of consistency and conservation of overall network structure between neural networks.

Comparison of neural networks to network models

Given that similar spectra reflect similar network structures, it has been noted that the distribution of Laplacian eigenvalues can be used for classification of networks (Banerjee and Jost, 2008a; Cetinkaya et al., 2012; Ipsen and Mikhailov, 2002; Vukadinović et al., 2002). Spectral similarity was examined by visual inspection of the characteristics of the spectral plots and quantified by computing the average Euclidean distance between spectra. Comparing the Laplacian spectra of the neural networks to the spectra of conceptual Erdős–Rényi (ER) random networks (Erdős and Rényi, 1959), Watts-Strogatz (WS) small-world networks (Watts and Strogatz, 1998), and Barabási-Albert (BA) scale-free networks (Barabási and Albert, 1999), revealed distinct dissimilarities (Figure 9.1.2). ER random and BA scale-free networks showed oval shaped Laplacian spectra, which were – except for a small bump at $\lambda = 0$ reflecting the number of connected components of the network – completely symmetric around one. WS small-world networks showed an asymmetric spectrum, with similarities to both the spectrum of a regular ring lattice and a random network (Banerjee and Jost,

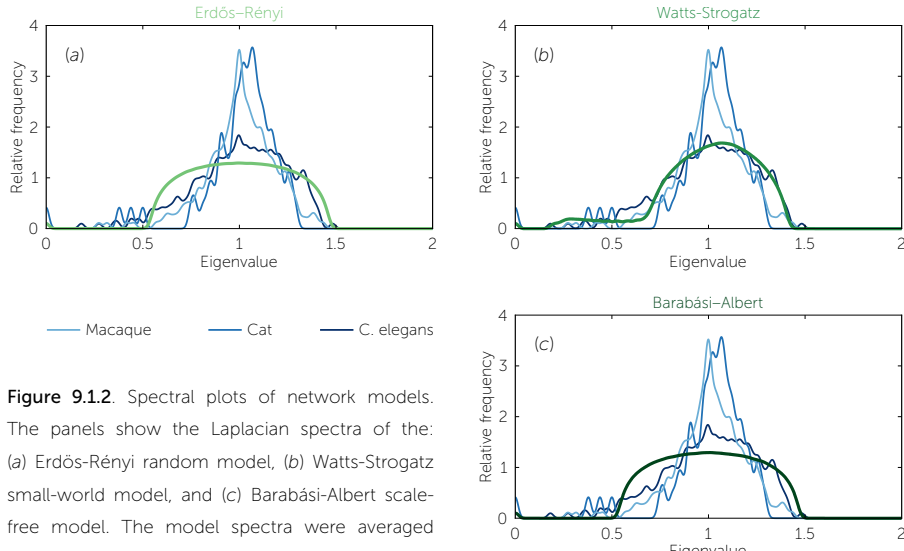


Figure 9.1.2. Spectral plots of network models. The panels show the Laplacian spectra of the: (a) Erdős-Rényi random model, (b) Watts-Strogatz small-world model, and (c) Barabási-Albert scale-free model. The model spectra were averaged over a set of 1000 generated networks. All model networks had 274 nodes and densities close to 6%, comparable to the *C. elegans* connectome map. The spectra of the examined neural networks are plotted in the background.

2008a). ER random and BA scale-free networks showed a maximum, but no sharp peak around one and did not show the characteristic skewed distribution that was observed in the neural networks. In contrast, the spectra of the WS small-world networks showed a skewed distribution with small eigenvalues, but these eigenvalues did not form scattered small peaks as seen in the neural spectra.

Confirming visual observation, the average Euclidean distance (see Table 9.1.1) between the Laplacian spectra of the macaque and cat connectome revealed to be small, indicating a high level of overlap in anatomical network organization. Comparing across scales, the spectra of, on the one hand, the *C. elegans* connectome and, on the other hand, the cat and macaque connectome, were found to be more distant (Table 9.1.1), potentially indicating organizational differences between neural networks on the micro- and macroscale. It appears that this distance results from differences in the density of eigenvalues close to one, as the Laplacian spectra of the cat and macaque showed a stronger

	Cat	C. elegans	ER	WS	BA	Food web	Email	Power grid	Football
Macaque	0.0334	0.0625	0.1047 (0.0021)	0.0645 (0.0023)	0.1014 (0.0023)	0.0389	0.1087	0.2482	0.0705
Cat	-	0.0888	0.1347 (0.0023)	0.0920 (0.0026)	0.1315 (0.0025)	0.0433	0.1245	0.2196	0.0858
C. elegans		-	0.0548 (0.0021)	0.0256 (0.0015)	0.0522 (0.0022)	0.1090	0.0701	0.2399	0.0424
ER			-	0.0838	0.0056	0.1461 (0.0017)	0.3362 (0.0012)	0.2606 (0.0009)	0.0707 (0.0015)
WS				-	0.0801	0.1137 (0.0023)	0.3422 (0.0023)	0.2371 (0.0027)	0.0291 (0.0010)
BA					-	0.1430 (0.0020)	0.3333 (0.0013)	0.2610 (0.0008)	0.0680 (0.0017)
Food web						-	0.1454	0.2380	0.1095
Email							-	0.2028	0.0810
Power grid								-	0.2027

Table 9.1.1. Spectral distances. Table summarizes the spectral distances (computed as the average Euclidean distance between the plots of the two spectra) between the three neural networks (macaque, cat, and *C. elegans*), three network models (ER: Erdős-Rényi random model, WS: Watts-Strogatz small-world model, and BA: Barabási-Albert scale-free model), and four non-neural empirical networks. Values represent mean distances and, where applicable, standard deviations.

peak around one than the Laplacian spectrum of the *C. elegans*. In line with this observation, the spectrum of the *C. elegans* was found to be relatively well approximated by the spectra of WS small-world networks, while the spectra of the macaque and cat were clearly distinct from the conceptual ER random, WS small-world, and BA scale-free models.

Comparison of neural networks to empirical networks

In addition to the spectra of conceptual network models, the Laplacian neural network spectra were also compared to spectra observed in an ensemble of non-neural empirical networks. Empirical networks included the food web of Florida Bay during wet season (abbreviation: Food web), a network describing email interchange at Rovira i Virgili University (Email), a network of American football games between college teams (Football), and the power grid of the western United States (Power grid). Spectra of these networks are plotted in Figure 9.1.3.

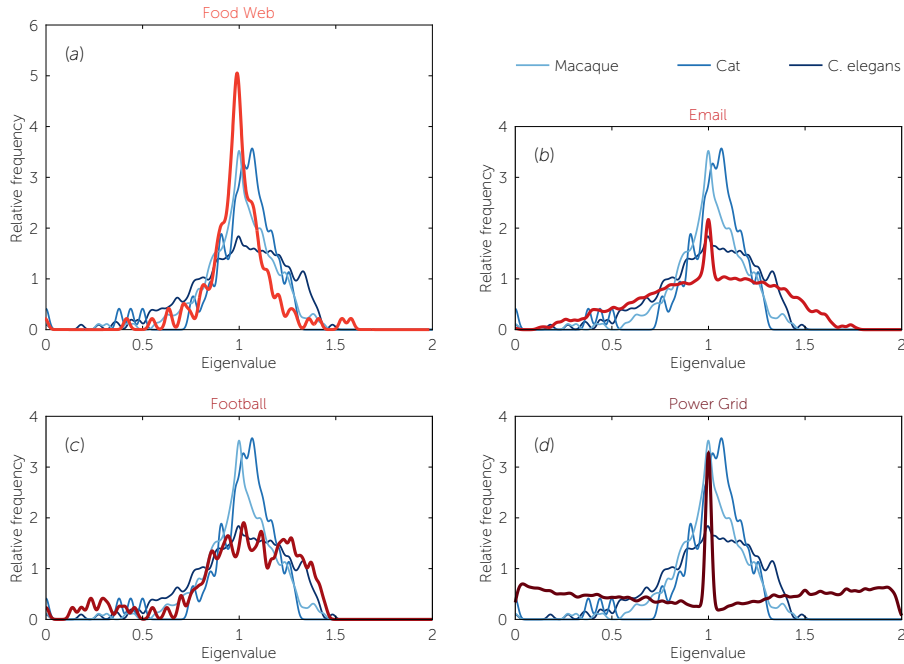


Figure 9.1.3. Spectral plots of empirical networks. The panels show the Laplacian spectra of a: (a) food web (121 nodes, 23.9% density), (b) email interchange network (1133, 0.85%), (c) network of football games (115, 9.35%), and (d) power grid (4941, 0.05%). The spectra of the neural networks of the macaque, cat, and *C. elegans* are plotted in the background.

The spectrum of the power grid and email network both showed a peak around one, but – opposed to the spectra of the neural networks – were not asymmetrically skewed and did not display scattered smallest eigenvalues (Figure 9.1.3). Consistent with this observation, the power grid and email network showed a large spectral distance to all neural networks (Table 9.1.1), suggesting relatively large differences in global topological organization between these two networks and the neural networks. Also the food web showed a spectrum with a pronounced peak around one, displaying a somewhat similar – but more symmetric – shape as the peak in the spectra of the macaque and cat connectome. Moreover, the food web showed scattered small eigenvalues, overlapping with the characteristics of the neural spectra. Both visually and in terms of spectral distance, the food web was more similar to the macaque and cat connectome than to the *C. elegans* connectome, suggesting that the food web may in part

ticular share some organizational features with macroscopic neural networks. Finally, the football network showed a similarly skewed spectrum as reported for the neural networks. The first eigenvalues were scattered, but the corresponding peaks were placed relatively far to the left. Moreover, the football spectrum displayed a maximum around one, but, similar to the spectrum of the *C. elegans*, there was only a modest peak observed around this maximum (Figure 9.1.3). These resemblances were also found when evaluating the spectral distances, showing that the football network was spectrally close to the *C. elegans* network, but distant from the neural networks of the macaque and cat (Table 9.1.1).

Spectral properties: smallest eigenvalues

The smallest eigenvalues of the Laplacian spectrum – meaning the first few eigenvalues of the ordered sequence $0 = \lambda_1 \leq \dots \leq \lambda_n \leq 2$ – have been noted to contain information on the community structure of a network (Figure 9.1.4a) (Donetti and Muñoz, 2005; Fortunato, 2010; Shen and Cheng, 2010; Shi and Malik, 2000). Each eigenvector v_i describes a bisection of the network by assigning a positive or negative value to each node (the eigenvector components) and the associated eigenvalue λ_i describes the inverse diffusion time of this subdivision to the homogeneous stationary state (Cheng and Shen, 2010). As such, smaller eigenvalues indicate longer diffusion times, attributable to a large proportion of intramodule connections and a low number of intermodule connections. The smallest nonzero eigenvalue λ_2 (in connected networks) thus provides information on the best possible cut of the network into two modules (Chung, 1997). To achieve finer subdivisions, the information of all eigenvectors up to v_i can be combined to separate the nodes of the network into i communities, where a possible number of communities for an optimal subdivision might be suggested by the largest eigengap: $\lambda_{i+1} - \lambda_i$ (Cheng and Shen, 2010; Shi and Malik, 2000).

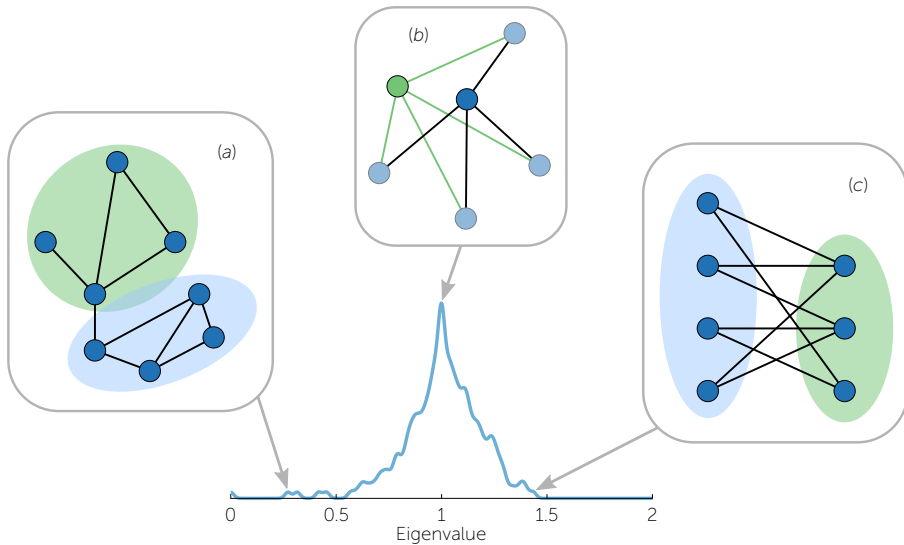


Figure 9.1.4. Topological properties reflected in the Laplacian spectrum. (a) The first eigenvalues reflect community structure, with smaller first eigenvalues indicating the existence of better subdivisions of the network into communities. (b) Motif manipulations, such as motif addition or duplication, result in specific eigenvalues in the spectrum. Recursive manipulations can therefore result in eigenvalues with high multiplicities, giving rise to peaks in the Laplacian spectrum. (c) The largest eigenvalue reflects the level of bipartiteness of the most bipartite subpart of the network, which is closely related to the number of odd cycles in the network.

Macaque

The smallest nonzero eigenvalue of the macaque dataset was $\lambda_2 = 0.2718$, which was significantly lower than the smallest nonzero eigenvalue observed in the randomized reference networks (mean [std]: 0.61 [0.06], $p < 0.001$) (see Materials and methods, 1000 randomized networks were examined). This finding indicates a good cut of the network into two parts and therefore a relatively high level of community structure. This was endorsed by $\lambda_6 - \lambda_5 = 0.1153$ being the largest eigengap, indicating that an optimal subdivision of the network may involve five communities.

Cat

For the cat dataset, the smallest nonzero eigenvalue revealed to be $\lambda_2 = 0.3782$, which was again significantly lower compared to matched random networks (mean [std]: 0.6937 [0.0134], $p < 0.001$). Additionally, $\lambda_5 - \lambda_4 = 0.2512$ was the largest eigengap, suggesting an optimal subdivision of the network into four communities.

C. elegans

For the *C. elegans* network, the smallest nonzero eigenvalue $\lambda_2 = 0.1818$ was also found to be significantly lower relative to randomized networks (mean [std]: 0.5438 [0.0142], $p < 0.001$). Various small eigenvalues showed relatively large eigengaps, demonstrating the existence of a number of stable communities, but the eigengap $\lambda_2 - \lambda_1$ revealed to be the largest, indicating that there is no clear optimal subdivision of the neural network map of the *C. elegans*. This showed that although there is a certain level of community structure within the *C. elegans* connectome dataset, this community structure is relatively weak.

Spectral properties: largest eigenvalue

The largest eigenvalue of the Laplacian spectrum provides information on the level of *bipartiteness* of (subparts of) a network (Figure 9.1.4c) (Bauer and Jost, 2009). A (sub)network is said to be (fully) bipartite if its nodes can be divided into two groups in such a way that nodes within the same group are not connected. As a result, bipartite networks lack cycles with an odd number of nodes. Subdividing the nodes based on the eigenvector associated to the largest eigenvalue, again using the sign of the eigenvector components for the subdivision, provides an indication of the most bipartite configuration of the network. The largest eigenvalue λ_n itself reflects the level of bipartiteness of this configuration. Considering the possibility that only a subset of the nodes may be explicitly positive or negative in the largest eigenvector, λ_n does not always reflect a global property of the entire network.

Macaque

The largest eigenvalue λ_n of the macaque was equal to 1.4341, not significantly higher than the largest eigenvalues observed in a set of comparable random networks (mean [std]: 1.3927 [0.0558], $p = 0.2291$). Additional visual inspection of the eigenvector linked to the largest eigenvalue showed that this eigenvector was localized on two of the five structural communities identified by Harriger et al. (2012), including frontal/orbitofrontal and temporal regions.

Cat

The largest eigenvalue in the cat dataset was found to be $\lambda_n = 1.2875$. For comparable random networks, the largest eigenvalue was on average 1.3319 (std: 0.0119), indicating that the specific wiring of the cat cortex significantly decreased the level of bipartiteness ($p < 0.001$). Visual inspection of the associated eigenvector showed that this eigenvalue represented the entire network, suggesting an overall weaker bipartiteness in the network of the cat cortex, potentially due to the existence of many simple (i.e., non-reducible) odd cycles.

C. elegans

The largest eigenvalue of the *C. elegans* showed to be $\lambda_n = 1.4827$, which was higher than in comparable random networks (mean [std]: 1.4613 [0.0136]), although this effect was marginal and only present at a trend level ($p = 0.0574$). Additional visual inspection showed that the eigenvector associated with this eigenvalue was restricted to one of four identified communities. This community included mostly ventral cord motor neurons, indicating that this class constitutes a relatively bipartite community.

Spectral properties: motif manipulations

Repeated addition and duplication of nodes and motifs in the formation of a network has been shown to leave traces in a network's Laplacian spectrum (Banerjee and Jost, 2008b; Banerjee and Jost, 2009). For example, node duplication, referring to the process of introducing a new node to the network with the exact

same connectivity pattern as an already existing node (Figure 9.1.4b), has been shown to result in an increase in the multiplicity of the eigenvalue $\lambda = 1$ (Banerjee and Jost, 2008b). As a result, recursive node duplication may create a peak in the spectrum at $\lambda = 1$. Moreover, edge duplication, referring to duplication of two connected nodes i and j and their connections, has been noted to produce eigenvalues symmetrically placed around 1, given by $\lambda = 1 \pm (k_i k_j)^{1/2}$ (where k_i and k_j are equal to the degree of node i and node j , respectively). Also addition of simple motifs to the network generates specific eigenvalues, with the inclusion of a new triangular motif, for instance, resulting in the addition of an eigenvalue $\lambda = 1.5$ to the spectrum (Banerjee and Jost, 2008b). So, in general, motif duplication and addition produce specific exact eigenvalues and subsequent repetition of these processes may result in characteristic high eigenvalue multiplicities, visible as peaks in the Laplacian spectrum. The presence of eigenvalues with high multiplicities (e.g., a high peak at $\lambda = 1$) may therefore provide an indication of local network patterns resulting from recursive motif manipulations.

Macaque, cat, and *C. elegans*

The spectra of all three neural networks showed a peak around one, suggesting traces of node duplication. Additionally, the observed peaks around one revealed to be rather symmetric, indicating traces of edge duplication in the networks. Comparison between the neural spectra showed that the peak around one and its symmetry was most clearly seen in the spectra of the macaque and cat network and to a lesser extent in the *C. elegans* network. This might indicate higher levels of duplication in the macroscopic neural networks of the macaque and cat compared to the microscopic neuronal network of the *C. elegans*. The spectra showed no other clear peaks indicative of recurrent motif manipulations.

Robustness

To investigate the influence of small amounts of noise on the examined neural spectra, the spectra of the macaque, cat, and *C. elegans* were compared to those of 1000 “noise including networks”, generated by rewiring a small proportion

of the edges of the original networks (ranging from 1 to 5%, see Materials and methods). The lower and upper boundaries of the spectra observed for these noise including networks are shown in Figure 9.1.5, together with the original spectra. For all three neural networks, large overlap was found between the spectra of the original and noise including networks, underscored by small spectral distances (see Table 9.1.2). As expected, with the inclusion of increasing levels of random noise, the spectra of the noise including neural networks started to reveal slightly more random properties, including higher smallest eigenvalues and a less pronounced peak around one.

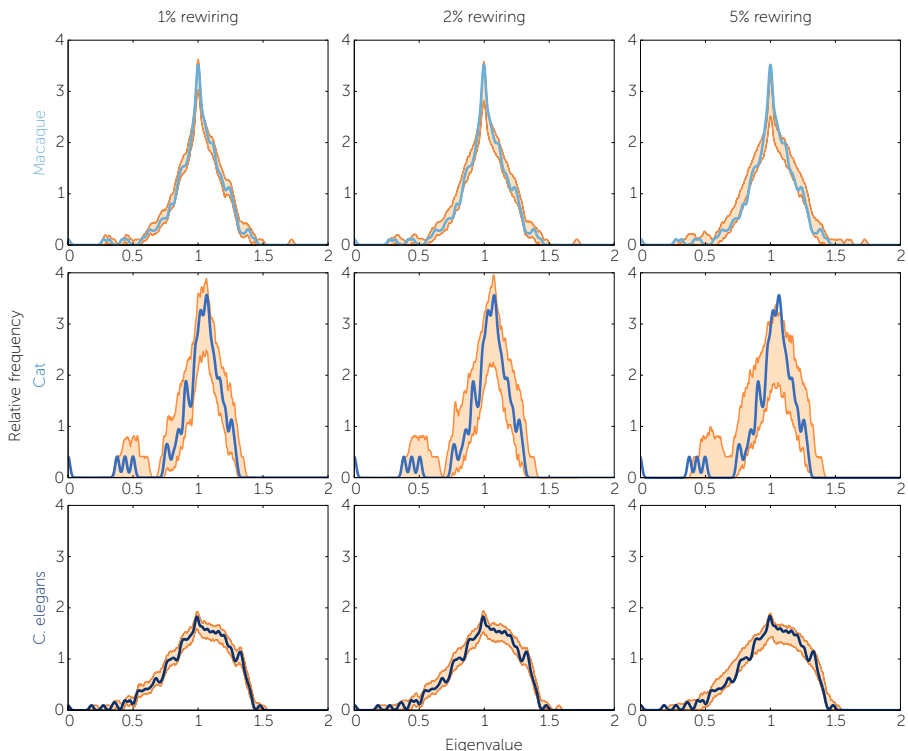


Figure 9.1.5. Robustness of neural network spectra to edge rewiring. Panels show how rewiring a small percentage of the edges (1, 2, or 5%) affects the spectra of the macaque, cat, and *C. elegans*, simulating potential effects of noise. For each eigenvalue, the plots show the lower and upper boundary of spectra of 1000 “noise including networks”. The cat network appears the most affected by the rewiring process, which is likely a consequence of its relatively small network size. In general, the spectra of the noise including networks show large overlap with the original spectra, indicating that the spectra are robust to small modifications in the datasets.

	1% rewiring	2% rewiring	5% rewiring
Macaque	0.0062 (0.0011)	0.0095 (0.0015)	0.0176 (0.0022)
Cat	0.0092 (0.0025)	0.0141 (0.0038)	0.0287 (0.0056)
<i>C. elegans</i>	0.0079 (0.0011)	0.0108 (0.0011)	0.0158 (0.0014)

Table 9.1.2. Robustness of neural network spectra to edge rewiring as measured by spectral distance. Table shows the spectral distances between the examined neural networks and networks in which a small proportion (1, 2, or 5%) of the edges was randomly rewired. Values represent mean distances and standard deviations.

Discussion

The main finding of this study is that the network spectra of anatomical neural networks of three different species showed mutual overlap on several characteristics, potentially providing evidence for a common underlying structural organization of neural networks. Examining and comparing the Laplacian spectrum of a microscopic neuronal network map of the *C. elegans* connectome and macroscopic maps of the macaque and cat connectome (Figure 9.1.1), it was found that the neural spectra all showed a few scattered peaks at the start of the spectrum, a high peak around one, and an overall skewness to the left. Conceptual ER random, WS small-world, or BA scale-free models could not reproduce these properties (Figure 9.1.2) and also the spectra of an email and power grid network were found to be clearly distinct from the neural spectra (Figure 9.1.3). As such, our findings indicate a relatively unique shape of the spectra of neural networks, suggesting that neural networks may form, to some extent, a specific network class.

Consistent with earlier observations (Arenas et al., 2008; Hilgetag et al., 2000), examination of the small eigenvalues in the neural spectra, causing the scattered peaks at the start, revealed the presence of community structure in all three neural networks. Interestingly, the optimal number of communities for the brain networks of the cat (four) and macaque (five) suggested by analysis of the eigengaps in their Laplacian spectra coincided with numbers of communities previously reported for these networks (Harriger et al., 2012; Scannell et al., 1995). Furthermore, the relatively symmetric peak around one observed in the

neural spectra suggested traces of node and edge duplication in neural networks. It should be noted, though, that the macaque and cat spectrum showed a more evident central peak than the spectrum of the *C. elegans*, suggesting higher levels of duplication in the macroscopic brain networks of the macaque and cat than in the microscopic neuronal network of the *C. elegans*. With respect to the largest Laplacian eigenvalue, reflecting the level of bipartiteness of (a subpart of) the network, the three neural spectra were less consistent. As bipartiteness is inversely related to the presence of simple odd cycles, one might expect that the commonly observed small-world properties of neural networks, predicting the presence of many triangular motifs (Bassett and Bullmore, 2006; Bullmore and Sporns, 2012; van den Heuvel et al., 2008a; Sporns and Zwi, 2004; Stam, 2004), would decrease their largest eigenvalues. However, only the largest eigenvalue of the cat dataset, and not those of the macaque and *C. elegans* datasets, revealed to be significantly smaller compared to randomized reference networks. A possible explanation for this observation is that the random levels of bipartiteness reflected by the largest eigenvalues of the *C. elegans* and macaque network were found to be specific for (small) subparts of these networks. Moreover, high numbers of triangles (i.e., simple cycles with three nodes) may be compensated by low numbers of simple odd cycles with five nodes or more.

In terms of spectral distance, the spectrum of the *C. elegans* was found to be relatively well approximated by the spectra of WS small-world model networks. However, the spectra of the macaque and cat were clearly distinct from the spectra of the ER random, WS small-world, and BA scale-free model networks. In addition, none of the network models could explain the three above-described characteristics of neural spectra. This may suggest that the rich architecture of neural networks, and perhaps in particular the macroscopic network architecture of the mammalian brain, cannot be fully explained by simple network models. Indeed, several network studies have shown that neural networks of the human brain deviate from the simple BA scale-free or WS small-world network model. For example, studies have suggested that brain networks tend to display a truncated power-law degree distribution rather than the true power-law distri-

butions seen in BA scale-free networks (Achard et al., 2006; Barabási and Albert, 1999; Iturria-Medina et al., 2008). Furthermore, studies have shown that neural networks display properties such as a rich community structure (van den Heuvel et al., 2008b; Meunier et al., 2010; Rubinov and Sporns, 2011; Salvador et al., 2005; Wu et al., 2011) and high levels of intermodule connectivity (van den Heuvel and Sporns, 2013) (**chapter 5**); complex properties which cannot be expected to emerge in WS small-world models created by rewiring a small number of edges of an otherwise regular lattice.

Comparison of the neural spectra to Laplacian spectra of other empirical networks demonstrated that two non-neural empirical networks, a food web and football network, may show organizational resemblances with the examined neural networks. Underscoring the relatively large spectral distance observed between neural networks of different spatial scales, the food web was spectrally closest to the macroscopic macaque and cat brain network, while the spectrum of the football network was closest to the microscopic *C. elegans* network. Searching for specific characteristics of the two non-neural empirical networks, the football network has been noted to display a geographically constrained community structure, with a high number of matches between teams from the same conference and sparse inter-conference matches with a strong preference for geographically close teams (Girvan and Newman, 2002). In addition, the food web has been noted to be the result of a long interplay between the introduction of new species due to differentiation and immigration, and the survival or extinction of species on the basis of fitness (Drossel and McKane, 2005). Hence, the spectral similarities between the neural networks and the food web and football network possibly suggest that neural networks on the microscopic level may exhibit organizational properties related to a spatially driven community structure, while macroscopic neural interactions might be shaped by a long developmental trajectory influenced by evolutionary constraints. Such constraints could include a limit on the amount of resources available for brain wiring, in agreement with a proposed balance in brain architecture between minimizing wiring cost and establishing advantageous topological properties

such as efficiency or robustness (Bullmore and Sporns, 2012; Collin et al., 2014; van den Heuvel et al., 2012).

When interpreting our findings, some potential limitations should be considered. First, connectome research is a rapidly moving field and the connectivity data as used in this study is likely to be complemented with additional data in the near future, something which may result in (small) modifications in the connectivity matrices. To understand the robustness of network spectra to such modifications and to noise in general, modifications to the neural network maps were simulated by randomly rewiring a small proportion (1-5%) of the edges in the networks. Spectra of these noise including neural networks were found to show large overlap with the original networks, illustrating a high level of robustness to small variations in overall wiring layout (Figure 9.2.5). However, the simulations also showed that in networks of smaller size, such as that of the cat brain, small variations in the eigenvalues have a relatively larger impact on the spectrum. Hence, in these networks, small spikes in the spectra should be interpreted with caution and may not reflect global network properties. Second, more generally, the size and density of a network – describing the number of nodes and edges representing the network – may have a strong influence on the distribution of the eigenvalues (Chung et al., 2003). In random networks, a higher density is associated with a larger smallest eigenvalue λ_2 and a smaller largest eigenvalue λ_n and this trend is consistent with observed differences in λ_2 and λ_n between the macaque, cat, and *C. elegans* spectrum. Third, all networks were regarded as binary and undirected, which made the connectivity data less accurate. Although generalizations of the normalized Laplacian have been proposed to produce similar spectra (with only real eigenvalues) of directed networks (Chung, 2005), this approach is relatively new and it is still unclear to what extent interpretations valid for spectra of the undirected Laplacian can be generalized to spectra of directed Laplacians. Future studies examining the link between spectra of directed and undirected networks would therefore be of high interest.

Part II: The role of symmetry in neural networks and their Laplacian spectra

Abstract

Human and animal neural systems constitute complexly wired networks that form an infrastructure for efficient processing and integration of information. An intriguing aspect of the organization of many neural networks is their level of symmetry, resulting from brain regions or neurons that exhibit similar wiring patterns. In the second part of this chapter, we propose a measure – labeled the duplication coefficient – to capture the global level of symmetry of a network and we link this measure to the so-called Laplacian spectrum of neural networks. Providing insight in the systems-level fingerprint provided by the Laplacian spectrum, we use the duplication coefficient to examine a characteristic central peak in the spectrum of anatomical network maps of the mouse, cat, macaque, and human brain. On the basis of both empirical networks and network models, we show that the height of the main peak in the Laplacian spectrum is largely attributable to symmetry in the underlying network. Moreover, spectral fitting of duplication-based model networks to neural networks showed that neural spectra are best approximated using a trade-off between duplication and diversification. Taken together, our results facilitate a better understanding of neural network spectra and the importance of symmetry in neural networks.

Introduction

The mammalian brain is a complexly wired network. On the macroscale systems level, anatomically segregated brain regions and their interconnecting white matter pathways together form a complex system of neural nodes and connections, commonly referred to as the macroscale *connectome* (Sporns et al., 2005). The architecture of this connectome can be examined using tools from graph theory, a branch of mathematics revolving around the formal study of networks (Bullmore and Sporns, 2009). Different from many more typical graph

metrics which describe neural systems on the basis of (average) node characteristics (see Rubinov and Sporns (2010) for an overview), the so-called Laplacian spectrum provides a unique systems-level fingerprint of brain networks and can therefore potentially provide new insights in their complex architecture (Banerjee and Jost, 2007; Varshney et al., 2011; Vukadinović et al., 2002). As shown in the first part of this chapter, characteristic features of neural spectra include the presence of a few scattered small peaks at the start of the spectrum and a pronounced peak in the middle.

Although some features of Laplacian spectra have been related to conventional network measures such as synchronization (Atay et al., 2006), local clustering (Bauer and Jost, 2009), and modularity (Cheng and Shen, 2010; Shen and Cheng, 2010; Shi and Malik, 2000), several other characteristics remain unexplained. For one, the large central peak in the spectra of neural networks – one of their most characteristic features – is not yet fully understood. Based on theoretical results showing that nodes with identical connectivity patterns increase the elevation precisely in the middle of the spectrum, it has been hypothesized that the central peak may describe nodal symmetry (Banerjee and Jost, 2008b), a property noted to be closely related to other features deemed relevant for neural systems such as parallel processing and functional specialization (Ballard, 1986; Bullmore and Sporns, 2009; Felleman and Van Essen, 1991; van den Heuvel and Hulshoff Pol, 2010).

In this study, we examine to what extent symmetry shapes neural spectra and whether overlap in the wiring pattern of brain regions can indeed explain the large central peak observed in spectra of neural networks. We explore the relationship between network symmetry, measured by the here introduced duplication coefficient, and the central spectral peak across and within macroscale reconstructions of the mouse, cat, macaque, and human connectome, as well as across several non-neural empirical networks. Next, we investigate this relationship also for commonly used network models, each incorporating a specific feature of neural networks. Finally, the interplay between regional symmetry and

regional diversity in neural networks is investigated by fitting the spectra of a duplication-based network model to the observed neural spectra.

Materials and methods

Network formalism

Laplacian spectra and network symmetry were investigated for brain networks of multiple species, including the human, macaque, cat, and mouse. Networks were mathematically represented by a connectivity matrix, formally known as the network's *adjacency matrix*. The rows and columns of this matrix represented the nodes of the network and an entry in row i and column j represented a connection (also referred to as *edge*) between node i and node j . In the examined neural networks, nodes represented brain regions and connections represented (the existence of) large-scale anatomical pathways between brain regions.

Neural networks

Human, standard resolution

The human brain connectivity network was obtained from high-quality diffusion-weighted MRI data from 215 subjects, provided in the Q3 data release of the Human Connectome Project (Glasser et al., 2013; Van Essen et al., 2012), as previously described in **chapter 6**. Briefly, white matter pathways were reconstructed using generalized q -sampling imaging and streamline tractography (Yeh et al., 2010) and the cortex was parcellated into 68 distinct regions based on FreeSurfer's Desikan-Killiany atlas (Desikan et al., 2006). Two brain regions were considered connected if in at least 60% of the subjects (see **chapter 4**) a reconstructed white matter fiber pathway touched both regions. This procedure resulted in a group-averaged connectome map with 68 nodes and a density of 20.2%.

Human, high resolution

By combining the aforementioned reconstructed white matter pathways with an additional cortical parcellation based on a high-resolution subdivision of the Desikan-Killiany atlas (Cammoun et al., 2012), a second group-averaged connectome map was formed. This high-resolution human brain network, again including connections if present in at least 60% of the subjects, comprised 219 nodes and had a density of 5.0%.

Macaque

The macaque connectivity dataset was extracted from the publicly available *Collation of Connectivity data on the Macaque brain* (CoCoMac) database, containing information on macroscale white matter pathways as reported in macaque anatomical tracer studies (Stephan et al., 2001). The connectivity matrix used here, previously adopted in a study of Scholtens et al. (2014), described interareal connectivity between 78 non-overlapping cerebral brain regions, parcellated according to a scheme proposed by Felleman and Van Essen (1991). An anatomical tract between two brain regions was included in the matrix if the tract was reported as existing in two-thirds of the reports which investigated the tract. The resulting connectivity matrix for the macaque had 78 nodes and a density of 23.0%.

Cat

The macroscale cat connectivity network was taken from a study by Scannell et al. (1995), presenting a connectivity dataset based on a comprehensive collation of neural tracing studies in the cat brain (also see **chapter 5**). The dataset contained information on projections between 65 non-overlapping brain regions, covering the cat cortex. Here, information about the presence of connections was used to form a network with 65 nodes and a density of 35.1%.

Mouse

The mouse connectivity matrix was based on the recently presented Allen Mouse Brain Connectivity Atlas (<http://connectivity.brain-map.org>), which describes the axonal projections between brain regions obtained from anterograde tracer examinations performed by a single research group (Oh et al., 2014) (see **chapter 7** for a brief discussion of this dataset). The connectivity matrix presented by Oh et al. (2014) contained information on the neural wiring of 213 brain regions, including data about the confidence of every connection. For this study, a connection between two regions was included if its reported α -level was lower than 0.05. The resulting connectivity matrix had 213 nodes and its density was 11.7%.

Non-neural empirical networks

In addition to the neural networks described above, also five non-neural empirical networks were examined, representing a food web, a network of frequently combined words, a social network describing book characters from the novel *Les Misérables*, a social network of interactions between dolphins, and a network of co-purchased books on US politics. Table 9.2.1 provides a brief overview of these empirical networks.

	Description	No. nodes	Density	Source
Food web	Food web of Florida Bay during wet season	121	24.3%	www.cbl.umces.edu/~atlss/ATLSS.html
Words	Adjacencies of common adjectives and nouns in the novel <i>David Copperfield</i>	112	6.8%	www.cise.ufl.edu/research/sparse/matrices
Books	Co-purchases of books on US politics	105	8.1%	www.cise.ufl.edu/research/sparse/matrices
Dolphins	Social interactions in a community of dolphins	62	8.4%	www.cise.ufl.edu/research/sparse/matrices
Les Miserables	Co-appearances of characters in the novel <i>Les Misérables</i>	77	8.7%	www.cise.ufl.edu/research/sparse/matrices

Table 9.2.1. Overview of the analyzed non-neural empirical networks.

Duplication coefficient

To measure the level of global symmetry in a network, we propose a measure that we will refer to as the *duplication coefficient* of the network. Described in words, the duplication coefficient measures to what extent network nodes have a “copy” or, phrased differently, how much nodes look like their most similar peer. In our formal implementation of the duplication coefficient, the similarity between nodes i and j was inferred from the overlap between their connectivity pattern, measured by the matching index (Hilgetag et al., 2002):

$$\frac{|N(i) \setminus j \cap N(j) \setminus i|}{|N(i) \setminus j \cup N(j) \setminus i|}, \quad (9.4)$$

where $N(i)$ denotes the set of nodes connected to node i (i.e., node i 's neighbors), $N(i) \setminus j$ are all neighbors of i excluding possibly j , and $|N|$ denotes the number of nodes in set N . The matching index takes values between 0 (for disjoint connectivity patterns) and 1 (for identical connectivity patterns). The duplication coefficient of an individual node was then defined as its maximum similarity to any other node in the network and the duplication coefficient of the entire network was defined as the average duplication coefficient over all nodes.

Laplacian spectrum

As in the first part of this chapter, network spectra were obtained by means of spectral analysis of the so-called normalized Laplacian matrix. Formally, the normalized Laplacian spectrum is given by the collection of all eigenvalues of the matrix $L = I - D^{-1}A$, where A is the adjacency matrix of the network and D is a diagonal matrix with the degree of the nodes on the diagonal (Chung, 1997). An important feature of the normalized Laplacian matrix L is that all eigenvalues are normalized between 0 and 2, enabling comparison of spectra for differently sized networks. For plotting and investigation of Laplacian spectra as continuous curves $\Gamma(x)$, rather than discrete collections of eigenvalues λ_i , eigenvalue densities were convolved with a Gaussian kernel of standard deviation $\sigma = 0.015$,

$$\Gamma(x) = \sum_{i=1}^n \frac{1}{\sqrt{2\pi}\sigma^2} \exp\left(\frac{-|x - \lambda_i|^2}{2\sigma^2}\right), \quad (9.5)$$

and then normalized such that the total area under the curve was one (Banerjee and Jost, 2007). The height of the main peak in the Laplacian spectrum was taken to be the maximum value of this normalized continuous function.

Relationship between peak height and symmetry

The relationship between the height of the main peak in the Laplacian spectrum and the global level of network symmetry – the existence of such a relationship being the main hypothesis of our study – was examined across and within networks. Across neural and non-neural empirical networks, the correlation between main peak height and duplication coefficient was considered. Furthermore, the absolute values of the duplication coefficient and central peak height were compared. In addition, within neural networks, the effect of symmetry on the Laplacian spectrum was investigated by comparing how the main peak in the spectrum was altered under two edge rewiring strategies. First, in the *random strategy*, a small group of nodes (10%) was randomly selected and the edges of these nodes were rewired to randomly chosen new neighbors. Second, in the *targeted strategy*, optimized to decrease network symmetry, the same approach as used in the random strategy was applied to produce 100 rewired networks of which the network with the lowest duplication coefficient was then selected. For both the random and targeted strategy, 1000 altered networks were constructed and the rewiring effect on the main peak of the spectrum was assessed by comparing the difference in peak height decrease between random and targeted rewiring.

Network models

Four common network models, each featuring their own characteristic network properties, were investigated to further examine how certain network organizations relate to symmetry and main spectral peak height:

Erdős-Rényi (ER) model. ER model networks are completely random networks with no other specified structure than their size n and density d and were obtained by randomly placing $L = d \times n(n - 1)/2$ connections between n nodes (Erdős and Rényi, 1959). ER random networks show no community structure, low levels of clustering, and short path lengths.

Watts-Strogatz (WS) model. WS model networks were obtained by rewiring a percentage of the edges of a lattice ring network of nodes with equal degrees (Watts and Strogatz, 1998). WS model networks display a small-world organization, characterized by high levels of local clustering and short path lengths, as also reported for many neural networks (Bassett and Bullmore, 2006; Bullmore and Sporns, 2009; Hagmann et al., 2008; van den Heuvel et al., 2008a).

Barabási-Albert (BA) model. BA model networks were grown from a so-called seed network by iteratively introducing new nodes to the network. Each new node was randomly connected to a constant number of already present nodes according to a degree-biased probability function (Barabási and Albert, 1999). The probability for a connection of a new node i to be attached to an already present node j was

$$P_j = \frac{k_j}{\sum_I k_I}, \quad (9.6)$$

where k_j is the degree of node j and the sum is over all existing nodes I . BA model networks have scale-free degree distributions and thus comprise small numbers of highly connected hub nodes (Barabási and Albert, 1999).

Spatial model. In the spatial model, networks grew in a similar manner as in the BA model, but nodes were randomly embedded in a three-dimensional cube and newly added nodes were connected with existing nodes in order of proximity (as given by the Euclidean distance). This cost-minimizing model helped to understand how symmetry and the central spectral peak interact with optimal wiring, a topic of special interest because connectivity in neural networks has

been suggested to result from a trade-off between acquiring beneficial topological properties and minimizing wiring cost (Bassett et al., 2010; Bullmore and Sporns, 2012; van den Heuvel et al., 2012; Sporns et al., 2004; Vértes et al., 2012).

To investigate spectra and symmetry in the network models, 1000 instances of each model were generated with the number of nodes and any other model parameters matched to the human high-resolution connectome. Specifically, for the WS model, nodes were set to have 10 connections and 12% of the edges were randomly rewired, such that the density and clustering coefficient of the generated small-world networks matched that of the human connectome. In the BA and spatial model, a fully connected network of 5 nodes was taken as seed network and the number of edges added to each new node was taken to be equal to 5. Model instances were used to calculate main spectral peak height and duplication coefficient distributions for each model, which were examined and compared to the values obtained for the high-resolution human brain network.

Duplication model

The extent to which the architecture and spectra of neural networks may be driven by local symmetry patterns was investigated using a duplication-based model in which symmetry naturally emerges from iterative (partial) node duplication (Bhan et al., 2002). Starting with a seed network, the model network grew by duplication of randomly selected nodes. Duplication of a node, referred to as the *parent* node, involved the introduction of a new node to the network which was connected to all neighbors of the randomly chosen parent node. For diversification, one connection of the new node was rewired such that the new node was connected to its parent, while the other connections of the new node were rewired with probability $1 - \gamma$ to nodes not in the neighborhood of the parent node.

To empirically establish the balance between regional diversity and regional

symmetry in neural networks (modeled by parameter γ), a grid search was applied to find the values of γ for which the spectra of the duplication model best resembled the examined neural spectra. Resemblance was measured using a simple concept of spectral distance (Gu et al., 2014), estimating the difference between two spectral plots Γ_1 and Γ_2 by

$$D(\Gamma_1, \Gamma_2) = \int_0^2 |\Gamma_1(x) - \Gamma_2(x)| dx, \quad (9.7)$$

where the integral was discretely evaluated using intervals of length 0.001. In the grid search, the performance of parameter γ was evaluated on the interval $[0, 1]$ with steps of 0.01 on the basis of spectra of 100 model realizations. Seed networks were taken to be randomly wired networks with an average degree of two and the size of the seed networks was chosen such that the density of the seed network matched the density of the neural network that was to be approximated.

Results

Spectral peak height and symmetry across empirical networks

The relationship between network symmetry and the main central peak in Laplacian spectra was first investigated by comparing the duplication coefficient and height of the spectral peak in an ensemble of empirical networks, including both neural and non-neural networks. As shown in Figure 9.2.1, a clear linear relationship was observed between a network's duplication coefficient and central peak height ($r = 0.63, p = 0.04$). The duplication coefficient of the examined neural networks revealed to range between 0.48 and 0.69 and the central peak height between 2.0 and 3.6, causing the neural networks to form a "cluster" positioned in between the non-neural empirical networks. Non-neural empirical networks showed a distinction between, on the one hand, the dolphins, words, and books networks, having lower duplication coefficients (between 0.33 and 0.46) and smaller central peaks (between 1.4 and 1.7) than the class of neural networks, and, on the other hand, the food web and Les Misérables network, reporting

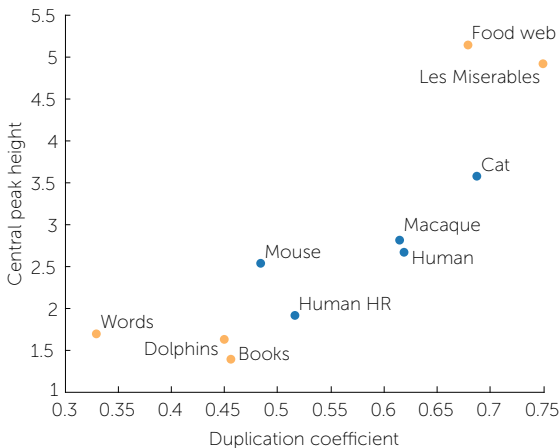


Figure 9.2.1. Duplication coefficient and central peak height in empirical networks. Across empirical networks, including five neural and five non-neural networks, a correlation was observed between the duplication coefficient, measuring network symmetry, and the height of the central peak in the Laplacian spectrum ($r = 0.63, p = 0.04$). This correlation suggests that network symmetry may be an important factor contributing to the high central peaks in neural spectra.

high levels of duplication (0.68 and 0.75, respectively) and a high central peak (5.1 and 4.9). The high spectral peak and symmetry level observed for the food web is in agreement with earlier suggestions of node duplication playing a major role in the formation of food webs (Drossel and McKane, 2005).

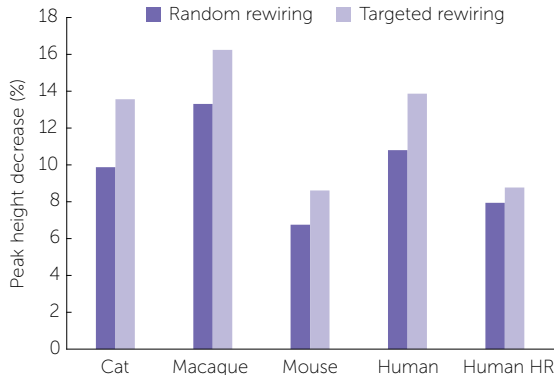
Effects of targeted and non-targeted rewiring

The influence of symmetry on the main spectral peak was further investigated within neural networks by examining targeted and non-targeted edge rewiring. For all neural networks, targeted rewiring of edges (optimized to decrease network symmetry) induced a stronger decrease of the main spectral peak than random rewiring, see Figure 9.2.2 ($p < 0.001$, t -tests, Bonferroni corrected). The largest effect was observed for the cat connectome, where targeted rewiring decreased the height of the main central peak 1.4x more than non-targeted rewiring; in the other networks this was 1.1x (human, high resolution), 1.2x (macaque), and 1.3x (human, standard resolution; mouse).

Validation using network models

The existence of a relationship between duplication coefficient and spectral peak height was verified using four network models. In comparison with the high-resolution human brain network, to which the model networks were matched, the

Figure 9.2.2. Effect of edge rewiring on the height of the central spectral peak. Targeted rewiring of edges optimized to reduce the duplication coefficient of neural networks was found to induce a significantly larger decrease of the central spectral peak than randomly rewiring edges (all $p < 0.001$, t -tests, Bonferroni corrected).



ER random and BA scale-free model networks showed lower peak heights and lower duplication coefficients (Figure 9.2.3). Instances of the WS small-world model and spatial model showed similar symmetry levels, but generally lower peak heights (average height for WS: 1.85, average height for spatial: 1.73) than the human high-resolution network (height 1.97). The relationship between duplication coefficient and peak height observed within and between the network models was in line with the trend seen for the empirical networks: all network models revealed a significant linear association between peak height and dupli-

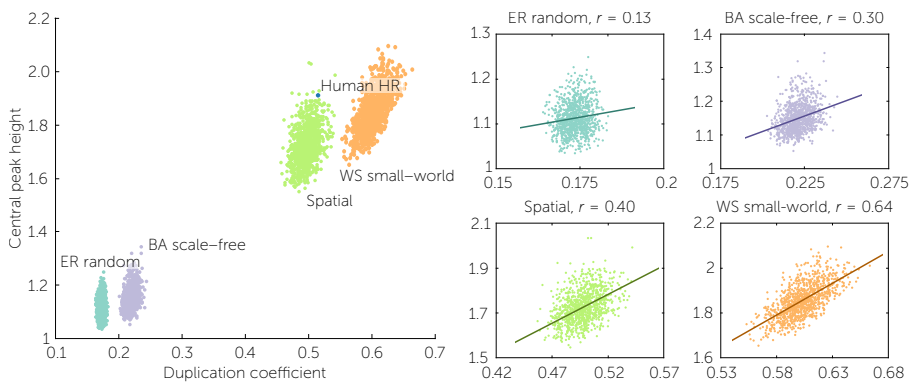


Figure 9.2.3. Duplication coefficient and central peak height in model networks. The duplication coefficients and central spectral peak heights observed across four different network models underscored the existence of an association between these measures. As the inserts show, significant associations were also found between the instances of each model separately (x-axis: duplication coefficient, y-axis: central peak height; all $p < 0.001$, Bonferroni corrected).

cation coefficient across the 1000 generated model instances (ER: $r = 0.13$, WS: $r = 0.64$, BA: $r = 0.30$, spatial: $r = 0.40$, with $p < 0.001$ for all models) and also the relative arrangement of the four populations was found to be in support of such an association (Figure 9.2.3).

Approximating neural spectra using nodal duplication

As indicated by the observed duplication coefficient scores for neural networks (ranging between 0.48 and 0.69), perfect symmetry is rare in neural networks. That is, the connectivity overlap between a brain region and its most similar peer is generally only partial. To provide insight in the balance between symmetry and diversity in the connectivity of brain regions, the spectrum of each neural network was approximated by the spectra of duplication-based model networks using a spectral fitting procedure (see Materials and methods). The best-fitting model spectra and the associated empirically established optimal parameters γ of the duplication model are shown in Figure 9.2.4. Values of γ , reflecting the expected percentage of connections that was copied from the parent during duplication and thus providing a “symmetry vs. diversity” estimate, were found to range from 0.74 for the best-fitting model of the mouse connectome, to 0.93 for the best-fitting model of the cat connectome. These relatively high values for γ indicate that duplication played a prominent role during the growth of the best-fitting model networks, but also that a certain amount of regional diversification (established by rewiring 7–26% of the connections after duplication) was essential to obtain spectra that resemble those of neural networks.

Providing insight in the influence of the model parameter γ on the duplication coefficient and central spectral peak height, Figure 9.2.5 shows the duplication coefficient and central peak height for instances of the duplication-based network model generated using different values of γ . As in the analysis of the four common network models, all instances were matched (in terms of density and network size) to the high-resolution human brain network. In line with our expectations, both the central peak height and the duplication coefficient increased with γ (Figure 9.2.5), again underscoring the relationship between those

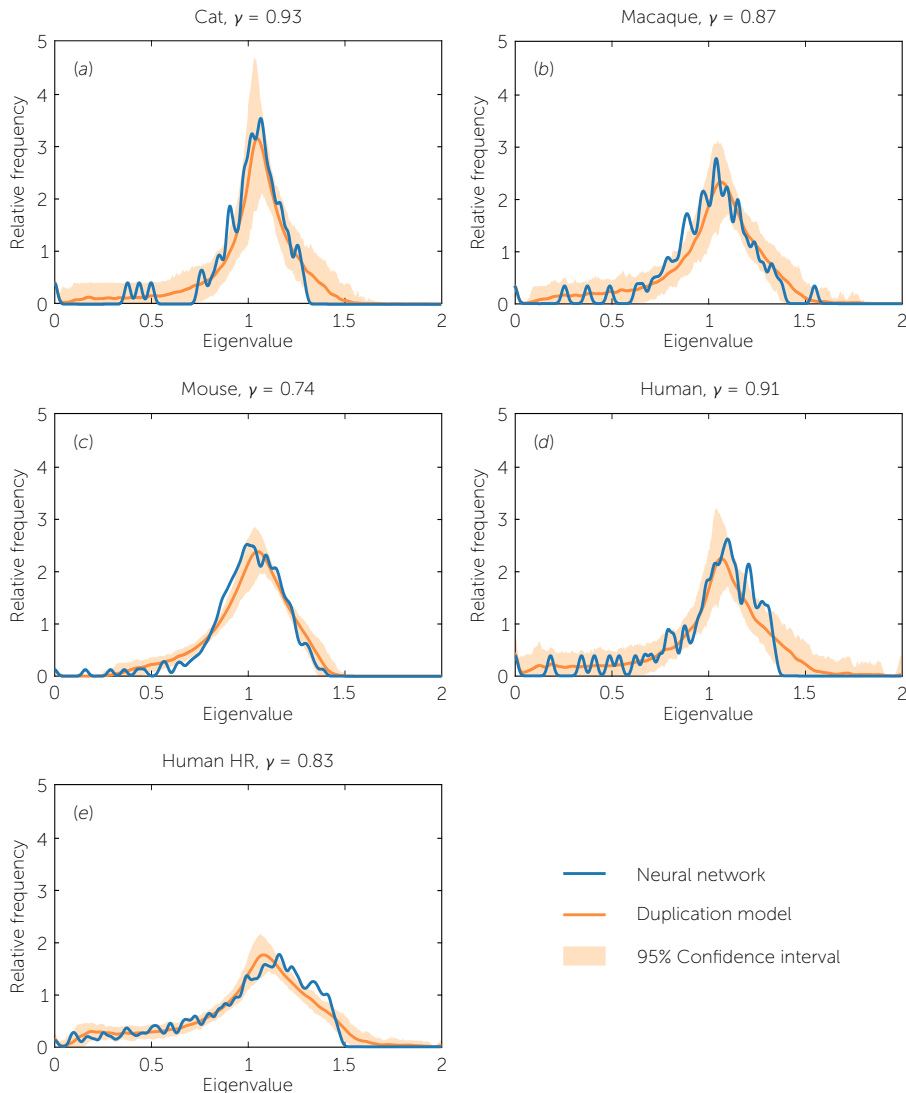


Figure 9.2.4. Approximation of neural spectra using duplication-based model networks. The optimal fraction γ of copied connections during the growth of duplication-based model networks ($\gamma = 1$ indicating full duplication and $\gamma = 0$ full diversification) was empirically determined by spectrally fitting the model networks to the connectivity maps of the (a) cat (optimal $\gamma = 0.93$), (b) macaque ($\gamma = 0.87$), (c) mouse ($\gamma = 0.74$), (d) human ($\gamma = 0.91$), and (e) high-resolution human ($\gamma = 0.83$) brain networks. The reported optimal gamma values suggest a balance in the interplay between symmetry and diversity of brain regions.

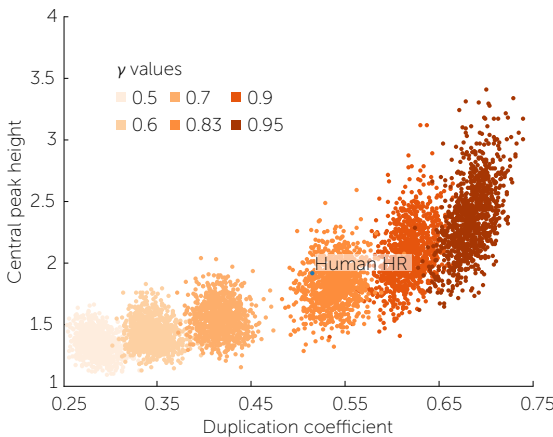


Figure 9.2.5. Effect of duplication-based model parameter γ on duplication coefficient and central peak height. Increasing the local symmetry during the growth of the duplication-based model networks, reflected by the parameter γ , increased both the duplication coefficient and central peak height. Comparison with the high-resolution human connectome showed that duplication-based model networks generated with optimal parameter $\gamma = 0.83$ match the human connectome in terms of both central peak height and duplication coefficient.

measures. Furthermore, even though the duplication coefficient played no role in the spectrum-based fitting procedure, the duplication coefficients (mean [std]: 0.53 [0.02]) of the best-fitting model networks, corresponding to $\gamma = 0.83$, were found to be approximately equal to the duplication coefficient (0.52) of the high-resolution human connectome ($p = 0.21$).

Discussion

This study describes the role of symmetry in the architecture of neural networks as revealed through their Laplacian spectra. Investigation of both empirical and model networks demonstrated that the large peak observed in the center of neural network spectra is strongly related to patterns of node symmetry. This observed relation is in line with earlier theoretical results identifying the occurrence of perfectly symmetric nodes as a source for eigenvalues positioned exactly in the middle of the spectral domain (Banerjee and Jost, 2008b; Yadav and Jalan, 2015).

That the occurrence of node symmetry in neural networks is an important factor for the height of the central spectral peak was shown in three ways. First,

the height of the central peak as observed in the spectra of multiple neural and non-neural empirical networks was found to be linearly related to the networks' duplication coefficient; a measure based on the overlap between nodal wiring patterns, introduced to assess the global level of network symmetry (Figure 9.2.1). Second, this relationship between duplication coefficient and spectral peak height was reproduced across and within commonly used network models (Figure 9.2.3), with significant correlations between duplication coefficient and spectral peak height being observed among realizations of each model. Third, investigation of the role of symmetry in neural networks revealed perturbations (in the form of edge rewiring) targeting network symmetry to have a significantly larger impact on the spectral peak height than random perturbations (Figure 9.2.2).

Acknowledging the importance of node symmetry for the characteristic central peak in the spectra of neural networks, it would be interesting to explore potential mechanisms behind the occurrence of such patterns of node symmetry. Since the Watts-Strogatz small-world model and the spatial model showed levels of duplication comparable to that of the human brain network to which they were matched (Figure 9.2.3), especially the small-world and spatial features of neural networks may be related to network symmetry. In the spatial model, proximate nodes are likely to have similar wiring patterns (Song et al., 2014), enlarging the duplication coefficient. Interestingly, the principle of minimizing wiring length or "cost" – being the driving mechanism behind the spatial model – has been suggested as an important factor for the wiring of neural networks (Bassett et al., 2010; Bullmore and Sporns, 2012; Kaiser and Hilgetag, 2006; Raj and Chen, 2011), which might be echoed by the Laplacian spectrum via the occurrence of spatially driven symmetries.

The high duplication coefficient in the Watts-Strogatz small-world model could be explained by its high clustering coefficient (directly induced by the model's design), which is a normalized measure of the number of triangles in the network, referring to subgroups of three mutually connected nodes. Since any two

nodes from such a triangle have at least one projection in common, the presence of triangles induces a certain level of node symmetry. However, that the clustering coefficient and duplication coefficient are inherently different measures is illustrated by the food web, which showed the highest spectral peak among all empirical networks and a high duplication coefficient (0.68 compared to 0.52 in the high-resolution human connectome), but a low clustering coefficient (0.29 compared to 0.48 in the high-resolution connectome). This combination of low clustering and high symmetry is a consequence of the nature of the food web, in which species that feed on the same prey (or are eaten by the same predators) are likely to be at the same level in the food chain and hence unlikely to have a predator-prey relation with one another. In such a situation where similar nodes are often unconnected, high overlap between the wiring pattern of nodes will generate many “open” triangles and thus decrease the clustering coefficient of the network. Hence, the spatial organization, clustering, and symmetry of neural networks appear to be related, but must also be noted to cover intrinsically different concepts.

Taking a closer look at the duplication coefficient values observed for the neural networks (cat: 0.69; macaque: 0.61; mouse: 0.48; human: 0.62; human, high resolution: 0.52), the occurrence of completely symmetric brain regions appears to be quite rare. Indeed, a post-hoc analysis confirmed that none of the neural networks possess perfectly symmetric brain regions and that only few brain regions have near perfect “copies” (indicated by a node-wise duplication coefficient greater than 0.9; cat: 3.1% of the regions; human, standard resolution: 5.9%; other networks: 0%). That is, most brain regions exhibit only partially overlapping wiring patterns, suggesting a balance between connectivity symmetry and diversity in neural systems. As hypothesized by Passingham et al. (2002), brain areas with overlapping anatomical connectivity are likely to show functional similarity, linking the issue of symmetry and diversity to functional specialization. In this light, both symmetry and diversity may have beneficial effects. On the one hand, connectivity diversification and functional specialization may support effective global communication and information integration in the

network (Markov et al., 2013). On the other hand, connectivity symmetry can provide redundancy and robustness (MacArthur et al., 2008) and may facilitate parallel processing (Ballard, 1986). Fitting duplication-based model networks to the neural networks, we found that the architecture of neural networks is best approximated if the fraction of connections copied during duplication ranges between 0.74 and 0.93, suggesting that neural systems are shaped by relatively high levels of symmetry and relatively low levels of diversification.

Although our findings demonstrate a clear link between the introduced duplication coefficient and spectral peak height, it should be noted that the duplication coefficient could not explain all variance in the height of the main spectral peak. One potential source of variation not incorporated in the duplication coefficient is given by the existence of symmetries more complex than overlap in node wiring (Silva et al., 2014). Indeed, the notion of perfect node symmetry – in which the label of two nodes can be permuted without altering the network structure – can be extended to higher-level symmetries, including, for instance, the scenario in which two groups of nodes have the same combined wiring pattern (Yadav and Jalan, 2015). Specific higher-level symmetries have been shown to induce a peak exactly in the middle of the spectrum (Dorogovtsev et al., 2003; Vukadinović et al., 2002; Yadav and Jalan, 2015), suggesting that also (approximate) higher-level symmetries will contribute to the central spectral peak. Future attempts to quantify the presence of higher-level symmetries should reveal the relevance of such symmetries in neural networks and their spectra.

Another future direction would be the adoption of the Laplacian spectrum as an instrument to describe network abnormalities in brain disorders. Relating the characteristic central peak in the Laplacian spectrum to node symmetry, this study shows how particular deviations in spectral fingerprints may correspond to concrete aspects of network architecture relevant for the study of brain disorders. For instance, a recent study showed that Alzheimer’s disease affects the symmetry between brain regions (Prasad et al., 2015), which – in view of our current findings – is likely to be reflected in the Laplacian spectra of Alzheimer

patients. Although the height of the central peak in network spectra can now be captured by the duplication coefficient, disease-related deviations in other parts of the spectrum may reveal systems-level changes that can currently not be described or detected by standard network metrics.

Acknowledgments

Human neuroimaging data for this study was provided by the Human Connectome Project, WU-Minn Consortium (Principal Investigators: David Van Essen and Kamil Ugurbil; 1U54MH091657) funded by the 16 NIH Institutes and Centers that support the NIH Blueprint for Neuroscience Research; and by the McDonnell Center for Systems Neuroscience at Washington University.

References

- Achard, S., Salvador, R., Whitcher, B., Suckling, J., Bullmore, E., 2006. A Resilient, Low-Frequency, Small-World Human Brain Functional Network with Highly Connected Association Cortical Hubs. *The Journal of Neuroscience* 26, 63-72.
- Arenas, A., Fernández, A., Gómez, S., 2008. A Complex Network Approach to the Determination of Functional Groups in the Neural System of *C. elegans*. In: Liò, P., Yoneki, E., Crowcroft, J., Verma, D.C. (Ed.), *Lecture Notes in Computer Science*, 9-18. Springer.
- Atay, F.M., Biyikoglu, T., Jost, J., 2006. Network synchronization: Spectral versus statistical properties. *Physica D: Nonlinear Phenomena* 224, 35-41.
- Ballard, D.H., 1986. Cortical connections and parallel processing: Structure and function. *Behavioral and Brain Sciences* 9, 67-90.
- Banerjee, A., 2012. Structural distance and evolutionary relationship of networks. *Biosystems* 107, 186-196.
- Banerjee, A., Jost, J., 2007. Spectral plots and the representation and interpretation of biological data. *Theory in Biosciences* 126, 15-21.
- Banerjee, A., Jost, J., 2008b. On the spectrum of the normalized graph Laplacian. *Linear Algebra and its Applications* 428, 3015-3022.
- Banerjee, A., Jost, J., 2008a. Spectral plot properties: Towards a qualitative classification of networks. *Networks and Heterogeneous Media* 3, 395-411.
- Banerjee, A., Jost, J., 2009. Graph spectra as a systematic tool in computational biology. *Discrete Applied Mathematics* 157, 2425-2431.
- Barabási, A.L., Albert, R., 1999. Emergence of Scaling in Random Networks. *Science* 286, 509-512.
- Bassett, D.S., Bullmore, E., 2006. Small-World Brain Networks. *The Neuroscientist* 12, 512-523.
- Bassett, D.S., Greenfield, D.L., Meyer-Lindenberg, A., Weinberger, D.R., Moore, S.W., Bullmore, E.T., 2010. Efficient Physical Embedding of Topologically Complex Information Processing Networks in Brains and Computer Circuits. *PLoS Computational Biology* 6, e1000748.
- Bauer, F., Jost, J., 2009. Bipartite and neighborhood graphs and the spectrum of the normalized graph Laplacian. *arXiv preprint*, arXiv:0910.3118.
- Bhan, A., Galas, D.J., Dewey, T.G., 2002. A duplication growth model of gene expression networks. *Bioinformatics* 18, 1486-1493.
- Boccaletti, S., Latora, V., Moreno, Y., Chavez, M., Hwang, D.U., 2006. Complex networks: Structure and dynamics. *Physics Reports* 424, 175-308.
- Bonacich, P., 1972. Factoring and weighting approaches to status scores and clique identification. *The Journal of Mathematical Sociology* 2, 113-120.
- Bullmore, E., Sporns, O., 2009. Complex brain networks: graph theoretical analysis of structural and functional systems. *Nature Reviews Neuroscience* 10, 186-198.
- Bullmore, E., Sporns, O., 2012. The economy of brain network organization. *Nature Reviews Neuroscience* 13, 336-349.
- Cammoun, L., Gigandet, X., Meskaldji, D., Thiran, J.P., Sporns, O., Do, K.Q., Maeder, P., Meuli, R., Haggmann, P., 2012. Mapping the human connectome at multiple scales with diffusion spectrum MRI. *Journal of Neuroscience Methods* 203, 386-397.
- Cetinkaya, E.K., Alenazi, M.J.F., Rohrer, J.P., Sterbenz, J.P.G., 2012. Topology connectivity analysis of internet infrastructure using graph spectra. *Proceedings of the 4th International Congress on Ultra Modern Telecommunications and Control Systems and Workshops*, 752-758.
- Cheng, X.Q., Shen, H.W., 2010. Uncovering the community structure associated with the diffusion dynamics on networks. *Journal of Statistical Mechanics: Theory and Experiment* 2010, P04024.
- Chung, F., 1997. Spectral graph theory. American Mathematical Society, Rhode Island.
- Chung, F., 2005. Laplacians and the Cheeger Inequality for Directed Graphs. *Annals of Combinatorics* 9, 1-19.
- Chung, F., Lu, L., Vu, V., 2003. Spectra of random graphs with given expected degrees. *Proceedings of the National Academy of Sciences* 100, 6313-6318.
- Collin, G., Sporns, O., Mandl, R.C.W., van den Heuvel, M.P., 2014. Structural and Functional Aspects Relating to Cost and Benefit of Rich Club Organization in the Human Cerebral Cortex. *Cerebral Cortex* 24, 2258-2267.

- Desikan, R.S. et al., 2006. An automated labeling system for subdividing the human cerebral cortex on MRI scans into gyral based regions of interest. *NeuroImage* 31, 968-980.
- Donetti, L., Muñoz, M.A., 2005. Improved spectral algorithm for the detection of network communities. *AIP Conference Proceedings* 779, 104-107.
- Dorogovtsev, S.N., Goltsev, A.V., Mendes, J.F.F., Samukhin, A.N., 2003. Spectra of complex networks. *Physical Review E* 68, 046109.
- Drossel, B., McKane, A.J., 2005. Modelling food webs. In: Bornholdt, S., Schuster, H.G. (Ed.), *Handbook of Graphs and Networks: From the Genome to the Internet*, 218-247. Wiley-VCH.
- Erdős, P., Rényi, A., 1959. On random graphs. *Publicationes Mathematicae Debrecen* 6, 290-297.
- Felleman, D.J., Van Essen, D.C., 1991. Distributed hierarchical processing in the primate cerebral cortex. *Cerebral Cortex* 1, 1-47.
- Fortunato, S., 2010. Community detection in graphs. *Physics Reports* 486, 75-174.
- Girvan, M., Newman, M.E.J., 2002. Community structure in social and biological networks. *Proceedings of the National Academy of Sciences* 99, 7821-7826.
- Glasser, M.F. et al., 2013. The minimal preprocessing pipelines for the Human Connectome Project. *NeuroImage* 80, 105-124.
- Gu, J., Jost, J., Liu, S., Stadler, P.F., 2014. Spectral classes of regular, random, and empirical graphs. *arXiv preprint, arXiv:1406.6454*.
- Guimerá, R., Danon, L., Diaz-Guilera, A., Giralt, F., Arenas, A., 2003. Self-similar community structure in a network of human interactions. *Physical Review E* 68, 065103.
- Hagmann, P., Cammoun, L., Gigandet, X., Meuli, R., Honey, C.J., Wedeen, V.J., Sporns, O., 2008. Mapping the Structural Core of Human Cerebral Cortex. *PLOS Biology* 6, e159.
- Harriger, L., van den Heuvel, M.P., Sporns, O., 2012. Rich Club Organization of Macaque Cerebral Cortex and Its Role in Network Communication. *PLoS ONE* 7, e46497.
- van den Heuvel, M.P., Hulshoff Pol, H.E., 2010. Exploring the brain network: A review on resting-state fMRI functional connectivity. *European Neuropsychopharmacology* 20, 519-534.
- van den Heuvel, M.P., Kahn, R.S., Goñi, J., Sporns, O., 2012. High-cost, high-capacity backbone for global brain communication. *Proceedings of the National Academy of Sciences* 109, 11372-11377.
- van den Heuvel, M.P., Mandl, R.C.W., Hulshoff Pol, H.E., 2008b. Normalized Cut Group Clustering of Resting-State fMRI Data. *PLoS ONE* 3, e2001.
- van den Heuvel, M.P., Sporns, O., 2013. An Anatomical Substrate for Integration among Functional Networks in Human Cortex. *The Journal of Neuroscience* 33, 14489-14500.
- van den Heuvel, M.P., Stam, C.J., Boersma, M., Hulshoff Pol, H.E., 2008a. Small-world and scale-free organization of voxel-based resting-state functional connectivity in the human brain. *NeuroImage* 43, 528-539.
- Hilgetag, C.C., Burns, G.A., O'Neill, M.A., Scannell, J.W., Young, M.P., 2000. Anatomical connectivity defines the organization of clusters of cortical areas in the macaque monkey and the cat. *Philosophical Transactions of the Royal Society of London B: Biological Sciences* 355, 91-110.
- Hilgetag, C.C., Kötter, R., Stephan, K.E., Sporns, O., 2002. Computational Methods for the Analysis of Brain Connectivity. In: Ascoli, G.A. (Ed.), *Computational Neuroanatomy*, 295-335. Humana Press.
- Ipsen, M., Mikhailov, A.S., 2002. Evolutionary reconstruction of networks. *Physical Review E* 66, 046109.
- Iturria-Medina, Y., Sotero, R.C., Canales-Rodríguez, E.J., Alemán-Gómez, Y., Melie-García, L., 2008. Studying the human brain anatomical network via diffusion-weighted MRI and Graph Theory. *NeuroImage* 40, 1064-1076.
- Kaiser, M., 2011. A tutorial in connectome analysis: Topological and spatial features of brain networks. *NeuroImage* 57, 892-907.
- Kaiser, M., Hilgetag, C.C., 2006. Nonoptimal Component Placement, but Short Processing Paths, due to Long-Distance Projections in Neural Systems. *PLoS Computational Biology* 2, e95.
- Kötter, R., 2004. Online retrieval, processing, and visualization of primate connectivity data from the CoCoMac Database. *Neuroinformatics* 2, 127-144.
- Liang, Z., King, J., Zhang, N., 2011. Uncovering Intrinsic Connectional Architecture of Functional Networks in Awake Rat Brain. *The Journal of Neuroscience* 31, 3776-3783.

CHAPTER 9

- Lohmann, G., Margulies, D.S., Horstmann, A., Pleger, B., Lepsién, J., Goldhahn, D., Schloegl, H., Stumvoll, M., Villringer, A., Turner, R., 2010. Eigenvector Centrality Mapping for Analyzing Connectivity Patterns in fMRI Data of the Human Brain. *PLoS ONE* 5, e10232.
- MacArthur, B.D., Sánchez-García, R.J., Anderson, J.W., 2008. Symmetry in complex networks. *Discrete Applied Mathematics* 156, 3525-3531.
- Markov, N.T. et al., 2013. The role of long-range connections on the specificity of the macaque interareal cortical network. *Proceedings of the National Academy of Sciences* 110, 5187-5192.
- Maslov, S., Sneppen, K., 2002. Specificity and Stability in Topology of Protein Networks. *Science* 296, 910-913.
- McGraw, P.N., Menzinger, M., 2008. Laplacian spectra as a diagnostic tool for network structure and dynamics. *Physical Review E* 77, 031102.
- Meunier, D., Lambiotte, R., Bullmore, E.T., 2010. Modular and hierarchically modular organization of brain networks. *Frontiers in Neuroscience* 4, 200.
- Modha, D.S., Singh, R., 2010. Network architecture of the long-distance pathways in the macaque brain. *Proceedings of the National Academy of Sciences* 107, 13485-13490.
- Newman, M.E.J., 2003. The Structure and Function of Complex Networks. *SIAM Review* 45, 167-256.
- Newman, M.E.J., 2006. Finding community structure in networks using the eigenvectors of matrices. *Physical Review E* 74, 036104.
- Oh, S.W. et al., 2014. A mesoscale connectome of the mouse brain. *Nature* 508, 207-214.
- Page, L., Brin, S., Motwani, R., Winograd, T., 1999. The PageRank Citation Ranking: Bringing Order to the Web. Technical Report. Stanford InfoLab, 1999-66.
- Passingham, R.E., Stephan, K.E., Kotter, R., 2002. The anatomical basis of functional localization in the cortex. *Nature Reviews Neuroscience* 3, 606-616.
- Pavlou, H.J., Goodwin, S.F., 2013. Courtship behavior in *Drosophila melanogaster*: towards a "courtship connectome". *Current Opinion in Neurobiology* 23, 76-83.
- Prasad, G., Joshi, S.H., Nir, T.M., Toga, A.W., Thompson, P.M., 2015. Brain connectivity and novel network measures for Alzheimer's disease classification. *Neurobiology of Aging* 36, Supplement 1, S121-S131.
- Raj, A., Chen, Y., 2011. The Wiring Economy Principle: Connectivity Determines Anatomy in the Human Brain. *PLoS ONE* 6, e14832.
- Reijneveld, J.C., Ponten, S.C., Berendse, H.W., Stam, C.J., 2007. The application of graph theoretical analysis to complex networks in the brain. *Clinical Neurophysiology* 118, 2317-2331.
- Rubinov, M., Sporns, O., 2010. Complex network measures of brain connectivity: Uses and interpretations. *NeuroImage* 52, 1059-1069.
- Rubinov, M., Sporns, O., 2011. Weight-conserving characterization of complex functional brain networks. *NeuroImage* 56, 2068-2079.
- Salvador, R., Suckling, J., Coleman, M.R., Pickard, J.D., Menon, D., Bullmore, E., 2005. Neurophysiological Architecture of Functional Magnetic Resonance Images of Human Brain. *Cerebral Cortex* 15, 1332-1342.
- Scannell, J.W., Blakemore, C., Young, M.P., 1995. Analysis of connectivity in the cat cerebral cortex. *The Journal of Neuroscience* 15, 1463-1483.
- Scholtens, L.H., Schmidt, R., de Reus, M.A., van den Heuvel, M.P., 2014. Linking macroscale graph analytical organization to microscale neuroarchitectonics in the macaque connectome. *The Journal of Neuroscience* 34, 12192-12205.
- Shen, H.W., Cheng, X.Q., 2010. Spectral methods for the detection of network community structure: a comparative analysis. *Journal of Statistical Mechanics: Theory and Experiment* 2010, P10020.
- Shi, J., Malik, J., 2000. Normalized cuts and image segmentation. *IEEE Transactions on Pattern Analysis and Machine Intelligence* 22, 888-905.
- Silva, F.N., Comin, C.H., Peron, T.K., Rodrigues, F.A., Ye, C., Wilson, R.C., Hancock, E., Costa, L.D.F., 2014. Concentric Network Symmetry. *arXiv preprint*, arXiv:1407.0224.
- Song, H.F., Kennedy, H., Wang, X.J., 2014. Spatial embedding of structural similarity in the cerebral cortex. *Proceedings of the National Academy of Sciences* 111, 16580-16585.
- Sporns, O., 2011. *Networks of the Brain*. MIT Press, Cambridge.

- Sporns, O., Chialvo, D.R., Kaiser, M., Hilgetag, C.C., 2004. Organization, development and function of complex brain networks. *Trends in Cognitive Sciences* 8, 418-425.
- Sporns, O., Kötter, R., 2004. Motifs in Brain Networks. *PLoS Biology* 2, e369.
- Sporns, O., Tononi, G., Kötter, R., 2005. The Human Connectome: A Structural Description of the Human Brain. *PLoS Computational Biology* 1, e42.
- Sporns, O., Zwi, J., 2004. The small world of the cerebral cortex. *Neuroinformatics* 2, 145-162.
- Stam, C.J., 2004. Functional connectivity patterns of human magnetoencephalographic recordings: a 'small-world' network? *Neuroscience Letters* 355, 25-28.
- Stephan, K.E., Kamper, L., Bozkurt, A., Burns, G.A.P.C., Young, M.P., Kötter, R., 2001. Advanced database methodology for the Collation of Connectivity data on the Macaque brain (CoCoMac). *Philosophical Transactions of the Royal Society of London B: Biological Sciences* 356, 1159-1186.
- Ulanowicz, R.E., Bondavalli, C., Egnotovich, M.S., 1998. Network Analysis of Trophic Dynamics in South Florida Ecosystem, FY 97: The Florida Bay Ecosystem. Annual Report to the United States Geological Service. Chesapeake Biological Laboratory, [UMCES] CBL 98-123.
- Van Essen, D.C. et al., 2012. The Human Connectome Project: A data acquisition perspective. *NeuroImage* 62, 2222-2231.
- Varshney, L.R., Chen, B.L., Paniagua, E., Hall, D.H., Chklovskii, D.B., 2011. Structural Properties of the *Caenorhabditis elegans* Neuronal Network. *PLoS Computational Biology* 7, e1001066.
- Vértes, P.E., Alexander-Bloch, A.F., Gogtay, N., Giedd, J.N., Rapoport, J.L., Bullmore, E.T., 2012. Simple models of human brain functional networks. *Proceedings of the National Academy of Sciences* 109, 5868-5873.
- Vukadinović, D., Huang, P., Erlebach, T., 2002. On the Spectrum and Structure of Internet Topology Graphs. In: Unger, H., Böhme, T., Mikler, A. (Ed.), *Lecture Notes in Computer Science*, 83-95. Springer.
- Watts, D.J., Strogatz, S.H., 1998. Collective dynamics of 'small-world' networks. *Nature* 393, 440-442.
- White, J.G., Southgate, E., Thomson, J.N., Brenner, S., 1986. The Structure of the Nervous System of the Nematode *Caenorhabditis elegans*. *Philosophical Transactions of the Royal Society of London B: Biological Sciences* 314, 1-340.
- Wu, K. et al., 2011. The Overlapping Community Structure of Structural Brain Network in Young Healthy Individuals. *PLoS ONE* 6, e19608.
- Yadav, A., Jalan, S., 2015. Origin and implications of zero degeneracy in networks spectra. *Chaos: An Interdisciplinary Journal of Nonlinear Science* 25, 043110.
- Yeh, F.C., Wedeen, V.J., Tseng, W.Y.I., 2010. Generalized q-Sampling Imaging. *IEEE Transactions on Medical Imaging* 29, 1626-1635.
- Zamora-López, G., Zhou, C., Kurths, J., 2009. Graph analysis of cortical networks reveals complex anatomical communication substrate. *Chaos: An Interdisciplinary Journal of Nonlinear Science* 19, 015117.
- Zamora-López, G., Zhou, C., Kurths, J., 2011. Exploring brain function from anatomical connectivity. *Frontiers in Neuroscience* 5, 83.



Chapter 10

Summary and discussion

Summary

The 80-100 billion neurons in our brain form a network of almost incomprehensible complexity. Although this vast system of neurons and neuronal connections – known as the *connectome* – can (currently) not be mapped in full detail, the organization of the neural infrastructure which enables us to move, sense, memorize, and think does not have to remain elusive. On a larger and more comprehensible scale, neurons are organized into anatomically and functionally distinguishable brain regions and their neuronal connections form large-scale white matter fibers. Especially during the last two decades, mapping this *macroscale* connectome of brain regions and white matter fibers has become increasingly feasible and studies have gradually started to unravel its intriguing network architecture. To do so, a branch of mathematics known as *graph theory* proved to be of tremendous help, initiating an interesting marriage between mathematics and neuroscience. When reduced to its essence, macroscale connectome mapping basically results in two lists: a list of brain regions and a large list of seemingly haphazardly placed connections between those brain regions. This relatively simple structure of “dots” (brain regions) interconnected by “lines” (neural connections) is omnipresent in nature and society and can be mathematically described and analyzed as a *graph*.

The adoption of graph theory in neuroscience – formally representing brain regions by *nodes* or *vertices* and neural connections by *edges* or *links* – has led to the discovery of several important properties of the human and animal connectome (Bullmore and Sporns, 2009). For instance, brain networks have been shown to exhibit a *modular* (Girvan and Newman, 2002) and *small-world* (Watts and Strogatz, 1998) organization, combining the existence of local groups of highly clustered nodes (Betzel et al., 2013; Hilgetag et al., 2000; Meunier et al., 2010) with the presence of short global communication paths (Gong et al., 2009; He et al., 2007; van den Heuvel et al., 2008; Sporns and Zwi, 2004; Stam, 2004). Another prominent feature of brain networks is the existence of highly connected *hub* regions (Li et al., 2013a; Power et al., 2013; Sporns et al., 2007), whose

high metabolic demands (Liang et al., 2013; Tomasi et al., 2013; Vaishnavi et al., 2010) and frequent implication in brain-related disorders (Achard et al., 2012; Bassett et al., 2008; Buckner et al., 2009; Crossley et al., 2014; van den Heuvel et al., 2010; Stam et al., 2009) suggest an important role in healthy brain function. Moreover, it has been recently discovered that neural hubs are not only individually “rich” in connectivity, but also form a densely interconnected central core or *rich club* in the brain (Hagmann et al., 2008; van den Heuvel and Sporns, 2011; Zamora-López et al., 2010).

Even though a corner of the veil has thus clearly been lifted, our understanding of macroscale connectome architecture is still a work in progress. The aim of this thesis was to introduce and explore some unconventional, eccentric graph theoretical perspectives on brain networks to extend the knowledge obtained by previous studies and further uncover the network architecture of the healthy brain. In other words, sticking to our metaphor: by changing our point of view, we aspired to look slightly further under the veil. Below, we summarize our eccentric perspective on brain networks and the results it helped us obtain.

An edge-centric (and eccentric) approach

Many “conventional” graph theoretical measures used in connectome research describe the organization of the connectome by computing (and then typically averaging) properties of nodes or groups of nodes (Rubinov and Sporns, 2010). Although this central role for nodes, and hence brain regions, is perfectly reasonable as well as practical, it is odd that in a framework with two types of elements (i.e., nodes and edges), there is a strong imbalance towards investigating one of them. In our own connectome research, we therefore increasingly turned our attention to the network properties of the edges of the connectome, establishing a graph theoretical perspective on brain networks that can be characterized as both edge-centric and eccentric.

Existence of connections

To engage the mysteries of our brain's wiring, an essential first step is to make a (simplified) map of the brain regions and interconnecting white matter projections that constitute the macroscale connectome. Especially for the human brain, magnetic resonance imaging (MRI) is an indispensable technique in establishing such maps (Gong et al., 2009; Hagmann et al., 2007; Iturria-Medina et al., 2008). As discussed in **chapter 3**, the brain regions which form the nodes of the connectome are most commonly obtained by comparing a conventional anatomical (T1-weighted) MRI scan of a given subject to a reference atlas based on several manual delineations. For each brain region defined in the reference atlas, this procedure finds the corresponding portion of the brain on the subject's MRI scan. As a result, the number of brain regions, as well as their descriptions and approximate locations are completely determined by the choice of reference atlas and connectome maps for different subjects can be based on the same set of nodes.

With the nodes of the connectome map in place, completing the connectome map basically amounts to determining for each pair of brain regions whether or not there are white matter fibers connecting those regions. Reconstruction of these white matter fibers can be performed on the basis of different (diffusion-weighted) MRI scans, measuring the local diffusion of water molecules (**chapter 2**). Unfortunately, the resulting connectome reconstructions are not perfect; the involved MRI measurements are known to be prone to various sources of "measurement noise" and methodological limitations of diffusion tractography techniques make some white matter tracts more difficult to reconstruct than others (Jbabdi and Johansen-Berg, 2011; Jones and Pierpaoli, 2005). So, in contrast to the situation for the nodes of connectome maps, the existence of connectome edges goes paired with some uncertainty and, potentially, intersubject variation (Bassett et al., 2011; Cammoun et al., 2012). The uncertainty and variation in the presence of edges indirectly also affect conventional node-centric network measures (Bassett et al., 2011), but become especially relevant when shifting from a node-centric to an edge-centric perspective.

After all, it is rather convenient to know whether the main objects of investigation exist or not.

One way to approximate the ideal scenario of a uniform and reliable set of edges is to combine reconstructed connectome maps from multiple subjects and include only those edges that were found to be present in all subjects. Consistently detected white matter connections are namely very unlikely to be caused by measurement errors and intersubject variation in the presence of these edges is by definition eliminated. However, since this criterion is very strict, the resulting group-averaged connectome map will omit many connections that are also likely to be present, which in turn influences all graph theoretical analyses based on this map. A better strategy to create a representative group-averaged connectome map might therefore be to include only those connections that were detected in a “large enough” percentage of the subjects. In **chapter 4**, we showed that the precise setting of this cut-off percentage, or *group threshold*, indeed has a substantial effect on the resulting group-averaged connectome map and its network properties and should therefore be carefully chosen. To support a motivated threshold choice, we proposed a model to estimate the number of false positive (i.e., mistakenly present) and false negative (i.e., mistakenly absent) edges in the group-averaged map. The obtained estimates showed that the expected increase in false positives and decrease in false negatives when raising the group threshold generally occur at unequal rates, with especially pronounced differences at very low or very high thresholds. For instance, decreasing the group threshold from 30 to 1% was estimated to prevent only about 10 false negatives at the cost of more than 700 false positives, while increasing the group threshold from 90 to 100% eliminated one false positive at the cost of 100 false negatives. We therefore concluded that group thresholds should preferably be chosen between 30 and 90%. Moreover, our estimates further suggested that, in most situations, a group threshold of circa 60% is a suitable setting, providing a good balance between the elimination of false positives and false negatives and approximately minimizing the total number of errors.

Edge categories

Another important difference between the nodes and edges of the connectome is that the connectome's edges are much more plentiful and generally do not have specific names. Although one could describe each edge by its endpoints (i.e., the nodes connected by the edge) and present long lists of edge-wise scores, it would be rather difficult to scan such lists for patterns of interest and to provide a sensible interpretation of any discoveries. Moreover, in scenarios that require statistical testing, dealing with hundreds or thousands of individual edges strongly affects statistical power due to the necessary corrections for multiple testing. A good way to avoid such problems and get a better grip on the myriad of connectome edges is to divide the collection of all edges into logical subgroups or *edge categories*. Instead of investigating each edge individually, one can then examine and compare the (average) properties of edges in a limited number of clearly described categories. In this way, edge categories may provide a level of detail intermediate between the rather coarse *global* level – describing network properties using a single value for the entire connectome – and the perhaps too detailed single connection level.

An edge category that runs as a red line through this thesis is the category of so-called *rich club* connections. As alluded to before, brain networks have been reported to comprise highly connected hub regions and those hub regions form a densely interconnected central *core* or *rich club* in the brain (Hagmann et al., 2008; van den Heuvel and Sporns, 2011; Zamora-López et al., 2010). In view of the resources involved in creating and maintaining white matter pathways (Bullmore and Sporns, 2012), the dense connectivity within this central collective suggests that it may be playing an important role in the overall architecture of the connectome, and a considerable portion of this thesis has been dedicated to the question what this role might be. Given the classification of nodes into rich club nodes and non-rich club nodes, the edges of the connectome can be divided into: *rich club* connections, spanning between rich club nodes; *feeder* connections, spanning between a non-rich club node and a rich club node; and *local* connections, spanning between non-rich club nodes (van den Heuvel

et al., 2012). This approach was adopted in **chapters 5-7** for, respectively, the cat, human, and rat connectome, all of which were found to exhibit a clear rich club organization.

Cat connectome

Starting with our examination of the cat connectome presented in **chapter 5**, our general aim was to shed light on the role of rich club, feeder, and local connections in brain networks by further exploring the differences between those connection classes. Complementing recent studies based on *in vivo* human MRI data, demonstrating that rich club connections are generally longer and stronger than feeder and local connections and represent white matter pathways with higher levels of white matter integrity (Collin et al., 2014a; van den Heuvel et al., 2012), we were specifically interested in two unique features of the tract-tracing based cat connectome dataset as provided by Scannell et al. (1995). First, neuronal tract-tracing provides information on the directionality of white matter projections, allowing to distinguish between a projection from region *i* to region *j* and a projection from region *j* to region *i* – something which is, unfortunately, not possible to achieve with (currently available) MRI techniques. Second, the cat connectome dataset included an *a priori* subdivision of the nodes of the network into four functional modules based on neurophysiological information about the functional role of each included brain area.

Seen from an edge-centric perspective, the unique features of the cat dataset collated by Scannell et al. (1995) provide, among other things, two new subdivisions of the connectome's edges, namely a subdivision into *intramodule* (spanning between nodes of the same functional module) and *intermodule* (spanning between nodes of different functional modules) connections, and a subdivision into *bidirectional* and *unidirectional* connections, reflecting edges that are part of a two-way projection and edges without a reciprocal pathway, respectively. Examining the interaction between these new edge categories and the classes of rich club, feeder, and local connections, we found that a large portion of all rich club (67%) and feeder (57%) connections linked nodes of different functional

modules, compared to only a very small portion of the local connections (15%), suggesting an important role for rich club and feeder connections in intermodule communication. Moreover, rich club connections were frequently found to be part of a two-way projection (86% bidirectional vs. 14% unidirectional), more often than feeder (69 vs. 31%) and local (70 vs. 30%) connections.

Building towards a more extensive set of tools to examine graph theoretical properties of edges, the characteristics of rich club, feeder, and local connections were further examined using two *ad hoc* edge-centric measures. First, computing the *structural homogeneity* of an edge as the normalized overlap between the neighbors of its endpoints, feeder connections revealed significantly lower scores than rich club and local connections, nicely aligning with the intuitive notion that feeder connections generally connect very different types of nodes (i.e., hubs versus non-hubs). Second, introducing the *module diversity* of an edge as the product $p_i \times p_j$ of the fractions of modules to which its endpoints i and j are connected, rich club connections achieved a significantly higher score than both feeder and location connections, suggesting that rich club connections are positioned in areas in which information from many functional modules passes and merges. Combined with several node-based observations, including rich club nodes to be present in all functional modules and to be well-represented among intermodule hubs, these findings pinpointed the rich club as a central anatomical infrastructure that interconnects different functional domains of the mammalian brain; a conclusion in line with human findings based on diffusion tractography and resting-state functional magnetic resonance imaging (fMRI) (van den Heuvel and Sporns, 2013) and prior suggestions (Harriger et al., 2012; van den Heuvel et al., 2012; van den Heuvel and Sporns, 2011).

Interestingly, a *path motif* analysis (van den Heuvel et al., 2012), performed by labeling all shortest intermodule communication paths by the categories of the traversed edges (with F-RC-F, for instance, representing a path that first traverses a feeder, then a rich club and then again a feeder connection) and counting

the occurrence of each possible sequence or *motif*, demonstrated a high prevalence of intermodule paths involving feeder, but no rich club, connections. Although the F-RC-F motif was found to be the most prevalent motif, it was also the only motif involving rich club connections that represented a relevant portion of all intermodule communication paths. When taken together, the F-F, L-F-F, and F-F-L motifs comprised a much larger share of all paths, something which was also reflected by a relatively large difference in the proportion of intermodule paths traveling through a rich club *connection* (24.2%) and the proportion of paths traveling through a rich club *node* (89.5%). This suggested that feeder connections are likely to play an important role in maintaining high levels of direct connectivity between functional domains and that rich club connections may not necessarily be designed to only facilitate quick global communication routes, leaving room for the hypothesis that the dense connectivity within the rich club may in addition contribute to providing a “global workspace” (Dehaene and Naccache, 2001) for integration of information from different functional domains.

Edge removal metrics

Even when including new edge metrics such as the *structural homogeneity* and *module diversity* proposed above, the number of network metrics available to characterize individual network edges remains scarce, especially compared to the vast number of network metrics available to assess global properties of the network as a whole or properties of individual nodes. To allow a more systematic examination of the network role of individual edges and edge categories, we therefore proposed a simple framework to “translate” traditional network metrics such as the characteristic path length and clustering coefficient into edge-centric ones. Inspired by lesion models that assess the vulnerability of brain networks to simulated damage (He et al., 2008; He et al., 2009; van den Heuvel and Sporns, 2011; Kaiser and Hilgetag, 2004; Kaiser et al., 2007), the framework was based on the idea that the importance of a connection for a given network property may be estimated by measuring the impact of a hypothetical lesion in that connection. This “cutting-edge” strategy was formalized by comparing the out-

come of a network metric M for an intact connectome map with that of slightly modified maps, missing only the single connection whose features were to be estimated. The relevance of a connection with respect to network metric M was subsequently quantified as the percentage change $(M(B) - M(A))/M(A) \times 100\%$ between the metric value $M(B)$ observed for the modified map and the metric value $M(A)$ derived for the intact connectome map.

In **chapter 6**, we applied such edge removal metrics to measure the relevance of connections in a group-averaged connectome map derived from diffusion-weighted MRI data from 215 healthy participants of the Human Connectome Project (Glasser et al., 2013; Van Essen et al., 2012). Comparing the impact of edge removal on five network metrics across rich club, feeder, and local connections, we found that rich club connections had a pronounced impact on the *communicability* (Estrada and Hatano, 2008) within the network and on a measure by Tononi et al. (1994) used to express the integration between different functional modules (as previously derived on the basis of fMRI), substantially and significantly exceeding the relevance of both feeder and local connections for these measures. Providing further, edge-level, support for a role of the rich club as backbone for global communication (Harriger et al., 2012; van den Heuvel et al., 2012) and as a crucial structure for the integration of information from different functional domains (van den Heuvel and Sporns, 2013), these findings nicely aligned with other recent reports and with our analysis of the cat connectome presented in **chapter 5**. Indeed, an analogous edge removal analysis for the cat connectome confirmed the pronounced relevance of rich club connections with respect to Estrada's communicability (Estrada and Hatano, 2008) and Tononi's integration (Tononi et al., 1994) metric, establishing more direct evidence for the earlier hypothesized role of rich club connections in global integration of information.

In line with the conclusion drawn from **chapter 5**'s path motif analysis, the edge removal analyses also showed that rich club connections do not have a particularly pronounced impact on the characteristic (i.e., average shortest) path length

of the network. Both for the human and cat connectome, removal of rich club connections in fact led to a smaller increase in path length than removal of feeder connections, confirming an important role of feeder connections in facilitating short communication paths. The modest impact of rich club connections on the shortest paths in the network was also in concordance with a report by Irimia and Van Horn (2014), noting that a “scaffold” of white matter connections partially based on simulated lesioning effects with respect to characteristic path length presented only little overlap with the rich club.

Rodent connectome

A brief exploratory examination of a recently released *mesoscale* reconstruction of the mouse connectome established by a landmark effort of the Allen Institute for Brain Science (Oh et al., 2014) and a more elaborate analysis of a reconstruction of the rat connectome provided by the open-access BAMS-II connectivity database (Bota and Swanson, 2007), demonstrated that many organizational network principles that have, for instance, been observed for the human, macaque, and cat brain, may also hold for rodent connectomes (**chapter 7**). For example, the (tract-tracing based) mouse and rat connectome map both showed features of a modular and small-world topology and exhibited a right-tailed degree distribution, reflecting the presence of high-degree neural hubs. Moreover, both networks displayed above-chance levels of interconnectivity between their hubs and thus exhibited a rich club organization. Consistent with reports on rich club organization in the human, macaque (Harriger et al., 2012), and *C. elegans* (Towlson et al., 2013), the associated rich club connections of the mouse and rat were found to span longer physical distances than non-rich club connections.

A closer look on the categories of rich club, feeder, and local connections in the rat connectome – further classifying feeder connections into *feeder-in* connections (those connections that project from non-rich club to rich club nodes) and *feeder-out* connections (projections from rich club nodes to non-rich club nodes) – revealed largely similar characterizations as previously observed for the cat connectome (**chapter 5**). First, the percentages of intermodule rich club

(75%) and intermodule feeder (out: 72%, in: 76%) connections were again found to be much larger than the percentage of intermodule local connections (53%), with the noteworthy difference that, in the absence of information on the functional role of brain regions, the subdivision of nodes into modules was now established on the basis of the connectivity structure of the network itself by means of repeated community detection (Newman, 2006). Second, rich club connections were confirmed to be more often bidirectional (94% bidirectional) than feeder-in (70%), feeder-out (62%), and local (49%) connections, a property which is even more remarkable considering the large portion of intermodule rich club edges and the fact that, across all edge categories, intramodule connections were more often bidirectional than intermodule connections (75 vs. 56%) (similar percentages were found in the cat connectome, with 79% of the intramodule connections and 62% of the intermodule connections being bidirectional). Third, just as in the cat connectome, rich club connections scored higher on our module diversity metric than feeder and local connections. Our inspection of the rodent connectome thus confirmed neural rich club edges to involve long-range, bidirectional, and intermodule connections, which span between brain regions with access to many different modules, together constituting a set of characteristics highly overlapping with properties believed to be relevant for global workspace neurons (Dehaene and Naccache, 2001; van den Heuvel and Sporns, 2013).

Heading in a different direction, we also considered the weights provided for the edges of the rat connectome, expressing the strength of white matter projections as integers between 1 (very weak) and 7 (very strong). Almost as intriguing as the placement of the edges themselves, is the way in which these weights are distributed over the edges. Why is there such a strong difference in strength (Oh et al. (2014) mentioning a 10^5 -fold range for the mouse connectome) between individual connections? And, considering a certain connection c , why is precisely connection c strong, weak, or perhaps just of average strength? Exploring potential links between the placement of edge weights and network topology, a first analysis showed that intramodule connections had significantly higher

weights than intermodule connections and that rich club connections were significantly stronger than feeder and local connections. Moreover, more related to network geometry than topology, short connections were found to comprise higher weights than long connections, expressed through a significant difference between the top 10% longest and shortest edges and a significant negative correlation ($r = -0.21$) between projection length and strength across all edges.

Further relating connection strength to the role of connections in the network, the edges were subdivided into seven weight-based categories (one for every possible weight level) and these edge categories were – similar to the investigation of rich club, feeder, and local connections presented in **chapter 6** – “profiled” using edge removal metrics. Even though connection weights were in no way involved in the assessment of the effects of simulated connection lesioning (metrics before and after lesioning were purely based on the placement of the connections), the effect of connection lesioning on the network’s communicability and clustering increased with connection weight in a staircase-like manner, indicating a more pronounced topological relevance with respect to global communicability and clustering for stronger connections. Interestingly, the category comprising the weakest network connections formed an exception to this observation, as witnessed by a relatively high relevance for clustering and, especially, global communicability. It should also be noted that two other investigated edge removal metrics (assessing effects on shortest paths and a measure for local communication) did not show clear patterns with respect to edge weight. An alternative strategy, interpreting each weight-based edge category as a subnetwork and examining these subnetworks using traditional metrics, in addition suggested that strong connections were likely to appear in “packs”, while weak connections tended to be more scattered.

Link communities

Chapters 5-7 all involved some kind of subdivision of brain regions into densely interconnected modules or communities, either derived from the network structure itself or from additional functional information. Looking at the connec-

tome from an edge-centric perspective, one might wonder whether a similar arrangement into communities might also exist for the connectome's edges, forming coherent collections of white matter pathways and thus potential new edge categories. Motivated by the recent discovery of such *link communities* in other empirical networks and the notion that these link communities might reveal different subsystems than traditional node communities (Ahn et al., 2010; Boldi and Rosa, 2012; Evans and Lambiotte, 2009; Kim and Jeong, 2011), we combined a robust (random walk based) community detection method (Rosvall and Bergstrom, 2008) with a mathematically motivated link community identification strategy (Evans and Lambiotte, 2009) and identified a consistent pattern of eleven link communities in the human connectome (**chapter 8**). Five of these eleven communities spanned through the midline fissure, roughly describing a community of pathways situated in the occipital lobe, a community comprising anterior-posterior connections originating from the cingulum tract, a community of pathways between frontal and a few temporal regions, and two homologous communities centered around the left and right paracentral lobule. The six other communities were found to be predominantly confined to a single hemisphere and formed three communities in the left hemisphere and three homologous communities in the right hemisphere.

In order to obtain more insight into the identified link communities, five edge-centric metrics – four edge removal metrics, complemented with a conventional edge analogue of betweenness centrality (Girvan and Newman, 2002) – were computed for each individual connection and then aggregated per link community. A strong variation of edge scores within communities suggested that the identified link communities did not constitute collections of similar pathways, but rather formed subsystems comprising a mixture of connections with varying roles in the network. Moreover, four of the five edge-centric metrics displayed marginally fluctuating means across communities. Only the impact of edge removal on global communicability was found to show significant deviations, with a tendency for more centrally positioned link communities to display larger scores. Linking the existence of link communities back to our investigation

of the brain's rich club, we hypothesized that rich club hubs would form "community hot spots" where links from multiple communities come together at a single node. In line with this hypothesis, the edges of individual rich club hubs were found to be distributed over significantly more communities (mean [std]: 5.8 [1.9]) than the edges of non-rich club nodes (mean [std]: 1.9 [1.1]), even after a correction was applied for the high degree of hubs. Moreover, as a collective, rich club regions were found to be attached to links from all 11 link communities. In other words, rich club nodes appeared to occupy a similar role with respect to the newly identified link communities as observed for conventional node-based communities (**chapter 5**, **chapter 7**) (van den Heuvel and Sporns, 2013).

Spectral fingerprints

So far, the mental picture when talking about the connectome as a graph has been that of a collection of "dots" (the nodes), combined with a collection of interconnecting "lines" (the edges). Moreover, examining a connectome graph typically comprised the choice of one or more metrics with a relatively intuitive meaning in terms of these dots and lines, each of which encoded a single property of the graph, often obtained by averaging local (e.g., node-wise) values. A rather different way to look at graphs, explored in **chapter 9**, derives from the matrix representation of a graph, storing information about the presence (and, if applicable, strength) of connections in an adjacency matrix A , with the rows and columns of A representing the nodes of the network and an entry in row i and column j representing a connection between node i and node j . Around the 1950s, more than two hundred years after Euler's solution to the Königsberg bridge problem which initiated graph theory, this matrix representation of graphs became the foundation of *spectral graph theory*; a new branch of mathematical research into the properties of graphs, revolving around the so-called eigenvalues and eigenvectors of graph-related matrices (Kaveh, 2013). Conceptually somewhat comparable to how stellar spectra – "jiggly" curves showing the light intensity as a function of wavelength – can be used to identify the presence and abundance of chemical elements on stars, characteristics of networks can be derived from the *spectra* of graph-related matrices (Chung, 1997) – formally de-

fined as the collection of all eigenvalues of a matrix, but commonly represented by (often indeed jiggly) curves which show the relative frequency of each eigenvalue. Instead of providing scores for a set of intuitive and clear-cut metrics, spectra thus represent networks by a single curve, giving a systems-level “fingerprint” of the network as a whole.

In **chapter 9**, we aimed to extend pioneering efforts using spectral graph theory to describe neural networks (Banerjee and Jost, 2007; Varshney et al., 2011). To this end, we compared spectral fingerprints (based on the so-called normalized Laplacian matrix) of reconstructions of the cat, macaque, and *C. elegans* connectome with one another, as well as with the spectra of several non-neural empirical networks and random network models. Consistent with previously observed overlap across species of network attributes assessed with conventional graph metrics (small-worldness, rich club organization, etc.), the examined neural network spectra were found to be relatively similar, while at the same time providing a clear qualitative distinction between, on the one hand, the microscale connectome of the *C. elegans*, and, on the other hand, the tract-tracing based macroscale connectome reconstructions of the cat and macaque. The three neural networks all showed a pronounced peak in the middle of their spectrum, as well as a few much smaller peaks left of the center, indicative of a modular architecture. These spectral characteristics resulted in both qualitative as quantitative (measuring spectral distance) differences with the spectra of commonly used network models. Of the four examined non-neural empirical networks, two networks showed clear spectral differences compared to the neural networks; of the two others, one showed similarities with the spectrum of the *C. elegans* and one with the spectra of the cat and macaque.

To provide a solid underpinning for the pronounced central peak observed in the neural network spectra, we performed a second study considering the influence of network symmetry on the normalized Laplacian spectrum. Inspired by earlier theoretical evidence identifying the occurrence of perfectly symmetric nodes (i.e., nodes with the exact same wiring pattern) as a source for eigenvalues po-

sitioned exactly in the middle of the spectral domain (Banerjee and Jost, 2008; Yadav and Jalan, 2015), we introduced a measure – referred to as the *duplication coefficient* – to capture the approximate (i.e., non-perfect) symmetry in nodal wiring patterns typically witnessed in real-world networks. Across several neural and non-neural empirical networks, the height of the main spectral peak was found to be strongly ($r = 0.63$) and significantly correlated to the duplication coefficient, an observation which was subsequently replicated across and within several network models. Moreover, closer investigation of the role of symmetry in the examined neural networks (now also including human data) showed that perturbations optimized to reduce the duplication coefficient had a significantly larger impact on the spectral peak height than random perturbations. Taken together, these findings suggested the high central peak in neural network spectra to be strongly attributable to patterns of approximate symmetry between brain regions, providing further insight into the meaning behind specific features of spectral fingerprints of connectome maps.

Discussion

The beauty of scientific research is that for each question answered, other questions are raised. In the final part of this thesis, we would like to highlight and reflect on some of our findings and give our thoughts about directions for future research.

Eccentric? Why bother?

According to Merriam-Webster's online dictionary, "eccentric" means "deviating from an established or usual pattern or style". In this thesis, we have both adopted and developed graph theoretical methods that indeed deviate from the usual style of connectome analysis. Whereas many conventional graph analyses of brain networks involve the assessment of properties of brain regions or the network as a whole, the edge-centric perspective given here revolved around the definition and examination of classes of white matter pathways. Essentially three ways to define such edge categories have been considered: based on node labels (rich club and non-rich club nodes inducing rich club, feeder, and local connections, intra- and intermodule edges derived from modules), based on connection morphology (bidirectional vs. unidirectional, strength- and length-based categories), and by edge-wise community detection (link communities). Moreover, we have seen different ways to examine edge categories: computing the overlap between different types of categories (for instance, assessing the percentage of bidirectional rich club connections), charting the arrangement of edge categories along communication paths (path motif analysis), comparing (new) edge measures such as edge removal metrics across categories, and interpreting edge categories as subnetworks. Of course, our aim in pursuing this edge-centric perspective was not just to do something "strange or unusual" (another definition of eccentric provided by Merriam-Webster), but to do something useful. So why should one bother about our edge-centric perspective?

A central backbone for global integrative processes

Our understanding of macroscale connectome architecture is a work in progress. Since the 1990s, the emergence of network science as an interdisciplinary academic field and the increasing availability of datasets describing neural networks have led to numerous insights about the organization of brain networks, often showing remarkable parallels to other complex networks in nature and society (Bullmore and Sporns, 2009). Today, circa 20 years after the first pioneering endeavors (among which those of Scannell et al. (1995) and Tononi et al. (1994)) and 10 years after the birth of the term “connectome” (Sporns et al., 2005), it is safe to say that these developments – the booming expansion of both network science and data on neural networks – are still very much ongoing, with landmark publications in network science (Barabási and Albert, 1999; Watts and Strogatz, 1998) getting thousands of new citations every year (source: Google Scholar) and several recent projects offering open access to connectome data of unprecedented quality (Oh et al., 2014; Van Essen et al., 2012). Part of the progress in network science and connectomics – the application of network science to the brain – is fueled by a continuous “hunt” for meaningful network characterizations, revealing novel aspects of network organization. Especially since connectome graphs have edges which actually represent physical connections (in contrast to graphs of, for instance, social networks, food webs, protein-protein interaction networks, etc.), we anticipated that characterizations concerning these edges would be well-suited to provide a contribution to the current knowledge about brain networks and, in particular, about the dense connectivity between rich club hubs.

The existence of topologically central rich clubs of densely interconnected neural hubs has been consistently demonstrated across a variety of species. Recent literature on neural networks includes reports on rich club organization in the macroscale human (van den Heuvel and Sporns, 2011), macaque (Harriger et al., 2012), cat (Zamora-López et al., 2010), and pigeon connectome (Shanahan et al., 2013), as well as descriptions of rich club organization in the neural system of the *Caenorhabditis elegans* (Towlson et al., 2013) and *Drosophila melanogaster*.

ter (Shih et al., 2015) (a nematode and fruit fly, respectively). Moreover, **chapter 7** shows that the mouse and rat can be added to this list of “rich club enabled” species. A common idea about the relevance of neural hubs for healthy brain function, becoming supported by more and more pieces of graph theoretical evidence, is that hubs may provide efficient communication between different parts of the connectome (Harriger et al., 2012; van den Heuvel et al., 2012; Sporns et al., 2007) and thus promote integration of information (van den Heuvel and Sporns, 2013; Zamora-López et al., 2010), and that hubs may be involved in the coordination of different brain functions (Cole et al., 2010; Crossley et al., 2013). Providing more insight in the potential role of hub-to-hub rich club *connections* in this story (previously shown to comprise long, strong, high-quality, and therefore costly white matter pathways (Collin et al., 2014a)), we found that rich club connections are predominantly bidirectional and often intermodular (**chapter 5** and **chapter 7**), properties believed to be relevant for the formation of a “global workspace” that mobilizes parallel modular cerebral networks and allows neural information to become globally available (Dehaene et al., 1998; Dehaene and Naccache, 2001). Furthermore, we demonstrated that simulated lesioning of (individual) rich club connections caused a pronounced drop in a measure for global communication and a measure for integration between different functional modules, substantially and significantly exceeding the effects of lesioning non-rich club connections (**chapter 6**).

Interestingly, both the simulated lesioning approach (**chapter 6**) and a path motif analysis (**chapter 5**) suggested that although rich club nodes are of undeniable importance for the existence of short global shortcuts, rich club connections may not be particularly relevant for such routes, nicely aligning with recent reports by Irimia and Van Horn (2014) and Perry et al. (2015). Instead, considering the definition of the global communication metric that showed the strong drop after lesioning rich club connections – a measure believed to reflect the “ease of communication” in a network (Estrada and Hatano, 2008) and shown to be implicated after actual, non-simulated lesions (Crofts and Higham, 2009; Crofts et al., 2011) – rich club connections appear to be especially relevant for slightly

longer paths and the existence of many parallel paths between brain regions. Our interpretation of these observations is that neural hubs could be individually relevant as classical “ethernet hubs”, allowing information to quickly arrive at the intended recipient through simple rebroadcasting of their input, but that the dense and costly interconnectivity between neural hubs will be largely attributable to more complex tasks of the rich club as a collective, at least including the integration of information from different domains. Such a subtle role of rich club connections is consistent with theoretical evidence suggesting that dense connectivity between hubs promotes synchronization between brain regions (Gómez-Gardeñes et al., 2010; Watanabe, 2013) and creates a large repertoire of accessible functional states (Senden et al., 2014); the latter observation being in line with the strong bidirectional character of rich club connections and the proposed importance of such connections for metastable dynamics (Gollo et al., 2015). All together, we believe that our edge-centric perspective has provided some novel evidence contributing to the idea that rich clubs in neural networks may act as central backbones for global integrative processes, complementing recent literature by especially providing insight in the characteristics of rich club connections.

Potential for examining connectome differences

Another reason why we believe that our edge-centric perspective is of interest is its potential for studies on the changing (e.g., developing or aging) or diseased brain. Since intersubject variation in connectome graphs is expressed through the edges, we anticipate that the availability of meaningful edge categories and methods to systematically characterize (groups of) edges may be valuable instruments to reveal and interpret brain network differences. Given the common scenario of two (or more) groups of subjects whose connectome differences should be scrutinized, we roughly envision two possible approaches. First, edge categories such as the link communities revealed in **chapter 8** may provide the right level of detail to detect localized differences in the strength of connections. Compared to testing the connectivity strength of individual connections, testing for group differences in the mean connectivity strength of edge catego-

ries drastically improves statistical power (requiring only a mild correction for multiple testing) and adds valuable information about the topological role of the investigated connections, making detected differences easier to interpret. Moreover, edge categories have a somewhat “smoothing” effect, avoiding difficulties due to potential intersubject variation in the presence of connections or due to variation in the precise (edge-level) location of the effect (either biologically accurate or induced by methodological issues). Second, working the other way around, one could first identify those connections whose strength (or perhaps even presence) differs between groups (e.g., are affected in a certain brain disorder) and then use edge-centric network measures such as edge removal metrics to quantify the role of these connections in the network. Since statistical power will often not be sufficient to identify altered connections in the most straightforward manner (testing each connection separately while correcting for multiple testing), network-based statistic (Zalesky et al., 2010a) could be used to first identify a significantly altered component of connections (Verstraete et al., 2011; Zalesky et al., 2011).

In the literature, especially the first approach (using edge categories to identify and interpret changes) has already been applied successfully. Recent studies reported significantly reduced connectivity strength of rich club, but not feeder and local, connections in schizophrenia patients (van den Heuvel et al., 2013) and – to a lesser extent – in their unaffected siblings (Collin et al., 2014b), and the level of rich club connectivity in patients was subsequently found to be related to positive longitudinal changes in general functioning (as assessed during a follow-up several years after the acquisition of the connectome data) (Collin et al., 2015). Moreover, related to connectome development, Kim et al. (2014) found that the white matter integrity of rich club and feeder connections as measured in a group of children between 6 and 11 years (including several children which were born prematurely) was positively associated with the length of gestation (i.e., the time spent in the womb), with local connections showing a more marginal effect, and Ball et al. (2014) reported that, in contrast to a relatively stable number of rich club connections, the number of feeder connections in preterm

born infants significantly increased during the preterm period between 30 and 40 weeks of gestational age.

Considering these early successes of the concept of rich club, feeder, and local edges, we expect that also our intrinsic subdivision of the connectome's edges into eleven different link communities (**chapter 8**) may prove to be of value for studies on connectome differences. Of course, it should be noted that the relevance of rich club, feeder, and local connections may (at least partially) be explained by the natural relevance of hubs and their frequent implication in brain disorders (Crossley et al., 2014; Stam, 2014). However, link communities have their own defining characteristics which make them likely to be suitable for the study of brain disorders. Because of the choice of community detection algorithm, the link communities presented in **chapter 8** may be interpreted as subsystems of the brain in which signals that travel randomly from connection to connection tend to get "trapped". Interestingly, this diffusion-like signal movement underlying our link community detection coincides with a transneuronal spread model of disease agents, recently suggested as an important mechanism in diseases such as amyotrophic lateral sclerosis (Schmidt et al., 2015; Verstraete et al., 2014), Alzheimer's (Mallio et al., 2015), frontotemporal dementia (Raj et al., 2012), and other neurodegenerative diseases (Zhou et al., 2012) which have previously been noted to specifically target large-scale subsystems of the brain (Seeley et al., 2009). Link communities could therefore reflect zones in which disease agents may accumulate and connections of link communities involving the epicenters of the disease (Mallio et al., 2015; Schmidt et al., 2015; Zhou et al., 2012) may be particularly affected.

Spectral fingerprints

For the perspective offered by network spectra – the other, more briefly explored, eccentric approach considered in this thesis – the path towards applications in future connectome studies is less clear. Having a single connectome "fingerprint" which can be compared across subjects has a clear appeal for case-control studies, but the current absence of an intuitive interpretation for

specific peaks or troughs in network spectra, other than peaks associated to the smallest, largest, or central eigenvalues, poses some difficulties. For instance, assuming that we would be able to find consistent alterations in the spectral fingerprints of, say, schizophrenia patients, an inevitable question would be what these alterations reflect (i.e., what change in the underlying connectome causes them) and, ultimately, how these alterations relate to the disease. In other words, for the adoption of spectral fingerprints in studies on brain disorders, we must be able to translate results from the rather mathematical domain of eigenvalues and eigenvectors to the domain of neuroscience. The findings presented in the second part of **chapter 9** – providing a practical relationship between the pronounced central peak in neural spectra and a more conventional (node- and edge-based) metric of approximate symmetry – may provide a modest contribution to this challenge. However, these findings heavily relied on the existence of a good theoretical understanding of the occurrence of eigenvalues $\lambda = 1$ (Banerjee and Jost, 2008; Yadav and Jalan, 2015), being one of the better understood special cases. Achieving further improvements in our understanding of neural spectra is likely to require additional research on both the mathematical and “translational” part.

Methodological considerations

Biological meaning of graph metrics

In contrast to spectral fingerprints, most of the graph metrics commonly used in connectomics (clustering, path length, etc.) have a quite intuitive meaning. For example, the clustering coefficient measures how often neighbors of a node are also neighbors of each other, overlapping with our conceptual idea of what “clusters” should be. Furthermore, the interpretation of characteristic path length as a measure of network efficiency is inspired by the intuitive notion that the number of steps necessary to reach node j from node i may reflect the time it takes to send information from i to j . It is, however, important to realize that having a conceptual understanding of a graph metric in a network sense does not imply that we also know the biological meaning of that metric in the context

of brain networks. Although the success of graph metrics in revealing differences between the healthy and diseased brain (Bassett and Bullmore, 2009; Filippi et al., 2013; Fornito and Bullmore, 2014; Stam, 2014) and reported relationships between graph metrics and more clinical descriptives, for instance linking path length to intelligence (van den Heuvel et al., 2009; Li et al., 2009; Zalesky et al., 2011), leave little ambiguity about the biological relevance of graph metrics, the mechanisms that may drive these relationships are generally difficult to reveal. It is, for example, unclear whether the observed relationships between path length and intelligence emerge because “communication” in brain networks indeed tends to follow the shortest paths; there could also be hidden factors beneficial for both path length and intelligence, or more complex mechanisms (e.g., involving synchronization (Hipp et al., 2011; Rodriguez et al., 1999)) with the same net effect.

The relevance of a scientific debate and future research concerning the biological meaning of graph metrics is underscored by our simulated lesioning study presented in **chapter 6**, showing that the importance of connections as assessed by simulated lesioning largely depends on the graph metrics chosen to evaluate the outcome. Evaluating the outcome of simulated lesions using three different communication metrics also returned three qualitatively different patterns with respect to the relevance of rich club, feeder, and local connections. As already discussed, lesioning rich club connections resulted in a pronounced drop in the network’s communicability (sensitive to parallel and longer paths), but had more modest effects on the average shortest path length. Moreover, for a third metric based on randomly moving signals, lesioning rich club connections even had a positive effect on the communication efficiency, likely attributable to the fact that randomly moving signals cannot easily pass through the densely connected rich club because they tend to get trapped. Although the apparent contrast between these findings is not necessarily problematic and can even give a more detailed impression of the potential role of rich club connections, it would of course be extremely beneficial to know whether or not, from a biological point of view, these three estimates for “impact on communication” should be

considered equally plausible. In this context, it is worth mentioning that communicability has been demonstrated to be a suitable metric to capture effects of actual (non-simulated) lesions (Crofts and Higham, 2009; Crofts et al., 2011; Li et al., 2013b) and also has some theoretical advantages for the assessment of lesion effects (Andreotti et al., 2014). However, as for the relationships between path length and intelligence, it is difficult to draw strong conclusions from such findings. Avenues that may provide additional insight in the biological accuracy of communication metrics – including the efforts of Goñi and colleagues, who determined the extent to which the connectome is optimized for certain types of communication (Goñi et al., 2013) and how analytic measures of communication along structural pathways relate to functional connectivity (Goñi et al., 2014) – are therefore of high interest.

A cat or rat is not a human

In this thesis, we have examined both the human and animal (mostly cat and rat) connectome. Tract-tracing based reconstructions of animal brain networks and *in vivo* MRI-based reconstructions of the brain networks of human subjects have their own advantages and limitations and can therefore strengthen each other. Neuronal tracing of axonal connections in the animal brain is unique in its direct assessment of connectivity and provides valuable information on the direction of projections, but has the disadvantage of not being suitable for human research and requiring data from a vast number of animals for the construction of a single connectome map (Bota and Swanson, 2007; Oh et al., 2014; Scannell et al., 1995; Stephan et al., 2001). In contrast, MRI-based connectome reconstruction does allow human research and reconstruction of individual connectomes, but is based on an indirect measurement of connectivity that may not be equally suitable for all white matter pathways (Jbabdi and Johansen-Berg, 2011; Jones and Pierpaoli, 2005) and is therefore likely to involve higher levels of false positives and false negatives (**chapter 4**). Also, MRI-based connectome assessment does not allow inference of the directionality of connections (**chapter 2**).

By checking many of our findings for multiple species, either directly (**chap-**

ter 6 testing both the human and cat connectome; chapter 7 replicating many cat findings from chapter 5 in the mouse or rat) or via the literature (the cat findings from chapter 5 being highly consistent with the human findings of van den Heuvel and Sporns (2013)), we have tried to ensure that our insights and conclusions are not driven by current limitations of macroscale connectome mapping. The displayed consistency of, for instance, the characteristics of rich club connections is in agreement with other network organizational principles, such as small-worldness and the presence of hubs, being robustly found across a wide variety of both mammalian and non-mammalian species (Kaiser, 2015) – a general level of similarity also being reflected through the similarity of neural network spectra (chapter 9). It seems, however, obvious that there must be many differences between neural networks as well; after all, a cat or rat is not a human. A problem in delineating potential differences in connectome maps of different species is that these connectome maps are typically formed using very different procedures, making it hard to tell whether dissimilarities are biologically or methodologically driven. Moreover, the dependency of network metrics on the definition and number of nodes (Fornito et al., 2010; Zalesky et al., 2010b) (chapter 3), and basic characteristics such as the amount of edges (Albert and Barabási, 2002; van Wijk et al., 2010), adds another layer of complexity. Whereas human connectome findings can be made more comparable between studies by using the same reference atlas for parcellation, this is more difficult to achieve between species. Keeping methodological procedures as similar as possible and looking into more fine-grained aspects of brain connectivity, studies have nevertheless achieved to pinpoint across-species differences in macroscale brain wiring (Goulas et al., 2014; Li et al., 2013a; Neubert et al., 2014) between humans and monkeys, including differences in the connectivity fingerprints of frontal regions between the human and macaque brain. If future efforts succeed in improving the compatibility of network metrics between differently sized networks, similar investigations may result in reliable assessment of potential differences in global wiring architecture between species.

Intersubject variation

Perhaps even more important than the comparison of connectomes across species is the comparison of connectomes between human subjects – certainly from a clinical perspective. Although the potential for the assessment and interpretation of connectome differences was an important motivation to pursue an edge-centric point of view on connectomics, we did not focus much on intersubject variation in this thesis itself. The tract-tracing based connectome reconstructions of the cat and rat examined in **chapter 5** and **chapter 7**, respectively, were composed of small pieces of information on limited sets of connections originating from many different studies and were thus unsuitable to provide insight in intersubject connectome variation. Moreover, our human findings presented in **chapter 6** and **chapter 8** were predominantly based on group-averaged connectome maps, again eliminating information on intersubject variation. However, in both studies, additional analyses showed a good correspondence between results derived directly at the group-level (i.e., using the group-averaged connectome map as input) and aggregated findings derived from individual connectome reconstructions. The classification of hubs and link communities, for example, showed relatively modest levels of variation across subjects and this variation roughly “averaged out” to the group-level observations. As witnessed by the distributions of connection prevalence examined in **chapter 4**, a similarly modest variation is present in the connectome maps themselves, with most of the brain region pairs being (almost) consistently reported as connected or (almost) consistently reported as disconnected across subjects. It should be noted, though, that the remaining variation is large enough to induce substantial and significant differences in commonly used network metrics (**chapter 4**) and that these observations do not include variation in connection strength.

When it comes to binary variation (i.e., concerning the presence or absence of connections) in individual macroscale connectome maps, an interesting question is to what extent this variation is biologically accurate. Johansen-Berg and Rushworth (2009) argue that for measured variation in the presence of a large-scale white matter pathway within healthy adults “a more plausible explanation

is that anatomical variation (in, for example, fiber density, myelination, geometry, etc.) results in the path being easier to trace using tractography in some subjects compared with others". In other words, they argue that, in reality, the binary skeleton of macroscale connectome maps is (largely) identical across individuals and that true biological variation is more likely to involve differences in the strength (fiber density) or quality (myelination) of connectome connections – a theory which we fully endorse. Although it seems difficult to properly verify this hypothesis of little variation in the presence of large-scale pathways with the currently available techniques, we believe that there are several observations which point in this direction.

First, it is important to note that the overall level of observed connectome variation between subjects, including variation in both the presence and strength of connections, is relatively modest. Indeed, reported correlation coefficients between connectivity matrices of different subjects roughly range between 0.7 and almost 1, with median values for commonly used spatial resolutions ranging between 0.8 and 0.95 (Bassett et al., 2011; Cammoun et al., 2012). Moreover, considering that the same studies also report variation between connectome reconstructions based on different diffusion-weighted imaging datasets of the same subject (acquired shortly after each other, effectively ruling out actual changes in macroscale brain wiring), part of the modest variation reflected by these correlation coefficients should be attributed to "measurement noise" inherent to MRI-based connectome mapping. Exploratory assessment of animal-to-animal variability in tract-tracing studies of the macaque and mouse brain – based on small subsets of repeated or overlapping injection experiments – confirmed such a high consistency in both the presence and strength of anatomical pathways across specimens (Markov et al., 2014; Oh et al., 2014), with Oh et al. (2014) reporting intersubject correlation coefficients of about 0.9 between different mice. In our opinion, there is a rather large gap between this apparently general situation of pathways with a reasonably consistent strength across subjects and the possibility of large-scale pathways that are completely absent in some subjects and present in others. Interestingly, in line with the remark of Johan-

sen-Berg and Rushworth (2009) that measured binary variation may be caused by more subtle anatomical variation in fiber density or myelination, weak connections have been reported to be less reliably mapped than strong connections (Cammoun et al., 2012); an observation underscored by a recent study which revealed clear correlations between the strength and reproducibility of connections (Zhao et al., 2015).

Other observations in favor of little biological variation in the presence of large-scale white matter pathways include similarity in brain wiring between infants and adults and between humans and monkeys. To be precise, studies of the neonatal brain have shown a high level of overlap (85%) between binary connectome maps of newborn children and adults (van den Heuvel et al., 2014), suggesting a common “blueprint” for brain wiring which is already (largely) implemented at birth. Furthermore, the aforementioned differences in brain wiring between the human and monkey brain are remarkably subtle, with comparative studies reporting many more similarities than dissimilarities (Goulas et al., 2014; Li et al., 2013a; Neubert et al., 2014). For instance, Goulas et al. (2014) report that macroscale maps of the macaque and human connectome share 75% of their connections. With this similarity between the macroscale human and macaque connectome in mind, representing species with strongly differing mental capacities, it seems unlikely that there would be large differences in the presence of large-scale white matter pathways between healthy human subjects, or even between healthy subjects and patients with a certain neurological or neuropsychiatric disorder. This is why the suggested edge-centric approaches for future case-control studies discussed above mainly revolve around differences in connection weights.

Of course, the issue of binary connectome variation between subjects is largely dependent on the scale of investigation. Although Sebastian Seung’s widely publicized statement that “the brain’s wiring makes us who we are” (Seung, 2012) may be a little exaggerated – indeed, we should not forget that the complexity of our brain extends beyond its intricate wiring as, for instance, evidenced by

the fundamental role of neuromodulation (Hasselmo, 1999; McCormick, 1992) and the existence of complex gut-brain interactions (Mayer, 2011) –, it is safe to say that the connectome is a fundamental part of one's self and that there are bound to be many differences in the wiring of individual connectomes on the neuronal level. As the techniques available for connectome mapping will likely continue to improve, future studies may provide a more definite answer to the question at which scales these putative neuronal differences cause binary variation in more coarse-grained connectome maps.

Final words

Of all networks appearing in nature and society, the neural network inside our skull is probably the most fascinating one. Although it is doubtful that we will every fully understand all processes and mechanisms involved in the formation and operation of this connectome, its defining role in our lives and its susceptibility to disorders makes it more than worthwhile to learn as much about it as we can. With this thesis, we hope to have provided a modest contribution to this goal, learning a little more about the macroscale organization of the connectome – and especially about the role of white matter pathways between highly connected hub regions – by looking at the connectome from a somewhat unusual perspective. For me personally, having spent years to train my brain in understanding mathematics, it has been truly exciting to now use mathematics to understand the brain.

References

- Achard, S., Delon-Martin, C., Vértes, P.E., Renard, F., Schenck, M., Schneider, F., Heinrich, C., Kremer, S., Bullmore, E.T., 2012. Hubs of brain functional networks are radically reorganized in comatose patients. *Proceedings of the National Academy of Sciences* 109, 20608-20613.
- Ahn, Y.Y., Bagrow, J.P., Lehmann, S., 2010. Link communities reveal multiscale complexity in networks. *Nature* 466, 761-764.
- Albert, R., Barabási, A.L., 2002. Statistical mechanics of complex networks. *Reviews of Modern Physics* 74, 47-97.
- Andreotti, J., Jann, K., Melie-Garcia, L., Giezendanner, S., Abela, E., Wiest, R., Dierks, T., Federspiel, A., 2014. Validation of Network Communicability Metrics for the Analysis of Brain Structural Networks. *PLOS ONE* 9, e115503.
- Ball, G. et al., 2014. Rich-club organization of the newborn human brain. *Proceedings of the National Academy of Sciences* 111, 7456-7461.
- Banerjee, A., Jost, J., 2007. Spectral plots and the representation and interpretation of biological data. *Theory in Biosciences* 126, 15-21.
- Banerjee, A., Jost, J., 2008. On the spectrum of the normalized graph Laplacian. *Linear Algebra and its Applications* 428, 3015-3022.
- Barabási, A.L., Albert, R., 1999. Emergence of Scaling in Random Networks. *Science* 286, 509-512.
- Bassett, D.S., Brown, J.A., Deshpande, V., Carlson, J.M., Grafton, S.T., 2011. Conserved and variable architecture of human white matter connectivity. *NeuroImage* 54, 1262-1279.
- Bassett, D.S., Bullmore, E., Verchinski, B.A., Mattay, V.S., Weinberger, D.R., Meyer-Lindenberg, A., 2008. Hierarchical Organization of Human Cortical Networks in Health and Schizophrenia. *The Journal of Neuroscience* 28, 9239-9248.
- Bassett, D.S., Bullmore, E.T., 2009. Human brain networks in health and disease. *Current Opinion in Neurology* 22, 340-347.
- Betzel, R.F., Griffa, A., Avena-Koenigsberger, A., Goñi, J., Thiran, J.P., Hagmann, P., Sporns, O., 2013. Multi-scale community organization of the human structural connectome and its relationship with resting-state functional connectivity. *Network Science* 1, 353-373.
- Boldi, P., Rosa, M., 2012. Arc-Community Detection via Triangular Random Walks. *Proceedings of the 8th Latin American Web Congress*, 48-56.
- Bota, M., Swanson, L.W., 2007. Online workbenches for neural network connections. *Journal of Comparative Neurology* 500, 807-814.
- Buckner, R.L., Sepulcre, J., Talukdar, T., Krienen, F.M., Liu, H., Hedden, T., Andrews Hanna, J.R., Sperling, R.A., Johnson, K.A., 2009. Cortical Hubs Revealed by Intrinsic Functional Connectivity: Mapping, Assessment of Stability, and Relation to Alzheimer's Disease. *The Journal of Neuroscience* 29, 1860-1873.
- Bullmore, E., Sporns, O., 2009. Complex brain networks: graph theoretical analysis of structural and functional systems. *Nature Reviews Neuroscience* 10, 186-198.
- Bullmore, E., Sporns, O., 2012. The economy of brain network organization. *Nature Reviews Neuroscience* 13, 336-349.
- Camoun, L., Gigandet, X., Meskaldji, D., Thiran, J.P., Sporns, O., Do, K.Q., Maeder, P., Meuli, R., Hagmann, P., 2012. Mapping the human connectome at multiple scales with diffusion spectrum MRI. *Journal of Neuroscience Methods* 203, 386-397.
- Chung, F., 1997. Spectral graph theory. American Mathematical Society, Rhode Island.
- Cole, M.W., Pathak, S., Schneider, W., 2010. Identifying the brain's most globally connected regions. *NeuroImage* 49, 3132-3148.
- Collin, G., Kahn, R.S., de Reus, M.A., Cahn, W., van den Heuvel, M.P., 2014b. Impaired Rich Club Connectivity in Unaffected Siblings of Schizophrenia Patients. *Schizophrenia Bulletin* 40, 438-448.
- Collin, G., de Nijls, J., Hulshoff Pol, H.E., Cahn, W., van den Heuvel, M.P., 2015. Connectome organization is related to longitudinal changes in general functioning, symptoms and IQ in chronic schizophrenia. *Schizophrenia Research*, epub ahead of print.
- Collin, G., Sporns, O., Mandl, R.C.W., van den Heuvel, M.P., 2014a. Structural and Functional Aspects Relating to Cost and Benefit of Rich Club Organization in the Human Cerebral Cortex. *Cerebral Cortex* 24, 2258-2267.

- Crofts, J.J., Higham, D.J., 2009. A weighted communicability measure applied to complex brain networks. *Journal of the Royal Society Interface* 6, 411-414.
- Crofts, J.J., Higham, D.J., Bosnell, R., Jbabdi, S., Matthews, P.M., Behrens, T.E.J., Johansen-Berg, H., 2011. Network analysis detects changes in the contralesional hemisphere following stroke. *NeuroImage* 54, 161-169.
- Crossley, N.A., Mechelli, A., Scott, J., Carletti, F., Fox, P.T., McGuire, P., Bullmore, E.T., 2014. The hubs of the human connectome are generally implicated in the anatomy of brain disorders. *Brain*, epub ahead of print.
- Crossley, N.A., Mechelli, A., Vértes, P.E., Winton-Brown, T.T., Patel, A.X., Ginestet, C.E., McGuire, P., Bullmore, E.T., 2013. Cognitive relevance of the community structure of the human brain functional coactivation network. *Proceedings of the National Academy of Sciences* 110, 11583-11588.
- Dehaene, S., Kerszberg, M., Changeux, J.P., 1998. A neuronal model of a global workspace in effortful cognitive tasks. *Proceedings of the National Academy of Sciences* 95, 14529-14534.
- Dehaene, S., Naccache, L., 2001. Towards a cognitive neuroscience of consciousness: basic evidence and a workspace framework. *Cognition* 79, 1-37.
- Estrada, E., Hatano, N., 2008. Communicability in complex networks. *Physical Review E* 77, 036111.
- Evans, T.S., Lambiotte, R., 2009. Line graphs, link partitions, and overlapping communities. *Physical Review E* 80, 016105.
- Filippi, M., van den Heuvel, M.P., Fornito, A., He, Y., Hulshoff Pol, H.E., Agosta, F., Comi, G., Rocca, M.A., 2013. Assessment of system dysfunction in the brain through MRI-based connectomics. *The Lancet Neurology* 12, 1189-1199.
- Fornito, A., Bullmore, E.T., 2014. Connectomics: A new paradigm for understanding brain disease. *European Neuropsychopharmacology* 25, 733-748.
- Fornito, A., Zalesky, A., Bullmore, E.T., 2010. Network scaling effects in graph analytic studies of human resting-state fMRI data. *Frontiers in Systems Neuroscience* 4, 22.
- Girvan, M., Newman, M.E.J., 2002. Community structure in social and biological networks. *Proceedings of the National Academy of Sciences* 99, 7821-7826.
- Glasser, M.F. et al., 2013. The minimal preprocessing pipelines for the Human Connectome Project. *NeuroImage* 80, 105-124.
- Gollo, L.L., Zalesky, A., Hutchison, R.M., van den Heuvel, M., Breakspear, M., 2015. Dwelling quietly in the rich club: brain network determinants of slow cortical fluctuations. *Philosophical Transactions of the Royal Society of London B: Biological Sciences* 370, 20140165.
- Gómez-Gardeñes, J., Zamora-López, G., Moreno, Y., Arenas, A., 2010. From Modular to Centralized Organization of Synchronization in Functional Areas of the Cat Cerebral Cortex. *PLoS ONE* 5, e12313.
- Gong, G., He, Y., Concha, L., Lebel, C., Gross, D.W., Evans, A.C., Beaulieu, C., 2009. Mapping Anatomical Connectivity Patterns of Human Cerebral Cortex Using In Vivo Diffusion Tensor Imaging Tractography. *Cerebral Cortex* 19, 524-536.
- Goñi, J., Avena-Koenigsberger, A., de Mendizabal, N.V., van den Heuvel, M.P., Betzel, R.F., Sporns, O., 2013. Exploring the Morphospace of Communication Efficiency in Complex Networks. *PLoS ONE* 8, e58070.
- Goñi, J., van den Heuvel, M.P., Avena-Koenigsberger, A., de Mendizabal, N.V., Betzel, R.F., Griffa, A., Hagmann, P., Corominas-Murtra, B., Thiran, J.P., Sporns, O., 2014. Resting-brain functional connectivity predicted by analytic measures of network communication. *Proceedings of the National Academy of Sciences* 111, 833-838.
- Goulas, A., Bastiani, M., Bezgin, G., Uylings, H.B.M., Roebroeck, A., Stiers, P., 2014. Comparative Analysis of the Macroscale Structural Connectivity in the Macaque and Human Brain. *PLoS Computational Biology* 10, e1003529.
- Hagmann, P., Cammoun, L., Gigandet, X., Meuli, R., Honey, C.J., Wedeen, V.J., Sporns, O., 2008. Mapping the Structural Core of Human Cerebral Cortex. *PLoS Biology* 6, e159.
- Hagmann, P., Kurant, M., Gigandet, X., Thiran, P., Wedeen, V.J., Meuli, R., Thiran, J.P., 2007. Mapping Human Whole-Brain Structural Networks with Diffusion MRI. *PLoS ONE* 2, e597.
- Harriger, L., van den Heuvel, M.P., Sporns, O., 2012. Rich Club Organization of Macaque Cerebral Cortex and Its Role in Network Communication. *PLoS ONE* 7, e46497.
- Hasselmo, M.E., 1999. Neuromodulation: acetylcholine and memory consolidation. *Trends in Cognitive Sciences* 3, 351-359.

- He, Y., Chen, Z.J., Evans, A.C., 2007. Small-World Anatomical Networks in the Human Brain Revealed by Cortical Thickness from MRI. *Cerebral Cortex* 17, 2407-2419.
- He, Y., Chen, Z.J., Evans, A.C., 2008. Structural Insights into Aberrant Topological Patterns of Large-Scale Cortical Networks in Alzheimer's Disease. *The Journal of Neuroscience* 28, 4756-4766.
- He, Y. et al., 2009. Uncovering Intrinsic Modular Organization of Spontaneous Brain Activity in Humans. *PLoS ONE* 4, e5226.
- van den Heuvel, M.P., Kahn, R.S., Goñi, J., Sporns, O., 2012. High-cost, high-capacity backbone for global brain communication. *Proceedings of the National Academy of Sciences* 109, 11372-11377.
- van den Heuvel, M.P., Kersbergen, K.J., de Reus, M.A., Keunen, K., Kahn, R.S., Groenendaal, F., de Vries, L.S., Benders, M.J.N.L., 2014. The Neonatal Connectome During Preterm Brain Development. *Cerebral Cortex*, *epub ahead of print*.
- van den Heuvel, M.P., Mandl, R.C.W., Stam, C.J., Kahn, R.S., Hulshoff Pol, H.E., 2010. Aberrant Frontal and Temporal Complex Network Structure in Schizophrenia: A Graph Theoretical Analysis. *The Journal of Neuroscience* 30, 15915-15926.
- van den Heuvel, M.P., Sporns, O., 2011. Rich-Club Organization of the Human Connectome. *The Journal of Neuroscience* 31, 15775-15786.
- van den Heuvel, M.P., Sporns, O., 2013. An Anatomical Substrate for Integration among Functional Networks in Human Cortex. *The Journal of Neuroscience* 33, 14489-14500.
- van den Heuvel, M.P., Sporns, O., Collin, G., Scheewe, T., Mandl, R.C.W., Kahn, W., Goñi, J., Hulshoff Pol, H.E., Kahn, R.S., 2013. Abnormal rich club organization and functional brain dynamics in schizophrenia. *JAMA Psychiatry* 70, 783-792.
- van den Heuvel, M.P., Stam, C.J., Boersma, M., Hulshoff Pol, H.E., 2008. Small-world and scale-free organization of voxel-based resting-state functional connectivity in the human brain. *NeuroImage* 43, 528-539.
- van den Heuvel, M.P., Stam, C.J., Kahn, R.S., Hulshoff Pol, H.E., 2009. Efficiency of Functional Brain Networks and Intellectual Performance. *The Journal of Neuroscience* 29, 7619-7624.
- Hilgetag, C.C., Burns, G.A., O'Neill, M.A., Scannell, J.W., Young, M.P., 2000. Anatomical connectivity defines the organization of clusters of cortical areas in the macaque monkey and the cat. *Philosophical Transactions of the Royal Society of London B: Biological Sciences* 355, 91-110.
- Hipp, J.F., Engel, A.K., Siegel, M., 2011. Oscillatory Synchronization in Large-Scale Cortical Networks Predicts Perception. *Neuron* 69, 387-396.
- Irimia, A., Van Horn, J.D., 2014. Systematic network lesioning reveals the core white matter scaffold of the human brain. *Frontiers in Human Neuroscience* 8, 51.
- Iturria-Medina, Y., Sotero, R.C., Canales-Rodríguez, E.J., Alemán-Gómez, Y., Melie-García, L., 2008. Studying the human brain anatomical network via diffusion-weighted MRI and Graph Theory. *NeuroImage* 40, 1064-1076.
- Jbabdi, S., Johansen-Berg, H., 2011. Tractography: Where Do We Go from Here? *Brain Connectivity* 1, 169-183.
- Johansen-Berg, H., Rushworth, M.F.S., 2009. Using Diffusion Imaging to Study Human Connectional Anatomy. *Annual Review of Neuroscience* 32, 75-94.
- Jones, D.K., Pierpaoli, C., 2005. Confidence mapping in diffusion tensor magnetic resonance imaging tractography using a bootstrap approach. *Magnetic Resonance in Medicine* 53, 1143-1149.
- Kaiser, M., 2015. Neuroanatomy: Connectome Connects Fly and Mammalian Brain Networks. *Current Biology* 25, R416-R418.
- Kaiser, M., Hilgetag, C.C., 2004. Edge vulnerability in neural and metabolic networks. *Biological Cybernetics* 90, 311-317.
- Kaiser, M., Martin, R., Andras, P., Young, M.P., 2007. Simulation of robustness against lesions of cortical networks. *European Journal of Neuroscience* 25, 3185-3192.
- Kaveh, A., 2013. Optimal analysis of structures by concepts of symmetry and regularity. Springer, New York.
- Kim, D.J., Davis, E.P., Sandman, C.A., Sporns, O., O'Donnell, B.F., Buss, C., Hetrick, W.P., 2014. Longer gestation is associated with more efficient brain networks in preadolescent children. *NeuroImage* 100, 619-627.
- Kim, Y., Jeong, H., 2011. Map equation for link communities. *Physical Review E* 84, 026110.

- Li, L., Hu, X., Preuss, T.M., Glasser, M.F., Damen, F.W., Qiu, Y., Rilling, J., 2013a. Mapping putative hubs in human, chimpanzee and rhesus macaque connectomes via diffusion tractography. *NeuroImage* 80, 462-474.
- Li, Y., Jewells, V., Kim, M., Chen, Y., Moon, A., Armao, D., Troiani, L., Markovic-Plese, S., Lin, W., Shen, D., 2013b. Diffusion tensor imaging based network analysis detects alterations of neuroconnectivity in patients with clinically early relapsing-remitting multiple sclerosis. *Human Brain Mapping* 34, 3376-3391.
- Li, Y., Liu, Y., Li, J., Qin, W., Li, K., Yu, C., Jiang, T., 2009. Brain Anatomical Network and Intelligence. *PLoS Computational Biology* 5, e1000395.
- Liang, X., Zou, Q., He, Y., Yang, Y., 2013. Coupling of functional connectivity and regional cerebral blood flow reveals a physiological basis for network hubs of the human brain. *Proceedings of the National Academy of Sciences* 110, 1929-1934.
- Mallio, C.A., Schmidt, R., de Reus, M.A., Vernieri, F., Quintiliani, L., Curcio, G., Zobel, B.B., Quattracchi, C.C., van den Heuvel, M.P., 2015. Epicentral Disruption of Structural Connectivity in Alzheimer's Disease. *CNS Neuroscience & Therapeutics*, epub ahead of print.
- Markov, N.T. et al., 2014. A Weighted and Directed Interareal Connectivity Matrix for Macaque Cerebral Cortex. *Cerebral Cortex* 24, 17-36.
- Mayer, E.A., 2011. Gut feelings: the emerging biology of gut-brain communication. *Nature Reviews Neuroscience* 12, 453-466.
- McCormick, D.A., 1992. Neurotransmitter actions in the thalamus and cerebral cortex and their role in neuromodulation of thalamocortical activity. *Progress in Neurobiology* 39, 337-388.
- Meunier, D., Lambiotte, R., Bullmore, E.T., 2010. Modular and hierarchically modular organization of brain networks. *Frontiers in Neuroscience* 4, 200.
- Neubert, F.X., Mars, R., Thomas, A., Sallet, J., Rushworth, M.S., 2014. Comparison of Human Ventral Frontal Cortex Areas for Cognitive Control and Language with Areas in Monkey Frontal Cortex. *Neuron* 81, 700-713.
- Newman, M.E.J., 2006. Modularity and community structure in networks. *Proceedings of the National Academy of Sciences* 103, 8577-8582.
- Oh, S.W. et al., 2014. A mesoscale connectome of the mouse brain. *Nature* 508, 207-214.
- Perry, A., Wen, W., Lord, A., Thalamuthu, A., Roberts, G., Mitchell, P.B., Sachdev, P.S., Breakspear, M., 2015. The organisation of the elderly connectome. *NeuroImage* 114, 414-426.
- Power, J., Schlaggar, B., Lessov-Schlaggar, C., Petersen, S., 2013. Evidence for Hubs in Human Functional Brain Networks. *Neuron* 79, 798-813.
- Raj, A., Kuceyeski, A., Weiner, M., 2012. A Network Diffusion Model of Disease Progression in Dementia. *Neuron* 73, 1204-1215.
- Rodriguez, E., George, N., Lachaux, J.-P., Martinerie, J., Renault, B., Varela, F.J., 1999. Perception's shadow: long-distance synchronization of human brain activity. *Nature* 397, 430-433.
- Rosvall, M., Bergstrom, C.T., 2008. Maps of random walks on complex networks reveal community structure. *Proceedings of the National Academy of Sciences* 105, 1118-1123.
- Rubinov, M., Sporns, O., 2010. Complex network measures of brain connectivity: Uses and interpretations. *NeuroImage* 52, 1059-1069.
- Scannell, J.W., Blakemore, C., Young, M.P., 1995. Analysis of connectivity in the cat cerebral cortex. *The Journal of Neuroscience* 15, 1463-1483.
- Schmidt, R., de Reus, M.A., Scholtens, L.H., van den Berg, L.H., van den Heuvel, M.P., 2015. Simulating disease propagation across white matter connectome reveals anatomical substrate for neuropathology staging in amyotrophic lateral sclerosis. *NeuroImage*, epub ahead of print.
- Seeley, W.W., Crawford, R.K., Zhou, J., Miller, B.L., Greicius, M.D., 2009. Neurodegenerative Diseases Target Large-Scale Human Brain Networks. *Neuron* 62, 42-52.
- Senden, M., Deco, G., de Reus, M.A., Goebel, R., van den Heuvel, M., 2014. Rich club organization supports a diverse set of functional network configurations. *NeuroImage* 96, 174-182.
- Seung, S., 2012. Connectome: how the brain's wiring makes us who we are. Houghton Mifflin Harcourt, Boston.
- Shanahan, M., Bingman, V.P., Shimizu, T., Wild, M., Güntürkün, O., 2013. Large-Scale Network Organisation in the Avian Forebrain: A Connectivity Matrix and Theoretical Analysis. *Frontiers in Computational Neuroscience* 7, 89.

CHAPTER 10

- Shih, C.T., Sporns, O., Yuan, S.L., Su, T.S., Lin, Y.J., Chuang, C.C., Wang, T.Y., Lo, C.C., Greenspan, R., Chiang, A.S., 2015. Connectomics-Based Analysis of Information Flow in the Drosophila Brain. *Current Biology* 25, 1249-1258.
- Sporns, O., Honey, C.J., Kötter, R., 2007. Identification and Classification of Hubs in Brain Networks. *PLoS ONE* 2, e1049.
- Sporns, O., Tononi, G., Kötter, R., 2005. The Human Connectome: A Structural Description of the Human Brain. *PLoS Computational Biology* 1, e42.
- Sporns, O., Zwi, J., 2004. The small world of the cerebral cortex. *Neuroinformatics* 2, 145-162.
- Stam, C.J., 2004. Functional connectivity patterns of human magnetoencephalographic recordings: a 'small-world' network? *Neuroscience Letters* 355, 25-28.
- Stam, C.J., 2014. Modern network science of neurological disorders. *Nature Reviews. Neuroscience* 15, 683-695.
- Stam, C.J. et al., 2009. Graph theoretical analysis of magnetoencephalographic functional connectivity in Alzheimer's disease. *Brain* 132, 213-224.
- Stephan, K.E., Kamper, L., Bozkurt, A., Burns, G.A.P.C., Young, M.P., Kötter, R., 2001. Advanced database methodology for the Collation of Connectivity data on the Macaque brain (CoCoMac). *Philosophical Transactions of the Royal Society of London B: Biological Sciences* 356, 1159-1186.
- Tomasi, D., Wang, G.J., Volkow, N.D., 2013. Energetic cost of brain functional connectivity. *Proceedings of the National Academy of Sciences* 110, 13642-13647.
- Tononi, G., Sporns, O., Edelman, G.M., 1994. A measure for brain complexity: relating functional segregation and integration in the nervous system. *Proceedings of the National Academy of Sciences* 91, 5033-5037.
- Towlson, E.K., Vértes, P.E., Ahnert, S.E., Schafer, W.R., Bullmore, E.T., 2013. The Rich Club of the *C. elegans* Neuronal Connectome. *The Journal of Neuroscience* 33, 6380-6387.
- Vaishnavi, S.N., Vlassenko, A.G., Rundle, M.M., Snyder, A.Z., Mintun, M.A., Raichle, M.E., 2010. Regional aerobic glycolysis in the human brain. *Proceedings of the National Academy of Sciences* 107, 17757-17762.
- Van Essen, D.C. et al., 2012. The Human Connectome Project: A data acquisition perspective. *NeuroImage* 62, 2222-2231.
- Varshney, L.R., Chen, B.L., Paniagua, E., Hall, D.H., Chklovskii, D.B., 2011. Structural Properties of the *Caenorhabditis elegans* Neuronal Network. *PLoS Computational Biology* 7, e1001066.
- Verstraete, E., Veldink, J.H., van den Berg, L.H., van den Heuvel, M.P., 2014. Structural brain network imaging shows expanding disconnection of the motor system in amyotrophic lateral sclerosis. *Human Brain Mapping* 35, 1351-1361.
- Verstraete, E., Veldink, J.H., Mandl, R.C.W., van den Berg, L.H., van den Heuvel, M.P., 2011. Impaired Structural Motor Connectome in Amyotrophic Lateral Sclerosis. *PLoS ONE* 6, e24239.
- Watanabe, T., 2013. Rich-club network topology to minimize synchronization cost due to phase difference among frequency-synchronized oscillators. *Physica A: Statistical Mechanics and its Applications* 392, 1246-1255.
- Watts, D.J., Strogatz, S.H., 1998. Collective dynamics of 'small-world' networks. *Nature* 393, 440-442.
- van Wijk, B.C.M., Stam, C.J., Daffertshofer, A., 2010. Comparing Brain Networks of Different Size and Connectivity Density Using Graph Theory. *PLoS ONE* 5, e13701.
- Yadav, A., Jalan, S., 2015. Origin and implications of zero degeneracy in networks spectra. *Chaos: An Interdisciplinary Journal of Nonlinear Science* 25, 043110.
- Zalesky, A., Fornito, A., Bullmore, E.T., 2010a. Network-based statistic: Identifying differences in brain networks. *NeuroImage* 53, 1197-1207.
- Zalesky, A., Fornito, A., Harding, I.H., Cocchi, L., Yücel, M., Pantelis, C., Bullmore, E.T., 2010b. Whole-brain anatomical networks: Does the choice of nodes matter? *NeuroImage* 50, 970-983.
- Zalesky, A., Fornito, A., Seal, M.L., Cocchi, L., Westin, C.F., Bullmore, E.T., Egan, G.F., Pantelis, C., 2011. Disrupted Axonal Fiber Connectivity in Schizophrenia. *Biological Psychiatry* 69, 80-89.
- Zamora-López, G., Zhou, C., Kurths, J., 2010. Cortical hubs form a module for multisensory integration on top of the hierarchy of cortical networks. *Frontiers in Neuroinformatics* 4, 1.
- Zhao, T., Duan, F., Liao, X., Dai, Z., Cao, M., He, Y., Shu, N., 2015. Test-retest reliability of white matter structural brain networks: A multiband diffusion MRI study. *Frontiers in Human Neuroscience* 9, 59.

Zhou, J., Gennatas, E., Kramer, J., Miller, B., Seeley, W., 2012. Predicting Regional Neurodegeneration from the Healthy Brain Functional Connectome. *Neuron* 73, 1216-1227.

Nederlandse samenvatting

Volgens gangbare schattingen bevat het brein van een volwassen persoon ongeveer 80 tot 100 miljard neuronen. Deze neuronen functioneren niet onafhankelijk van elkaar, maar staan in verbinding via zo'n 100-500 biljoen neuronale connecties en vormen samen een uitgebreid en zeer complex netwerk. Het aantal neuronen en neuronale verbindingen in het brein is dus behoorlijk duidelingwekkend. Ter illustratie: als je naar het strand zou gaan en lege literflessen van je favoriete frisdrank zou vullen met zand, heb je circa honderdduizend flessen nodig om evenveel zandkorrels te verzamelen als neuronen in het brein en zelfs honderd miljoen flessen om het aantal neuronale connecties te benaderen. Hoewel het voorlopig verre van haalbaar is het volledige netwerk van neuronen en hun onderlinge verbindingen – het zogenaamde *connectoom* – van het menselijk brein in kaart te brengen, kunnen we de neurale infrastructuur die ons in staat stelt te bewegen, voelen, herinneringen te vormen en na te denken toch onderzoeken. Op een grovere en beter te bevatten schaal is het brein namelijk op te delen in diverse hersengebieden, ieder bestaande uit talloze neuronen met een vaak voor dat gebied karakteristieke interne organisatie, en de neuronale verbindingen tussen deze gebieden vormen dikke zenuwbanen. Dit *macroscopische* connectoom van hersengebieden en zenuwbanen is wel te reconstrueren, hetgeen ons in staat stelt de intrigerende architectuur van de bedrading van onze hersenen stukje bij beetje te ontrafelen.

Met name in de afgelopen twee decennia zijn verscheidene onderzoeksgroepen begonnen met het maken en bestuderen van goede connectoomreconstructies en is er geleidelijk aan steeds meer ontdekt over de manier waarop hersennetwerken georganiseerd zijn. Hierbij is gebleken dat concepten uit de *grafentheorie*, een onderzoeksgebied binnen de wiskunde, een onmisbaar hulpmiddel zijn bij het beschrijven van de architectuur van hersennetwerken. Simpel gezien resulteert connectoomreconstructie namelijk in een lijst van "punten" (de hersengebieden) en een lijst van "lijnen" (zenuwbanen) die deze punten met

elkaar verbinden, een structuur die precies overeenkomt met het wiskundige concept van een *graaf*. Ook in dit proefschrift gebruiken we grafentheorie om de organisatie van hersennetwerken te beschrijven. We richten ons hierbij met name op nieuwe onderzoekstechnieken voor grafen die nog niet gangbaar zijn binnen (en soms ook niet buiten) de neurowetenschappen. Hoewel reeds uitgevoerde studies met succes een tip van de sluier hebben weten op te lichten, zijn er nog vele vragen te beantwoorden over de bedrading van onze hersenen. Waarom lopen de zenuwbanen in ons brein bijvoorbeeld zoals ze lopen? Wat voor bijzondere eigenschappen hebben hersennetwerken ten opzichte van andere netwerken die voorkomen in de natuur en maatschappij? En hoe wordt informatie afkomstig van verschillende hersengebieden gecombineerd? Door op een andere manier naar grafen en hersennetwerken te kijken, hopen we een stap dichter bij de beantwoording van dergelijke vragen te komen. Oftewel, om bij onze beeldspraak te blijven: door ons perspectief te veranderen proberen we verder onder de sluier te kijken. Daarnaast verwachten we dat de hier onderzochte en toegepaste methodes van pas zullen komen om verschillen in bedrading tussen het gezonde en zieke brein bloot te leggen en hopen we dat dit proefschrift bij zal dragen aan toepassing van deze methodes in toekomstige, meer klinisch georiënteerde studies.

Het in kaart brengen van hersennetwerken

Om de organisatie van het (macroscopische) connectoom te kunnen bestuderen, moet het connectoom eerst in kaart gebracht worden. Afhankelijk van de gebuikte techniek, kan dit een enorme klus zijn. Zoals beschreven in **hoofdstuk 1**, wordt een techniek bekend als *virale tracing* vaak als gouden standaard gezien. Bij deze techniek, alleen geschikt voor onderzoek op dieren, wordt een gemodificeerd virus op een bepaalde plek in de hersenen ingebracht. Dit virus verplaatst zich via de verbindingen tussen neuronen en kan later aangekleurd worden zodat duidelijk wordt hoe het virus zich verspreid heeft, waaruit vervolgens kan worden afgeleid of er verbindingen liggen tussen de plek waarop het virus geïnjecteerd is en andere delen van de hersenen. Helaas kan een dergelijk experiment niet herhaald worden en kan er dus slechts inzicht verkregen

worden in de connectiviteit van één vooraf gekozen gebiedje. Om toch een volledige connectoomkaart te krijgen, worden de resultaten van verschillende experimenten met elkaar gecombineerd, vaak via grote online databases waarin alle in de literatuur gerapporteerde resultaten worden samengebracht. In dit proefschrift hebben we onder andere dergelijke reeds samengestelde connectoomkaarten van de kat, muis, rat en aap onderzocht.

Dankzij ontwikkelingen in beeldvormingstechnieken gebaseerd op magnetische resonantie (MR) is het heden ten dage echter ook mogelijk om connectoomkaarten te maken van het menselijk brein. Dit gebeurt op een veilige, niet-invasieve manier, waarbij de belasting van een proefpersoon beperkt blijft tot het stil in een MRI-scanner liggen (vaak zo'n twintig minuten). In **hoofdstuk 2** is geschetst hoe de hiervoor benodigde diffusie-gewogen beeldvorming werkt en wordt uitgebreid beschreven hoe de beelden geproduceerd door de MRI-scanner uiteindelijk worden omgezet in een kaart van het connectoom, een procedure die met behulp van speciaal hiervoor ontwikkelde software volledig automatisch kan worden uitgevoerd. Naast het feit dat deze op MRI gebaseerde procedure ons in staat stelt om hersennetwerken van menselijke subjecten (en nog levende dieren) te onderzoeken, heeft deze techniek als voordeel dat het een volledige macroscopische connectoomkaart van één individu oplevert en dat de meting eventueel op een later tijdstip herhaald kan worden. Hierdoor is het mogelijk hersennetwerken te vergelijken tussen verschillende subjecten (bijvoorbeeld patiënten en controles) of te monitoren over leeftijd, hetgeen een enorme impuls heeft gegeven aan de populariteit van connectoomonderzoek. Een nadeel ten opzichte van virale tracing is echter dat de aanwezigheid en sterkte van verbindingen met minder zekerheid kan worden vastgesteld. Bij diffusie-gewogen beeldvorming worden namelijk niet de verbindingen zelf – hetgeen momenteel simpelweg niet mogelijk is – maar de bewegingen (i.e., diffusie) van watermoleculen in kaart gebracht. Omdat deze watermoleculen de neiging hebben parallel aan de verbindingen te bewegen (bij beweging in andere richtingen “botsen” ze als het ware op de banen), kan de ligging van zenuwbanen hier indirect uit afgeleid worden.

Bij het maken van connectoomkaarten van het menselijk brein met behulp van MRI komen een aantal belangrijke methodologische aspecten om de hoek kijken. Om te beginnen moeten de hersenen opgedeeld worden in verschillende macroscopische hersengebieden. Gangbare methodes om deze *parcellatie* te bewerkstelligen zijn besproken in **hoofdstuk 3**. De verschillen tussen de diverse methodes zijn relatief groot; zowel het aantal gebieden waarin de hersenen worden onderverdeeld als de manier waarop de onderverdeling tot stand komt en naar een specifiek individu wordt vertaald loopt uiteen. Uit een analyse van bestaande literatuur bleek echter dat kwalitatieve uitspraken over hersennetwerken grotendeels onafhankelijk zijn van de gemaakte keuzes voor de parcellatie. Wat betreft kwantitatieve resultaten heeft met name de fijnmazigheid van de onderverdeling (i.e., het aantal onderscheiden gebiedjes) een sterke invloed, welke deels terug te voeren is op een algemene interactie tussen de resultaten van grafenanalyses en de grootte van de graaf.

Met de keuze voor een bepaalde parcellatiemethode liggen de *nodes* (i.e., "punten") van het te reconstrueren hersennetwerk in principe vast. Deze nodes zijn voor ieder subject hetzelfde en dragen in het formalisme van een graaf verder geen informatie. Om de connectoomkaart te voltooien moet er vervolgens aan de hand van de met diffusie-gewogen beeldvorming gereconstrueerde zenuwbanen voor ieder paar nodes besloten worden of er wel of geen verbinding tussen de bijbehorende hersengebieden ligt. Eventueel kan er ook nog een *gewicht* worden toegevoegd om de sterkte of kwaliteit van de verbinding uit te drukken. Vanwege de eerder genoemde onzekerheid en relatief ruizige aard van diffusie-gewogen beeldvorming, zullen de resulterende kaarten echter niet helemaal waarheidsgetrouw zijn. Met name in studies naar de netwerkeigenschappen van "het" gezonde brein – zoals de studies in dit proefschrift – is het daarom gebruikelijk de connectoomkaarten van meerdere proefpersonen te combineren tot één gemiddelde kaart. Hierbij worden alleen de verbindingen geïncludeerd die in een "groot genoeg" percentage – gespecificeerd door een bepaalde drempelwaarde – van de proefpersonen gedetecteerd zijn. De gedachte hierachter is dat het van consistent waargenomen verbindingen niet erg aannemelijk is dat

ze zijn toe te schrijven aan meetfouten. In **hoofdstuk 4** hebben we laten zien dat de keuze van de drempelwaarde een grote invloed heeft op de uiteindelijke connectoomkaart en hebben we onderzocht wat geschikte keuzes zouden zijn. De drempelwaarde simpelweg zo hoog mogelijk zetten volstaat namelijk niet; in dat geval zijn de overgebleven verbindingen weliswaar heel betrouwbaar en zijn er dus weinig fout-positieve verbindingen, maar zijn er waarschijnlijk ook veel daadwerkelijk bestaande verbindingen geëlimineerd die door een meetfout in een aantal subjecten niet gevonden zijn, resulterende in veel fout-negatieve verbindingen. Een inschatting van het aantal fout-positieve en fout-negatieve verbindingen per drempelwaarde – gemaakt met behulp van een simpel model – liet zien dat de drempelwaarde het beste tussen de 30 en 90% gekozen kan worden, met een mogelijk optimum bij 60%.

Een andere kijk: de verbindingen centraal

Het in kaart brengen van een connectoom levert in eerste instantie vooral een wirwar van punten en lijnen op en geeft nog niet direct nieuwe informatie over de netwerkarchitectuur van de hersenen. Om dergelijke informatie uit een connectoomkaart te destilleren wordt gebruik gemaakt van zogenaamde netwerkmaten, waarvan de meest gangbare kort zijn samengevat in **hoofdstuk 1**. Een simpel voorbeeld van een netwerkmaat is de karakteristieke padlengte van een netwerk, gedefinieerd als het aantal stappen dat je gemiddeld moet zetten als je langs de verbindingen van het netwerk van één node naar een andere node wilt reizen (iedere verbinding telt als één stap). Het toepassen van netwerkmaten op hersennetwerken heeft reeds diverse inzichten opgeleverd. Zo is aangeïntoond dat hersennetwerken een modulaire, “small-world” organisatie hebben, gekarakteriseerd door een relatief korte padlengte en het bestaan van groepen van sterk geclusterde hersengebieden. Een andere belangrijke eigenschap van hersennetwerken is het bestaan van gebieden met veel verbindingen en een centrale positie in het netwerk, de zogeheten *hubs*. Hubs en hun verbindingen lijken een cruciale rol te spelen in het brein en het beter duiden van deze rol is een belangrijk thema in dit proefschrift.

Opvallend is dat bijna alle netwerkmaten die voor connectoomonderzoek gebruikt worden een omschrijving geven van het netwerk door (gemiddelde) eigenschappen van de nodes van het netwerk uit te rekenen. Dit terwijl de verschillen in connectoomkaarten tussen individuen (inclusief eventuele verschillen gerelateerd aan hersenziekten) juist worden veroorzaakt door variatie in de (sterkte van) verbindingen van het netwerk. Hoewel het (impliciet) centraal stellen van hersengebieden op zich logisch is (hersengebieden zijn relatief beperkt in aantal en over het algemeen goed omschreven, waarbij er vaak extra informatie beschikbaar is over hun eventuele functie, micro- en macroscopische kenmerken, en genetische expressie), zou een omschrijving van hersennetwerken vanuit een perspectief waarin de verbindingen centraal staan van belangrijke aanvullende waarde kunnen zijn. In de studies beschreven in **hoofdstuk 5-8** hebben we daarom op verschillende manieren aandacht besteed aan het karakteriseren van de verbindingen van het connectoom.

Voortbordurend op recente studies die hebben laten zien dat de hubs in hersennetwerken een collectief vormen van sterk onderling verbonden hersengebieden, de zogenaamde *rich club*, is in **hoofdstuk 5** op basis van een connectoomkaart van de kat onderzocht wat de mogelijke rol van deze rich club is in de hersenen. Hierbij is met name gelet op de rol van drie verschillende typen verbindingen, namelijk (1) tussen hubs gelegen *rich club* verbindingen, (2) tussen hubs en niet-hubs gelegen *feeder* verbindingen, en (3) tussen niet-hubs gelegen *lokale* verbindingen. Dankzij twee unieke eigenschappen van de gebruikte connectoomkaart, zijnde een onderverdeling van de gebieden in functionele modules en de aanwezigheid van informatie over de richting van verbindingen, konden de verbindingen verder gelabeld worden als inter- of intramodulair en als uni- of bidirectioneel. Uit een beschouwing van de interactie tussen de verschillende *verbindingscategorieën* bleek dat rich club en feeder verbindingen veel vaker intermodulair zijn (i.e., hersengebieden uit verschillende functionele modules verbinden) dan lokale verbindingen en dat rich club verbindingen opvallend vaak bidirectioneel zijn. Verdere analyses bevestigden een belangrijke positie van de rich club tussen de diverse functionele modules, waarbij opviel

dat bijna 90% van de kortste intermodulaire paden in het netwerk langs een rich club node lagen, maar dat slechts 24% ook een rich club verbinding passeeerde. Dat verbindingen tussen hubs niet per se noodzakelijk lijken om een rol van de rich club als schakelstation tussen verschillende functionele modules mogelijk te maken, laat ruimte voor de hypothese dat deze (toch overvloedig aanwezige) verbindingen wellicht een andere rol vervullen, namelijk het faciliteren van integratie van informatie afkomstig uit verschillende functionele domeinen.

In **hoofdstuk 6** is deze hypothese vervolgens op directere wijze onderzocht. Om dit mogelijk te maken is het centraal stellen van de verbindingen in dit hoofdstuk verder uitgebouwd door een methode te introduceren om netwerkeigenschappen van individuele verbindingen te berekenen. Hierbij wordt de rol van een individuele verbinding in het netwerk bepaald door uit te rekenen hoe bestaande netwerkeigenschappen (zoals de karakteristieke padlengte) veranderen als de verbinding uit het netwerk wordt weggenomen. Een vergelijking van op deze manier bepaalde relevantie scores van verbindingen in het menselijk brein liet zien dat rich club verbindingen een significant hogere relevantie hebben ten aanzien van twee specifieke netwerkmaten: een maat die inschat hoe makkelijk hersengebieden met elkaar kunnen communiceren en een maat die beschrijft hoe goed verschillende functionele modules geïntegreerd zijn. Deze bevinding – succesvol gerepliceerd in de eerder onderzochte kaart van het connectoom van de kat – is in lijn met de gestelde hypothese en andere aanwijzingen dat de rich club een belangrijke rol speelt bij communicatie en integratie in het brein.

Dat kwalitatieve aspecten van de organisatie van hersennetwerken een grote gelijkenis vertonen over verschillende diersoorten wordt onderstreept door het in **hoofdstuk 7** beschreven onderzoek van connectoomreconstructies van de muis en rat. Zo bevatte zowel het hersennetwerk van de muis als het hersennetwerk van de rat een rich club van sterk onderling verbonden hub gebieden, waarmee deze diersoorten aansluiten in een steeds langer wordende lijst van soorten waarvoor dit fenomeen gerapporteerd is. Ook de gevonden

eigenschappen van de rich club verbindingen tussen hubs bleken consistent met eerder gerapporteerde resultaten, zowel uit dit proefschrift als de literatuur. Rich club verbindingen waren gemiddeld genomen langer en sterker dan andere verbindingen en waren bovendien vaak bidirectioneel, intermodulair en gepositioneerd tussen gebieden met toegang tot een groot aantal modules; eigenschappen waarvan gesuggereerd is dat ze ideaal zouden zijn voor verbindingen van een “globale werkplaats” waar informatie uit verschillende functionele domeinen kan samenkomen. De overeenstemming tussen resultaten afgeleid van verschillende connectoomkaarten – verkregen door middel van verschillende technieken – maakt aannemelijk dat de bevindingen niet zijn toe te schrijven aan eventuele methodologische artefacten.

Aansluitend op de prominente rol van het concept van modules in de tot nu toe beschreven analyses en ons voornemen om het brein te beschrijven vanuit een perspectief waarin de verbindingen centraal staan, hebben we in **hoofdstuk 8** onderzocht of – in plaats van de nodes – ook de verbindingen van het connectoom opgedeeld kunnen worden in modules. Door een bestaand algoritme voor het detecteren van modules van nodes met een wiskundige truc geschikt te maken voor het detecteren van modules van verbindingen, vonden we een verdeling van de connecties van het menselijk connectoom in elf verschillende modules. Vijf van deze modules waren geconcentreerd rondom de middenlijn tussen de twee hersenhelften; de overige zes modules waren overwegend geïsolseerd binnen één hersenhelft, met drie modules in de linkerhelft en drie vergelijkbare modules in de rechterhelft. Toepassing van de eerder omschreven methode om netwerkeigenschappen van verbindingen te bepalen, liet zien dat de gedetecteerde modules niet zozeer groepen van gelijksoortige verbindingen vormen, maar eerder gezien moeten worden als deelsystemen van het connectoom. Onderzoek naar de interactie tussen de gevonden modules en de aanwezigheid van hubs toonde bovendien aan dat hub gebieden “hot spots” vormen waar de verbindingen van een groot aantal modules samenkommen, hetgeen naadloos aansluit bij onze eerdere bevindingen betreffende de rol van de rich club.

Het gebruikte algoritme voor de detectie van de hierboven omschreven modulen is gebaseerd op het idee dat een goede onderverdeling in modules kan worden verkregen door te zoeken naar delen van het netwerk waarin een signaal dat willekeurig over het netwerk beweegt tijdelijk “gevangen” raakt doordat de elementen steeds naar elkaar verwijzen. Met het oog op recente bevindingen die suggereren dat een vergelijkbaar proces een rol speelt in diverse neurodegeneratieve ziekten, waarbij ziektefactoren zich mogelijk verspreiden via de verbindingen van het connectoom, zijn de hier gedetecteerde modules van verbindingen mogelijk een interessant doelwit voor toekomstige connectoomstudies naar deze ziekten. Hoewel we ons in dit proefschrift hebben toegelegd op het beter begrijpen van het gezonde brein, is de mogelijke toepassing van de hier onderzochte netwerkconcepten in meer klinisch georiënteerde studies wel een extra drijfveer geweest om ons specifiek te richten op de verbindingen van het connectoom, zijnde de elementen waarin verschillen tussen subjecten tot uiting komen. Zo hopen we dat de beschreven categorieën van verbindingen (waaronder de gedetecteerde modules) kunnen helpen om verschillen tussen het connectoom van patiënten en controles te identificeren. Bovendien verwachten we dat onze methode om netwerkeigenschappen van individuele verbindingen te bepalen bij kan dragen aan het schetsen van een beter beeld van verbindingen die ziekte-gerelateerde veranderingen tonen.

Netwerk spectra

Of je nu de nodes of de verbindingen als uitgangspunt neemt, in beide gevallen is het mentale beeld van een graaf dat van een verzameling “punten” en “lijnen”. Een graaf kan echter ook worden gezien als matrix, waarbij de rijen en kolommen van de matrix de nodes vertegenwoordigen en het element op positie (i, j) in de matrix aangeeft of node i en j met elkaar verbonden zijn. In plaats van een graaf te omschrijven met op nodes en verbindingen gebaseerde netwerkmaten, kan een graaf derhalve ook geanalyseerd worden door de zogenaamde eigenwaarden en eigenvectoren van aan de graaf gerelateerde matrices te bestuderen. In het bijzonder geeft het zogeheten *spectrum* van de *Laplaciaanse* matrix – formeel een discrete verzameling van eigenwaarden, maar vaak weergegeven

als een curve die de relatieve frequentie van de eigenwaarden aanduidt – een soort “vingerafdruk” van de graaf als geheel, zonder te refereren aan individuele nodes of verbindingen.

In **hoofdstuk 9** is verkend hoe een dergelijke (vrij wiskundige) analyse van grafen behorende bij connectoomkaarten kan worden gebruikt om inzicht te geven in de eigenschappen en organisatie van neurale netwerken. Het eerste deel van het hoofdstuk laat zien dat de spectrale vingerafdrukken van neurale netwerken van drie verschillende diersoorten een aantal karakteristieke eigenschappen in gemeen hebben, waaronder een uitgesproken piek in het midden van het spectrum. Het onderzoek in het tweede deel van het hoofdstuk toont aan dat deze centrale piek sterk gerelateerd is aan vormen van symmetrie in het onderliggende netwerk, gecreëerd door het bestaan van hersengebieden met een gedeeltelijk overlappend bedradingspatroon. Specifieke aspecten van spectrale vingerafdrukken zijn dus terug te vertalen naar concrete netwerkeigenschappen, al zal er nog veel van dit “vertaalwerk” nodig zijn voordat deze bijzondere kijk op hersennetwerken zich echt uitbetaalt.

Afsluiting

Van alle netwerken die voorkomen in de natuur en maatschappij is het neurale netwerk dat huist in onze schedel waarschijnlijk het meest fascinerende. Hoewel het twijfelachtig is of we de processen en mechanismes die komen kijken bij het ontstaan en functioneren van dit connectoom ooit volledig zullen begrijpen, maakt de bepalende rol van het connectoom in wie we zijn en de vatbaarheid van dit netwerk voor ziekten het absoluut de moeite waard om er zoveel mogelijk over te weten te komen. Met dit proefschrift hopen we hieraan een bescheiden bijdrage te hebben geleverd. Door op een andere manier naar hersennetwerken te kijken, zijn we meer te weten gekomen over de macroscopische organisatie van het connectoom, en met name over de rol van de verbindingen tussen centrale hub gebieden in de hersenen. Voor mij persoonlijk geldt dat na jaren mijn brein gebruikt te hebben om wiskunde te begrijpen, het enorm energerend is geweest om nu wiskunde te gebruiken om het brein te begrijpen.

List of publications

Publications incorporated in this thesis are marked by an *.

2015

van den Heuvel, M.P., de Reus, M.A., Barrett, L.F., Scholtens, L.H., Coopmans, F.M.T., Schmidt, R., Preuss, T.M., Rilling, J.K., Li, L., 2015. Comparison of diffusion tractography and tract-tracing measures of connectivity strength in rhesus macaque connectome. *Human Brain Mapping*, epub ahead of print.

Scholtens, L.H., de Reus, M.A., van den Heuvel, M.P., 2015. Linking Contemporary High Resolution Magnetic Resonance Imaging to the Von Economo Legacy: A Study on the Comparison of MRI Cortical Thickness and Histological Measurements of Cortical Structure. *Human Brain Mapping*, epub ahead of print.

Baggio, H.C., Segura, B., Junque, C., de Reus, M.A., Sala-Llonch, R., Van den Heuvel, M.P., 2015. Rich Club Organization and Cognitive Performance in Healthy Older Participants. *Journal of Cognitive Neuroscience*, epub ahead of print.

Mallio, C.A., Schmidt, R., de Reus, M.A., Vernier, F., Quintiliani, L., Curcio, G., Zobel, B.B., Quattrochi, C.C., van den Heuvel, M.P., 2015. Epicentral Disruption of Structural Connectivity in Alzheimer's Disease. *CNS Neuroscience & Therapeutics*, epub ahead of print.

Schmidt, R., de Reus, M.A., Scholtens, L.H., van den Berg, L.H., van den Heuvel, M.P., 2015. Simulating disease propagation across white matter connectome reveals anatomical substrate for neuropathology staging in amyotrophic lateral sclerosis. *NeuroImage*, epub ahead of print.

Peper, J.S., de Reus, M.A., van den Heuvel, M.P., Schutter, D.J.L.G., 2015. Short fused? associations between white matter connections, sex steroids, and aggression across adolescence. *Human Brain Mapping* 36, 1043-1052.

* van den Heuvel, M.P., Scholtens, L.H., de Reus, M.A., 2015. Topological organization of connectivity strength in the rat connectome. *Brain Structure and Function*, epub ahead of print.

Marqués-Iturria, I., Scholtens, L.H., Garolera, M., Pueyo, R., García-García, I., González-Tartiere, P., Segura, B., Junqué, C., Sender-Palacios, M.J., Vernet-Vernet, M., Sánchez-Garre, C., de Reus, M.A., Jurado, M.A., van den Heuvel, M.P., 2015. Affected connectivity organization of the reward system structure in obesity. *NeuroImage* 111, 100-106.

2014

Scholtens, L.H., Schmidt, R., de Reus, M.A., van den Heuvel, M.P., 2014. Linking macroscale graph analytical organization to microscale neuroarchitectonics in the macaque connectome. *The Journal of Neuroscience* 34, 12192-12205.

- * de Reus, M.A., Saenger, V.M., Kahn, R.S., van den Heuvel, M.P., 2014. An edge-centric perspective on the human connectome: link communities in the brain. *Philosophical Transactions of the Royal Society of London B: Biological Sciences* 369, 20130527.
- * de Reus, M.A., van den Heuvel, M.P., 2014. Simulated rich club lesioning in brain networks: a scaffold for communication and integration? *Frontiers in Human Neuroscience* 8, 647.
- Senden, M., Deco, G., de Reus, M.A., Goebel, R., van den Heuvel, M., 2014. Rich club organization supports a diverse set of functional network configurations. *NeuroImage* 96, 174-182.
- * van den Heuvel, M.P., de Reus, M.A., 2014. Chasing the Dreams of Early Connectionists. *ACS Chemical Neuroscience* 5, 491-493.
- van den Heuvel, M.P., Kersbergen, K.J., de Reus, M.A., Keunen, K., Kahn, R.S., Groenendaal, F., de Vries, L.S., Binders, M.J.N.L., 2014. The Neonatal Connectome During Preterm Brain Development. *Cerebral Cortex*, epub ahead of print.
- Schmidt, R., Verstraete, E., de Reus, M.A., Veldink, J.H., van den Berg, L.H., van den Heuvel, M.P., 2014. Correlation between structural and functional connectivity impairment in amyotrophic lateral sclerosis. *Human Brain Mapping* 35, 4386-4395.
- Collin, G., Kahn, R.S., de Reus, M.A., Cahn, W., van den Heuvel, M.P., 2013. Impaired Rich Club Connectivity in Unaffected Siblings of Schizophrenia Patients. *Schizophrenia Bulletin* 40, 438-448.
- * de Lange, S.C., de Reus, M.A., van den Heuvel, M.P., 2014. The Laplacian spectrum of neural networks. *Frontiers in Computational Neuroscience* 7, 189.

2013

- * de Reus, M.A., van den Heuvel, M.P., 2013. The parcellation-based connectome: Limitations and extensions. *NeuroImage* 80, 397-404.
- * de Reus, M.A., van den Heuvel, M.P., 2013. Rich Club Organization and Intermodule Communication in the Cat Connectome. *The Journal of Neuroscience* 33, 12929-12939.
- * de Reus, M.A., van den Heuvel, M.P., 2013. Estimating false positives and negatives in brain networks. *NeuroImage* 70, 402-409.
- Boersma, M., Kemner, C., de Reus, M.A., Collin, G., Snijders, T.M., Hofman, D., Buitelaar, J.K., Stam, C.J., van den Heuvel, M.P., 2013. Disrupted Functional Brain Networks in Autistic Toddlers. *Brain Connectivity* 3, 41-49.
- Collin, G., de Reus, M.A., Cahn, W., Hulshoff Pol, H.E., Kahn, R.S., van den Heuvel, M.P., 2013. Disturbed grey matter coupling in schizophrenia. *European Neuropsychopharmacology* 23, 46-54.

Acknowledgments

Modern science is becoming more and more of a team effort. As the boundaries of our knowledge continue to expand, there will be more ground to cover before reaching them and it will take more effort to push them. With an era of truly “big data” about to dawn, working together and building on each other’s strengths is crucial to make advances. This principle also applies to the work presented in this thesis, which I could never have done without the help of many fantastic people. Here, I would like to take a moment to thank them.

I would like to convey my heartfelt gratitude to my supervisor Prof. René Kahn, whose vast research experience and positive attitude helped me enormously to bring my PhD project to a (hopefully) successful end. Having such a kind and wise supervisor, with a great sense of humor, has been an absolute privilege. I am also grateful to Professor Kahn for his trust in the person to whom I am – without any doubt – indebted most: my daily supervisor Dr. Martijn van den Heuvel.

Martijn, working with you has been an incredible journey from the first day on. You are not only extremely smart and creative, but also a great motivator and coach who always strives for the best. During our mental sparring sessions, we would never be short of ideas and it would only take a few words to get up to speed with each other; a truly special experience. Thank you for your immense contribution to this work and for all the opportunities you have given me. It is much appreciated! With your talents and guidance, I am sure that the Dutch Connectome Lab will have a very bright future ahead of it and I would be honored to contribute to that future.

I would also like to thank the other researchers within the Brain Center Rudolf Magnus, and in particular the members of the Dutch Connectome Lab, for all the support and fun. Guusje, Ruben, Lianne, Fraukje, Kristin, Idoia, Ingrid, Hannelore, Siemon, and Claire, I could not have asked for better comrades to

pursue our scientific dreams and to enjoy our work and everything beyond that. You made coming to the lab a pleasure. Guusje and Ruben, thanks for being my paranympths. You are both fantastic and have so many qualities I admire you for. Lianne, thank you for the awesome figures you have made. You have a real eye for artwork and are a great colleague. Siemon, many thanks for your hard work on the spectral approach and for making tutoring easy.

Of course, I am very indebted to all of my co-authors, both those involved in the studies incorporated in this thesis and those with whom I worked on other projects. I much enjoyed being able to work with researchers from different research labs and with different areas of expertise, which has substantially broadened my horizon. Victor, thank you for your contributions to this thesis. Hugo, Carlo, Aldo, Tim, Sebastian, Karina, Jiska, Mario, Lara, Dienke, and many others, thank you for your trust. I hope we can continue to collaborate.

I am likewise grateful to the members of my thesis committee: Prof. Rick Dijkhuizen, Prof. Hilleke Hulshoff Pol, Prof. Roberto Fernández, Prof. Cornelis Stam, and Prof. Olaf Sporns. I am truly honored that such highly esteemed experts from a variety of institutions and backgrounds have been found willing to evaluate and discuss the work presented in this thesis, and – especially in the case of Prof. Sporns – travel a long distance to do so. Thank you!

Last but not the least, I would like to thank my family and girlfriend. To my parents and siblings, I am grateful for a wonderful youth and for unconditional support throughout my (educational) career and my life in general. To my girlfriend, my gratefulness can hardly be described in words. Nadja, your role in this thesis and my life is indispensable. Not only have you made many practical contributions by carefully reading all of the text and helping me out with the design and figures, you have also supported me mentally with your love and friendship, and made it possible for me to focus on my work when necessary. Thank you for everything.

Curriculum vitae

Marcel A. de Reus was born on February 1, 1987, in Rotterdam. He subsequently attended the Albert Plesmanschool (primary education) and Emmauscollege (high school) and completed his pre-university schooling in 2005. Marcel received a bachelor's degree in physics and mathematics (*cum laude*) from Utrecht University in 2008 and a master's degree in mathematics (also *cum laude*) from that institution in 2011. In the same year, he started a PhD project at the Brain Center Rudolf Magnus of the University Medical Center Utrecht under supervision of Dr. Martijn P. van den Heuvel and Prof. René S. Kahn, ultimately resulting in this thesis. As part of his research project, Marcel developed software for MRI-based reconstruction of large-scale brain networks, which is currently being used in collaborations with several international research labs and which he will continue to work on.